รายงานวิจัยฉบับสมบูรณ์

โครงการพัฒนากระบวนการผลิตเชื้อเพลิงชีวภาพ “แบบไร้ของเสีย” อย่างยั่งยืน จากวัตถุดิบภายในประเทศโดยบูรณาการกระบวนการผลิตเข้ากับการใช้ประโยชน์จากผลิตภัณฑ์พลอยได้

โดย

รศ.ดร. นวดล เหล่าศิริพจน์

บัณฑิตวิทยาลัยร่วมด้านพลังงานและสิ่งแวดล้อม

มหาวิทยาลัยเทคโนโลยีพระจอมเกล้าธนบุรี

30 มิถุนายน 2555

สัญญาเลขที่ BRG5280005

รายงานวิจัยฉบับสมบูรณ์

โครงการพัฒนากระบวนการผลิตเชื้อเพลิงชีวภาพ “แบบไร้ของเสีย” อย่างยั่งยืน จากวัตถุดิบภายในประเทศโดยบูรณาการกระบวนการผลิตเข้ากับการใช้ประโยชน์จากผลิตภัณฑ์พลอยได้

รศ.ดร. นวดล เหล่าศิริพจน์

บัณฑิตวิทยาลัยร่วมด้านพลังงานและสิ่งแวดล้อม

มหาวิทยาลัยเทคโนโลยีพระจอมเกล้าธนบุรี

สนับสนุนโดยสำนักงานคณะกรรมการการอุดมศึกษา

และสำนักงานกองทุนสนับสนุนการวิจัย

Project Title (in Thai) การพัฒนากระบวนการผลิตเชื้อเพลิงชีวภาพ ‘‘แบบไร้ของเสีย’’ อย่างยั่งยืนจากวัตถุดิบภายในประเทศโดยบูรณาการกระบวนการผลิตเข้ากับการใช้ประโยชน์จากผลิตภัณฑ์พลอยได้

(in English) Development of sustainable “zero-waste” biofuel production processes from local feedstock by integrating the production with by-product utilization processes

Project members

Project Head

Name	Mr. Navadol Laosiripojana (นายนวดล เหล่าศิริพจน์)
Qualification	Ph.D.
Position	Associate Professor
Address	The Joint Graduate School of Energy and Environment King Mongkut’s University of Technology Thonburi, Bangkok 10140, Thailand
Telephone	(02) 872-9014
Facsimile	(02) 872-6736
Email	navadol_l@jgsee.kmutt.ac.th

Project Member

Name	Mr. Verawat Champreda (นายวีระวัฒน์ แช่มปรีดา)
Qualification	Ph.D.
Position	Researcher
Address	National Center for Genetic Engineering and Biotechnology, BIOTEC, Bangkok, Thailand
Telephone	(02) 564-6700 ext 3473
Facsimile	(02) 564-6707
Email	verawat@biotec.or.th

Project Consultant

Name	Mr. Suttichai Assabumrungrat (นายสุทธิชัย อัสสะบำรุงรัตน์)
Qualification	Ph.D.
Position	Professor
Address	Department of Chemical Engineering, Faculty of Engineering, Chulalongkorn University, Bangkok 10330, Thailand
Telephone	(02) 218-6868
Facsimile	(02) 218-6877
Email	Suttichai.A@chula.ac.th

Abstract

Energy and environment crisis are currently among the world's most concerns. One interesting solution that several developed countries have been developing is the synthesis of clean alternative (and/or renewable) fuels to replace the conventional fossil-based fuels. On the basis of Thailand, as an agricultural country, several types and numerous amount of lignocellulosic biomass are available. Therefore, the uses of these biomasses as feedstock for biofuel (i.e. BTL and bioethanol) productions would help the nation to reduce the oil import rate as well as decrease CO_2 emission rate. In addition to biomass, palm oil is another important renewable feedstock for biodiesel production. Typically, it contains high amount of free fatty acid (FFA) that must be firstly processed or removed (as called palm fatty acid distilled or PFAD). The conversion of this PFAD to fatty acid methyl ester (FAME) is an alternative way to reduce cost and to make biodiesel enable to compete economically with conventional fuels. In this research, it involves the development of processes for converting several biomasses to BTL and bioethanol and converting waste PFAD to biodiesel. In addition, along with these biofuel productions, several by-products from the processes will be further converted to energy (e.g. hydrogen) and/or valuable products (e.g. bioplastic, oil, and useful chemicals) with an aim to develop the sustainable "zero-waste" process.

Keywords: biomass; alkane fuel; ethanol; biodiesel; waste; hydrogen

บทคัดย่อ

วิกฤตการณ์ด้านพลังงานและสิ่งแวดล้อมอันเป็นปัญหาสำคัญที่ทั่วโลกกำลังประสบ ซึ่งแนวทางที่นำเสนอคือ การพัฒนาเชื้อเพลิงชีวภาพขึ้นใช้ทดแทนน้ำมันฟอสซิล โดยประเทศไทยซึ่งเป็นประเทศเกษตรกรรมมีวัสดุชีวมวลเหลือใช้หลากหลายประเภทเป็นจำนวนมาก การนำวัสดุชีวมวลเหล่านี้มาใช้เป็นสารตั้งต้นในการสังเคราะห์เชื้อเพลิงชีวภาพ (อันได้แก่ เชื้อเพลิงเหลวจากชีวมวล (Biomass-to-Liquid; BTL) และไบโอเอทานอล) จะมีส่วนช่วยประเทศชาติในการลดอัตราการนำเข้าน้ำมันอย่างมีนัยสำคัญ อีกทั้งยังสามารถลดอัตราการปลดปล่อยก๊าซคาร์บอนไดออกไซด์ได้อีกด้วย อนึ่งนอกเหนือจากวัสดุชีวมวลแล้ว น้ำมันปาล์มก็เป็นวัตถุดิบที่สำคัญอีกชนิดหนึ่งที่ถูกนำมาใช้เพื่อผลิตโอดีเซลอย่างกว้างขวาง โดยทั่วไปแล้วน้ำมันปาล์มจะมีองค์ประกอบของกรดไขมันอิสระประเภทต่างๆ อยู่ในสัดส่วนที่สูง ซึ่งกรดไขมันอิสระเหล่านี้ต้องถูกแยกออกหรือบำบัดก่อนการแปรสภาพนำน้ำมันปาล์มเป็นไบโอดีเซล การแปรสภาพกรดไขมันอิสระเหล่านี้เป็นสารประกอบเมทิลเอสเทอร์ ซึ่งสามารถแปรสภาพเป็นไบโอดีเซลได้จะช่วยลดค่าใช้จ่ายของกระบวนการผลิตไบโอดีเซลและทำให้ราคาไบโอดีเซลที่ผลิตได้สามารถแข่งขันได้กับเชื้อเพลิงฟอสซิล ภาพรวมของโครงการวิจัยที่เสนอนี้เกี่ยวข้องกับการพัฒนากระบวนการผลิตเชื้อเพลิงชีวภาพ Biomass-to-Liquid (BTL) และไบโอเอทานอล จากวัสดุชีวมวลประเภทต่างๆ ในประเทศ รวมถึงการแปรสภาพกรดไขมันอิสระที่แยกได้จากน้ำมันปาล์มไปเป็นไบโอดีเซล นอกจากนั้นงานวิจัยนี้ยังได้เสนอการบูรณาการกระบวนการผลิตดังกล่าวเข้ากับการใช้ประโยชน์จากผลิตภัณฑ์พลอยได้ที่เกิดขึ้น ทั้งแง่ของการนำผลิตภัณฑ์พลอยได้เหล่านั้นไปแปรสภาพเป็นพลังงาน (อันได้แก่ ไฮโดรเจน ซึ่งเป็นพลังงานสะอาด) หรือแปรสภาพเป็นผลิตภัณฑ์ที่มีประโยชน์ (อันได้แก่ ไบโอพลาสติก เมทานอล น้ำมัน หรือสารประกอบเคมีต่างๆ) ซึ่งการบูรณาการดังกล่าวจะเป็นการสร้างกระบวนการผลิตเชื้อเพลิงชีวภาพ “แบบไร้ของเสีย” อย่างยั่งยืน ขึ้น

คำสำคัญ ชีวมวล เชื้อเพลิงอัลเคน เอทานอล ไบโอดีเซล ของเสีย ไฮโดรเจน

Executive Summary

In the present work, it involves the development of processes for converting several biomasses to BTL and bioethanol and converting waste PFAD to biodiesel. In addition, along with these biofuel productions, several by-products from the processes will be further converted to energy (e.g. hydrogen) and/or valuable products (e.g. bioplastic, oil, and useful chemicals) with an aim to develop the sustainable "zero-waste" process. The summaries of this project can be grouped in 4 main sections as presented below:

1. Production of BTL via single unit catalytic hot compressed water reactor

In this research, we successfully developed the process for converting biomass to alkane via sequential hydrolysis/dehydration/aldol-condensation/hydrogenation. The novelty of this work is that we combine all reactions in single unit hot compressed water (HCW) reactor. We also developed the novel catalyst (i.e. Pd/WO_3-ZrO_2) that has the reactivity for all reactions in this single unit system.

2. Production of lignocellulosic ethanol via hydrolysis & fermentation reactions

As for lignocellulosic ethanol production, it involves 2 main reactions i.e. hydrolysis of biomass to sugars and later fermentation to ethanol. For hydrolysis reaction, we proposed that the hot compressed water (HCW) can efficiently hydrolyze cellulose and hemicellulose in biomass to sugars. According to our study, we found that in the presence of a suitable catalyst (i.e. solid super-acid catalyst; H_3PO_4-activated carbon), the catalyst can promote the hydrolysis reaction simultaneously with the inhibition of the dehydration reaction. The biomass hydrolyzate was then converted to ethanol by fermentation process.

3. Production of biodiesel from waste palm fatty acid distilled (PFAD)

Regarding biodiesel production process, we successfully developed the solid super-acid catalyst (i.e. WO_3-ZrO_2) with a novel technique that provided excellent esterification reactivity with high stability toward long-term testing. Also, intrinsic kinetics for esterification reaction of several fatty acids e.g. palmitic acid, linoleic acid, and oleic acid over developed catalysts was carried out as a procedure to understand the role of catalyst and optimize the suitable conditions for esterification reaction. As another approach for biodiesel production in this project, the biocatalytic process using solid lipase-catalyst was developed and tested. From this research, we found that immobilized lipase from *C. antarctica* (Novozym 435®, Bagsvared, Denmark) and CLEA-lipase can efficiently convert palm oil, free fatty acids (FFA) and acid oil model (TAG/FFA mixes) to fatty acid methyl ester (FAME) and fatty acid ethyl ester (FAEE).

4. Utilization of by-products from the main processes

As for the last theme, the developments of technologies for converting several by-products from above processes to energy and/or valuable products were carried out. We found that several wastes from the processes i.e. fatty acids and lignin can be efficiently converted to synthesis gas or hydrogen-rich gas by the catalytic steam and authothermal reforming reactions.

Chapter 1

Background and Importance of the Project

Energy and environment are among the world's most concerns. Most countries around the worlds have been facing with the energy crisis due to the shortage of conventional oil as well as the dramatic rising of the oil price. These problems are believed to come from the high consumption rate of conventional oil. As a main consequence of energy crisis, several environmental problems occur. One of the current critical environmental problems is the global warming and climate change due to the high emission rate of CO_2 from the combustion of oil. Recently, there are several attempts around the world to minimize the environmental problems e.g. Kyoto protocol. According to the report of Intergovernmental Panel for Climate Change (IPCC), Thailand has signed this Protocol and has the commitment to reduce the level of green house gas releasing. Currently, although this value for Thailand is still below the world average, it has been rising up due to the growing of our fossil fuel consumption rate. Once, this value reaches or becomes higher than that of the world average, Thailand could possibly face the non-tariff trade barrier.

Typically, there are several procedures to minimize energy and environmental problems. One of the current interesting solution that several developed countries have been attempting to do is to develop the clean alternative (and/or renewable) fuels to replace the conventional oil. Some examples of these alternative fuels are hydrogen, gas-to-liquid (GTL), biomass-to-liquid (BTL), dimethyl-ether (DME), biodiesel, and bioethanol. Nowadays, the most practical biofuels for Thailand are bio-ethanol and biodiesel. Thai government has been attempting to promote the use of these two biofuels to replace conventional gasoline and diesel oil respectively. It should be noted that the current raw materials that have been applied to produce bioethanol and biodiesel are molasses from sugarcane, cassava, and palm oil. The major consideration for using these raw materials as feedstock for fuel production is the competition with food market, which could result in the food shortage and the rising of food price. On the basis of Thailand, as an agricultural country, we have several types and numerous amount of lignocellulosic biomass as presented in Table 1.

Table 1: Information of biomass in Thailand [1]

Crop	Production 2003 (ktons)	Residue	RPR	Surplus Availability Factor	Calorific Value (MJ/kg)	Potential Energy (TJ)
Rice	26,057	Husk	0.230	0.493	14.27	42,162
		Straw	0.447	0.684	10.24	81,581
Sugar Cane	64,973	Bagasse	0.291	0.207	14.40	56,358
		Top & Trashier	0.302	0.986	17.39	336,447
Maize	4,230	Corn Cob	0.273	0.670	18.04	13,958
Cassava	16,868	Stalk	0.088	0.407	18.42	11,128
Coconut	1,418	Husk	0.362	0.595	16.23	4,957
		Shell	0.160	0.378	17.93	1,538
		Empty Bunches	0.049	0.843	15.40	902
		Frond	0.225	0.809	16.00	4.130

Therefore, the uses of these biomasses as feedstock for biofuel (i.e. BTL and bioethanol) productions would be a great option for Thailand. If we can develop the efficient techniques to convert these feedstocks to biofuels, it will certainly help the nation to reduce the fuel import rate as well as decrease CO_2 emission rate from the combustion of fuel (as these alternative fuels are produced from renewable sources and the CO_2 emission from the combustion of these fuel is not considered as emission, according to Kyoto protocol).

Apart from the use of biomass as raw materials for bioethanol and BTL production, palm oil is currently the main raw material for biodiesel production. Typically, palm oil always contains high amount of free fatty acid (FFA) and the presence of too high FFA easily results in high amount of soap produced during transesterification reaction. Therefore, to avoid this reaction, most of FFA in palm oil must be firstly processed or removed (as called palm fatty acid distilled or PFAD). The conversion of this PFAD to fatty acid methyl ester (FAME), which can be used as biodiesel, is an alternative way to increase the overall biodiesel yield, thus reducing the cost for biodiesel production and to make biodiesel enable to compete economically with conventional petroleum diesel fuels.

In summary, the main objective of this research proposal is to develop the processes for converting several biomasses (e.g. bagasse, rice husk, rice straw, cassava stalk) to biofuels (i.e. BTL and bioethanol; as called cellulosic ethanol) and also converting waste PFAD to biodiesel (as called fatty acid methyl-ester; FAME). It should be noted that, along with these biofuel productions, several by-products e.g. glycerol, lignin, and undefined residues are also generated from the reactions. As another research theme, we plan to study the processes for utilizing or converting these by-products to energy and/or valuable products with an aim to develop the sustainable "zero-waste" process. On this basis, it will provide the great benefit in terms of energy, environmental, and economical aspects. As the final step, technical and economical feasibilities for these processes will be studied to identify the possible use in commercial scale. For the clear understanding, Figure 1 explains the schematic diagram of this whole research proposal.

In details, BTL is one of the promising 2^{nd} generation fuels. Theoretically, its physical and chemical properties are identical to those of conventional diesel and/or gasoline oil (depending on the process). As for its production technology, currently, there are 2 main procedures to produce BTL i.e. Gasification/Fischer-Tropsch (FT) and fast pyrolysis processes. According to the first process, gasification/Fischer-Tropsch (FT), biomass is firstly converted to synthesis gas via gasification reaction, and then secondary reformed to liquid C_9-C_{15} alkanes via catalytic Fischer-Tropsch (FT) process. The great advantage of gasification/Fischer-Tropsch (FT) process is the achievement of high product selectivity, nevertheless, the major barrier is its poor economic feasibility. It has widely been reported that this process is economically feasible only at large scale production (3 million standard cubic meters per day; MSCMD). In contrast, for the fast pyrolysis process, it is the cheaper process and feasible for the small scale production unit, but the weakness of this process is its low product selectivity, as various types of by-products are also generated during the process. Consequently, the expensive distillation or extraction system is required.

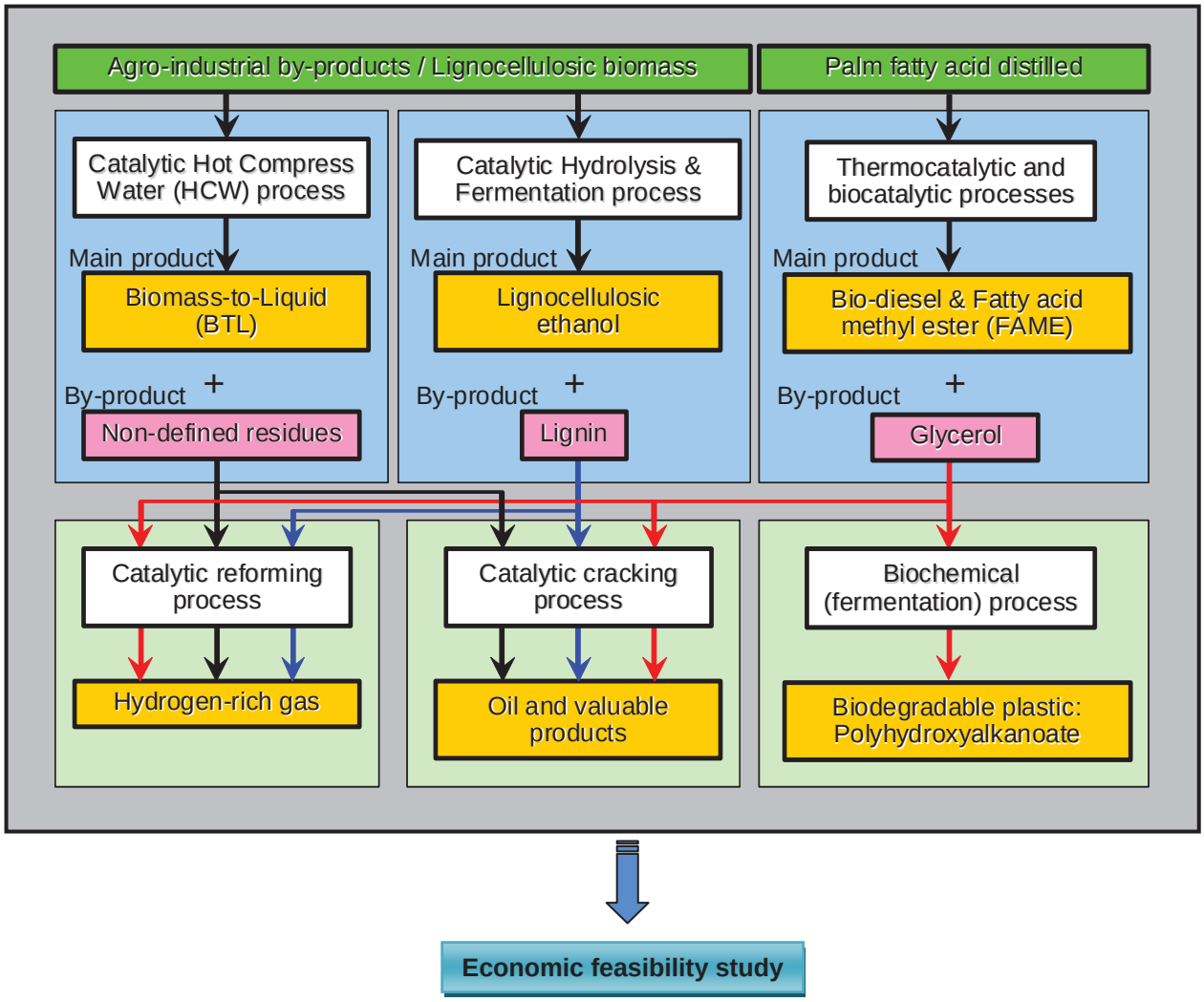

Figure 1: Overall scope of work proposed in this research proposal

In the year 2005, there was one article published in Science magazine (G.W. Huber et al. [2]) reporting the novel pathway for converting C_6 sugar to C_9, C_{12} and C_{15} alkanes (details are given in literature review section). Their reaction pathways involve dehydration, hydrogenation and aldol condensation reactions. We previously developed the process related to these reaction pathways, but instead of C_6 sugar, biomass (e.g. bagasse) was applied as our raw material. As the typical compositions of biomass are cellulose, hemicellulose and lignin, in order to convert biomass to alkane, one more reaction i.e. hydrolysis is required to convert cellulose and hemicellulose in biomass to C_6 and C_5 sugars, respectively. Another difference between the work by G.W. Huber et al. and our work is the hydrogen source for hydrogenation reaction. Instead of using high-consumed energy "aqueous phase reforming" to produce hydrogen from sugar, we found that at relevant condition lignin in biomass can be converted to phenol and eventually cracked to H_2 in the presence of a suitable catalyst (i.e. high content Ni-based catalysts). Figure 2 shows the comparison between G.W. Huber et al. and our reaction pathway.

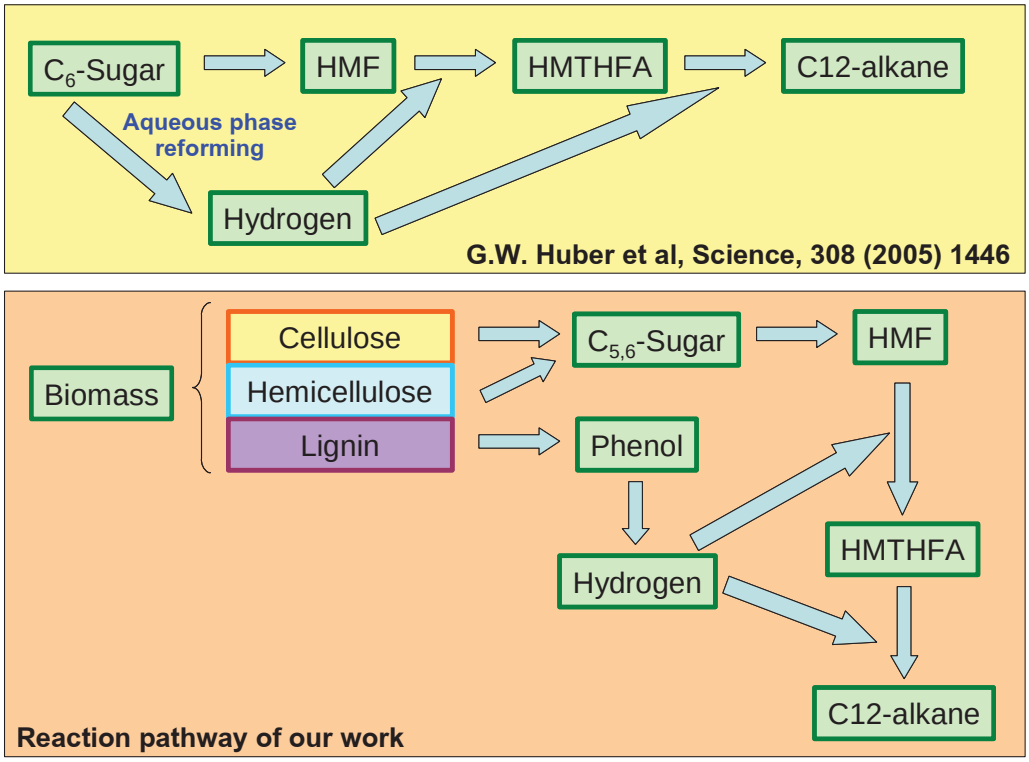

Figure 2: Comparison of reaction pathway in G.W. Huber et al. and our work

Another novelty of our previous work is that we combined all reactions (i.e. hydrolysis, dehydration, hydrogenation and aldol condensation reactions) in a single reactor unit; the type of reactor we selected is hot compressed water (HCW) reactor. Hot compressed water is one of the potent methods for biomass decomposition and conversion, which is operated in the presence of a catalyst and at different reaction temperatures between 200-350˚C. Details of HCW operation is also given in literature review section. The great benefit for the use of single reactor unit is its user-friendly and easy operation. As the major difficulty for biomass utilization is its low density and high distribution, consequently the cost for biomass transportation is high and thus it may not be suitable for large-scale plant. The decentralized biomass conversion would be a good option to overcome the above problem, and the user-friendly system with simple operation is required. It should be noted that the main difficulty of using HCW reactor to convert biomass to oil in a single unit is the selection of catalyst. For all relevant reactions (i.e. hydrolysis, dehydration, hydrogenation and aldol condensation reactions), the catalyst plays an important role on the reactivity and each reaction required different types of catalyst. For instance, hydrolysis reaction always requires acid catalysts e.g. H_2SO_4 or solid TiO_2-based catalysts, whereas the dehydration reaction favors base catalysts e.g. NaOH or ZrO_2-based catalysts. The cracking of phenol to hydrogen and the hydrogenation of HMF to HMTHFA require metallic-based catalysts i.e. Ni and Pd based catalysts, respectively. Therefore, the use of catalyst that has the good reactivity for all reactions is necessary for the single unit system. According to our preliminary testing, we found that bimetallic (Pd-Ni) catalysts over mixed oxide support (TiO_2-ZrO_2) have reactivity for converting biomass to liquid alkane under hot compressed water condition. Nevertheless, its reactivity remains relatively low and requires further development.

According to the research theme on lignocellulosic ethanol production, there are 2 main reactions involved i.e. hydrolysis of biomass to C_5 and C_6 sugars and fermentation of these sugars to ethanol. For the hydrolysis reaction, currently, the technology is based on the acid hydrolysis (using sulfuric acid). Nevertheless, environmental concern is the barrier of this process. The use of enzymatic technology can solve the above problem but the high cost of enzymes and the requirement for prior physical or chemical pretreatment of biomass limits the use of this process in commercial scale. As another novel process, hot compressed water (HCW) technology has been proposed to have good capability to hydrolyze cellulose and hemicellulose in biomass to C_6 and C_5 sugars, respectively. It should be noted that the key barrier of HCW technology is the occurring of side reaction i.e. dehydration simultaneously with hydrolysis reaction, which further converts sugar to furfural components (e.g. furfural and hydroxyl-methyl-furfural; HMF). According to our preliminary study, we found that in the presence of suitable catalyst (e.g. solid super-acid catalyst) under HCW condition, our catalyst can promote the hydrolysis reaction simultaneously with inhibit the dehydration reaction. We therefore would like to study and develop more on this catalyst as well as to determine the suitable conditions. The successful development of this catalyst and reaction condition will help promote the use of this technology for lignocellulosic ethanol production. As for the fermentation part, ethanol fermentation is a biological process in which organic materials, mainly sugars, are converted by microorganisms to ethanol. The most commonly used microbe is *Saccharomyces cereviciae*, which is the preferred one for most ethanol fermentation, while research and develoment on alternative ethanologenic microorganisms has been an important issue. *Candida tropicalis* has been a promising candidate for ethanol fermentation from lignocellulosic biomass as it can use xylose for fermentation and tolerates to polyphenolic compounds in biomass hydrolyzate. Here, we aim to develop fermentation process using this potent yeast, preliminarily in small-scale and further up-scaling to bioreactor system to optimize conditions for improving ethanol yield.

Regarding biodiesel production process, currently, palm oil is the main raw material since it constitutes a renewable and sustainable source of energy. Importantly, palm oil always contains high amount of free fatty acid (FFA) and the presence of too high FFA easily results in high amounts of soap produced simultaneously with the transesterification reaction. To avoid this reaction, most of FFA in palm oil must be firstly processed or removed (as called palm fatty acid distilled or PFAD). Recently, several works in the literature have reported the possible conversion of this PFAD to fatty acid methyl ester (FAME) via esterification as a good procedure to reduce the cost for biodiesel production and consequently to make biodiesel enable to compete economically with conventional petroleum diesel fuels. The typical catalyst for this reaction is sulfuric acid, nevertheless, the main problem of using this liquid acid catalyst is the requirements of separation process as well as the good waste management system. Recently, some literatures have proposed the use of solid super acid catalyst e.g. sulfate zirconia (SO_4-ZrO_2) for this reaction. The great benefit of the solid catalyst is the easy separation from the product solution, but the current problem of typical solid catalyst is its relatively low reactivity compared to liquid sulfuric acid and also its easily loss of reactivity for long-term operation. Therefore, the development of soild super acid catalyst that provides high reactivity with long term stability is an important step to improve the reaction performance. In our previous work, we prepared sulfate zirconia with a novel technique that can provide the material with high dispersion percentage of sulfate over zirconia surface. According to our testing, the reactivity of our developed catalyst is 4 times higher than that of the commercial sulfate zirconia and closed to that of liquid phase

sulfuric acid catalyst. Nevertheless, our testing performed in the small-scale batch system. Therefore, as proposed in this research proposal, further testing on the semibatch and continuous systems as well as the development of larger scale system should be performed.

In addition, as another approach for biodiesel production, the biocatalytic process using solid lipase-catalyst. Although the chemocatalytic transesterification and esterification reactions are the main processes for biodiesel production nowadays, these processes also has several drawbacks, including being energy intensive, difficulty in recovering glycerol, the need for removal of catalyst from the products, and requirement for waste water treatment. In addition, without the good control, free fatty acids present in the oil interfere with the reaction, especially for alkali-catalyst case, leading to undesirable side products from saponification. Recently, several research works have moved to the less energy intensive and environmental friendly biodiesel production process by applying enzyme as a catalyst. The biocatalytic approaches allow mild reaction conditions with no chemical waste and overcome many problems facing the conventional chemical methods without compromising their advantages. Importantly, glycerol can be easily recovered without any complex process. Free fatty acids contained in the oils can be completely converted to methyl esters and subsequent wastewater treatment is not required. Therefore, we propose to develop the lipase-catalytic process for biodiesel production in small scale and explore different forms of biocatalysts including commercial immobilized lipase from *C. antarctica* (Novozym435®, Bagsvared, Denmark) and the recently introduced CLEA-lipase (prepared based on Shah et al, 2006) in comparison to free lipase for biodiesel synthesis using palm oil, its composite free fatty acids (FFA) and acid oil model (TAG/FFA mixes). Reactions parameters will be optimized for kinetic study of the process for further up-scaling of the system.

As for our last research theme, the development of technologies for converting several by-products from above processes to energy and/or valuable products are proposed as follows:

(1) *Hydrogen production for utilization in Solid Oxide Fuel Cells*: hydrogen is the major fuel for fuel cell; it can be produced efficiently from catalytic steam reforming of several conventional hydrocarbon fuels such as methane, natural gas, liquefied petroleum gas (LPG), gasoline and other oil derivatives. Nevertheless, due to the current oil crisis and the shortage of fossil fuels, the development of the hydrogen production process from biomass-based fuels and/or from wastes attracts much attention. According to our proposed of studies, we aims to convert by-products from the above reactions i.e. glycerol, waste PFAD left from the reaction, lignin and undefined residues from the HCW of biomass to hydrogen for later utilization in fuel cell. This by-product utilization will provide the great benefit in terms of energy, environmental, and economical aspects to the overall production unit.

According to our previous studies, we successfully developed the hydrogen production unit (as called reformer) that can reform several hydrocarbon feedstock i.e. methane, natural gas, biogas, bioethanol, methanol, and LPG to hydrogen with high efficiency comparable to several works in the literature. Here, we propose the further development of hydrogen production unit that can reform all types of hydrocarbon feedstock to hydrogen in a single unit as called “flexible fuel reformer”. Details of our development are explained in literature review section.

(2) *Production of oil and valuable products*: apart from the conversions of by-products to hydrogen, recently, there are some reports indicate the possible conversion of these components e.g. fatty acids, glycerol to valuable products e.g. liquid alkane via catalytic cracking reaction. As for this kind of reaction, catalyst and operation condition play an important role on the degree of conversion and product selectivity. Thus, we here propose the investigation of the suitable type of catalyst and reaction that can efficiently convert by-products from the main reaction to valuable products.

(3) *Bioplastic production*: glycerol-rich stream generated in large amounts by the biofuel industry, especially from the production of biodiesel, presents an excellent staring material for co-production of value-added products. Once considered a valuable "co-product", crude glycerol is rapidly becoming a "waste product" with a disposal cost attributed to it. The development of processes to convert crude glycerol into higher value product is the way to establish biorefinery process which can be readily integrated to the existing biodiesel industry for improved process economics. Biological conversion could help circumvent the disadvantages of chemical catalysis (***e.g.*** low product specificity, use of high pressure and/or temperatures, inability to use crude glycerol with high levels of contaminants, *etc*), while offering the opportunity to synthesize a large array of products and functionalities. The use of glycerol as a substrate for polyhydroxyalkanoates (PHAs) bioplastic production is addressed. In this proposal, we will focus on the construction of a recombinant *E. coli* containing the *pha* gene cluster (*pha*CAB) along with the phasin encoding gene from *Cupriavidus necator* (formerly *Ralstonia eutropha* or *Alcaligenes eutrophus* (from TISTR)), which was shown to produce poly(3-hydroxybutyrate-co-3-hydroxyvalerate) using glucose as the carbon source (from previous project granted from NRCT). The *pha* gene cluster will be isolated based on the sequences of the corresponding gene cluster in *Ralstonia eutropha* reference strain H16 in the GenBank (NC_008313) and cloned into an expression vector under the control of a strong external promoter. The recombinant *E. coli* will be used for preliminary study on bioplastic production from (1) pure glycerol, (2) crude glycerol model, containing glycerol, free fatty acid and FAME and (3) crude glycerol stream from biodiesel industry under aerobic and microaerobic systems. After achieving the preliminary results, the optimization of recombinant cell cultivation in bioreactor system will be carried out for further up-scaling of the process.

Objectives of the project

- To develop the scientific knowledge for the production of clean alternative fuels from local feedstock
- To achieve the technology for sustainable "zero-waste" process for clean alternative fuel productions
- To improve the national security for energy/fuel reservation
- To reduce the social, environmental and economic impacts from the high import and utilization rates of conventional fuels
- To develop highly qualified Thai researchers in the field of "energy and fuel"
- To publish research outputs in well-recognized international journals
- To promote and strengthen research collaborations with researchers both in Thailand and other countries as well as the partnership in the industries

Scope of the works

This research project is focused on the development of clean alternative and renewable fuels i.e. BTL, bioethanol and biodiesel from local feedstock e.g. lignocellulosic biomass, ago-industrial by-products and waste palm fatty acid distilled by applying some new concepts of reactors e.g. catalytic hot compressed water reactor and biocatalytic transesterification reactor. Various types of chemical reactions (e.g. hydrolysis, dehydration, hydrogenation, thermocatalytic and biocatalytic esterification, reforming) and reactors under several types of operation are considered aiming to improve the performance of alternative fuel production. Furthermore, the by-product utilization will also be integrated with the main reaction unit to improve the overall system performance as "zero-waste" process. In summary, this research work is divided in 4 main themes:

1st research theme:
Production of BTL via single unit catalytic hot compressed water reactor

As described, we previously developed the process and catalyst that enable to combine hydrolysis, dehydration, hydrogenation and aldol condensation reactions in single unit hot compressed water (HCW) reactor. We preliminarily found that bimetallic (Pd-Ni) catalyst over mixed oxide support (TiO_2-ZrO_2) have reactivity for converting biomass to liquid alkane under hot compressed water condition. Nevertheless, its reactivity remains relatively low (around 4.6%) and requires further development. Therefore, the main scope of work for this research theme is to:

- Investigate the most suitable catalyst for converting biomass to alkane in single step under hot compressed water condition
- Optimize the suitable conditions of hot compressed water reactor e.g. temperature, pressure, water concentration, ratio of catalyst to biomass that enable to convert biomass to alkane efficiently
- Determine the overall reaction pathway for BTL production from biomass via single unit catalytic hot compressed water reactor
- Study the production of alkane from various types of biomass to determine the most suitable type of biomass for converting to BTL (in terms of conversion percentage, product selectivity, and energy requirement)

2nd research theme:
Production of lignocellulosic ethanol via catalytic hydrolysis & fermentation reactions

As for lignocellulosic ethanol production, it involves with 2 main reactions i.e. hydrolysis of biomass to sugars and fermentation of sugars to ethanol. For the hydrolysis reaction, currently, the technology is based on the acid hydrolysis (using sulfuric acid). Nevertheless, environmental concern is the main barrier of this process. The use of enzymatic technology can solve the above problem but the relatively high cost of enzymes and the requirement for prior physical or chemical pretreatment of biomass limits the use of this process in commercial scale.

We therefore proposes the process of hot compressed water (HCW) to hydrolyze cellulose and hemicellulose in biomass to C_6 and C_5 sugars, respectively. As mentioned, the key barrier of HCW technology is the side reaction i.e. dehydration, which further converts sugar to furfural components (e.g. furfural and hydroxyl-methyl-furfural; HMF). According to our preliminary study, we found that the in the presence of suitable catalyst (e.g. solid super-acid catalyst) under HCW condition, the catalyst can promote the hydrolysis reaction simultaneously with the inhibition of the dehydration reaction. As for the fermentation part, lignocellulosic biomass hydrolysate will be used for ethanol fermentation using *C. tropicalis* BCC7755. The preliminary optimization for media, biomass loading, temperature, and pH will be based on small-scale cultures. The work will then focus on scaling up the fermentation process in bioreactor and optimizing glucose and xylose assimilation using a potentio-stat system for improving ethanol yield. Therefore, the main scope of work for this research theme can be summarized as:

- Further develop the catalyst for hydrolyzing biomass to C_6 and C_5 sugars under hot compressed water condition with less affect of dehydration reaction
- Optimize the suitable conditions of hot compressed water reactor e.g. temperature, pressure, water concentration, ratio of catalyst to biomass that maximize the yield of sugar production for later fermentation process
- Study of fermentation conditions to maximize the yield of lignocellulosic ethanol production

3rd research theme:

Production of biodiesel from waste palm fatty acid distilled (PFAD)

1. Thermocatalytic process

As presented, palm oil always contain high amount of free fatty acid (FFA) and the presence of too high FFA easily results in high amounts of soap produced simultaneously with the transesterification reaction. Therefore, to avoid this reaction, most of FFA in palm oil must be firstly processed or removed (as called palm fatty acid distilled or PFAD). Recently, several works in the literature have reported the possible conversion of this PFAD to fatty acid methyl ester (FAME) via esterification as an alternative way to increase the FAME yield which thus reducing the cost for biodiesel production and consequently make biodiesel enable to compete economically with conventional petroleum diesel fuels. According to our previous work, we prepared sulfate zirconia (SO_4-ZrO_2) with a novel technique that can provide the material with high dispersion percentage of sulfate over zirconia surface and the esterification reactivity of our developed catalyst is 4 times higher than that of the commercial sulfate zirconia. The scope of work for this research theme is to:

- Modify and characterize SO_4-ZrO_2 to have better esterification reactivity with high stability toward long-term testing
- Test the esterification reaction of several fatty acids e.g. palmitic acid ($CH_3(CH_2)_{14}COOH$), oleic acid ($C_{18}H_{34}O_2$; $CH_3(CH_2)_7CH{=}CH(CH_2)_7COOH$) and linoleic acid ($C_{18}H_{32}O_2$; $CH_3(CH_2)_4CH{=}CHCH_2CH{=}CH(CH_2)_7CO_2H$) over developed catalysts and compared to the commercial and typical catalysts
- Optimize the suitable conditions for esterification reaction e.g. temperature, alcohol concentration, ratio of catalyst to PFAD that maximize the yield of FAME production

- Determine the kinetics and reaction pathway for the esterification reaction over solid super acid catalyst
- Develop the semibatch and continuous operation for esterification reaction and scale-up the system

2. Biocatalytic process

The study in this theme consists of two parts. The first one is the exploration and establishment of the lipase-catalytic process for biodiesel production in small scale. This work includes the exploration of different forms of biocatalysts including commercial immobilized lipase from *C. antarctica* (Novozym 435®, Bagsvared, Denmark) and a recently introduced CLEA-lipase (prepared based on Shah et al, 2006) in comparison to free lipase for biodiesel synthesis using palm oil, its composite free fatty acids (FFA) and acid oil model (TAG/FFA mixes) with different alcohols (methanol and ethanol). Reaction parameters including reactant molar ratio, enzyme loading, temperature and time will be optimized. The effect of solvent *e.g.* the recently introduced *tert*-butanol on reaction rate and enzyme reusability will be studied in comparison to the solvent-free system. The second part includes the study on the reaction kinetics in a laboratory-scale reactor as a prototype for further up-scaling based the data from the first part.

4th research theme:

Utilization of by-products from the main processes

Along with the above biofuel productions, several by-products are also generated from the reactions e.g. glycerol, lignin, and undefined residues. The scope of work for this research theme is to study the processes for utilizing or converting of these by-products to energy and/or value-added products (with an aim to develop the sustainable "zero-waste" process). There are 3 main approaches for these by-product utilizations i.e. hydrogen production, oil and valuable product generation, and bioplastic synthesis. Details of these works are presented below:

1. *Hydrogen production for utilization in Solid Oxide Fuel Cells*

According to our previous studies, we successfully developed the hydrogen production unit (as called reformer) that can reform several hydrocarbon feedstock i.e. methane, natural gas, biogas, bioethanol, methanol, and LPG to hydrogen with high efficiency comparable to several works in the literature. Here, we aim to further develop the hydrogen production unit fueled by the by-products from main reactions, which are glycerol, waste PFAD left from reaction, lignin and undefined residues from the HCW of biomass. Details of this work are presented below:

- Select and synthesize suitable reforming catalysts for each raw material
- Test and optimize the reforming conditions that can maximize the yield of hydrogen production from each raw material
- Determine the kinetics and reaction pathway for the above reforming reactions over selected reforming catalysts
- Design and construct novel hydrogen production unit that can reform all types of hydrocarbon to hydrogen in a single unit as called "flexible fuel reformer"

- Apply mathematical modeling to indicate the suitable sizing and all dimensions of this "reformer" and to predict the behavior and performance of this reformer
- Real testing of the "flexible fuel reformer" to determine the yield of hydrogen production from various feedstock

2. *Production of oil and valuable products:*

As described, some reports indicated the possible conversions of glycerol and lignin to valuable products e.g. liquid alkane via catalytic cracking reaction. As for this kind of reaction, catalyst and operation condition play an important role on the degree of conversion and product selectivity. Details of this work are presented below:

- Investigation of the suitable type of catalyst and reactions that can efficiently convert glycerol and lignin to valuable products
- Development and testing of catalysts for the above reactions
- Optimization of the suitable conditions for the reactions e.g. temperature, pressure, co-fed reactants, and catalyst that maximize the yield of products

3. *Bioplastic production*

Firstly, the work will focus on the construction of a recombinant *E. coli* containing the *pha* gene cluster (*pha*CAB) along with the phasin encoding gene from *Cupriviadus necator* (formerly *Ralstonia eutropha* or *Alcaligenes eutrophus* (from TISTR)), which was shown to produce poly(3-hydroxybutyrate-co-3-hydroxyvalerate) using glucose as the carbon source (from previous project granted from NRCT). The *pha* gene cluster will be isolated based on the sequences of the corresponding gene cluster in *Ralstonia eutropha* reference strain H16 in the GenBank (NC_008313) and cloned into an expression vector under the control of a strong external promoter. The recombinant *E. coli* will be used for preliminary study on PHB production using (1) pure glycerol, (2) crude glycerol model, containing glycerol, free fatty acid and FAME and (3) crude glycerol stream from biodiesel industry as the sole carbon sources under aerobic and microaerobic systems.

As the second stage, the work will include the design of recombinant *E. coli* with additional genetic improvement e.g. *pha*P and study its effect on PHB fermentation based on metabolic flux analysis to further enhance the production efficiency of PHB. The last phase will focus on optimization of the recombinant cell cultivation in bioreactor system to obtaining important data for further up-scaling of the process. It should be noted that PHB will be quantitatively analysed using gas chromatography based on standard method at KMITNB. The physico-chemical properties of PHB granules will be analysed using gel permeation chromatography for polymer molecular weight and differential scanning calorimerty for thermal properties at MTEC. This section will be in collaboration with the Institute of Molecular Biology and Genetics, Mahidol University and the Faculty of Agro-industry, King Mongkut's Institute of Technology North Bangkok. Below is the list of proposed works for this research theme:

- Construction of a recombinant *E. coli* containing the *pha* gene cluster (*pha*CAB) along with the phasin encoding gene from *Cupriavidus necator*

- PHB production using (1) pure glycerol, (2) crude glycerol model, containing glycerol, free fatty acid and FAME and (3) crude glycerol stream from biodiesel industry as the sole carbon sources under aerobic and microaerobic systems
- Design of recombinant *E. coli* with additional genetic modificationand study the effect on PHB fermentation based on metabolic flux analysis to further enhance the production efficiency of PHB
- Optimization of the recombinant cell cultivation in bioreactor system to obtaining important data for further up-scaling of the process

Chapter 2

Literature review

2.1 Current status of Thailand's energy and environment

Thailand, along with several countries around the world, has been facing several energy and environmental crisis e.g. security for energy reservation, efficiency of energy utilization, social and environmental impacts and global climate change due to the high energy consumption. Below are some details of these problems.

Security for energy reservation

Thailand is now facing high risk for long term security of energy reservation because half of our energy consumption has been imported with the total cost of 900,000 million baht per year (or 10% of country GDP). The value is now rising up dramatically due to the increasing of oil price in the world market. Apart from this problem, the ratio of fuel usages in Thailand is another concern as we have too much relied on the use of natural gas for power generation and the import of petroleum oil for transportation section. More than 65% of the local power generation comes from natural gas, while the proportion of import petroleum oil for transportation application is 38% of our total energy consumption. The high energy consumption is another major problem for Thailand. Figure 3 presents the rate of energy consumption from the past, present and also projecting to the future. It can be seen that the rate of oil consumption has been increasing rapidly [3].

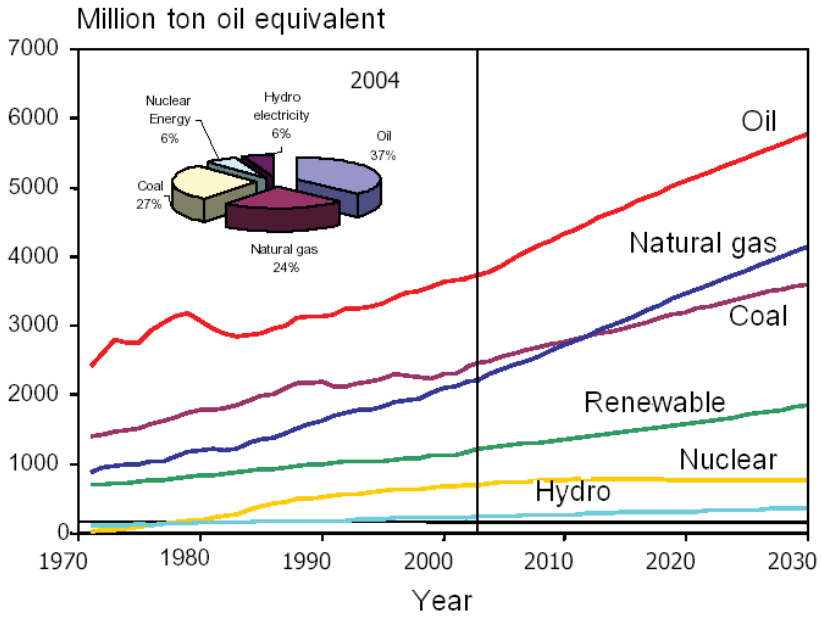

Figure 3 Rate of energy consumption from the past, present and projecting to future [3]

Efficiency of energy utilization

According to the report of World Resources Institute (2003), Thailand energy consumption was 1,405.7 kilograms of oil equivalent (kgoe) per capita, which is less than the world average (1,674.4 kgoe per capita) and still far away from that of the developed countries (4,623.1 kgoe per capita). Therefore, there still have high opportunity that the need of energy in Thailand will grow up significantly in the near future due to the improvement of our economic and life quality. By considering the energy intensity in term of energy consumption per GDP, this proportion for Thailand is now at 199.1, which is still less than that of the world average (212.9) and of the developed countries (211.8). Nevertheless, if compared that to some countries, which have been attempting to improve the efficiency of energy utilization, e.g. Japan (154.0), Germany (163.9) and France (170.5), the efficiency of energy utilization in Thailand in terms of the conversion of fuel to energy and energy utilize at end use can still be improved considerably.

Social and environmental impacts

More than 80% of energy produced in Thailand comes from the combustion of fossil fuels, which typically generates some emissions as by-product and consequently results in the social and environmental problems. Figure 4 below indicates that the rate of CO_2 emission has been increasing rapidly with the rate nearly in the same trend as that of oil use. According to the report of Intergovernmental Panel for Climate Change (IPCC), Thailand has signed Kyoto Protocol and has the commitment to reduce the level of green house gas releasing. Currently, although this value for Thailand is still below the world average, it is rising up due to the growing of our fossil fuel consumption rate. Once, this value reaches or higher than that of the world average, Thailand could possibly face the non-tariff trade barrier.

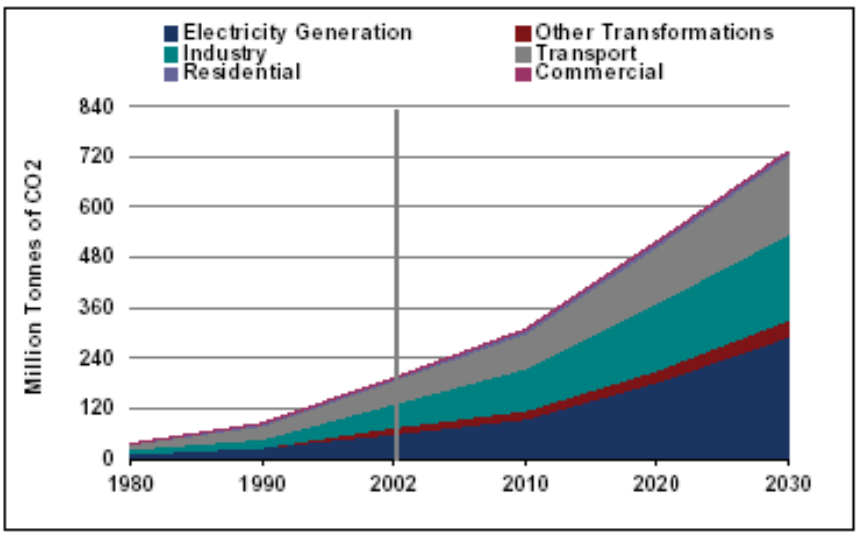

Figure 4 Rate of CO_2 emission from the past, present and projecting to future [4]

2.2 Literature review on BTL production from lignocellulosic biomass

Lignocellulosic biomass has been considered as a potent renewable resource for agricultural countries like Thailand. Some important types of biomass that generally

applied for energy production aspect are rice husk, rice straw, corncob, coconut shell, palm shell, cassava pulp and sugarcane bagasse. With advances in chemical engineering and biotechnology, several novel processes have been established for effective energy production processes from biomass. For instance, these materials can be used as fuel to vaporize water to steam and later be used for electrical generation. As another aspect, biomass can also be used to synthesize liquid and/or gaseous fuels via thermochemical and biochemical conversion processes. The important liquid and gaseous fuels produced from biomass are biodiesel (mainly RME and FAME), alcohols (ethanol/methanol), biogas, synthetic fuel (BTL - biomass to liquid) and hydrogen, as shown in Figure 5 below.

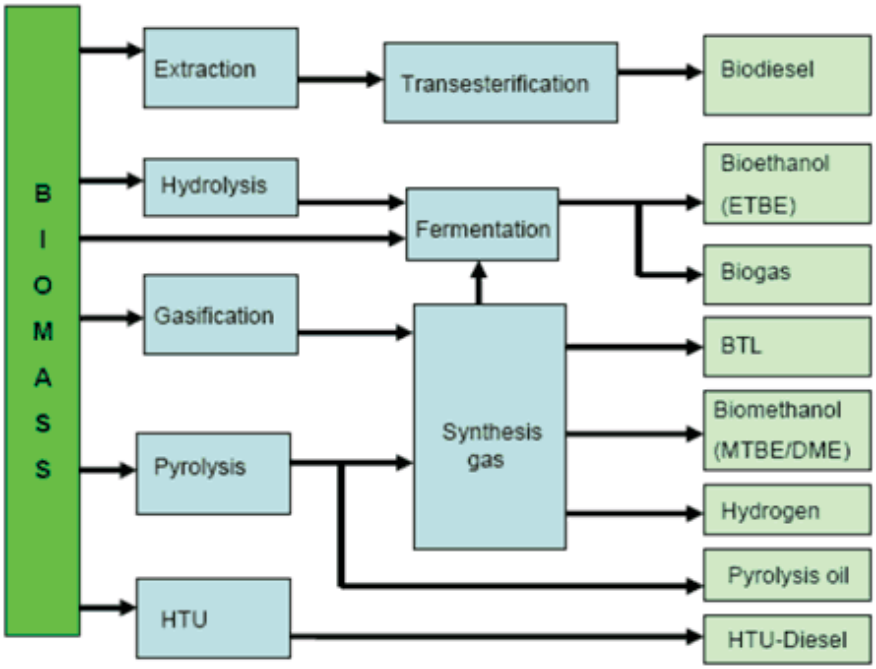

Figure 5 Biofuel conversion routes

Among them, Biomass-to-Liquid (BTL) is one of the premising alternative fuel technologies. The great advantage of BTL is its excellent quality, which is not subject to any limitations of use in either today's engine or foreseeable next-generation engines, and cleaner than the conventional oil. In addition, as it is produced from renewable biomass resource, BTL provides high potential to reduce CO_2 emissions (by over 90%) with great potential for securing supply, mitigating climate change and providing added value in rural areas. As described, currently, there are 2 main procedures to produce BTL i.e. Gasification/Fischer-Tropsch (FT) and fast pyrolysis processes. According to the first process, gasification/Fischer-Tropsch (FT), biomass is firstly converted to synthesis gas via gasification reaction, then secondary reformed to liquid C_9-C_{15} alkanes via catalytic Fischer-Tropsch (FT) process. The great advantage of gasification/Fischer-Tropsch (FT) process is the achievement of high product selectivity, nevertheless, the major barrier is its economic feasible. It has widely been reported that this process is economically feasible only at large scale production. In contrast, for the fast pyrolysis process, it is the cheaper process and feasible for the small scale production unit, but the weakness of this

process is its low product selectivity, as various types of by-products are also generated during the process. Consequently, the expensive distillation or extraction system is required. In the year 2005, there is one article published in Science magazine (G.W. Huber *et al* [2]) reporting the novel pathway for converting of C_6 sugar to C_9, C_{12} and C_{15} alkanes. Their reaction pathways involve dehydration, hydrogenation and aldol condensation reactions. We previously developed the process related to these reaction pathways, but instead of C_6 sugar, biomass (e.g. bagasse) was applied as raw material. In general, biomass composes of cellulose, hemicellulose, and lignin. The most important process in conversion of biomass to liquid fuel is the cellulose conversion. It involves the conversion of cellulose into intermediates e.g. sugars, furfural, 5-hydroxymethylfurfural (HMF) and others by acid hydrolysis and dehydration reactions. These intermediates are then further converted via thermochemical or chemical processes into the final biofuels.

Keikhosro et *al. (2006)* [5] studied conversion of rice straw to sugars by dilute-acid hydrolysis. Dilute-acid hydrolysis to produce sugars from rice straw at high temperature and pressure was investigated in one and two stages. Optimization of the first-stage hydrolysis with dilute sulfuric acid to depolymerize xylan to xylose achieved the highest yield of 80.8% at hydrolysis pressure of 15 bar, 10 min, and 0.5% acid. As presented in Table 2, hydrolysis pressure, acid concentration, and retention time were the function of furfural and HMF, however, the concentration of acetic acid was almost constant at pressure higher than 10 bar and a total retention time of 10 min.

Table 2 The yields of the hydrolysis products in two-stage hydrolysis with addition of 0.5% sulfuric acid prior to each of the two stages [5]

First stage pressure (bar)	Second stage pressure (bar)	Retention time (min)	Yield of glucose	Yield of xylose	Yield of acetic acid	Yield of HMF	Yield of furfural
10	25	10	117.7(142.6)	4.7(137)	2.4(14.9)	9.2(14.9)	0.3(1.0)
10	30	10	87.2(112.1)	3.8(136.1)	3.7(16.2)	10.8(12.9)	0.8(1.5)
15	30	10	67.5(95.2)	4.3(193.3)	0.7(20.7)	11.7(15.8)	0.9(2.6)
20	30	10	82.8(131.6)	3.4(92.1)	2.9(23.7)	11.8(18.7)	0.3(13.5)
20	35	10	38.7(78.9)	0(80.6)	2.4(23.9)	12.7(19.9)	0.7(13.7)
15	25	3	128.2(157.1)	5.8(193.8)	1.3(26.9)	3.8(8.9)	0.8(2.4)
15	30	3	164(194.3)	3(184.7)	1.3(22.9)	4.6(9.1)	0.7(2.5)
15	35	3	132(160.6)	0(184.6)	2.7(25.6)	7.3(12.2)	0.8(2.5)

Biomass conversion via hot compressed water process

Hot-compressed water (HCW) is one of the potent methods for biomass decomposition and conversion [6]. This process is environmental friendly as it decreases the emission of air pollutants (PM, NO_x, and SO_x). HCW is operated in the presence of a catalyst and at different reaction temperatures from 200-350˚C. The important parameters on HCW process are temperature, retention time and pressure, which must be optimized to enhance the high production efficiency, particularly when different types of lignocellulosic biomass are applied due to the difference in their chemical structure and composition. In general, cellulose starts decompose to glucose when the temperature of HCW is higher than 230˚C, while hemicellulose decomposes when the temperature of HCW reaches 180˚C and lignin is extracted by HCW at relatively low temperature. Generally, the rate of glucose production increases according to HCW temperature. Besides glucose, products from dehydration reaction e.g. furfural and HMF are generated in HCW process of lignocellulosic biomass, especially at high temperature and pressure in the presence of some homogeneous and/or heterogeneous catalysts e.g. H_2SO_4, NaOH,

TiO_2 and ZrO_2 [6]. Furfural is commonly used as a solvent. It is soluble in ethanol and ether and somewhat soluble in water. Furan derivatives, such as HMF and furfural, obtained from renewable biomass-derived carbohydrates have potential to be sustainable substitutes for petroleum-based building blocks used in production of fine chemicals and plastics [7]. The production of HMF and furfural from dehydration of lignocellulosic biomass constituents, including glucose, fructose and xylose using HCW is thus of great interest for research and application.

The properties of HCW related with chemical reactions and water characteristic [8-9]. A. Kruse and E. Dinjus *(2007)* [8] reviewed that the properties of HCW change with temperature and density. The properties of water below the critical point, the vapor pressure curve is separated the liquid and vapor phase below the critical point and the vapor pressure curve ends at the critical point (T_c = 373 °C, p_c = 22.1 MPa and ρ_c = 320 kg m^{-3}). The supercritical water (SCW) density beyond the critical point can be varied continuously from liquid-like to gas-like values without any phase transition over a wide range of conditions. At ambient conditions (T = 25 °C, p = 0.1 MPa), liquid water is poorly miscible with hydrocarbons and gases. The complete miscibility of supercritical water and gases as well as many organic compounds makes SCW an excellent solvent for homogeneous reactions of organic compounds with gases, like the oxidation of organic compounds with oxygen and air but SCW is a poor solvent for salts. The absence of phase boundaries leads to a rapid and complete reaction. Asghari *et al.(2006)* [10] studied acid-catalyzed production of 5-hydroxymethyl furfural from D-fructose in subcritical water by batch-type. The best yield of HMF (65%) was obtained when the optimum condition at 513 K, 120 s in the presence of phosphoric acid (H_3PO_4) pH 2 [10]. The pH of acid catalyst and the nature of the acid showed strong influence on the decomposition pathway. The scheme below shows a general type of the reaction that is an acid induced elimination of 3 mol of water from saccharides.

Bicker *et al. (2003)* [11] studied the dehydration of fructose to 5-hydroxymethylfurfural in sub- and supercritical acetone. HMF is a key substance between carbohydrate chemistry and mineral oil-based industry. However, in aqueous systems (supercritical water) achieved low selectivities. This makes the use of an acetone–water mixture even more preferable to water only as the reaction media. The dehydration of fructose was also performed in sub- and supercritical methanol and acetic acid. Watanabe *et al. (2005)* [6] then studied the effect of homogeneous catalysts (H_2SO_4 and NaOH) and heterogeneous catalysts (TiO_2 and ZrO_2) on glucose reactions were investigated in HCW at 473 K by a batch-type reactor [6]. They reported that the homogeneous acid catalyst (H_2SO_4) promoted dehydration while homogeneous base catalyst (NaOH) promoted isomerization of glucose to fructose. As for heterogeneous catalysts, anatase TiO_2 was an acid catalyst that promoted the formation of 5-hydroxymethylfuraldehyde (HMF), whereas Zirconia (ZrO_2) was a base catalyst that promoted the isomerization of glucose. Figure 6 shows the products from glucose conversion including fructose, AHG, HMF, and furfural over several catalysts. It is clear that NaOH and ZrO_2 promoted isomerization of glucose and fructose, while H_2SO_4 and anatase TiO_2 promoted dehydration and condensation reactions. They also indicated that

anatase TiO_2 acted as a base catalyst for the fructose reaction and its acidity and basidity might be the reason for the high yield of HMF from glucose (Figure 7).

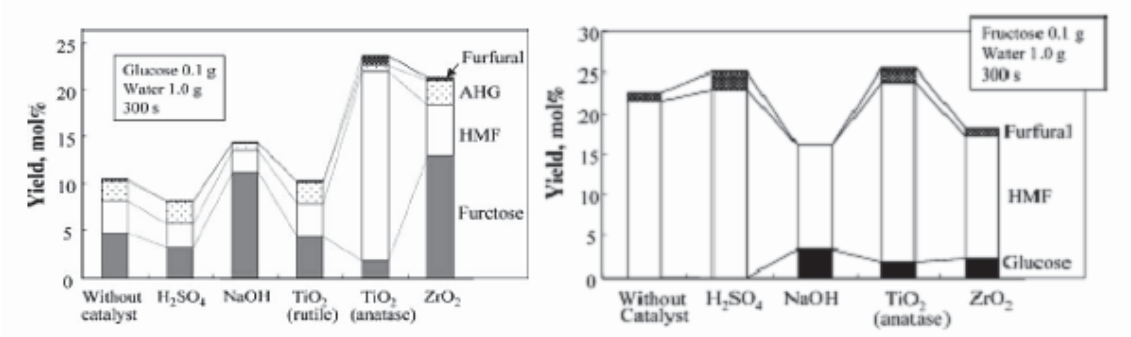

Figure 6 Effect of the additives on the yield of the liquid products (473 K, 300 s) [6]

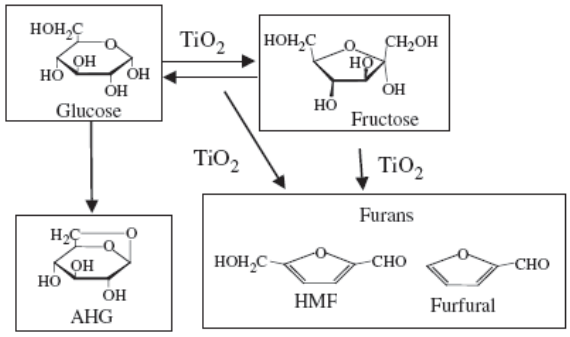

Figure 7 Effects of anatase TiO_2 on glucose primary reactions at 473 K [6]

Aida *et al. (2007)* [12] studied the dehydration of D-glucose at high temperature and pressure conditions (up to 673 K and 80 MPa) in the flow reactor. They indicated that the yield of furfural production increased with increasing temperature and pressure. They concluded that the increase of pressure from 40 to 80 MPa led to an increase in yields of 1,2,4-benzenetriol (BTO), 5-HMF and furfural, while the increase of temperature to 673 K enhanced the hydrolysis of 5-HMF to BTO, which resulted in low yield of 5-HMF in the products (below 10%). Bernard *et al.(1997* and *1999)* [13, 14] studied the decomposition of glucose and fructose to elucidate the reaction pathway and evaluate the kinetics in subcritical and supercritical water at temperature of 300-400°C and pressure of 25-40 MPa for extremely short residence times between 0.02 and 2 s. This study was proposed the kinetic constants and evaluated for glucose decomposition. They found that the main products of glucose decomposition were fructose, erythrose, glycolaldehyde, dihydroxyacetone, glyceraldehyde, 1,6-anhydroglucose, and pyruvaldehyde. The decomposition products of fructose were mainly glyceraldehyde, dihydroxyacetone, and erythrose. The reactions involved are mainly three types, namely isomerization, bond cleavage, and dehydration. The pathway of glucose decomposition isomerized to fructose while decomposed to erythrose, glycolaldehyde, dihydroxyacetone, glyceraldehyde, and 1,6-anhydroglucose. Then, fructose also decomposed to the same products except for 1,6-anhydroglucose (Figure 8). The supercritical region, the rate of glucose decomposition decreased with increasing pressure at a given temperature due to the decrease in the

epimerization rate of glucose to fructose. Nevertheless, in the subcritical region, glucose decomposition rates did not vary significantly with pressure. The pressure effect in the supercritical region proposed the possibility of controlling the selectivity for glucose when decomposing cellulosic materials.

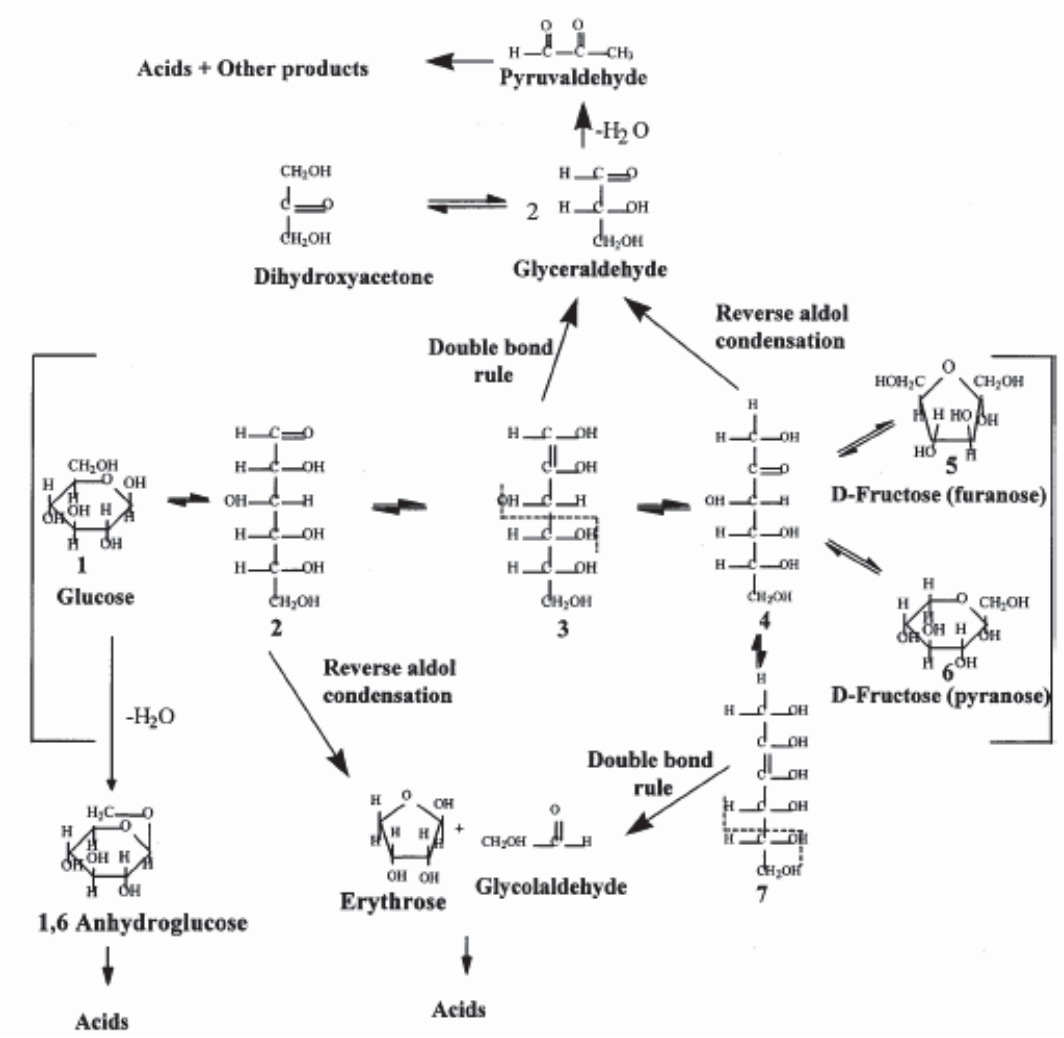

Figure 8 Mechanism of glucose decomposition in sub- and supercritical water [13]

Liquid fuel production via dehydration / aldol condensation / hydrogenation

Importantly, it was recently reported that furfural and HMF are efficiently converted to liquid alkanes. Huber *et al.(2005)* [2] studied production of liquid alkanes with the number of carbon atoms ranging from C_7 to C_{15} were selectively produced from sugar via acid-catalyzed dehydration, followed by aldol condensation over solid base catalysts to form large organic compounds (Figure 9). They reported that hydrogenated furfural-acetone (2:1) produced primarily C_{11} to C_{13} alkanes from the 4-PD/H reactor. They prepared an aqueous solution of 12.5 wt % hydrogenated furfural-acetone (1:1), and this feed produced primarily C_7 and C_8 alkanes in the 4-PD/H reactor. The results from these experiments indicate that the process for producing liquid alkanes from biomass-derived resources does not require the use of alcohol solvents, and it is not limited to dilute aqueous feeds. Crossed aldol condensation of HMF with acetone was carried out with HMF:acetone molar ratios of 1:1 and 1:10 by using a mixed Mg-Al–oxide catalyst at

room temperature. The condensed HMF:acetone feeds produced mainly C_8 to C_{15} alkanes in the 4-PD/H reactor, depending on the HMF:acetone ratio used in the aldol-condensation step. When the HMF: acetone ratio decreases, the alkane distribution shifts to lighter alkanes. The selectivity can also be shifted to heavier alkanes by increasing the extent of conversion for the aldol condensation step of HMF: acetone.

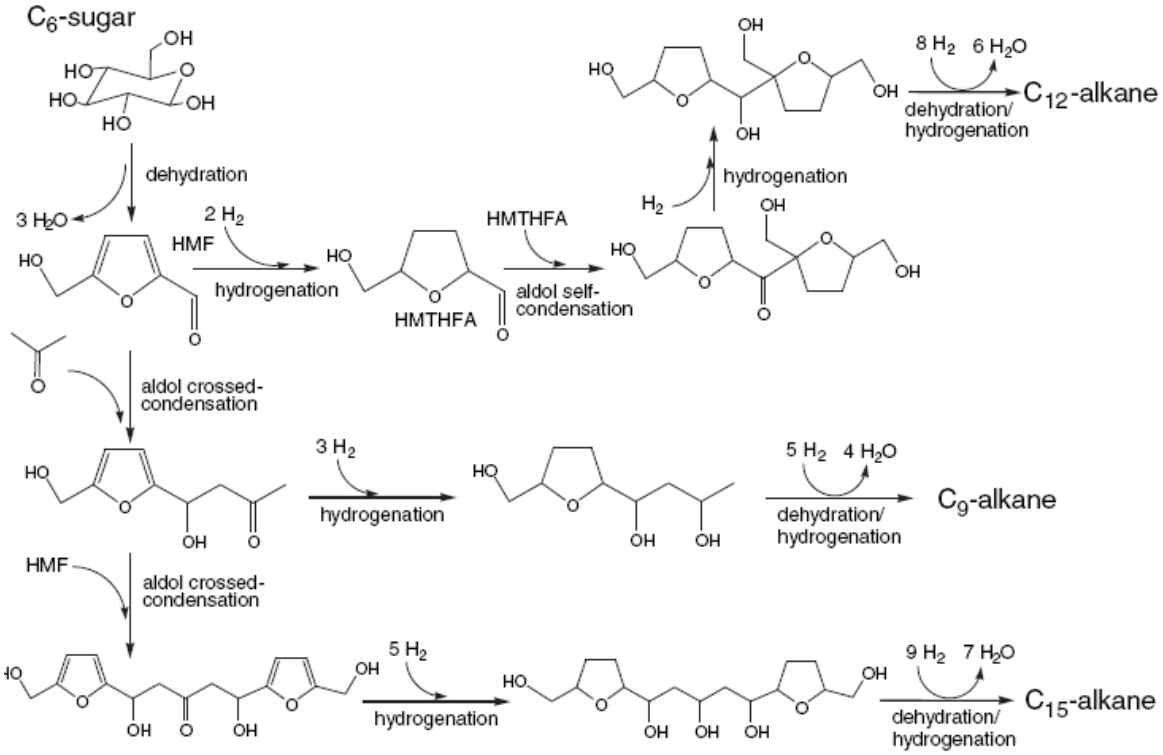

Figure 9 Reaction pathways for conversion of glucose to liquid alkanes [2]

2.3 Literature review on lignocellulosic ethanol production from biomass

Lignocellulose is a complex substrate, consisting of a mixture of carbohydrate polymers (cellulose and hemicellulose) and lignin. The carbohydrate polymers are tightly bound to lignin, mainly by hydrogen bonds but also by some covalent bonds. The biological process to convert lignocellulose to bioethanol requires: delignification to liberate cellulose and hemicellulose from their complex with lignin, depolymerisation of the carbohydrate polymers to produce sugars, and fermentation of the released glucose and pentose to produce ethanol. Among the key steps described above, the delignification of lignocellulosic biomass is the rate-limiting and most difficult step to be solved, in addition to the formation of by-products from sugars in hydrolysis process using aqueous acid. Enzymatic hydrolysis of lignocellulose is considered a desirable approach. However, the process is still relatively expensive due to the enzyme cost and the need for the pretreatment process for efficient enzyme hydrolysis. The development of an efficient hydrolysis technology for biomass is thus of great interest for research and industry. The first demonstration plant using lignocellulosic feedstocks has been in operation in Canada since April 2004. The first industrial-scale demonstration ethanolplant using sugarcane bagasse as the feedstock has been recently established in Thailand.

Ethanol fermentation is a biological process in which organic material, mainly sugars is converted by microorganisms to ethanol. Several microorganisms, including yeast, bacteria and fungi have been reported for ethanol production. The most commonly used microbe is yeast. Among the yeasts, *Saccharomyces cereviciae* is the preferred one for most ethanol fermentation which can produce ethanol as high as 18% of the fermentation broth [15]. This yeast can grow both in simple sugars, such as glucose and on disaccharide sucrose. *S. cereviciae* is also a generally recognized as safe (GRAS) microorganism. However, it cannot use pentose as a carbon source and does not tolerate to high temperature (>40^{o}C). *Zymomonas mobilis* is an unusual Gram-negative bacteria that has several appealing properties for bioethanol production. The microbe has a homoethanol fermentation pathway and tolerates up to 120 g/l ethanol. It has a higher ethanol yield and a much higher specific ethanol productivity (2.5x) than *Saccharomyces* sp. [16]. Furthermore, *Z. mobilis* is GRAS and has simple nutritional needs. Despite its advantages, *Z. mobilis* is not well suited for ethanol production from lignocellulosic biomass as it ferments only glucose, fructose and sucrose. Engineered *Escherichia coli* is another potent microorganism for ethanol production [17]. *E. coli* has several advantages as a biocatalyst for ethanol production, including the ability to ferment a wide spectrum of sugars, no requirements for complex growth factors, and prior industrial use for recombinant protein production. The major disadvantages in using *E. coli* are a narrow and neutral pH growth range, less hardy cultures compared to yeast, and public perceptions regarding the danger of pathogenic *E. coli* strains. Due to the composition of lignocellulosic biomass, recent researches have been focused on genetic engineering of microorganisms for xylose utilisation in order to convert all available fermentable sugars to ethanol for improving production yield. The recombinant *E. coli* was able to convert glucose and xylose to ethanol at high yield [18]. *Z. mobilis* was metabolically engineered to broaden the range of fermentable substrate to include xylose [19]. Engineering *S. cereviciae* for xylose fermentation is also considered an attractive approach [20].

Screening yeast strains for ethanol fermentation from xylose is another interesting approach. Among the yeasts, *Candida tropicalis* has been considered one of the most potent microorganisms for ethanol production from glucose and xylose [21] at relatively high temperature under mild acidic condition. The use of *C. tropicalis* for ethanol fermentation from a range of substrates has been investigated, in addition to its conventional utilisation in xylitol production [22]. The yeast also produces glucoamylase and ferments ethanol from starch at low rate in the absence of extra α-amylases, suggesting its potential on ethanol fermentation from starch-based substrate [23]. Together with its ability to tolerate and decompose phenols and polyphenols generated during pretreatment of lignocellulosic biomass [24], *C. tropicalis* is considered an attractive system for ethanol and chemical production from renewable plant-derived biomass. However, in respiratory yeast, metabolism of glucose and xylose is tightly regulated by dissolved oxygen concentration, reflected by the redox potential. In the presence of mixed sugars, glucose also represses xylose metabolism and is primarily assimilated until consumed below the sub-repressive levels [22]. While conversion of glucose to ethanol occurs under a wide redox potential range, the shift between ethanol and xylitol production from xylose in *C. tropicalis* is dependent on the redox balance of the cells [21]. Optimization of the process conditions *e.g.* by using potentio-stat control system to achieve the optimal redox potential would lead to more efficient xylose assimilation and, thus, improving ethanol yield. Process development on fermentation conditions, including media optimisation, oxygen concentration, and reactor design is needed for maximizing ethanol productivity.

2.4 Literature review on biodiesel production

Biodiesel is a promising alternative energy produced from renewable agricultural resources. It can be produced by several approaches, including pyrolysis in the presence of metal salts, supercritical alcohol process and by chemocatalytic as well as biocatalytic processes [25]. Currently, most of biodiesel are produced from transesterification reaction of palm oil. This reaction involves with the reaction of triglyceride in palm oil with alcohol in the presence of alkali catalyst e.g. NaOH. According to this reaction, triglyceride reacts with alcohol to produce diglyceride, which further converts to monoglyceride. Lastly, monoglycerides react with alcohol to produce esters and glycerol as by-product [26]. Typically, this reaction requires three moles of alcohol per one mole of triglyceride.

As described, palm oil always contain high amount of free fatty acid (FFA) and the presence of too high FFA easily results in high amounts of soap produced during transesterification reaction. To avoid this reaction, some literature works reported that FFA in palm oil (as called palm fatty acid distilled or PFAD) should be firstly converted to fatty acid methyl ester (FAME) via esterification reaction. Regarding this reaction, fatty acids will react with alcohol in the presence of acid catalyst e.g. H_2SO_4 and produce methyl ester. Below are some important summarizes of the literature works on FAME production via esterification and biocatalytic processes.

FAME production via esterification reaction

According to this reaction, there are several parameters that affect the reaction performance [27-31]. The reaction temperature is one of the most important factors that directly affect the reaction. At room temperature, the yield of product is relatively low. Inversely, when the temperature increases, the yield of product rapidly increases (Figure 10) but the possible loss of methanol and the cost of biodiesel production could be increased.

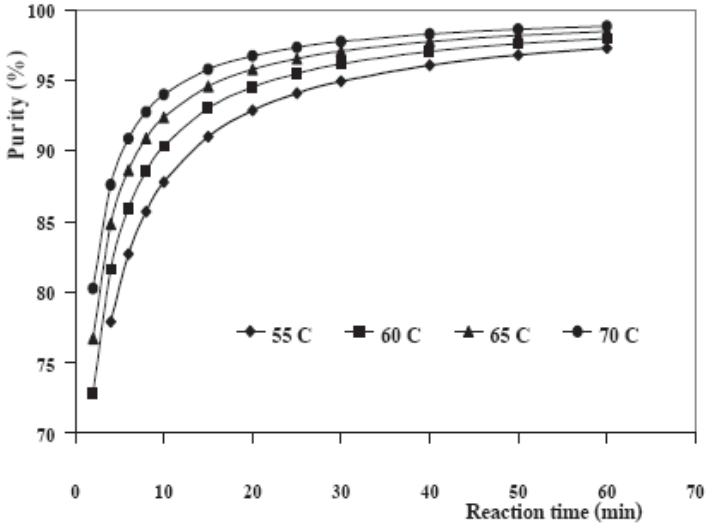

Figure 10 Effects of duration and temperature on the esterification reaction [30]

As for the effect of alcohol to feedstock molar ratio, the yield of methyl ester normally increases when the molar ratio increases. Nevertheless, after the optimum point, the use of higher alcohol ratio is not affect the yield of ester, Figure 11.

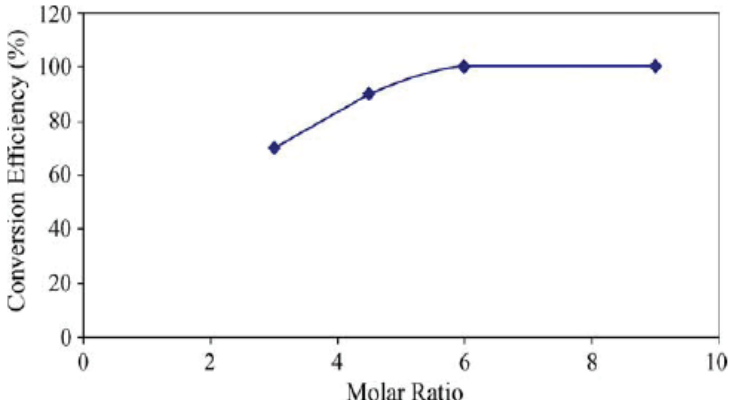

Figure 11 Effect of alcohol to feedstock molar ratio on the esterification reaction [30]

Importantly, it was reported that, the amount of catalyst strongly affects the conversion efficiency. Usually, the higher concentration of catalyst is required in order to drive the forward reaction and yield more products. However, the excess amount of catalyst also causes of the saponification reaction to produce soap and results in lower yield of alkyl esters, Figure 12.

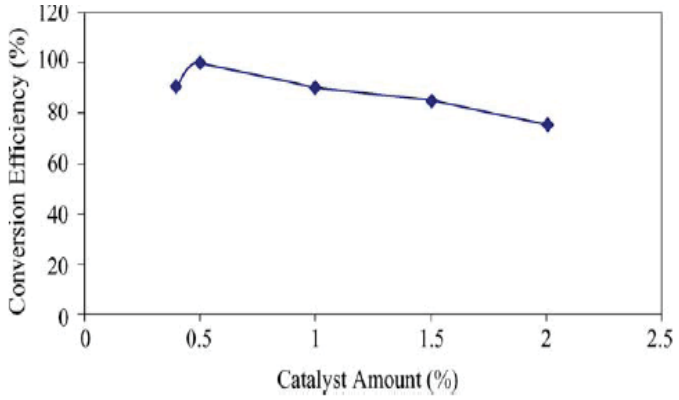

Figure 12 Effect of amount of catalyst on the esterification reaction [30]

The mixing speed is also another significant factor that affects the performance of the reaction as it strongly impacts the interfacial area by reducing diffusion-related rate limitations and mass transfer rate. It was reported that the stirring helps increasing the conversion rate and the yield of alkyl esters [32]. Nevertheless, some previous work reports that mixing speed in range of 100 to 600 round per minute (RPM) has no significant difference on the yield of methyl esters [33].

Catalysts for esterification and transesterification reactions

Theoretically, the catalyst for biodiesel production can be divided into 2 main groups i.e. acid catalyst and alkaline catalyst, which are applied for esterification and transesterification reaction, respectively.

Acid catalyst

The acid catalyst is normally used for esterification process. The most common acid catalyst is sulfuric acid (H_2SO_4). Theoretically, hydrochloric acid (HCl) and hydrogen iodide (HI) are also effective for the esterification reaction, but H_2SO_4 is the most favorite one due to it high esterification reactivity. It should be noted that the use of homogeneous catalyst cause some problems to the process e.g. corrosion, loss of catalyst since it cannot be reused and encounter the problems of handling and transportation. Therefore, development of heterogeneous catalyst is received interesting [34]. Recently, some literatures have proposed the use of solid super acid catalyst e.g. amberlyst-15, nafion NR50, sulphated zirconia (SZ), tungsta zirconia (WZ), supported phosphoric acid (SPA), titanosilicate (ETS-10H), zeolite for this reaction [35, 36]. The great benefit of the solid catalyst is the easy separation from the product solution, but the current problem of typical solid catalyst is its relatively low reactivity compared to liquid acid and also its easily loss of reactivity for long-term operation. According to the work from Lopez et al. (2005) [26], the catalytic activity of amberlyst-15, nafion NR50, sulphated zirconia (SZ), tungsta zirconia (WZ), supported phosphoric acid (SPA), titanosilicate (ETS-10H), zeolite and H_2SO_4 were compared and the results are shown in Figure 13. The sequence of reactivity is H_2SO_4 > SZ > WZ > SPA > zeolite > ETS-10H.

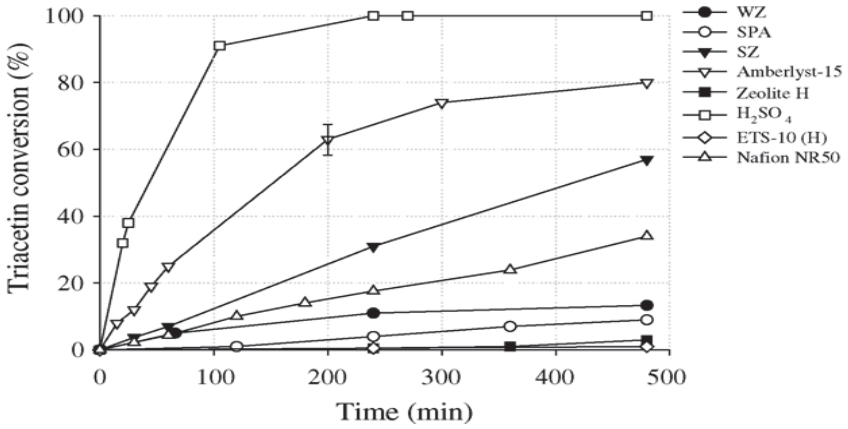

Figure 13 Esterification reactivity over several acid catalysts [26]

Alkaline catalyst

The alkaline catalyst is normally used for transesterification process. The most of common type of alkaline used are sodium hydroxide (NaOH) and potassium hydroxide (KOH), while the novel types are sodium methoxide ($NaOCH_3$) and potassium methoxide ($KOCH_3$) [37, 38]. According to Vicente et al. (2007), several types of liquid catalysts were compared (Figure 14).

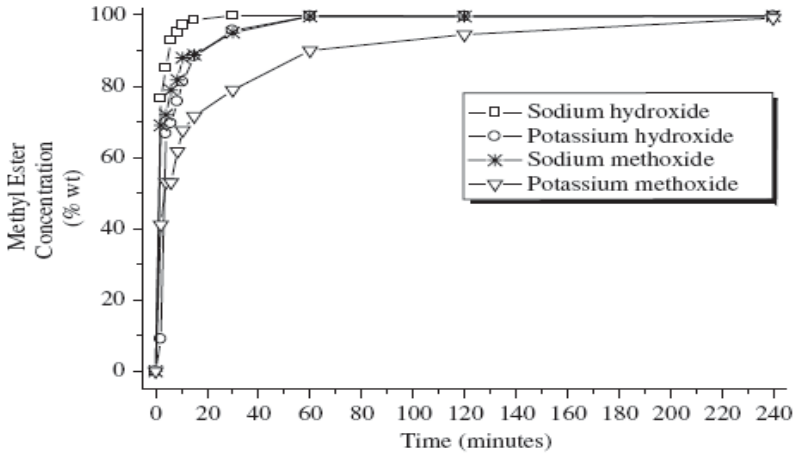

Figure 14 Methyl ester production from transesterification process over several catalysts (at 65°C, methanol:oil = 6:1, and 1% weight of catalyst) [37]

It can be seen that the uses of NaOH and KOH can provide higher reactivity than $NaOCH_3$ and $KOCH_3$ which is in good agreement with the literature by Leung et al. (2006) [28] as shown in Figure 15. Compared between NaOH and KOH, the solubility of KOH in alcohol is better than NaOH, therefore, the transesterification reaction with KOH is more efficient at the same concentration.

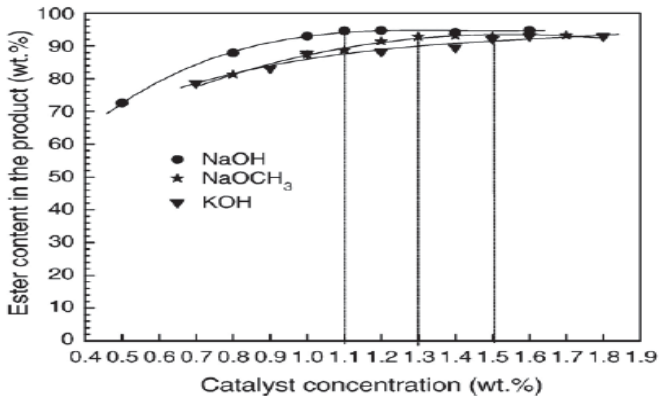

Figure 15 Methyl ester production from transesterification process over several catalysts (at 70°C, methanol:oil = 7.5:1, and 1% weight of catalyst) [28]

FAME production via biocatalytic processes

Although the chemocatalytic transesterification and esterification reactions are the main processes for biodiesel production nowadays, these processes also has several drawbacks, including being energy intensive, difficulty in recovering glycerol, the need for removal of catalyst from the products, and requirement for waste water treatment. In addition, without the good control, free fatty acids present in the oil interfere with the reaction, especially for alkali-catalyst case, leading to undesirable side products from saponification.

Recently, it has been proposed in several research works in the literature that the less energy intensive and environmental friendly biodiesel production process is using enzyme as a catalyst for transesterification. The biocatalytic approaches allow mild reaction conditions with no chemical waste and overcome many problems facing the conventional chemical methods without compromising their advantages. Importantly, glycerol can be easily recovered without any complex process. Free fatty acids contained in the oils can be completely converted to methyl esters and subsequent waste water treatment is not required.

Table 3: Comparison of different technologies to produce biodiesel [25]

Variable	Alkali catalysis	Lipase catalysis	Supercritical alcohol	Acid catalysis
Reaction temperature (^{o}C)	60-70	30-40	239-385	55-80
Free fatty acid in raw materials	Saponified products	Methyl esters	Esters	Esters
Water in raw materials	Interference with reaction	No influence		Interference with reaction
Yield of methyl esters	Normal	Higher	Good	Normal
Recovery of glycerol	Difficult	Easy		Difficult
Purification of methyl esters	Repeated washing	None		Repeated washing
Production cost of catalyst	Cheap	Relatively expensive	Medium	Cheap

Lipases are enzymes that catalyse the hydrolysis of ester bonds in triglycerides. In nonaqueous systems, lipases catalyse the reverse reaction, namely synthesis and transesterification. The use of a variety of vegetable oils, such as soybean oil [39], palm oil [40], rapeseed oil [41], rice bran oil [42], sunflower oil [43], jatropha oil [44], canola oil [45] and waste edible oil [46] as feedstocks for enzymatic production of biodiesel has been reported. An earlier attempt to model lipase-catalytsed transesterification was based on a consecutive two-step reaction consisting of hydrolysis of triglycerides followed by esterification of the released fatty acids [47, 48]. However, a kinetic model based on a single step direct alcholysis of triglycerides has been recently reported [40]. Various reaction parameters has been investigated for optimization of lipase-catalysed biodiesel synthesis, including enzyme forms and loading, acyl donors (methanol, ethanol and butanol), substrate molar ratio, temperature and added water content and reaction medium (solvent-free, organic solvents and ionic liquids). Systematic approaches *e.g.* response surface methodology (RSM) and central composite rotable design (CCRD) were used for reaction parameter optimization [45]. Lipase efficiently catalyses reactions when the substrates dissolved each other. When methanol amount exceeds its solubility limits, lipase is deactivated by the insoluble methanol that exists as drops in the oil due to its instability in short-chain alcohol. A moderate polar solvent *tert*-butanol has been recently introduced to improve stability of the enzyme in organic system by eliminating of the negative effects caused by methanol and by-product glycerol [41, 49]. The enhancement effect on conversion in ionic liquids was also recently reported [50]. A two-step lipase-catalysed reaction composed of methyl esterification of FFAs and methanolysis of TAGs was also reported for efficient FAME synthesis from acid oil [51]. The typical yield of FAME from lipase catalysed reaction after process optimization has been around 80%-nearly 100% conversion after incubation for 8-25 h under mild conditions [41] with more than 200 repeated uses of the biocatalyst.

Lipases from various microorganisms, including *Candida antarctica* [52], *Pseudomonas cepasia* [53], *Rhizomucor miehei* [54] and *Thermomyces lanuginosus* [39] in different forms have been used for biodiesel synthesis, either in soluble and immobilized forms [40, 45]. In addition, processes using whole-cell biocatalysts expressing lipase have also been reported *e.g. Rhizopus oryzae* immobilized on polyurethane [55, 56] and *Saccharomyces cereviciae* with intracellular expression of lipase from *R. oryzae* [57]. Though the use of whole-cell catalyst is simple and cost-effective, majority of the research are based on isolated enzyme, especially in immobilized form due to its stability and convenient reusability.

As an alternative approach to the conventional immobilized enzyme on solid support commercially available, several simple and cost-effective heterogeneous enzyme preparation have been reported, including cross-linked enzyme crystals (CLECs) [58] and cross-linked enzyme aggregates (CLEAs) [59]. These high-performance biocatalyst designs show improved stability, catalytic efficiency and reusability in aqueous and/or nonaqueous media. Several advantages of CLEA over CLEC have been described [60], including the unnecessary for extensive protein purification. CLEA-lipase has recently been used for FAME synthesis with a high conversion yield at 90% and reduced reaction time in 6 h compared to free lipase (77% conversion in 8 h) [61]. Although the application of lipase in the production of biodiesel from vegetable oils has been thoroughly addressed in many literatures and become more and more attractive, the industrial biodiesel production using enzymatic process has not yet been implemented. Currently almost biodiesel production in Thailand is based on alkali-catalytic reaction using sodium hydroxide. However, this process is energy intensive and sensitive to the presence of free fatty acid in the feedstocks. It is thus of great interest to establish the enzymatic biodiesel synthesis technology which can overcome the limitations of the conventional process as the option for future research and development. However, intensive research is needed in order to overcome the key limitations for future industrial application including the cost of the biocatalyst production, downstream processing and immobilization as well as enzyme inactivation and reusability. Optimisation of the reaction process parameters for feedstock of interest and exploration of available catalysts and technology are thus necessary for establishment of an efficient enzymatic biodiesel synthesis process aimed for an efficient and environmental-friendly biodiesel production in the future.

2.5 Literature review on hydrogen production technologies

Hydrogen is currently an important feedstock in various chemical and petrochemical industries and it is expected to be a potential alternative fuel to replace refined petroleum products, i.e. gasoline and diesel, in the near future. Recently, the demand of hydrogen is progressively increased since hydrogen is considered as a primary pollution-free energy source for future transportation and electricity generation as a result from the successful development in fuel cell technology. At present, about 48% of the world's hydrogen production is from the well-established steam reforming technology using methane as the major feedstock. The methane steam reforming is a widely practiced technology for production of hydrogen or synthesis gas for later utilization in fuel cells. Three main reactions are always carried out as presented in the following equations:

$CH_4 + H_2O \Leftrightarrow CO + 3H_2$ (1)
$CO + H_2O \Leftrightarrow CO_2 + H_2$ (2)
$CH_4 + 2H_2O \Leftrightarrow CO_2 + 4H_2$ (3)

Both water-gas shift reaction (Eq. 2) and reverse methanation (Eq. 3) are associated with the steam reforming over a catalyst at elevated temperatures. The reverse methanation (Eq. 3) is thermodynamically linearly dependent on methane steam reforming and water-gas shift reaction, but it is kinetically independent [62-66]. Due to the overall high endothermic nature of the reactions, they are carried out at high temperature (700-900^oC).

Apart from steam reforming, carbon dioxide (or dry) reforming reaction is another beneficial reforming processes to convert feedstock that have some content of carbon dioxide (e.g. biogas) to hydrogen. Compared to the steam reforming, both steam and dry reforming reactions have similar thermodynamic characteristics except that the carbon formation in the dry reforming is more severe than in the steam reforming due to the lower H/C ratio of this reaction [67]. The attractive feature of the dry reforming reaction is the utilisation of CO_2, which is a greenhouse effect gas. In general, the dry reforming reaction (Eq. 4) is typically accompanied by the simultaneous occurrence of the reverse water-gas shift reaction (RWGS) (Eq. 5).

$CH_4 + CO_2 \Leftrightarrow 2CO + 2H_2 \quad \Delta H = 247$ kJ/mol (4)
$CO_2 + H_2 \Leftrightarrow CO + H_2O \quad \Delta H = 41.1$ kJ/mol (5)

The hydrogen to carbon monoxide production ratio (H_2/CO ratio) from the dry reforming reaction is always less than 1. M. A. Vannice et al. [68] presented the apparent activation energies for the consumption of methane and carbon dioxide, as well as the production of carbon monoxide, hydrogen, and water in order to investigate the influence of the RWGS reaction. They observed that the apparent activation energy for hydrogen formation is greater than that for the formation of carbon monoxide, in which supported the influence of the reverse water-gas shift reaction on the reaction mechanism. Sodesawa et al. [69] studied the dry reforming reaction at a stoichiometric feed ratio over several catalysts. They found that the activities of most catalysts deactivated rapidly due to the carbon deposition. Topor et al. [70] suggested that the use of excess carbon dioxide could avoid carbon formation. Chubb et al [71, 72] studied the carbon dioxide reforming using an excess of carbon dioxide with carbon dioxide to methane ratios of 3:1 and 5:1 over Ni/Al_2O_3. They reported that the rate of disintegration is smaller for the higher one. Rostrup-Nielsen and Bak Hansen [73] investigated the activity toward dry reforming over several metals. Their order of reactivity for this reaction was Ru > Rh > Ni ~ Ir > Pt > Pd, in which similar to their proposed order for steam reforming. They also observed that the replacing of steam with carbon dioxide gave similar activation energies, which indicated a similar rate-determining step in these two reactions. In addition, low levels or no carbon formation was detected from dry reforming over Rh metal at low temperature and CO_2 content [74]. Erdohelyi et al. [75, 76] studied the influence of the catalyst support on the dry reforming of rhodium-based catalyst, and reported that the support had no effect on the activity of Rh. In contrast, Nakamura et al. [77] and Zhang et al. [78] observed that the initial turnover frequency (specific activity) of Rh crystallities was significantly affected by their supports. Zhang et al. [78] also reported that the deactivation of Rh crystallities was strongly dependent on their supports.

Recently, there is another proposed reforming process, as called autothermal reforming. This reaction is a combination of steam reforming and partial oxidation process. The former is a highly endothermic process that requires an efficient external heat supply to the system. Although the present steam reforming technology is very efficient, offering nearly 90% of the maximum thermodynamic efficiency, it is still considered as a very energy- and capital-intensive process which is particularly unattractive for a small scale and low-pressure hydrogen production. The latter process, partial oxidation, is an exothermic process, using pure oxygen or air to react either thermally or catalytically with a fuel to generate synthesis gas (the combination of hydrogen and carbon monoxide) with H_2/CO ratios from 1.6 to 1. Theoretically, the autothermal reforming can be categorized into 2 main groups, i.e. conventional autothermal reforming and catalytic autothermal reforming. In the first process, a mixture of fuel, steam and oxygen (at a substoichiometric ratio) is fed to a burner where the partial oxidation takes place, supplying the heat required for the endothermic reactions taking place in a subsequent bed of reforming catalyst where the steam reforming and water gas shift reactions take place to produce synthesis gas with H_2/CO ratios of 2 to 1. Catalytic autothermal reforming has received much attention in research over the conventional autothermal reforming nowadays as it offers advantages of smaller unit size, lower operating temperature, easier start-up, and wider choice of materials.

Fuel selection for reforming reactions

Fuel source for hydrogen/syngas production is highly flexible, varying from several gaseous hydrocarbons e.g. methane, natural gas, liquefied petroleum gas (LPG) and also liquid hydrocarbons e.g. gasoline, diesel, alcohols, naphtha, residual oil, ethylene glycol, and glycerol. Fuel selection depends strongly on its application, the availability of the feedstock, and the site location. The reforming of methane has been proposed as a suitable process to produce CO-rich synthesis gas to further utilize in Fischer–Tropsch process for GTL production as well as methanol and dimethyl ether synthesis. Liquefied petroleum gas (LPG) is an appropriate fuel for a small stand-alone system with no connection to a natural gas grid. Previously, the steam reforming of LPG has been studied by a few researchers [79-85], and most of them have investigated the reforming of LPG over noble metal catalysts (e.g. Rh, Ru, and Pt) on oxide supports. The uses of gasoline and diesel compounds, i.e. n-dodecane, tetralin, n-heptane, n-dodecane, toluene, and methylcyclohexane, glycerol and dimethyl ether (DME) for hydrogen production have also been widely investigated owing to their high hydrogen density and well-established infrastructures. DME has several advantages; it is harmless and does not cause ozone layer destruction, and it is easy to handle like LPG. Previously, hydrogen production from the reforming of DME has been studied over acid catalysts and Cu-based catalysts by several researchers; however, most of them have investigated the reforming of DME at low temperature [86-91]. Glycerol is a major byproduct from biodiesel production. The use of glycerol for hydrogen or synthesis gas productions can further improve an economic incentive for biodiesel plant.

Alcohol (e.g. methanol), ethylene glycol, and glycerol, which have recently been studied, are also interesting fuels for autothermal reforming. They are volatile carbohydrates with the formula of $C_n(H_2O)_nH_2$. Methanol is favorable due to its ready availability, high-specific energy and storage transportation convenience [92, 93], while ethanol is also a promising candidate, since it is readily produced from renewable resources (e.g., fermentation of biomasses) and has reasonably high hydrogen content

[94, 95]. Previously, the reforming of ethanol has been studied by several researchers [96-116]. Most of them reported that the major difficulty to reform ethanol is the possible degradation of the catalyst due to the carbon deposition. Therefore, most of the recent works on the reforming of ethanol have been based on the noble metal catalysts (e.g. Rh, Ru, Pt, Pd) over several oxide supports (e.g. Al_2O_3, MgO, SiO_2, TiO_2) [100, 102, 103, 105, 113, 114, 115], as these precious metals were reported to provide high resistance to the carbon formation compared to the conventional catalysts (i.e. Ni based catalyst). Nevertheless, the current prices of these metals are very high for commercial uses, and the availability of some precious metals such as ruthenium was too low to have a major impact on the total reforming catalyst market [117].

It should be noted that the reforming from several types of fuel always requires different operation conditions; e.g. catalysts, temperature, fuel/oxidant ratio and treatment process. For instance, the heavy hydrocarbons, i.e. isooctane and hexadecane can be easily decomposed by thermal cracking and have higher possibility of coke formation compared to the light hydrocarbon compounds. Gasoline and diesel, which generally contain high aromatic compounds, would, as well, have higher tendency for coke formation when compared to paraffinic fuels. Thus, these heavy hydrocarbons normally require precious metal catalysts, e.g. Rh or Pt, which have high resistance toward carbon formation. Sulfur content in feed also has a strong impact on catalyst life and performance. A sulfur removal unit and/or sulfur tolerant catalysts may be required.

Catalysts for Reforming

Recently, a number of publications have reported the studies on the development of catalyst for several reforming reactions fueled by several hydrocarbon compounds. Several precious metals, i.e. Rh, Pd, and Pt have been studied, since there is evidence that lower amount of carbon can be dissolved in precious metal particles compared to conventional Ni, coke formation is suppressed. It is well established that Rh seems to be the most active metal giving the highest activity and stability toward the reforming reaction. Nevertheless, the major drawback for using precious metals is their high prices. Thus, the attempt to minimize precious metal loading has been widely investigated. In addition, recently, several investigations have also been focusing on the development of other alternative reforming catalysts, i.e. bimetallic catalysts, ceria-based catalysts, and perovskite-based catalysts. A number of publications have reported the benefits of bimetallic catalysts in terms of stability, activity and resistance toward the poisonings compared to the conventional monometallic catalysts.

It has been reported that cerium oxide (or ceria; CeO_2) based material can also act as an important catalyst for various reactions involving oxidation of hydrocarbons. This material has been widely used as a promoter or a support in several industrial processes. It is also a key component in the formulation for noxious emissions control catalyst, wildly applied in transportation section. Ceria-based material contains a high concentration of highly mobile oxygen vacancies, which act as local sources or sinks for oxygen involved in reactions taking place on its surface [118-125]. Because of high oxygen mobility, high oxygen storage capacity, and its modifiable ability, the ceria-based material becomes a very attractive material for a wide range of catalytic applications. Recently, one of the great potential applications of ceria is for an in-stack reforming catalyst in an Internal Reforming-Solid Oxide Fuel Cell (IR-SOFC) [126-133]. The advantage of ceria as a reforming catalyst is arisen from its high resistance toward carbon

deposition compared to the conventional metal catalysts, i.e. Ni-based catalysts; nevertheless, the main drawback of ceria is its low specific surface area and high deactivation due to the thermal sintering particularly when operated at a high temperature. Several researches have been conducted to overcome these constraints. Recently, the synthesized ceria with improved textural, structural and chemical properties for environmental applications by using a novel cationic surfactant-assisted approach was suggested. In addition to the investigation on preparation method, the addition of zirconium oxide (ZrO_2) has also been reported to improve the specific surface area, oxygen storage capacity, redox property, thermal stability and catalytic activity of ceria. These benefits are associated with enhanced reducibility of cerium (IV) in Ce-ZrO_2, which is a consequence of high O^{2-} mobility inside the fluorite lattice. The reason for the increasing mobility might be related to the lattice strain, which is generated by the introduction of a smaller isovalent Zr cation into the ceria lattice (Zr^{4+} has a crystal ionic radius of 0.84 Å, which is smaller than 0.97 Å for Ce^{4+} in the same co-ordination environment) [134-135].

Along with ceria-based catalyst, perovskite-based catalysts have also been considered as a promising catalyst for reforming reaction. Typically, $LaCrO_3$-based perovskite materials have been reported to be active for reforming reactions at high temperatures with relatively good stability and resistance toward carbon deposition. Furthermore, from perovskite formula, ABO_3, the substitution on the A and B sites with alkali earth could modify the material electronic and catalytic properties. For instance, $La_{1-x}Ce_xNiO_3$ was developed by partially substituting La at the A-site with Ce and tested its catalytic performance toward the autothermal reforming of gasoline. It was reported that, at the temperature range of 650–800°C, the catalyst exhibited excellent performance in terms of thermal stability, resistance toward carbon formation and sulfur poisoning compared to un-doped $LaNiO_3$.

2.6 Literature review on bioplastic production from glycerol

Polyhydroxyalkanoates (PHAs) or bioplastic are a group of polyesters produced by a number of bacteria which accumulated them as intracellular granules under unfavorable growth conditions. PHAs are carbon and energy reserves and also act as electron sinks, enhancing the fitness and stress resistance of bacteria and contributing to redox balance [136]. These thermoplastic polyesters have properties that vary according to their monomer compositions. PHAs were produced industrially by bacterial fermentation from the late 1980s, first by Imperial Chemical Industries and then by other industries *e.g.* Metabolix/ADM with current production of 50,000 tones/year. However, high production costs have hindered the use of PHAs as commodity plastics since their final price is considerably higher than that of petrochemical-based synthetic plastics. Growing concern about environmental pollution and increasing petroleum price has led to the interest on industrial production of PHAs, which are totally biodegradable by microorganisms in most environments and can be produced from different renewable carbon sources [137].

Poly(3-hydroxybutyrate) (PHB) is the best known PHA and is often used as a model product in the development of fermentation strategies. Accumulation of PHB in recombinant *Escherichia coli* from several carbon sources has been studied [138]. PHB production costs can be reduced by several means, including the use of cheap substrates,

or by enhancement of product yield *e.g.* by genetic engineering approach. In majority of PHB-accumulating species, it is synthesized in three sequential enzymatic steps: a 3-ketothiolase condenses two acetyl-CoA) moieties to form acetoacetyl COA; a NADPH-dependent acetoacetyl-CoA reductase catalyses the stereoselective reduction of acetoacetyl CoA to D-(-)-3-hydroxybutyryl CoA mononers, which are then link to the growing PHB chain by ester bond formation catalysed by a PHB synthase [139]. PHB and its copolymers are accumulated in a wide range of bacteria. Based on the results of economic evaluation, *Ralstonia eutropha*, *Alcaligenes latus* and recombinant *Escherichia coli* have been suggested as good candidates for the production of SCL-PHAs, like PHB [140]. The development of PHB producing microorganisms is an attractive approach for commercial production of PHAs. Genes encoding for PHB synthesis have been transferred into heterologous hosts including *E. coli*, *S. cereviciae* [141] and transgenic plants [142, 143]. The use of recombinant *E. coli* is a promising approach for development of economical PHB production strategy. *E. coli* is a suitable host as a heterologous expression background for foreign genes that can be easily manipulated and improved by means of recombinant DNA methodologies. Also, high-cell-density cultivation strategies for *E. coli* strains are well established [144]. *E. coli* cells that accumulate large amount of PHB become fragile, facilitating the isolation and purification of the biopolymer, and the bacterium does not express PHA-degrading enzymes, thus allowing high level accumulation of PHB in the cells [145].

The three *pha* structural genes, *pha*CAB were introduced in expression plasmids and used for the construction of recombinant *E. coli* strains that accumulate the polymer from different carbon sources. Genes responsible for PHB synthesis from a number of microorganisms, such as *Cupriavidus necator* (formerly *Ralstonia eutropha or Alcaligenes eutrophus*) [146], *Pseudomonas aeruginosa* [147], *Alcaligenes latus* [148], *Thiocapsa pfennigii* [149], *Streptomyces aureofaciens* [150], *Azotobacter* sp. [138] have been introduced into *E. coli*. In most cases, the biosynthetic genes were expressed either under the control of their native promoters or external promoters, and the recombinant bacteria were able to accumulate PHA from different carbon sources, up to 70-80% of their cell dry weight.

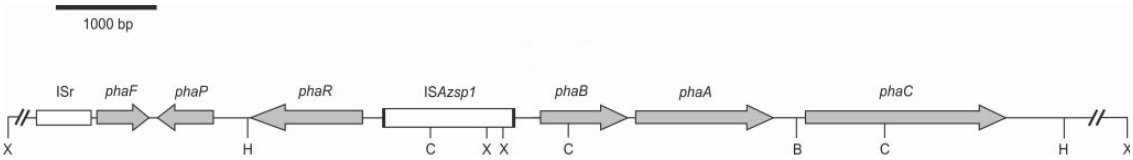

Figure 16 Organisation of the *Azotobacter* sp. strain FA8 genomic region containing the *pha* gene cluster [138]

Apart from the genes that catalyse polymer biosynthesis, natural PHA producers have several genes for proteins involved in granule formation and/or with respiratory functions. Among this group of gene products, phasins, such as PhaP1 from *Cupriavidus necator*, are granule-associated proteins that have been shown to affect polymer biosynthesis and the number and size of PHA granules [151]. Increased growth and PHB production in recombinant *E. coli* carrying PhaP from *Paracoccus denitrificans* [152] and *C. necator* [153] have been reported. Metabolic flux analysis revealed the enhancement of PHB synthesis by increasing the amount of acetoacetyl CoA and reducing equivalent

(such as NADH and NADPH) [140]. *E. coli arc* mutant with unrepressed TCA enzymes resulting in elevated amount of reducing equivalent was reported for increasing amount of PHB accumulation under microanaerobic conditions [154].

Glycerol-rich stream generated in large amounts by the biofuel industry, especially from the production of biodiesel, presents an excellent staring material for co-production of value-added products. Once considered a valuable "co-product", crude glycerol is rapidly becoming a "waste product" with a disposal cost attributed to it. The development of processes to convert crude glycerol into higher value product is the way to establish biorefinery process which can be readily integrated to the existing biodiesel industry for improved process economics. Several strategies based on chemical and biological transformation are being pursued to convert glycerol into more valuable products. Biological conversion could help circumvent the disadvantages of chemical catalysis (*e.g.* low product specificity, use of high pressure and/or temperatures, inability to use crude glycerol with high levels of contaminants, *etc*), while offering the opportunity to synthesise a large array of products and functionalities. Anaerobic fermentation of glycerol to a range of products, including 1,3-propanediol, succinic acid, co-production of ethanol-hydrogen and ethanol-formate have been reported [155]. The use of glycerol as a substrate for PHA production is addressed. Microbial PHA synthesis from glycerol has been studied in natural PHA producers, such as *Methylobacterium rhodesianum*, *Pseudomonas* strains*, Paracoccus denitrificans* and *Cupriavidus necator* [156-158]. However, many natural PHA producers are not suitable for industrial process, as they cannot grow at sufficiently high densities. Some of them also accumulate by-products such as exo-polysaccharides that complicate oxygen transfer in the bioreactor and PHA extraction process [159]. Production of PHB from glycerol by recombinant *E. coli* has been investigated. Recombinant *E. coli* harboring PHB synthesing genes from *Streptomyces aureofaciens* was constructed and the maximum PHB accumulation of 60% cell dry weight was achieved after 48-h fermentation using glycerol as the sole carbon source [150]. Expression of PhaP from *Azotobacter* sp. strain FA8 in the recombinant *E. coli* containing *pha*BAC was reported with increased growth and PHB accumulation from glycerol, especially at high cell density, allowing 7.9 g/l PHB in 48-h batch cultures [160].

Based on the strong platform in plastic industry in Thailand and the potential of biodegradable plastic market, a national roadmap on biodegradable plastic industry has been established, with the first phase from 2008-2012. The roadmap includes the establishment of technology for production of key bio-based plastics including PHAs. The development of PHA producing strains and process using glycerol as the substrate is thus of great interest for improving the economics of biodiesel production process.

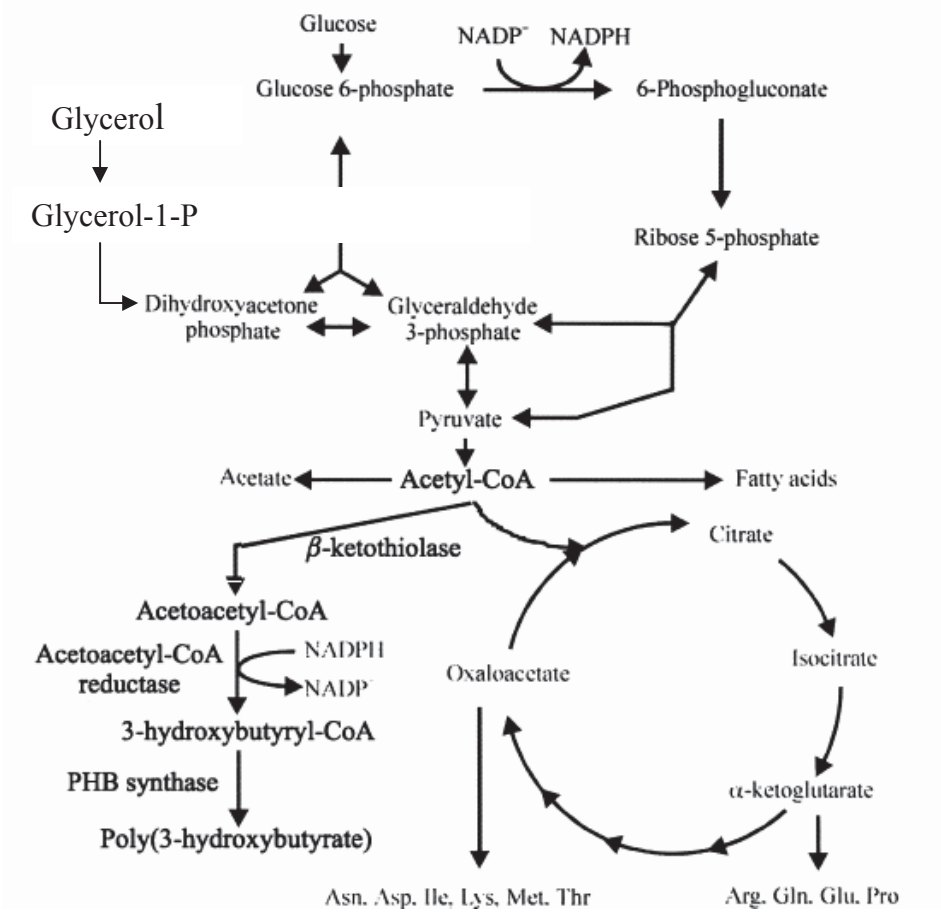

Figure 17: Simplified central metabolic pathway on PHB synthesis from glycerol in recombinant *E. coli* [140]

References

[1] National Statistics Office, 2007
[2] Huber G.W., Chheda J.N., Barrett C.J., and Dumesic J.A. (2005), Production of Liquid Alkanes by Aqueous-Phase Processing of Biomass-Derived Carbohydrates, *Science*, 308, pp.1446-1450.
[3] BP Statistical Review of World Energy, June 2004
[4] APERC Analysis (2006), Thailand case
[5] Keikhosro K., Shauker K. and Mohammad J.T. (2006), Conversion of rice straw to sugars by dilute-acid hydrolysis, *Biomass and Bioenergy*, 30, pp. 247–253.
[6] Watanabe M., Aizawa Y., Iida T., Aida T.M., Levy C., Sue K. and Inomata H.(2005), Glucose reactions with acid and base catalysts in hot compressed water at 473 K, *Carbohydrate Research*, 340, pp.1925-1930.
[7] Weil J.R., Dien B., Bothast R., Hendrickson R., Mosier N.S. and Ladisch M.C.(2002), Removal of Fermentation Inhibitors Formed during Pretreatment of Biomass by Polymeric Adsorbents, *Ind. Eng. Chem. Res.*, 41, pp. 6132-6138.
[8] Kruse A. and Dinjus E.(2007), Hot compressed water as reaction medium and reactant properties and synthesis reactions, J. of Supercritical Fluids, 39, pp.362-380.

[9] Kruse A. and Dinjus E.(2007), Hot compressed water as reaction medium and reactant 2. Degradation reactions, J. of Supercritical Fluids, 41, pp.361-397
[10] Asghari F.S., Yoshida H.(2006), Acid-Catalyzed Production of 5-Hydroxymethyl Furfural from D-Fructose in Subcritical Water, *Ind. Eng. Chem. Res.*, 45, pp. 2163-2173.
[11] Bicker M., Hirth J. and Vogel H. (2003), Dehydration of fructose to 5-hydroxymethyl furfural in sub- and supercritical acetone, *Green Chemistry*, 5 , pp. 280–284
[12] Aida T.M., Watanabe M., Aizawa Y., Iida T., Levy C., Sue K. and Inomata H. (2007), Dehydration of d-glucose in high temperature water at pressures up to 80MPa, *J. of Supercritical Fluids*, 40, pp. 381–388.
[13] Bernard M. K., Tadafumi A., Roberto M. M., and Kunio A. (1997), Kinetics of Glucose Epimerization and Decomposition in Subcritical and Supercritical Water, Ind. Eng. Chem. Res., 36, pp.1552-1558.
[14] Bernard M. K., Tadafumi A., Roberto M. M., and Kunio A. (1999), Glucose and Fructose Decomposition in Subcritical and Supercritical Water: Detailed Reaction Pathway, Mechanisms, and Kinetics, *Ind. Eng. Chem. Res.*, 38, pp. 2888-2895.
[15] Lin Y., Tanaka S. (2006) Ethanol fermentation from biomass resources: current state and prospects. Appl. Microbiol. Biotechnol. 69, 627-642.ess Biochem. 24, 141-145.
[16] Sprenger G.A. (1996) Carbohydrate metabolism in Zymomonas mobilis: a catabolic highway with some scenic routes. FEMS Microbiol. Lett. 145, 403-407.
[17] Dien B.S., Cotta M.A., Jeffries T.W. (2003) Bacteria engineered for fuel ethanol production current status. Appl. Microbiol. Biotechnol. 63, 258-266.
[18] Gonzalez R., Tao H., Purvis J.E., York S.W., Shanmugam K.T., Ingram L.O. (2003) Gene array-based identification of changes that contribute to ethanol tolerance in ethanologenic Escherichia coli: comparison of KO11 (parent) to LY01 (resistant mutant). Biotechnol. Prog. 19, 612-623.
[19] Lynd L.R., Weimer P.J., van Zyl W.H., Pretorius I.S. (2002) Microbial cellulose utilization: fundamentals and biotechnology. Microbiol. Mol. Biol. Rev. 66, 506-577.
[20] Sonderregger M., Sauer U. (2003) Evolutionary engineering of Saccharomyces cereviciae for anaerobic growth on xylose. Appl. Environ. Microbiol. 69, 1990-1998.
[21] Kastner J.R., Eitema M.A., Lee S.A. (2003) Effect of redox potential on stationary-phase xylitol fermentations using Candida tropicalis. Appl. Microbiol. Biotechnol. 63, 96-100.
[22] Kastner J.R., Eiteman M.A., Lee S.A. (2001) Glucose repression of xylitol production in Candida tropicalis mixed sugar fermentations. Biotechnol. Lett. 23, 1663-1668.
[23] Jamai L., Ettayebi K., Yamani J.E., Ettayebi M. (2007) Production of ethanol from starch by free and immobilized Candida tropicalis in the presence of □-amylase. Bioresour. Technol. 98, 2765-2770.
[24] Klinke H.B., Thomsen A.B., Arhing B.K. (2004) Inhibition of ethanol-producing yeast and bacteria by degradation products produced during pre-treatment of biomass. Appl. Microbiol. Biotechnol. 66, 10-16.
[25] Marchetti J.M., Miguel V.U., Errazu A.F. (2007) Possible methods for biodiesel production. Renew. Sustain. Energ. Rev. 11, 1300-1311.

[26] Lopez E.D., Goodwin Jr.G.J., Bruce A.D. and Lotero, E.(2005), Transesterification of triacetin with methanol on solid acid and base catalyst, Applied Catalysis, 295, pp.97-105.
[27] Demirbas, A.(2006), Biodiesel production via non-catalytic SCF method and biodiesel fuel characteristics, Energy Conversion and Management, 47, pp.2271-2282.
[28] Leung D.Y.C. and Guo, Y.(2006), Transesterification of neat and used frying oil: Optimization for biodiesel production, Fuel Processing Technology, 87, pp.883-890.
[29] Gerpen, V.J.(2005), Biodiesel processing and production, Fuel Processing Technology, 86, pp.1097-1107.
[30] Ramadhas A.S., Jayaraj S. and Muraleedharan, C.(2005), Biodiesel production from high FFA rubber seed oil, Fuel, 84, pp.335-340.
[31] Vicente G., Maetinez M. and Aracil, J.(2004), Integrated biodiesel production: a comparison of different homogeneous catalysts systems, Bioresource Technology, 92, pp.297-305.
[32] Feezol industries (2006). "Biodiesel in India" Available online: http://www.feezol.com/biodiesel.htm
[33] Zheng S., Kates M., Dube M.A. and Mclean, D.D.(2006), Acid-catalyzed production of biodiesel from waste frying oil, Biomass and Bioenergy, 30, pp.267-272.
[34] Nijhuis T.A., Beers A.E.W., Kapteijn F. and Moulijn, J.A.(2002), Water removal by reactive stripping for a solid-acid actalyzed esterification in a monolithic reactor, Chemical Engineering Science, 57, p.1627.
[35] Omota F., Dimian A.C. and Bliek, A.(2003), Fatty acid esterification by reactive distillation: Part I: equilibrium-based design, Chemical Engineering Science, 58, pp. 3159-3161.
[36] Omota F., Dimian A.C. and Bliek, A.(2003), Fatty acid esterification by reactive distillation: Part I: kinetics-based design for sulphated zirconia catalysts, Chemical Engineering Science, 58, pp. 3175-3176.
[37] Vicente G., Maetinez M. and Aracil, J.(2007), Optimisation of integrated biodiesel production. Part I. A study of the biodiesel purity and yield, Bioresource Technology, 98, pp.1724-1733.
[38] Vicente G., Maetinez M. and Aracil, J.(2007), Optimisation of integrated biodiesel production. Part II. A study of the material balance, Bioresource Technology, 98, pp.1754-1761.
[39] Du W., Xu Y., Liu D., Zeng J. (2004) Comparative study on lipase-catalyzed transformation of soybean oil for biodiesel production with different acyl acceptors. J. Mol. Catal. B: Enzym. 30, 125–129.
[40] Al-Zahair S., Ling F.W., Jun L.S. (2007) Proposed kinetic mechanism of production of biodiesel from palm oil using lipase. Proc. Biochem. 42, 951-960.
[41] Du W., Liu D., Li L., Dai L. (2007a) Mechanism exploration during lipase-mediated methanolysis of renewable oils for biodiesel production in a tert-butanol system. Biotechnol. Prog. 23, 1087-1090.
[42] Lai C.C., Zullaikah S., Vali R.R., Ju Y.H. (2005) Lipase-catalyzed production of biodiesel from rice bran oil. J. Chem. Technol. Biot. 80, 331–337.
[43] Oliveira, A.C., Rosa, M.F. (2006) Enzymatic transesterification of sunflower oil in an aqueous-oil biphasic system. J. Am. Oil Chem. Soc. 83, 21-25.
[44] Shah S., Gupta M.N. (2007) Lipase catalyzed preparation of biodiesel from Jatropha oil in a solvent free system. Proc. Biochem. 42, 409-414.

[45] Chang H.-M., Liao H.-F., Lee C.-C., Shieh C.-J. (2005) Optimized synthesis of lipase-catalyzed biodiesel by Novozyme 435. J. Chem. Technol. Biotechnol. 80, 307-312.
[46] Shimada Y., Watanabe Y., Sugihara A., Tominaga Y. (2002) Enzymatic alcoholysis for biodiesel fuel production and application of the reaction to oil processing. J. Mol. Catal. B: Enzym. 17, 133–142.
[47] Al-Zuhair S. (2005) Production of biodiesel by lipase-catalysed transesterification of vegetable oils: a kinetics study. Biotechnol. Prog. 21(5), 1442-1448.
[48] Al-Zuhair S. (2006) The effect of substrate concentrations on the production of biodiesel by lipase-catalysed transesterification of vegetable oils. J. Chem. Technol. Biotechnol. 81, 299-305.
[49] Li L., Du W., Liu D., Wang L., Li Z. (2006) Lipase-catazed transesterification of rapeseed oils for biodiesel production with a novel organic solvent as the reaction medium. J. Mol. Cat. B: Enzymatic 43, 58-62.
[50] Ha S.H., Lan M.N. Lee S.H., Hwang S.M., Koo Y.-M. (2007) Lipase-catalyzed biodiesel production from soybean oil in ionic liquids. Enz. Microb. Technol. 41, 480-483.
[51] Watanabe Y., Pinsirodom P., Nagao T., Yamauchi A., Kobayashi T., Nishida Y., Takagi Y., Shimada Y. (2007) Conversion of acid oil by-produced in vegetable oil refining to biodiesel fuel by immobilized Candida tropicalis lipase. J. Mol. Cat. B: Enzymatic 44, 99-105.
[52] Samukawa T., Kaieda M., Matsumoto T., Ban K., Kondo A., Shimada Y., Noda H., Fukuda H. (2000) Pretreatment of immobilized Candida antarctica lipase for biodiesel production from plant oil. J. Biosci. Bioeng. 90, 180–183.
[53] Noureddini H., Gao X., Philkana R.S. (2005) Immobilized Pseudomonas cepacia lipase for biodiesel fuel production from soybean oil. Bioresource Technol. 96, 769–777.
[54] Hernández-Mártin E., Otero C. (2008) Different enzyme requirements for the synthesis of biodiesel: Novozym®435 and Lipozyme® TL IM. Bioresoure Technol 99, 277-286.
[55] Li W., Du W., Liu D. (2007) Rhizopus oryzae IFO 4967 whole cell catalyzed methanolysis of crude and acidified rapeseed oils for biodiesel production in tert-butanol system. Proc. Biochem. 1481-1485.
[56] Hama S., Yamaji H., Fukumizu T., Numata T., Tamalampudi S., Kondo A., Noda H., Fukuda H. (2007) Biodiesel-fuel production in a packed-bed reactor using lipase-producing Rhizopus oryzae cells immobilized within biomas support particles. Biochem. Eng, J. 34, 273-278.
[57] Matsumoto T., Takahashi S., Kaida M. Ueda M., Tanaka A., Fukuda H., Kondo A. (2001) Yeast whole-cell biocatalyst constructed by intracellular overexproduction of Rhizopus oryzae lipase is applicable to biodiesel fuel production. Appl. Microbiol. Biotechnol. 57, 515-520.
[58] Clair N.L.S. Navia M.A. (1992) Cross-linked enzyme crystals as robust biocatalysts. J. Am. Chem. Soc. 114, 7314-7316.
[59] Cao L., Van Rantwijk F., Sheldon R.A. (2000) Cross-linked enzyme aggregates: a simple and effective method for the immobilization of penicillin acylase. Org. Lett. 2, 665-670.
[60] Cao L., Van Langen F., Sheldon R.A. (2003) Immobilized enzymes: carrier-bound or carrier-free? Curr. Opin. Biotechnol. 14, 387-394.

[61] Shah S., Sharma A., Gupta M.N. (2006) Preparation of cross-linked enzyme aggregates by using bovine serum albumin as a proteic feeder. Anal. Biochem. 207-213.
[62] J. Xu,1986, Ph.D. Thesis, Laboratorium Voor Petrochemische Techniek, Rijkuniversiteit, Gent, Belgium.
[63] J. Xu, G.F. Froment, AIChE., 35 (1989) 88.
[64] J. Xu, G.F. Froment, AIChE., 35 (1989) 97.
[65] S. S. E. H. Elnashaie, A. M. Adris, A. S. Al-Ubaid, M. A. Soliman, Chem. Eng. Sci., 45 (1990) 491.
[66] S.S.E.H. Elnashaie, S.S. Elshishini, "Modeling, Simulation and Optimization of Industrial Fixed Bed Catalytic Reactors", Gordon and Breach Science Publishers, UK, 1993.
[67] J.H. Edwards and A.M. Maitra, Fuel Processing Technology, 42, (1995), 269.
[68] M. A. Vannice and M. C. J. Bradford, Applied Catalysis A: General, 142(1), (1996), 97-122.
[69] T. Sodesawa, A. Dobashi and F. Nozaki, React. Kinet. Catal. Lett., 12, (1979), 107.
[70] L. Topor, L. Bejan, E. Ivana, N. Georgescu, Revue Chim. Bucharest, 30, (1979), 539.
[71] T.A. Chubb, Sol. Energy, 24, (1980), 341.
[72] T.A. Chubb, J.H. McCrary, G.E. McCrary, J.J. Nemecek and D.E. Simmons, Proc. Meet. Am. Sect. Int. Sol. Eng. Soc., 4, (1981), 166.
[73] J.R. Rostrup-Nielsen and J.H. Bak Hansen, J. Catalysis, 144, (1993), 38.
[74] P. Gronchi, C. Mazzocchia, E. Tempesti and R. Del Rosso, in Enviromental Catalysis, Edited by G. Centi et al., SCI Publi., Roma, (1995), 627.
[75] A. Erdöhelyi, J. Cserényi and F. Solymosi., J. Catal., 141, (1993), 287.
[76] A. Erdöhelyi, J. Cserényi, E. Rapp and F. Solymosi., Appl. Catal. A: Gen., 108, (1994), 205.
[77] J. Nakamura, K. Aikawa, K. Sato and T. Uchijima., Catal. Lett., 25, (1994), 265.
[78] Z.L. Zhang, V.A. Tsipouriari, A.M. Efstathiou and X.E. Verykios., J. Catal., 158, (1996), 51.
[79] K. Ahmed, J. Gamman and K. Föger, Solid State Ionics, 152-153, p. 485-492
[80] Takashi Suzuki, Hiko-ichi Iwanami, Osamu Iwamoto and Tamio Kitahara, Int. J. Hydrogen Energy, 26(9), p. 935-940
[81] Avci AK, Trimm DL, Aksoylu AE, Önsan ZI. Catal Lett, 88, p. 17–22.
[82] A.F. Ghenciu, Curr Opinion Solid State Mater Sci 6 (2002), p. 389–399
[83] T. Rampe, A. Heinzel and B. Vogel, J Power Sources, 86 (2000), p. 536–541
[84] F. Joensen and J.R. Rostrup-Nielsen, J Power Sources 105 (2002), pp. 195–201.
[85] Vincenzo Recupero, Lidia Pino, Antonio Vita, Francesco Cipitı`, Manuela Cordaro and Massimo Laganà, Int. J. Hydrogen Energy, 30(9), p. 963-971
[86] K. Oka, T. Nishiguchi, H. Kanai, K. Utani and S. Imamura, Appl. Catal. A: General, 309(2), (2006), 187-191
[87] T.A. Semelsberger, K.C. Ott, R.L. Borup and H.L. Greene, Appl. Catal. A: General, 309(2), (2006), 210-223
[88] T. Kawabata, H. Matsuoka, T. Shishido, D. Li, Y. Tian, T. Sano and K. Takehira, Appl. Catal. A: General, 308, (2006), 82-90
[89] T.A. Semelsberger, K.C. Ott, R.L. Borup and H.L. Greene, Appl. Catal. B: Environmental, 65(3-4), (2006), 291-300
[90] K. Faungnawakij, Y. Tanaka, N. Shimoda, T. Fukunaga, S. Kawashima, R. Kikuchi and K. Eguchi, Appl. Catal. A: General, 304, (2006), 40-48

[91] T. Nishiguchi, K. Oka, T. Matsumoto, H. Kanai, K. Utani and S. Imamura, Appl. Catal. A: General, 301(1), (2006), 66-74
[92] Emonts B., Hansen J.B., Jorgensen S.L., Hohlein B. and Peters R., J. Power Sources, 71, (1998), 288
[93] Ledjeff-Hey K., Formanski V., Kalk T. and Roes J., J. Power Sources, 71(1-2), (1998), 199
[94] S. Cavallaro, S. Freni, Int. J. Hydrogen Energy, 21 (6), (1996), 465
[95] A.N. Fatsikostas, X.E. Verykios, J. Catal., 225 (4), (2004), 439
[96] L. Garcia, R. French, S. Czernik and E. Chornet. Appl. Catal. A: Gen. 201 (2000), 225.
[97] I. Fishtik, A. Alexander, R. Datta and D. Geana. Int. J. Hydrogen Energy 25 (2000) 31.
[98] S. Freni, G. Maggio and S. Cavallaro. J. Power Sour. 62 (1996) 67.
[99] K. Vasudera, N. Mitra, P. Umasankar and S.C. Dhinga. Int. J. Hydrogen Energy 21 (1996) 13.
[100] S. Cavallaro and S. Freni. Int. J. Hydrogen Energy 21 (1996) 465.
[101] F. Marino, E.G. Cerrella, S. Duhalde, M. Jobbagy and M.A. Laborde. Int. J. Hydrogen Energy 23 (1998) 1095.
[102] S. Cavallaro. Energy and Fuels 14 (2000) 1195.
[103] S. Freni. J. Power Sour. 94 (2001) 14.
[104] A. Fatsikostas, D. Kondarides and X. Verykios. Catal. Today 75 (2002) 145.
[105] S. Freni, S. Cavallaro, N. Mondello, L. Spadaro and F. Frusteri. J. Power Sour. 108 (2002) 53.
[106] A. Fatsikostas, D. Kondarides and X. Verykios. Catal. Today 75 (2002) 145.
[107] F. Marino, G. Baronetti, M. Jobbagy and M. Laborde. Appl. Catal. A: Gen. 6043 (2002) 1.
[108] J.P. Breen, R. Burch and H.M. Coleman. Appl. Catal. B: Environ. 39 (2002) 65.
[109] J. Llorca, N. Homs, J. Sales and P. Ramirez de la Piscina. J. Catal. 209 (2002), 306.
[110] V. Fierro, V. Klouz, O. Akdim and C. Mirodatos. Catal. Today 75 (2002) 141.
[111] D. Liguras, D. Kondarides and X. Verykios. Appl. Catal. B: Environ. 43 (2003) 345.
[112] J. Llorca, P. Ramirez de la Piscina, J.-A. Dalmon, J. Sales and N. Homs. Appl. Catal. B: Environ. 43 (2003) 355.
[113] S. Cavallaro, V. Chiodo, S. Freni, N. Mondello and F. Frusteri. Appl. Catal. A: Gen. 249 (2003) 119.
[114] S. Freni, S. Cavallaro, N. Mondello, L. Sadaro and F. Frusteri. Catal. Commun. 4 (2003) 259.
[115] S. Cavallaro, V. Chiodo, A. Vita and S. Freni. J. Power Sour. 123 (2003) 10.
[116] D. Srinivas, C.V.V. Satyanarayana, H.S. Potdar and P. Ratnasamy. Appl. Catal. A: Gen. 243 (2003) 261.
[117] J.R. Rostrup-Nielsen and J.-H. Bak-Hansen, J. Catal. 144 (1993) 38.
[118] A. Trovarelli, Catal. Rev.-Sci. Eng. 38 (1996) 439.
[119] P. Fornasiero, G. Balducci, R.D. Monte, J. Kaspar, V. Sergo, G. Gubitosa, A. Ferrero, M. Graziani, J. Catal. 164 (1996) 173.
[120] T. Miki, T. Ogawa, M. Haneda, N. Kakuta, A. Ueno, S. Tateishi, S. Matsuura, M. Sato, J. Phys. Chem. 94 (1990) 339.
[121] C. Padeste, N.W. Cant, D.L. Trimm, Catal. Lett. 18 (1993) 305.
[122] S. Kacimi, J. Barbier Jr., R. Taha, D. Duprez, Catal. Lett. 22 (1993) 343.
[123] G.S. Zafiris, R.J. Gorte, J. Catal. 143 (1993) 86.
[124] G.S. Zafiris, R.J. Gorte, J. Catal. 139 (1993) 561.

[125] S. Imamura, M. Shono, N. Okamoto, R. Hamada, S. Ishida, Appl. Catal. A 142 (1996) 279.
[126] E. Ramírez-Cabrera, A. Atkinson, D. Chadwick, Appl. Catal. B 47 (2004), 127.
[127] E. Ramírez-Cabrera, N. Laosiripojana, A. Atkinson, D. Chadwick, Catal. Today 78 (2003) 433.
[128] R.J. Gorte, J.M. Vohs, S. McIntosh, Solid State Ionics 175 (2004) 1.
[129] S. Jung, C. Lu, H. He, K. Ahn, R.J. Gorte, J.M. Vohs, J. Power Sources (2005) In Press.
[130] T. Kim, G. Liu, M. Boaro, S.-I. Lee, J.M. Vohs, R.J. Gorte, O.H. Al-Madhi, B.O. Dabbousi, J. Power Sources (2005) In Press.
[131] O. Costa-Nunes, R.J. Gorte, J.M. Vohs, J. Power Sources 141 (2005) 241.
[132] S. An, Lu C., W.L. Worrell, R.J. Gorte, J.M. Vohs, Solid State Ionics 175 (2004) 135.
[133] D.J.L. Brett, A. Atkinson, D. Cumming, E. Ramírez-Cabrera, R. Rudkin, N.P. Brandon, Chem. Eng. Sci. 60 (2005) 5649.
[134] P. Fornasiero, R. Dimonte, G.R. Rao, J. Kaspar, S. Meriani, A. Trovarelli, M. Graziani, J. Catal. 151 (1995) 168.
[135] M.H. Yao, T.E. Hoost, R.J. Baird, F.W. Kunz, J. Catal. 166 (1997) 67.
[136] Reddy C.S.K., Ghai R., Rashmi, Kalia V.C. (2003) Polyhydroxyalkanotes: an overview. Bioresource -Technol. 87, 137-146.
[137] Khanna S. and Srivastara A.K. (2005) Recent advances in microbial polyhydroxyalkanoates. Process Biochem. 40, 607-619.
[138] Nikel P.I., de Almeida A., Melillo E.C., Galvagno M.A., Pettinari M.J. (2006a) New recombinant *Escherichia coli* strain tailored for the production of poly(3-hydroxybutyrate) from agroindustrial by-products. Appl. Environ. Microbiol. 72, 3949-3954.
[139] Steinbüchel A., Füchtenbusch B. (1998) Bacterial and other biological systems for polyester production. Trends Biotechnol. 16, 419-427.
[140] Lee S.Y., Hong S.H., Park S.J., van Wegen R., Middelberg A.P.J. Metabolic flux analysis on the production of poly(3-hydroxybutyrate): in Doi Y., Steinbüchel A. (Eds), Biopolymers vol.3a, Wiley/VCH, Weinheim, 2002, 249-261.
[141] Carlson R., Fell D., Srienc F. (2002) Metabolic pathway analysis of a recombinant yeast for rational strain development. Biotechnol. Bioeng. 79, 121-134.
[142] Petrasovits L.A., Purnell M.P., Nielsen L.K., Brumbley S.M. (2007) Production of polyhydroxybutyrate in sugarcane. Plant Biotechnol. J. 5, 162-172.
[143] Poirier Y., Dennis D.E., Klomparens K., Somerville C. (1992) Polyhydroxybutyrate, a biodegradable thermoplastic, produced in transgenic plants. Science 256, 520-523.
[144] Shiloach J., Fass R. (2005) Growing *E. coli* to high cell density- a historical perspective on method development. Biotechnol. Adv. 23, 345-357.
[145] Aldor I.S., Keasling J.D. (2003) Process design for microbial plastic factories: metabolic engineering of polyhydroxyalkanoates. Curr. Opin. Biotechnol. 14, 475-483.
[146] Schubert P., Steinbüchel A., Schlegel H.G. (1988) Cloning of theAlcaligenes eutrophus genes for synthesis of poly(β-hydroxybutyric acid) (PHB) and synthesis of PHB in Escherichia coli. J. Bacteriol. 170, 5837-5847.
[147] Langenbach S., Rehm B.H., Steinbüchel A. (1997) Functional expression of PHA synthase gene *phaC1* in *Pseudomonas aeruginosa* in *Escherichia coli*

results in poly(3-hydroxyalkanoate) synthesis. FEMS Microbiol. Lett. 7, 229-236.

[148] Choi J.I., Lee S.Y., Han K. (1998) Cloning of *the Alcaligenes latus* polyhydroxyalkanoate biosynthesis genes and use of these genes for enhanced production of poly(3-hydroxybutyrate) in *Escherichia coli*. Appl. Environ. Microbiol. 64, 4897-4803.

[149] Liu S.J., Steinbüchel A. (2000) A novel genetically engineered pathway for synthesis of poly(hydroxyalkanoic acids) in *Escherichia coli*. Appl. Environ. Microbiol. 66,739-743.

[150] Mahishi L.H.,Tripathi G., Rawal S.K. (2003) Poly(3-hydroxybutyrate) (PHB) synthesis by recombinant *Escherichia coli* harbouring *Streptomyces aureofaciens* PHB biosynthesis genes: effect of different carbon source and nitrogen sources. Microbiol. Res. 158, 19-27.

[151] Pötter M., Muller H., Reinecke F., Wieczorek R., Fricke F., Bowien B., Friedrich B., Steinbüchel A. (2004) The complex structure of polyhydroxbutyrate (PHB) granules: four orthologous and paralogous phasins occur in *Ralstonia eutropha*. Microbiology 150, 2301-2311.

[152] Machara A., Ueda S. Nakano H., Yamane T. (1999) Analyses of a polyhydroxyalkanoic acid granule-associated 16-kilodalton protein and its putative regulator in the pha locus of *Paracoccus denitrificans*. J. Bacteriol. 181, 2914-2921.

[153] York G. M., Stunne J., Sinskey A.J. (2001) New insight into the role of the PhaP phasing *of Ralstonia eutropha* in promoting synthesis of polyhydroxybutyrate. J. Bacteriol. 183, 2394-2397.

[154] Nikel P.I., Pettinari M.J., Galvagno M.A., Méndez B.S. (2006b) Poly(3-hydroxybutyrate) synthesis by recombinant *Escherchia coli arcA* mutants in microaerobiosis. Appl. Environ. Microbiol. 72, 2614-2620.

[155] Yazdani S.S., Gonzalez R. (2007) Anaerobic fermentation of glycerol: a path to economic viability for the biofuels industry. Curr. Opin. Biotechnol. 18, 213-219.

[156] Ashby R.D., Solaiman D.K.Y., Foglia T.A. (2004) Bacterial poly(hydroxyalkanoate) polymer production from the biodiesel co-product stream. J. Polym. Environ. 12, 105-112.

[157] Solaiman D.K., Ashby R.D., Foglia T.A., Marmer W.N. (2006) Conversion of agricultural feedstock and coproducts into poly(hydroxyalkanoates). Appl. Microbiol. Biotechnol. 71, 783-789.

[158] Mothes G., Schnorpfeil C., Achermann J.-U. (2007) Production of PHB from crude glycerol. Eng. Life Sci. 7, 475-479.

[159] Quagliano J.C., Alegre P., Miyazaki S.S. (1994) Isolation and characterization of *Azotobacter* sp. For the production of poly-β-hydroxyalkanoates. Rev. Argent. Microbiol. 26, 21-27.

[160] De Almeida A., Nikel P.I., Giordano A.M., Pettinari M.J. (2007) Effects of granule-associated protein PhaP on glycerol-dependent growth and polymer production in poly(3-hydroxybutyrate)-producing *Escherichia coli.* Appl. Environ. Microbiol. 73, 7912-7016.

Chapter 3

Results and Discussion: Biomass conversion studies

3.1 Introduction and research objectives

Due to the current rapid declining of petroleum resources and the global concern over environmental crisis, the developments of energies and/or fuels from natural resources (e.g. lignocellulosic biomass) are now being interested since it is known that the combustions of biomass as well as biomass-derived fuels are not considered as the contribution for global warming and climate change. For agricultural countries, various types and enormous amount of biomass (e.g. bagasse, rice husk, rice straw, corncob, coconut, and palm) are available. These materials can be effectively converted to energies (in the form of electricity and/or heat) and liquid fuels (e.g. biodiesel, alcohols, and biomass-to-liquid (BTL)) via several thermo-chemical, physico-chemical, and biological processes. Among these biomass-derived fuels, BTL is one of the promising fuels to replace fossil oils in transportation section. The advantage of BTL is its identical properties to conventional gasoline and diesel; hence BTL can be entirely replaced these fuels without engine modification required. Currently, the typical process for BTL production is the gasification/Fischer–Tropsch process. Nevertheless, this technology is feasible economically only for large scale application and the cost of synthesized BTL form this technology remains relatively high.

Recently, Huber et al. (2005) reported an alternative low-cost process to convert carbohydrate compounds to C_7-C_{15} alkanes, which can be efficiently used as fuel for transportation and industrial applications. Their conversion route involves a series of reaction steps starting with acid-catalyzed dehydration of carbohydrates to carbonyl-containing furan compounds (i.e. 5-hydroxymethylfurfural (HMF) and furfural). This reaction typically occurs in the presence of solid acid catalysts (Moreau et al., 1998; Lourvanij et al., 1993). Subsequently, these compounds are condensed via aldol reaction to produce larger organic molecules (>C_6). Generally, the aldol-condensation is carried out in the presence of base catalysts to form a C-C bond between two carbonyl-containing compounds. Importantly, HMF and furfural cannot undergo self-condensation reactions since these compounds do not have a-H atom; nevertheless, both HMF and furfural have aldehyde groups, which can efficiently condense with acetone to form carbanion species. Solid base catalysts e.g. magnesia–zirconia (MgO-ZrO_2) and magnesia–titania (MgO-TiO_2) have been proved to active for vapor phase condensation of acetone to form C–C bonds (Aramendia et al., 2004). Apart from the solid-catalyzed process, aldol-condensation in aqueous environment for carbohydrate-derived molecules has also been reported to be efficiently catalyzed by homogeneous mineral bases (e.g. NaOH) (Gutsche et al., 1967; Shigemasa et al., 1994). After the aldol-condensation step, the aldol-products were further hydrogenated to form large water-soluble organic compounds. In the presence of specific metal catalysts (i.e. Pd), selective hydrogenation of the furan ring in HMF and furfural can lead to additional carbonyl-containing compounds that can undergo

aldol self-condensation to form heavier alkanes. Lastly, these hydrogenated molecules were converted to liquid alkanes (ranging from C_7-C_{15}) by aqueous-phase dehydration/hydrogenation (APD/H) over a bifunctional catalyst containing acid (e.g. SiO_2-Al_2O_3) and metal sites (e.g. Pd or Pt) with two feed streams i.e. an aqueous stream containing the organic reactant and a hexadecane sweep stream. The large aqueous organic reactants become more hydrophobic during APD/H processing, and the hexadecane sweep stream removes these hydrophobic species from the catalyst before they react further to form coke. In order to convert lignocellulosic biomass to alkane-based fuel via the above pathway, the feedstock must be firstly hydrolyzed to form sugar compounds and later dehydrated to HMF and furfural. Previously, several research and development on the production of these compounds via acid-catalyzed reaction, hot compressed water (HCW), subcritical water and supercritical water technologies have been reported (Laopaiboon et al., 2010; Yat et al., 2008; Karimi et al., 2006; Bower et al., 2008; Watanabe et al., 2005a, 2005b; Asghari et al., 2006; Bicker et al., 2003; Aida et al., 2007; Yang et al., 1996; Kabyemela et al., 1997; Moreau et al., 2000; Sasaki et al., 2002).

In the present work, we firstly aim at the coupling of hydrolysis and dehydration reactions to produce HMF and furfural from three promising lignocellulosic biomasses (i.e. sugarcane bagasse, rice husk and corncob) in a single unit for later utilization as intermediate compounds for alkane-based fuel production. The HCW operation in the presence of several heterogeneous catalysts i.e. TiO_2, ZrO_2 and mixed oxide TiO_2-ZrO_2 (with three different Ti/Zr ratios i.e. 3/1, 1/1, and 1/3 and three different calcination temperatures i.e. 773 K, 873 K and 973 K) will be applied. The impact of these catalysts on the hydrolysis and dehydration of selected biomasses will be compared at various operating conditions to determine the suitable catalyst system for enhancing maximum yield of HMF and furfural productions. It is noted that the effect of catalyst preparation methods i.e. sol-gel, (co-) precipitation and physical mixing (for TiO_2-ZrO_2) on the catalytic reactivity will be also studied since several reports indicated the significant impact of catalyst preparation method on its catalytic reactivity. Lastly the physical characteristics of these synthesized catalysts, i.e. acidity-basicity properties, phase formation and catalyst surface properties will be also carried out in order to relate these properties with the preparation method and catalytic performance.

As the next step, we investigated the integration of hydrolysis/dehydration reactions with aldol-condensation/hydrogenation reactions in order to convert the selected lignocellulosic biomass (i.e. corncob) and biomass-derived carbohydrate (i.e. waste cassava) to water-soluble organic compounds (C_5-C_{15}) in the single unit; these compounds can be later converted to alkane-based fuel by APD/H process (Huber et al., 2005). Following our studies in the first part, TiO_2-ZrO_2 was applied as the hydrolysis/dehydration catalyst, while Pd-based catalyst (i.e. Pd/MgO-ZrO_2) was used for the sequential aldol-condensation/hydrogenation reactions (Barrett et al., 2006). Furthermore, for comparison, WO_3-ZrO_2 and H_3PO_4 were also tested as hydrolysis/dehydration catalysts since liquid H_3PO_4 is widely known to have activity toward hydrolysis/dehydration reaction, whereas WO_3-ZrO_2 was also reported to active for several acid-catalyzed reactions (Furuta et al., 2004; Lopez et al., 2005; Rao et al., 2006). As the next step, the sequential aldol-condensation/hydrogenation of HMF and furfural over Pd/TiO_2-ZrO_2 and Pd/WO_3-ZrO_2 were also carried out and compared to Pd/MgO-ZrO_2 (as previously reported in the literature (Barrett et al.,

2006)). Based on all information observed, the integrative hydrolysis/dehydration/ aldol-condensation/ hydrogenation of lignocellulosic biomass and biomass-derived carbohydrate for water-soluble organic compounds (C_5-C_{15}) production in the single reactor were studied over selected catalyst systems and the optimum conditions for this conversion process were determined.

3.2 Materials and methods

3.2.1 Material preparation

Sugarcane bagasse, rice husk, corncob and waste cassava were used as the samples of lignocellulosic biomasses in the present work. The percentages of cellulose, hemicellulose, and lignin for these samples are 0.44:0.29:0.20, 0.28:0.28:0.24, and 0.50:0.31:0.15 (the rest of the compounds are minerals). Before undergoes the reaction testing, these feedstocks were ground with a ball-milling to become fine particle with the average particle size of 75 μm. It should be noted that the reactions of sugar (i.e. glucose and xylose), cellulose, and xylan (representative for hemicellulose) were also carried out. These materials were supplied from Aldrich and Ajax Finechem.

3.2.2 Catalyst preparation and characterization

In the present work, tentatively zirconia (ZrO_2), titania (TiO_2) and titania-zirconia (TiO_2-ZrO_2) will be applied as catalyst for the interested reactions. ZrO_2 and TiO_2 will be synthesized by precipitation and sol-gel methods. For the precipitation method, a solution of either zirconium or titanium salt precursors (i.e. zirconyl chloride ($ZrOCl_2$) and titanium chloride ($TiCl_4$) (0.15 M)) will be slowly dropped into a well-stirred precipitating solution of ammonium hydroxide (NH_4OH) (2.5 wt%) at room temperature. The solution will be controlled at pH of 11. The obtained precipitate will be removed, and then washed with deionized water until Cl^- is not detected by a silver nitrate ($AgNO_3$) solution. Then, the solid sample will be dried overnight at 383 K and calcined at various temperatures (i.e. 773 K, 873 K and 973 K) under continuous air flow for 6 h with a temperature ramping rate of 10 K min^{-1}. For sol-gel method, titanium-tetra-isopropoxide (TTIP) and Zirconium (IV) isopropoxide isopropanol (supplied from Aldrich) will be applied as the starting precursors. They will be dissolved in 2-propanol with the molecular ratio of 1:40 and stirred for 15 minutes. The reaction will then be maintained at pH 2 for 30 minutes by adding HNO_3. After that, the solution will be kept at ambient temperature until become gel then it will be dried at 373 K for 12 h and calcined at 773 K, 873 K and 973 K for 6 h.

As for TiO_2-ZrO_2, this catalyst (with Ti/Zr molar ratios of 1/3, 1/1, and 3/1) will be prepared by co-precipitation (using $ZrOCl_2$ and $TiCl_4$ as salt precursors), sol-gel (using titanium-tetra-isopropoxide and zirconium (IV) isopropoxide isopropanol as precursors; Figure 1), and physical mixing of TiO_2 and ZrO_2 (obtained from precipitation method). After similar treatment to ZrO_2 and TiO_2, several characterizations i.e. BET, XRD and TPD will be performed over all synthesized catalysts. BET measurements will be carried out by N2 physisorption technique using Micromeritics ASAP 2020 surface area and porosity analyzer to determine the specific surface area, cumulative pore volume and average pore diameter of material.

The X-ray diffraction (XRD) patterns of powder will be analyzed by X-ray diffractometer, in which the crystallite size was estimated from line broadening according to the Scherrer equation. Temperature-programmed desorption techniques with ammonia and carbon dioxide (NH_3- and CO_2-TPD) will be applied to determine the acid-base properties of catalysts. In detail, TPD experiments will be carried out using a flow apparatus; the catalyst sample (0.1g) will be treated at 773 K in helium for 1 h and then saturated with 15% NH_3/He mixture or pure CO_2 flow after cooling to 373 K. After purging with helium, the sample will be heated to 923 K under helium and the amount of acid-base sites on the catalyst surface will be calculated from the desorption amount of NH_3 and CO_2, which will be determined by measuring the areas of the desorption profiles obtained from the Chemisorption System analyzer.

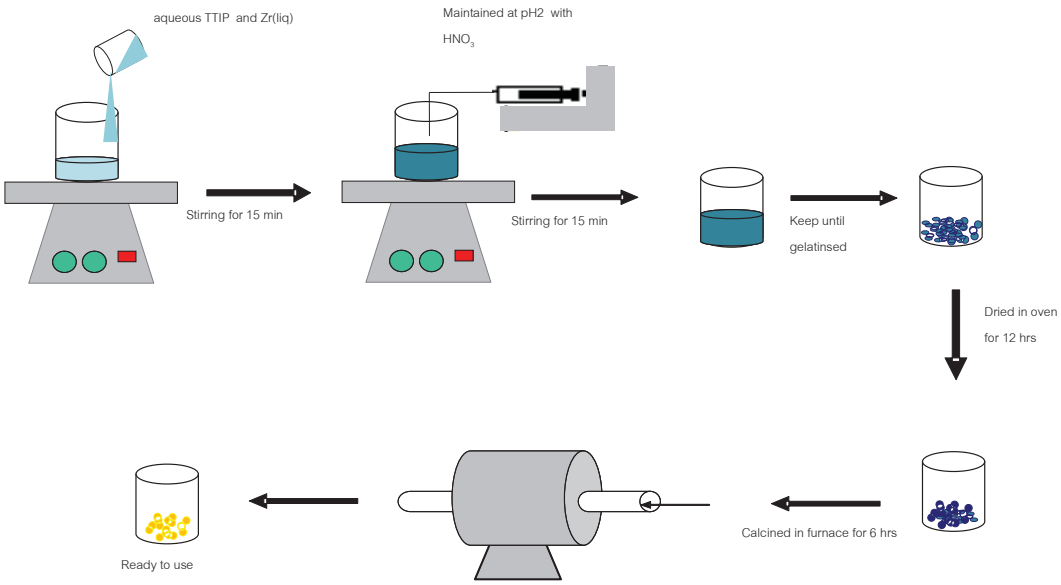

Fig. 3.1 Preparation of $TiZrO_4$ catalyst by sol-gel method

WO_3-ZrO_2 was prepared by incipient wetness impregnation of ammonium metatungstate over ZrO_2 (prepared from the co-precipitation of $ZrO(NO_3)_2$ precursor) providing tungsten weight contents of 20 wt% at 343 K for 30 min, then dried overnight at 383 K and calcined at 1073 K for 3 h. After preparation, the characterizations (i.e. BET and Temperature-programmed desorption techniques with ammonia and carbon dioxide (NH_3- and CO_2-TPD)) were performed over these synthesized catalysts. BET measurements was carried out by N2 physisorption technique using Micromeritics ASAP 2020 surface area and porosity analyzer to determine the specific surface area, cumulative pore volume and average pore diameter of these synthesized materials (as shown in Table 1). NH_3- and CO_2-TPD were applied to determine the acid-base properties of catalysts. In detail, TPD experiments were carried out using a flow apparatus; the catalyst sample (0.1g) was treated at 773 K in helium for 1 h and then saturated with 15% NH_3/He mixture or pure CO_2 flow after cooling to 373 K. After purging with helium, the sample was heated to 923 K under helium and the amount of acid-base sites on the catalyst surface was calculated from the desorption amount of NH_3 and CO_2, which was determined

by measuring the areas of the desorption profiles obtained from the Chemisorption System analyzer. According to these studies, the amount of acid sites for WO_3-ZrO_2, MgO-ZrO_2, and TiO_2-ZrO_2 are 281.5, 82.4 and 492 μmol g^{-1}, while the amount of base sites for these catalysts are 42.1, 44.9 and 693 μmol g^{-1}. Pd/MgO-ZrO_2, Pd/TiO_2-ZrO_2 and Pd/WO_3-ZrO_2 (5 wt% Pd) were prepared by impregnating MgO-ZrO_2, TiO_2-ZrO_2 and WO_3-ZrO_2 with $Pd(NO_3)_2$ solution (from Aldrich). The catalysts were further calcined and reduced with 10%H_2/He at 773 K for 6 h before use. The weight contents of Pd in Pd/MgO-ZrO_2, Pd/TiO_2-ZrO_2 and Pd/WO_3-ZrO_2 were determined by X-ray fluorescence (XRF) analysis. The reducibility percentage of Pd was measured and calculated from the degree of H_2 uptakes from the temperature-programmed reduction (TPR) test using 5% H_2 with the total flow rate of 100 cm^3 min^{-1} and temperature from room temperature to 773 K, while the dispersion percentage of Pd was identified from the volumetric H_2 chemisorption measurement using chemisorption analyzer. Furthermore, the catalyst specific surface areas were obtained from BET measurement. All physicochemical properties of the synthesized catalysts are presented in Table 3.1.

3.2.3 Experimental setting-up

In the present work, the reaction will be carried out in a 0.5 inch diameter stainless steel reactor placing vertically inside tubular furnace. Nitrogen will be used to purge and increase the pressure of the reactor. For the base condition, 0.1 g of sample will be mixed with 1 cm^3 of water (with and without the presence of 0.1 g catalyst) and N_2 will be loaded to raise the reactor pressure up to 2.5 MPa before placing the reactor in the furnace. In our system, a Type-K thermocouple will be placed into the annular space between the reactor and furnace with close contact to the catalyst bed to minimize the temperature difference between the furnace temperature and reaction temperature), Figure 3.2. The reaction temperature will be varied from 473 to 523, 573, 623, and 673 K, while the pressure inside the reactor will be measured by a pressure transducer (Kyowa, PGM-500 KD) connected to the reactor. After the reaction time is reached, the reactor will be quenched in a water bath to stop the reaction. After the reactions, the quantification and identification of gaseous and liquid-products will be conducted by GC-TCD (Shimadzu GC-14B) and HPLC (equipped with a Dionex PDA-100 photodiode array detector with a Shodex RSpak KC-811 of 8.0mmID x 300mm column). In this study, we focus on the hydrolysis and dehydration reactions with the possible side reaction of isomerization; therefore, the possible product species i.e. glucose, fructose, xylose, furfural, HMF and 1,6-anhydroglucose (AHG) were quantified.

Table 3.1 Physicochemical properties of synthesized catalysts

Catalysts	BET Surface Area[a] (m^2/g)	Cumulative Pore Volume[b] (cm^3/g)	Average Pore Diameter[c] (nm)	Metal loading[d] (wt.%)	Metal reducibility[e] (Pd%)	Metal dispersion[f] (Pd%)
WO_3-ZrO_2	92	0.189	3.4	-	-	-
TiO_2-ZrO_2	173	0.335	3.1	-	-	-
MgO-ZrO_2	112	0.245	3.0	-	-	-
Pd/WO_3-ZrO_2	88	0.172	3.6	4.9	94.9	4.83
Pd/TiO_2-ZrO_2	164	0.289	3.3	5.0	94.1	4.96
Pd/MgO-ZrO_2	103	0.216	3.1	4.9	95.2	4.92

[a] Error of measurement = ±5%.
[b] BJH desorption cumulative volume of pores between 1.7 and 300 nm diameter.
[c] BJH desorption average pore diameter.
[d] Measured from X-ray fluorescence analysis
[e] Pd reducibility (from temperature-programmed reduction with 5%hydrogen)
[f] Pd dispersion (from the volumetric H_2 chemisorption measurement using chemisorption analyze

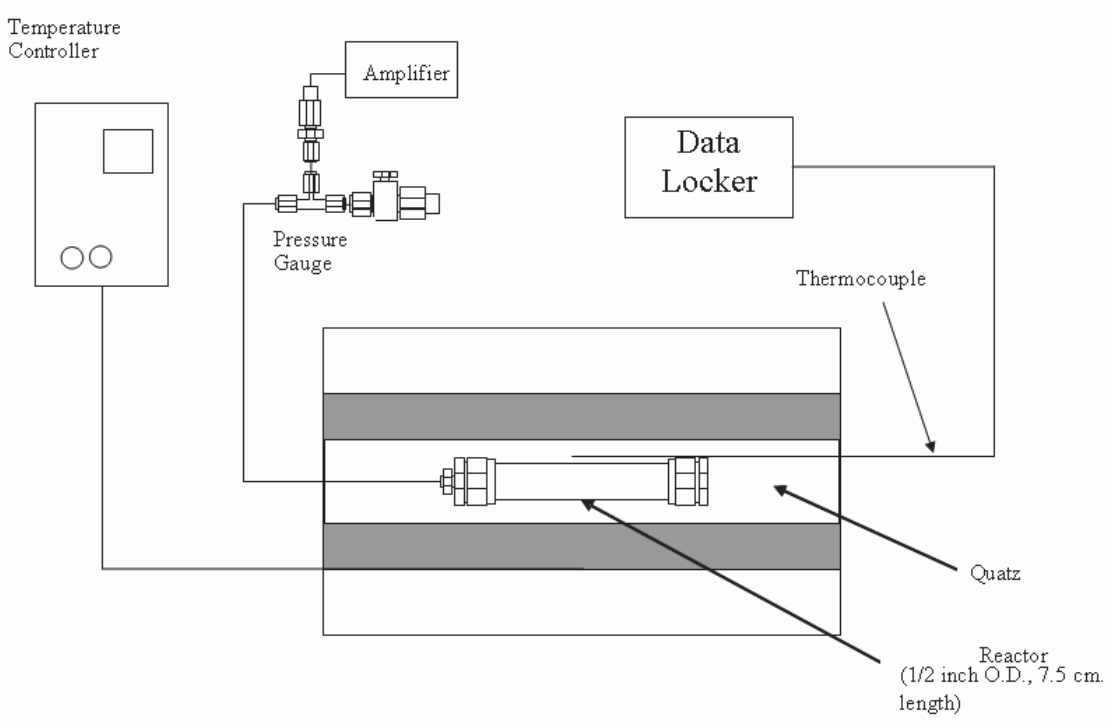

Fig. 3.2 Reactor set-up

The reaction temperature will be varied from 473 to 523, 573, 623, and 673 K, while the pressure inside the reactor will be measured by a pressure transducer (Kyowa, PGM-500 KD) connected to the reactor. After the reaction time is reached, the reactor will be quenched in a water bath to stop the reaction.

3.2.4 Experimental procedure

In the present work, the experiments are divided into 3 main parts (i) the study of aldol-condensation and subsequent hydrogenation reactions, (ii) the study of hydrolysis and dehydration reactions, and (iii) the integration of hydrolysis, dehydration, aldol-condensation and subsequent hydrogenation reactions in the single unit. Details of these three experimental steps are described more in the following sub-sections.

Hydrolysis and dehydration

A similar reactor was performed over these reactions under pressurized water and solvent (i.e. acetone). The reactor was initially loaded with the reaction mixture with catalyst and N_2 gas 25 bars was added before the reactor was loaded into the heating furnace. After the reaction temperature and time were reached, the reaction was immediately stopped by quenching in the water bath.

Aldol-condensation and hydrogenation

The reaction was carried out in a SS 316 stainless steel small tube bomb reactor (1/2 inch O.D. and 7.5 cm. length). This reactor was mounted vertically inside a tube furnace. The temperature controller was connected to the furnace in order to heat up and control the desired temperatures. The reactor was initially loaded with the reaction mixture with catalysts and added helium up to 10 bars before starting the aldol-condensation reaction which was controlled in reaction temperature. After stopping the aldol-condensation reaction, the hydrogenation reaction was then continued by adding H_2 in the reactor and the reactor was heated to 393 K. After the controlled reaction time was reached, the reactor was quenched in a water bath to stop the reaction. This study focuses on the liquid alkanes production. The overall product yields were analyzed by gas chromatography (Shimadzu 2010 model).

According to the hydrolysis/dehydration testing, constant amount of sample (i.e. corncob and waste cassava) and catalyst (i.e. TiO_2-ZrO_2, WO_3-ZrO_2 and H_3PO_4) were mixed with 1 cm^3 of aqueous solution (acetone with and without DMSO as co-solvent in water); then N_2 was loaded to raise the reactor pressure up before placing the reactor in the furnace. In our system, a Type-K thermocouple was placed into the annular space between the reactor and furnace with close contact to the catalyst bed to minimize the temperature difference between the furnace temperature and reaction temperature). The reaction temperature was varied from 473 to 523, 573, 623, and 673 K, while the pressure inside the reactor, measured by a pressure transducer (Kyowa, PGM-500 KD) connected to the reactor, was kept constant at 34.5 MPa in all experiments. After the reaction time was reached, the reactor was quenched in a water bath to stop the reaction. For the aldol-condensation/hydrogenation testing, the reactor was initially loaded with the reactant mixture (HMF, furfural and acetone) and catalysts; then helium was added up to 10 bar to start the aldol-condensation reaction at constant temperature (53^oC for the reaction of HMF with acetone and 80^oC for the reaction of furfural with acetone (Barrett et al., 2006)) for 30 h. After stopping the aldol-condensation reaction, the hydrogenation reaction was then continued by adding H_2 in the reactor and the reactor was heated and held at 393 K, 50 bar for 6 h (Barrett et al., 2006); then, the reactor was quenched in the water bath to stop the reaction.

According to the integrative hydrolysis/dehydration/aldol-condensation/ hydrogenation testing, the reactant mixture (i.e. corncob and waste cassava) and catalyst (i.e. Pd/TiO_2-ZrO_2, Pd/WO_3-ZrO_2 and Pd/MgO-ZrO_2) were mixed with acetone/DMSO in water and loaded in the reactor. Then, the experiment was carried out following the steps as described above; starting with the hydrolysis/dehydration, subsequently with the aldol-condensation and hydrogenation before stop the reaction in the water bath and withdrawn the samples out from the reactor for further analyses.

3.2.5 Product analysis

The quantification and identification of gaseous products were conducted by Gas Chromatography (Shimadzu GC-14B with Porapak Q column) connected with a thermal conductivity detector (TCD) and a frame ionization detector (FID). In order to satisfactorily separate all elements, the temperature setting inside the GC column was programmed varying with time. In the first 3 min, the column temperature was constant at 333 K, it was then increased steadily by the rate of 15 K min^{-1} until 393 K and lastly decreased to 333 K. The amounts of HMF and furfural were analyzed by High Performance Liquid Chromatography (Summit, Dionex Co., Germany), which consists of a Dionex PDA-100 photodiode array detector, a Dionex P680 pump system, a Dionex STH585 column oven and a Dionex ASI-100 automated sample injector equipped with a Shodex RSpak KC-811 (8.0mmID*300mm) column. HPLC system was based on UV absorbance at 280 nm by comparing to the corresponding standard curves and H_3PO_4 was used as the eluent with the injection volume of 20 μl at a flow rate of 0.4 ml/min. The retention time for HMF and furfural was 49.5 and 80.5 min, respectively. The selectivity and yield of water-soluble organic compounds (C_5-C_{15}) production were analyzed by the GC-FID (Shimadzu 2010 model) with capillary column (50m x 0.2mm and 0.5μm); the GC was accomplished with the injector, detector and column temperature of 220^oC, 280^oC and 200^oC, respectively.

It is noted according to the measurement of total carbon amount in the aqueous solution after reaction that the TOC (total organic carbon) values for all experiments were always higher than 86% indicated that the quantity of gaseous products from the reactions were considerably less than that of liquid products. Hence, we here reported the results and discussion only for the liquid products from the reactions. For the hydrolysis/dehydration reactions, the possible product species i.e. glucose, fructose (from the isomerization of glucose), xylose, furfural, HMF and 1,6-anhydroglucose (AHG) were quantified. For the aldol-condensation reaction, the conversion of HMF and furfural was identified, whereas for the aldol-condensation/hydrogenation and the integrative hydrolysis/dehydration/aldol-condensation/hydrogenation reactions, the analyzed product species were water-soluble organic compounds (C_5-C_{15}). The yield of each product was calculated by the carbon balance, defined as the ratios of the amount of carbon atom in the specified product to the amount of carbon atom in the loaded feedstock, while the selectivity of water-soluble organic compounds (C_5-C_{15}) was reported as the ratio of specified water-soluble organic compound species to the total water-soluble organic compounds in the final liquid product.

3.3 Results and discussion

3.3.1 Results on hydrolysis/dehydration reactions

Sugarcane bagasse, rice husk and corncob were used as the samples of lignocellulosic biomasses in the present work. The percentages of cellulose, hemicellulose, and lignin for these samples are 0.44:0.29:0.20, 0.28:0.28:0.24, and 0.50:0.31:0.15. Before undergoes the reaction testing, these feedstocks were ground with a ball-milling to become fine particle with the average particle size of 75 μm. It should be noted that the reactions of sugar (i.e. glucose and xylose), cellulose, and xylan (representative for hemicellulose) were also carried out. These materials were supplied from Aldrich and Ajax Finechem. The reactions in the presence of various catalysts i.e. TiO_2, ZrO_2 and TiO_2-ZrO_2 prepared by various methods and treated under different conditions were studied. The synthesized TiO_2, ZrO_2 and TiO_2-ZrO_2 by (co-) precipitation, sol-gel, and physical mixing were denoted as Ti-P, Ti-S, Zr-P, Zr-S, TiZr-P, TiZr-S and TiZr-M. The catalysts calcined at different temperatures (i.e. 773, 873 and 973 K) were denoted as Ti-P-773, Ti-P-873 and Ti-P-973 (which means TiO_2 prepared by precipitation method and calcined at 773, 873 and 973 K).

Lignocellulosic biomass reactions under HCW condition

As the base condition, the reaction of sugarcane bagasse was firstly studied under HCW condition with and without adding of solid catalysts. It was found that the main products from the reaction were glucose, fructose, xylose, furfural, HMF and AHG indicated the occurring of hydrolysis, isomerization and dehydration reactions. The yields of these liquid products from the reaction at various conditions are shown in Figs. 3.5-3.7. It can be seen from Fig. 3.5 (a)-(c) that, at 523 K with the reaction time of 5 min, the presence of catalyst makes significant impact on the yield and selectivity of products; furthermore, the preparation procedure and calcination temperature also affect the catalyst performance. For TiO_2 and ZrO_2, the precipitation method with low calcination temperature (773 K) provide higher yield of total liquid products than the catalysts prepared by sol-gel method with high calcination temperature (873 and 973 K), whereas for TiO_2-ZrO_2 the highest total product yield was observed from the catalyst prepared by co-precipitation method with the calcination temperature of 873 K.

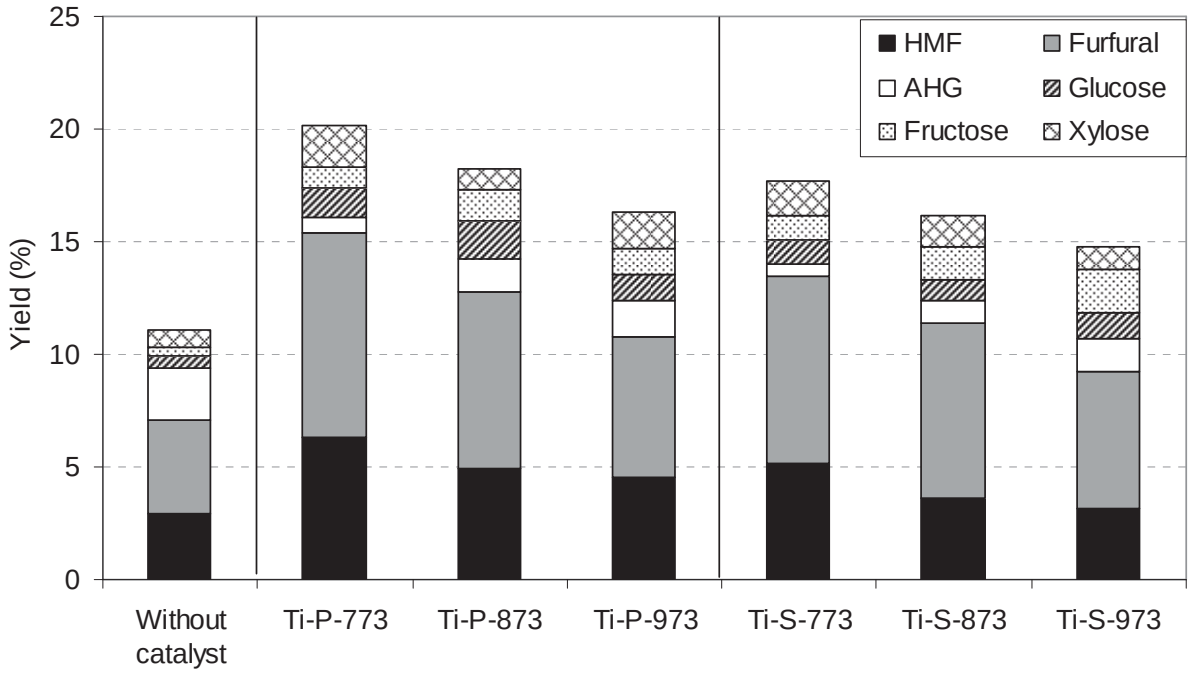

Fig. 3.5 (a)

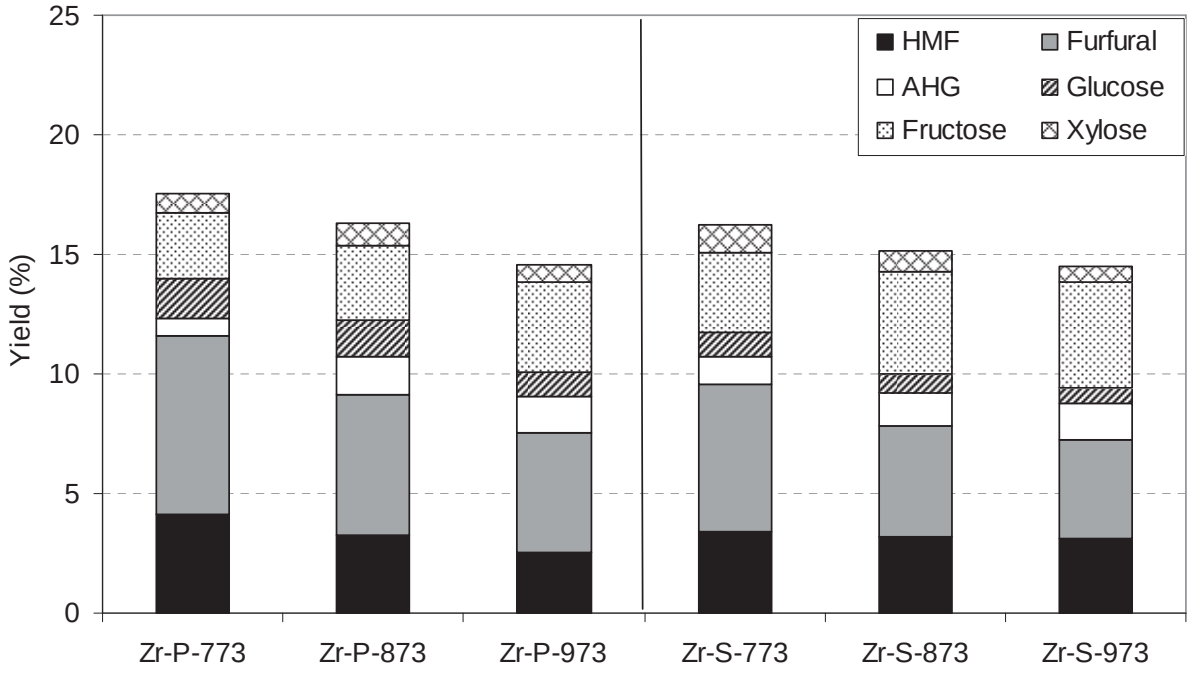

Fig. 3.5 (b)

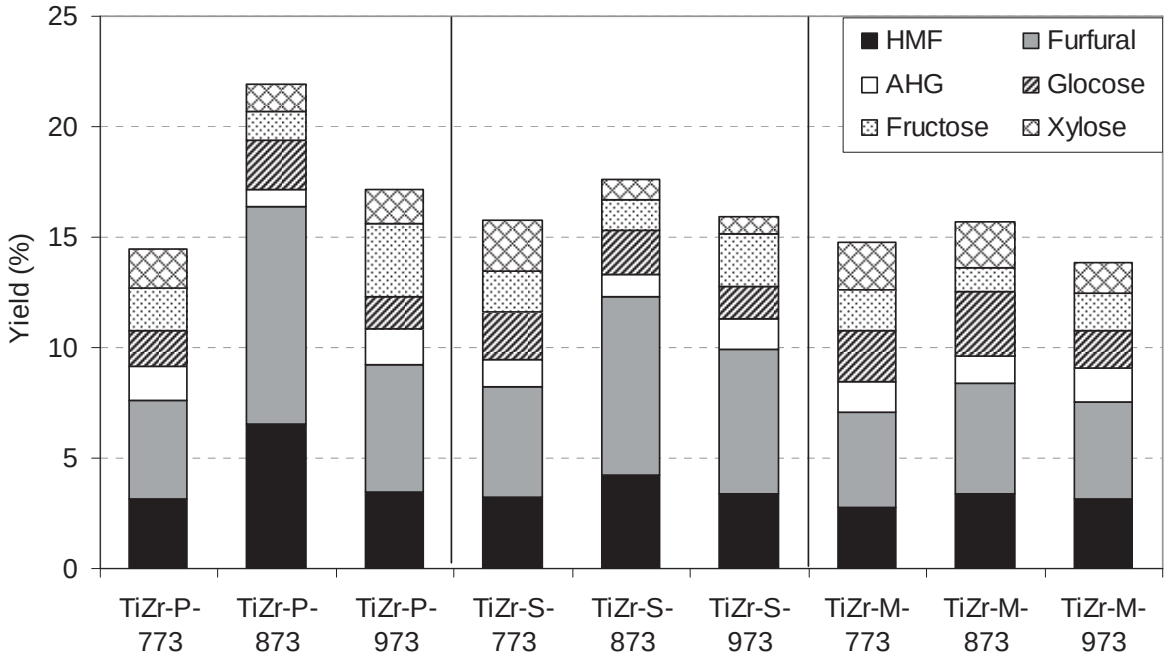

Fig. 3.5 (c)

Fig. 3.5 Yield of liquid products from the reaction of sugarcane bagasse at 523 K and 5 min in the presence of (a) TiO_2, (b) ZrO_2 and (c) TiO_2-ZrO_2 (prepared by various methods and treated under different conditions)

Clearly, among all catalysts, TiO_2-ZrO_2 was the most active one in terms of total product yields and HMF-furfural selectivities. It can also be seen that the reaction in the presence of ZrO_2 provided the greatest amount of fructose in the product indicated the promotion of isomerization reaction by this catalyst as previously reported by Watanabe *et al* [8, 10], whereas the presence of TiO_2 and TiO_2-ZrO_2 obviously inhibited the yield of AHG. The high HMF and furfural productions with low AHG and fructose formations observed over TiO_2 and TiO_2-ZrO_2 could be due to the strong isomerization of glucose to fructose following with the rapid dehydration of fructose to HMF by these catalysts. To prove this clarification, the experiments with various reaction times (1, 2, 3, 4 and 5 min) were carried out. It was found that initially within the first 1-2 min, high amount of fructose was observed; but it decreased with increasing reaction time, whereas the yield of HMF increased rapidly with increasing reaction time before reaching steady state value at 5 min. Fig. 3.6 shows the effect of Ti/Zr molar ratio for TiO_2-ZrO_2 (prepared by co-precipitation) on the catalyst reactivity; it can be seen that TiO_2-ZrO_2 with Ti/Zr molar ratio of 1/1 provides the highest HMF and furfural productions. The effect of reaction temperature was also studied by varying the temperature from 473-673 K as shown in Fig. 3.7; the highest yield of liquid products can be achieved at the reaction temperature of 523 K for all catalysts.

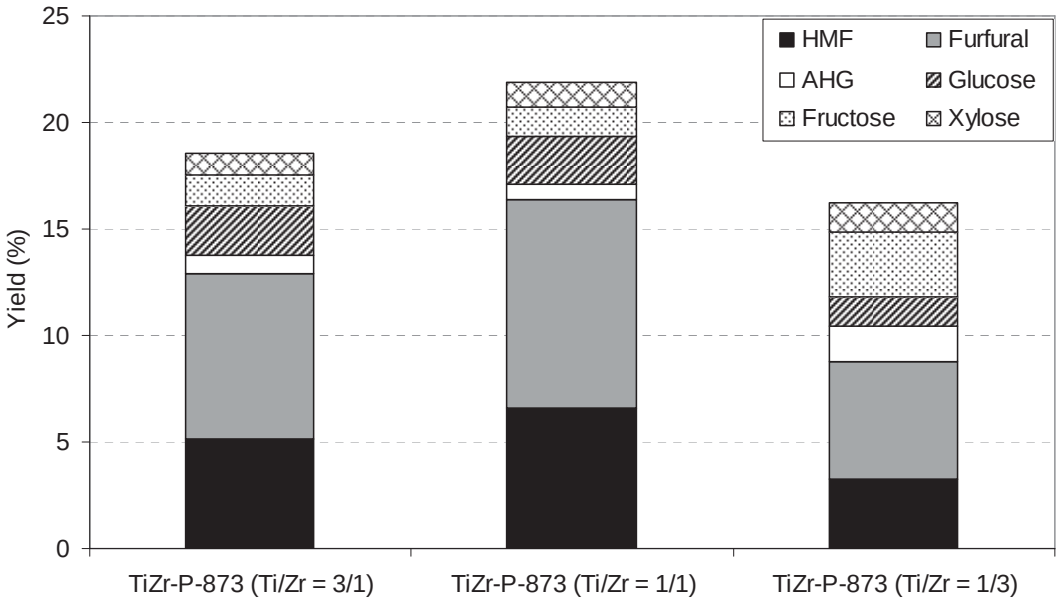

Fig. 3.6 Yield of liquid products from the reaction of sugarcane bagasse at 523 K and 5 min in the presence of TiO_2-ZrO_2 with various Ti/Zr ratios

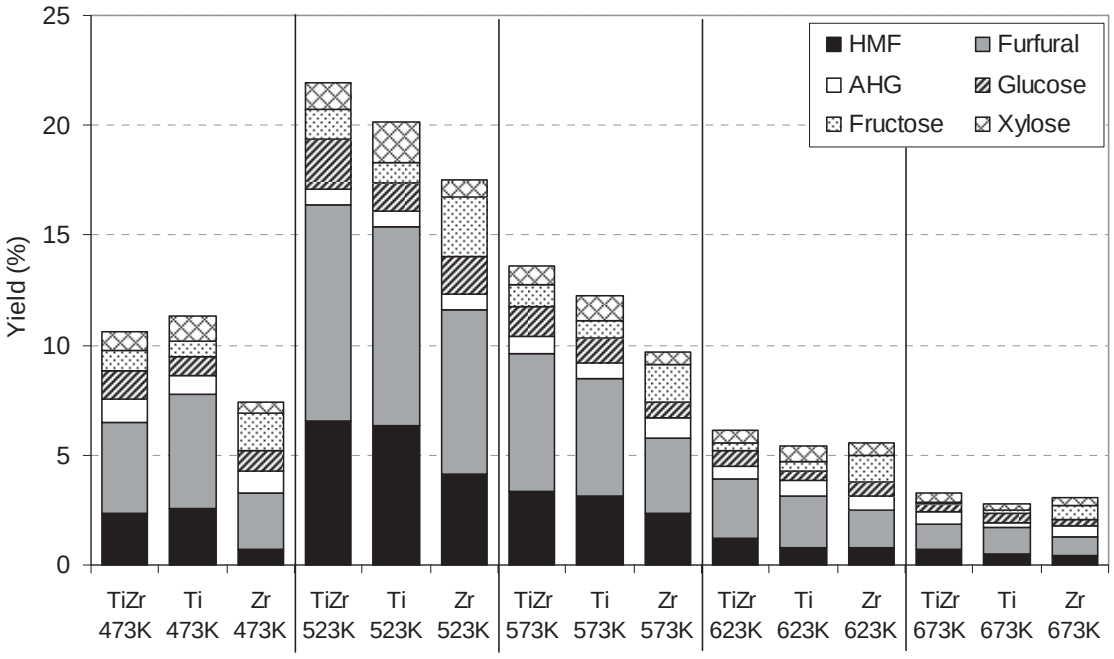

Fig. 3.7 Effect of reaction temperature (473 to 673 K) on the yield of liquid products from the reaction of sugarcane bagasse in the presence of various catalysts

For comparison, the reactions of rice husk and corncob were then studied at selected conditions (523 K in the presence of TiO_2-ZrO_2 with Ti/Zr molar ratio of 1/1 and calcined at 873 K). The yields of liquid products from these three different lignocellulosic

biomasses are presented in Fig. 3.8. Among them, the reaction of corncob provided the highest furfural and HMF productions, whereas those produced from the reaction of rice husk were the lowest. These results are closely related to the amounts of cellulose and hemicellulose in each feedstock since the portions of cellulose and hemicellulose in corncob are significantly higher than those in sugarcane bagasse and rice huck.

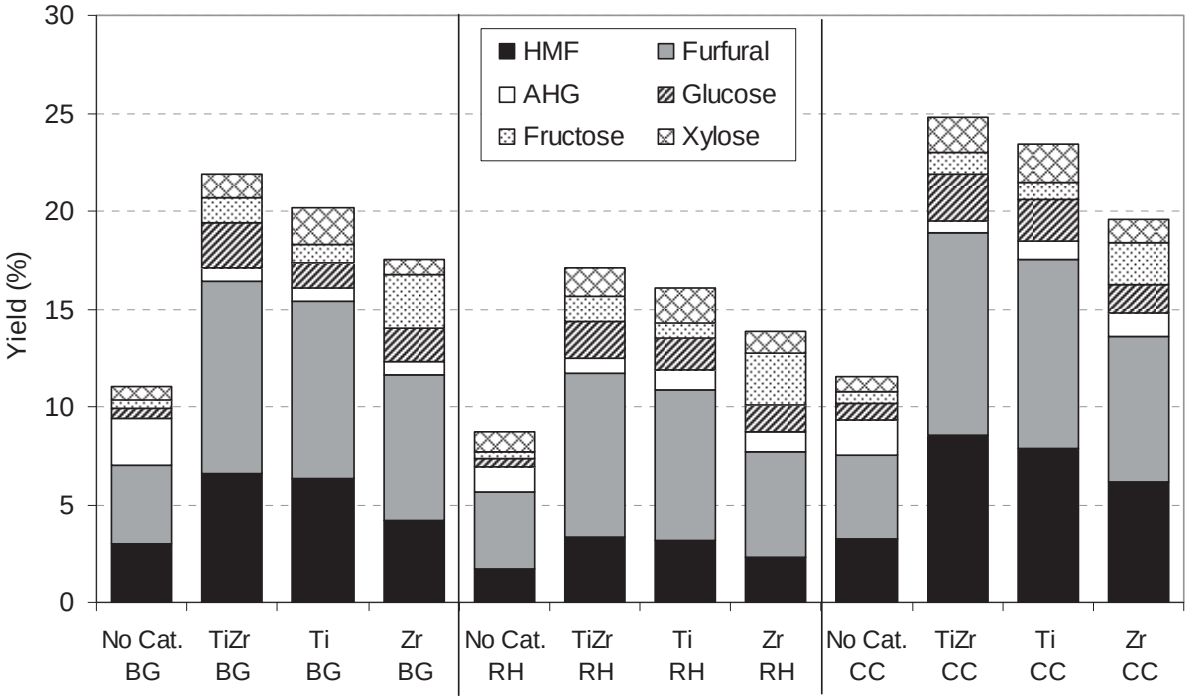

Fig. 3.8 Yield of liquid products from the reaction of sugarcane bagasse (BG), rice husk (RH) and corncob (CC) (at 523 K and 5 min with and without the presence of catalysts)

It is noted that the reusability of catalysts was also tested. After separated from water solution, the catalysts were washed and dried before re-testing the reaction at the same operating conditions. As shown in Fig. 3.9, the reactivities of spent catalysts are almost identical to the fresh one indicated its well-reusable. This highlights the great benefit of heterogeneous oxide-based catalyst compared to the typical homogeneous catalysts (e.g. H_2SO_4).

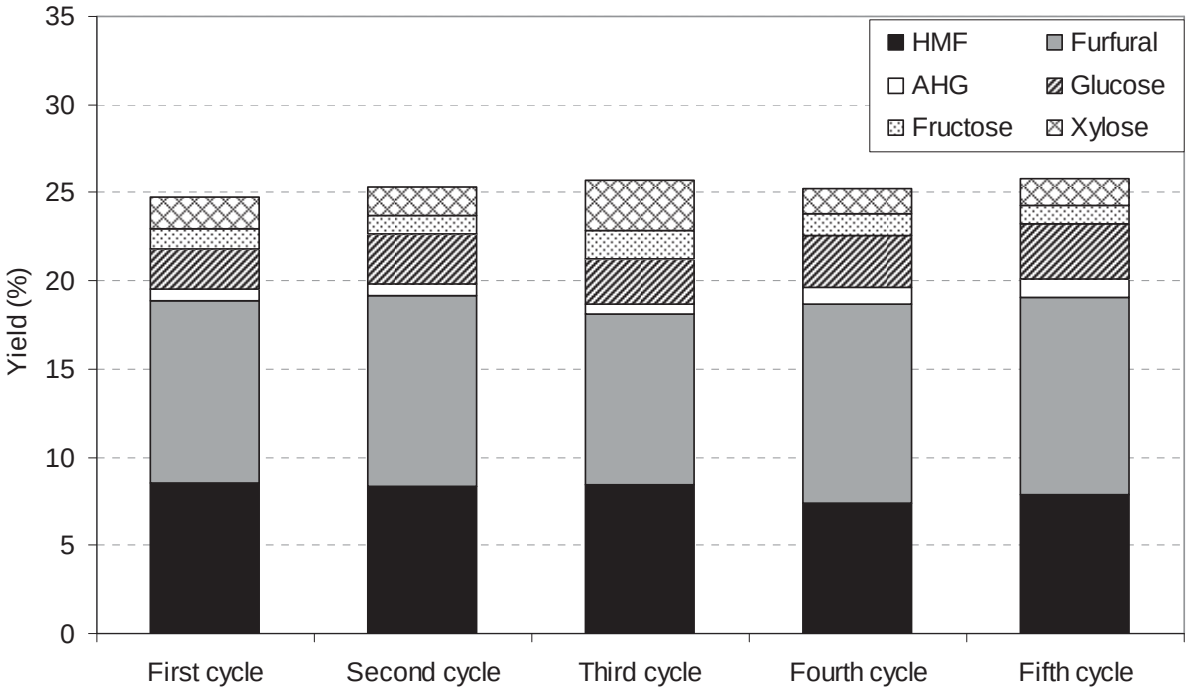

Fig. 3.9 Reusability testing of TiZr-P-883 toward the reaction of corncob at 523 K

After getting the optimum conditions for hydrolysis/dehydration of lignocellulosic biomass, the reaction testing of TiZr-P-883 toward the reaction of waste cassava at 523 K was carried out for comparison. From the study, it was found that higher yields of HMF, furfural, glucose, fructose and xylose than corncob can be achieved (11.3% HMF, 14.3% furfural, 4.4% glucose, 3.7% fructose and 3.5% xylose). This could be due to the easier hydrolysis/dehydration of starch compound when compared to cellulose and hemicellulose.

Catalyst characterizations

To understand the role of each catalyst (prepared by different methods and conditions) on the interested reactions, the physical characteristics of all synthesized catalysts i.e. surface properties, phase formation, and acidity-basicity properties were determined by BET, XRD and NH_3- and CO_2-TPD measurements; the results of these characterizations are summarized in Tables 3.2 and 3.3 and Fig. 3.10.

Table 3.2 N_2 Physisorption (BET) results of TiO_2, ZrO_2 and TiO_2-ZrO_2 (prepared by various methods and treated under different conditions)

Catalysts	BET Surface Area[a] (m^2/g)	Cumulative Pore Volume[b] (cm^3/g)	Average Pore Diameter[c] (nm)
Ti-P-773	48.2	0.120	4.6
Ti-P-873	35.9	0.109	4.9
Ti-P-973	20.1	0.098	5.2
Ti-S-773	36.3	0.096	4.9
Ti-S-873	25.9	0.073	5.3
Ti-S-973	11.7	0.051	5.4
Zr-P-773	124	0.234	4.3

Zr-P-873	101	0.217	4.6
Zr-P-973	76.3	0.210	4.6
Zr-S-773	95.2	0.147	4.6
Zr-S-873	73.9	0.110	5.1
Zr-S-973	54.0	0.079	5.3
TiZr-P-773 (Ti/Zr=1/1)	198	0.394	2.5
TiZr-P-873 (Ti/Zr=1/1)	187	0.391	2.5
TiZr-P-973 (Ti/Zr=1/1)	165	0.382	2.7
TiZr-S-773 (Ti/Zr=1/1)	163	0.259	3.3
TiZr-S-873 (Ti/Zr=1/1)	149	0.217	3.9
TiZr-S-973 (Ti/Zr=1/1)	119	0.194	4.2
TiZr-M-773 (Ti/Zr=1/1)	121	0.201	3.8
TiZr-M-873 (Ti/Zr=1/1)	109	0.155	4.4
TiZr-M-973 (Ti/Zr=1/1)	97.4	0.150	4.9
TiZr-P-873 (Ti/Zr=3/1)	109	0.181	3.9
TiZr-P-873 (Ti/Zr=1/3)	130	0.271	4.3

[a] Error of measurement = ±5%.
[b] BJH desorption cumulative volume of pores between 1.7 and 300 nm diameter.
[c] BJH desorption average pore diameter.

Table 3.3 acid-base properties of TiO_2, ZrO_2 and TiO_2-ZrO_2 (prepared by various methods and treated under different conditions)

Catalysts	Amount of acid site (μmol/g)	Density of acid site (μmol/m^2)	Amount of base site (μmol/g)	Density of base site (μmol/m^2)
Ti-P-773	161	3.34	84	1.74
Ti-P-873	108	3.00	86	2.39
Ti-P-973	59.1	2.94	92	4.58
Ti-S-773	70.7	1.95	84	2.32
Ti-S-873	47.3	1.83	87	3.37
Ti-S-973	18.0	1.54	88	7.51
Zr-P-773	232	1.87	129	1.04
Zr-P-873	177	1.75	145	1.44
Zr-P-973	119	1.56	166	2.19
Zr-S-773	171	1.80	138	1.45
Zr-S-873	119	1.61	149	2.02
Zr-S-973	62.1	1.15	170	3.14
TiZr-P-773 (Ti/Zr=1/1)	692	3.49	697	3.52
TiZr-P-873 (Ti/Zr=1/1)	645	3.45	712	3.81
TiZr-P-973 (Ti/Zr=1/1)	554	3.35	806	4.89
TiZr-S-773 (Ti/Zr=1/1)	471	2.89	654	4.01
TiZr-S-873 (Ti/Zr=1/1)	393	2.64	672	4.51
TiZr-S-973 (Ti/Zr=1/1)	301	2.53	687	5.78
TiZr-M-773 (Ti/Zr=1/1)	216	1.79	215	1.78
TiZr-M-873 (Ti/Zr=1/1)	183	1.68	219	2.01
TiZr-M-973 (Ti/Zr=1/1)	137	1.41	226	2.33
TiZr-P-873 (Ti/Zr=3/1)	309	2.84	84	1.74
TiZr-P-873 (Ti/Zr=1/3)	256	1.97	86	2.39

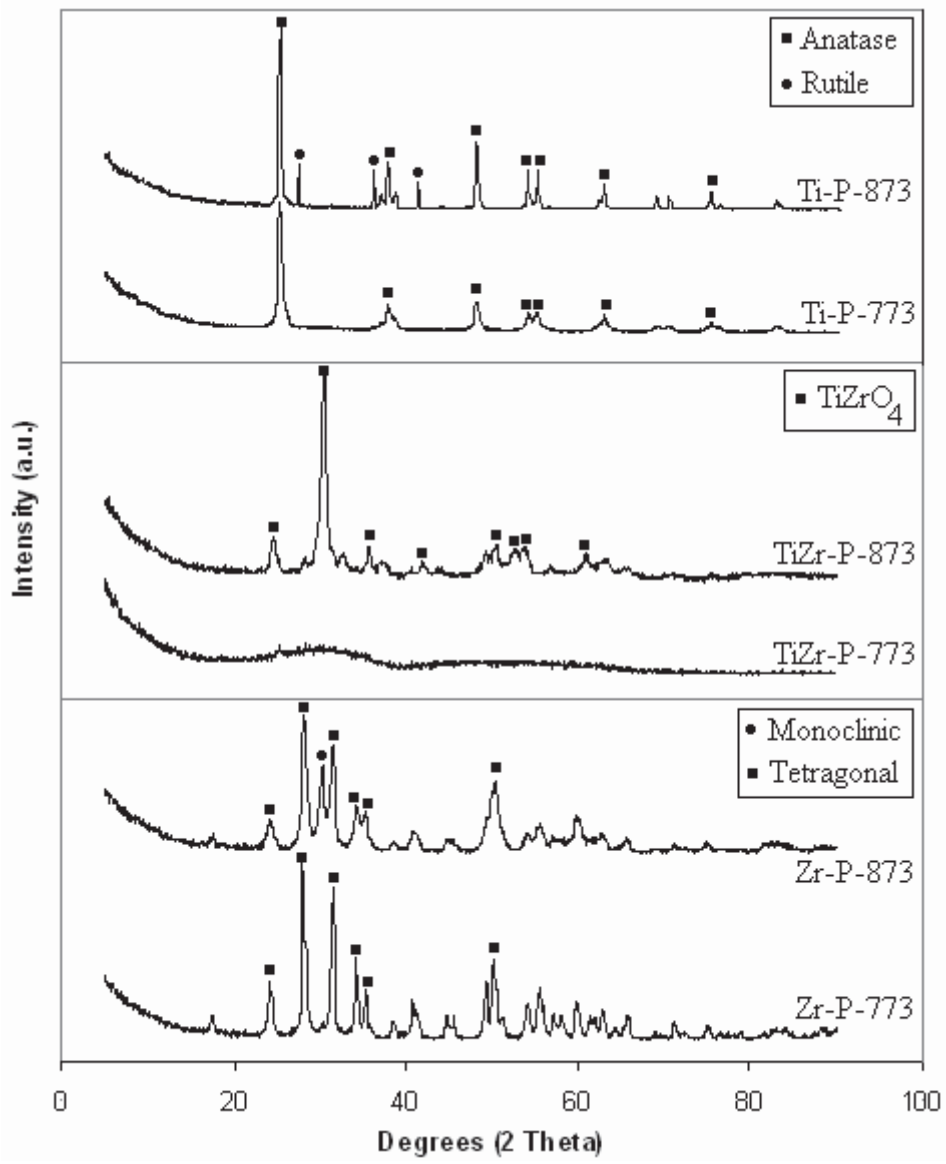

Fig. 3.10 XRD patterns of TiO_2, TiO_2-ZrO_2 and ZrO_2 calcined at different temperatures

As seen in Table 3.2, the BET results indicated that among all catalyst TiO_2-ZrO_2 (with Ti/Zr molar ratio of 1/1) shows the greatest specific surface area. It can also be seen that the calcination temperature, preparation procedure and Ti/Zr molar ratio (for TiO_2-ZrO_2) significantly affect the specific surface area, cumulative pore volume and average pore diameter of all synthesized catalysts. The specific surface area and cumulative pore volume linearly decreased with increasing calcination temperature, whereas the average pore diameter dramatically increased. Furthermore, among all preparation procedures, (co-) precipitation method can synthesize material with highest specific surface area. According to the XRD measurements (Fig. 10), the main phase observed for TiO_2-ZrO_2 is $TiZrO_4$. It is noted that TiO_2-ZrO_2 is in amorphous phase when calcined at 773 K, but the phase turns to be crystalline at higher alcinations temperature (> 873 K). As for TiO_2, the anatase crystalline phase was mainly found when calcined at 773 K; however, with increasing the alcinations temperature (973 K), rutile phase was also detected

along with anatase crystalline phase. Lastly, the XRD pattern of ZrO_2 indicated the containing of both tetragonal and monoclinic phases with various contents depending on the calcinations temperature; we found that the crystal size in monoclinic phase and the fraction of monoclinic phase increased considerably with increasing calcinations temperature, whereas tetragonal phase decreased.

NH_3- and CO_2-TPD techniques were used to measure the acid-base properties of the catalysts; the amounts of acid and base sites, which were calculated from the area below curves of these TPD profiles, are listed in Table 3.3. Along with these values, the distribution of acid and base site on the catalyst surface (namely the density of acid and base site; μmol m^{-2}) and the strength of acid and base sites (the top peak of TPD spectra) are also given in the table since these parameters are important indicators to determine the catalytic reactivity of acid and base reactions. Among all catalysts, TiO_2-ZrO_2 with Ti/Zr molar ratio of 1/1 shows the greatest amounts and densities for both acid and base sites; in addition, the highest peaks of NH_3- and CO_2-TPD spectra for this catalyst was relatively lower than other two catalysts indicated that the strengths of acid and base sites for TiO_2-ZrO_2 were weak. It should be noted that the calcinations temperature and preparation procedure also affect the acidity-basicity properties of catalysts; the amount of acid sites decreased with increasing the calcinations temperature whereas the base sites increased for all catalysts. As for the preparation procedure, the catalysts prepared by co- precipitation method gained the greatest acidity-basicity properties, whereas those from physical mixing were the lowest.

According to the catalyst reactivity and all characterization results, it can be concluded that the catalyst reactivity, phase formation and acidity-basicity properties are closely related. The catalyst with "high acid site density" and "weak acid site" can enhance the great reactivity toward hydrolysis and dehydration reactions, while the catalyst with "high base site density" and "weak base site" provides high reactivity toward isomerization reaction. Hence, high HMF and furfural productions can be achieved from TiO_2-ZrO_2 (prepared by co-precipitation method with Ti/Zr molar ratio of 1/1) since this catalyst shows the bifunctionality for both acidity and basicity properties, according to the TPD experiments. It is noted that the acidity of TiO_2 and ZrO_2 decreased with increasing temperature, thus the reactivities of catalysts that calcined at low temperature (773 K) is greater than those calcined at higher temperatures. Nevertheless, for TiO_2-ZrO_2 the best reactivity was observed from the catalyst calcined at 873 K; the use of lower calcinations temperature (773 K) resulted in the low reaction reactivity, whereas the catalyst calcined at higher temperature (973 and 1073 K) was also found inactive (due to the reducing of catalyst acidity at high calcinations temperature). According to the XRD patterns of TiO_2-ZrO_2, the phase of TiO_2-ZrO_2 turns from amorphous to crystalline phase at 873 K; hence this revealed the impact of catalyst phase formation on its reaction reactivity (the crystalline phase is the active one for the interested reactions). It can also be seen from the studies that the phase TiO_2 and ZrO_2 also affected its reaction reactivity i.e. TiO_2 calcined at low temperature of 773 K (mainly anatase phase) showed better reactivity than that calcined at higher temperature (slight formation of rutile phase detected); this result is in good agreement with the results reported by Watanabe et al who indicated that anatase-TiO_2 showed better dehydration reactivity than rutile-TiO_2. As for ZrO_2, we found that the catalyst with larger portion of tetragonal phase (compared to monoclinic phase) shows greater reactivities toward hydrolysis and dehydration.

3.3.2 Sequential aldol-condensation/hydrogenation of HMF and furfural

Following the hydrolysis/dehydration studies, the aldol-condensation and hydrogenation reactions were then carried out over HMF and furfural compounds (representative as the major intermediate products from the hydrolysis/dehydration step). Firstly, the aldol-condensation reaction was carried out in the presence of WO_3-ZrO_2, TiO_2-ZrO_2, and MgO-ZrO_2 at 353 K with inlet HMF/acetone and furfural/acetone molar ratios of 1/1 (Barrett et al., 2006). Fig. 3.11 shows the variations of HMF and furfural conversions with time; it can be seen that the conversions of both compounds steadily increased with increasing reaction time and reached steady state after 27-30 h. Among these three catalysts, WO_3-ZrO_2 and MgO-ZrO_2 showed considerably greater activity than TiO_2-ZrO_2 (86-90% HMF and furfural conversions compared to 68-71% HMF and furfural conversions). This result also supports the suggestion that TiO_2-ZrO_2 is unsuitable for the reaction in the presence of acetone, while the comparable activities of WO_3-ZrO_2 and MgO-ZrO_2 toward this reaction could be due to their almost identical amount of base site (42.1 and 44.9 μmol g^{-1}), according to the CO_2-TPD study since Barrett et al. (2006) and Huber et al (2006) indicated that the aldol-condensation is the base-catalyzed reaction.

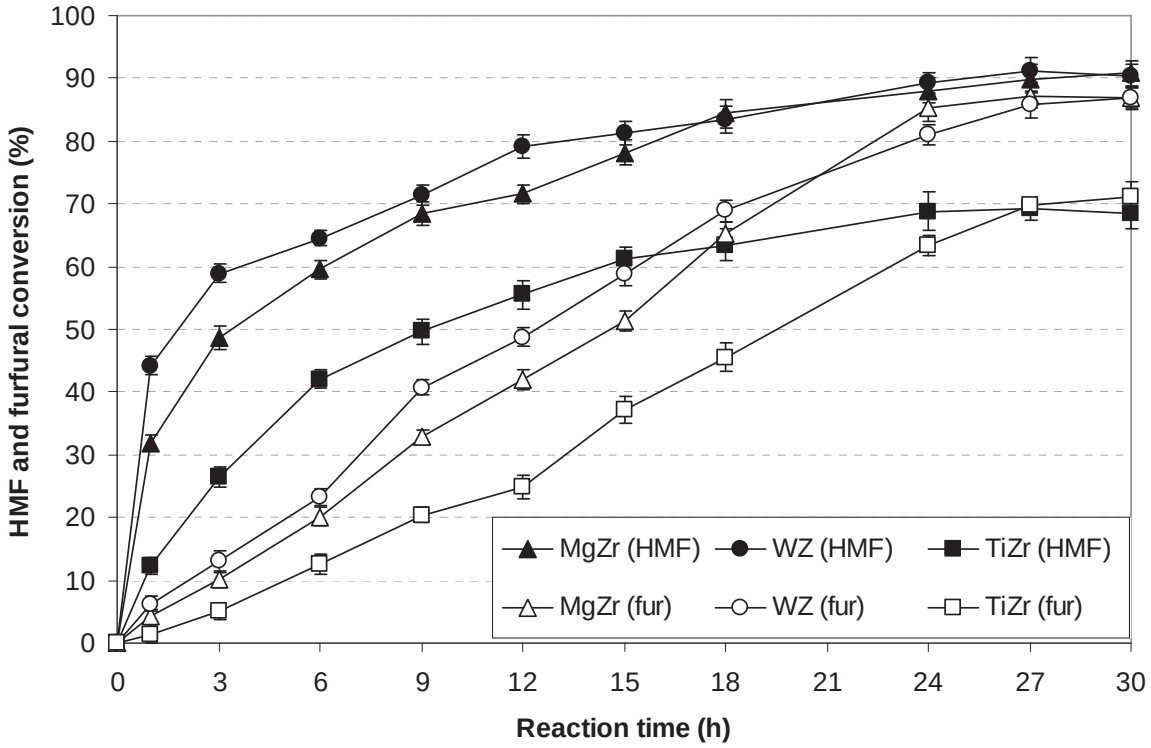

Fig. 3.11 Variations of HMF and furfural conversions with time from the aldol-condensation reaction in the presence of WO_3-ZrO_2, TiO_2-ZrO_2, and MgO-ZrO_2 (at 353 K with inlet reactant/acetone molar ratio of 1/1)

As the next step, the sequential aldol-condensation/hydrogenation of HMF and furfural were carried out. Instead of WO_3-ZrO_2, TiO_2-ZrO_2, and MgO-ZrO_2, Pd/WO_3-ZrO_2, Pd/TiO_2-ZrO_2, and Pd/MgO-ZrO_2 were applied as catalysts. It is noted that we also examined the activities of these catalysts toward the aldol-condensation reaction and found that the catalytic activities of Pd/WO_3-ZrO_2, Pd/TiO_2-ZrO_2, and Pd/MgO-ZrO_2 are almost identical to WO_3-ZrO_2, TiO_2-ZrO_2, and MgO-ZrO_2 respectively; hence it can be

indicated that the impregnating of Pd shows no affect on the aldol-condensation reaction. After the aldol-condensation step (with the reaction time of 30 h in all experiments), the hydrogenation reaction was started by pressurizing the reactor with hydrogen to 55 bar, heating up to 393 K and holding for 6 h (Barrett et al., 2006). From the reactions, C_5-C_{13} and C_6-C_{15} water-soluble organic compounds were produced from the combined aldol-condensation/hydrogenation reactions of furfural and HMF, respectively, as shown in Fig. 3.12.

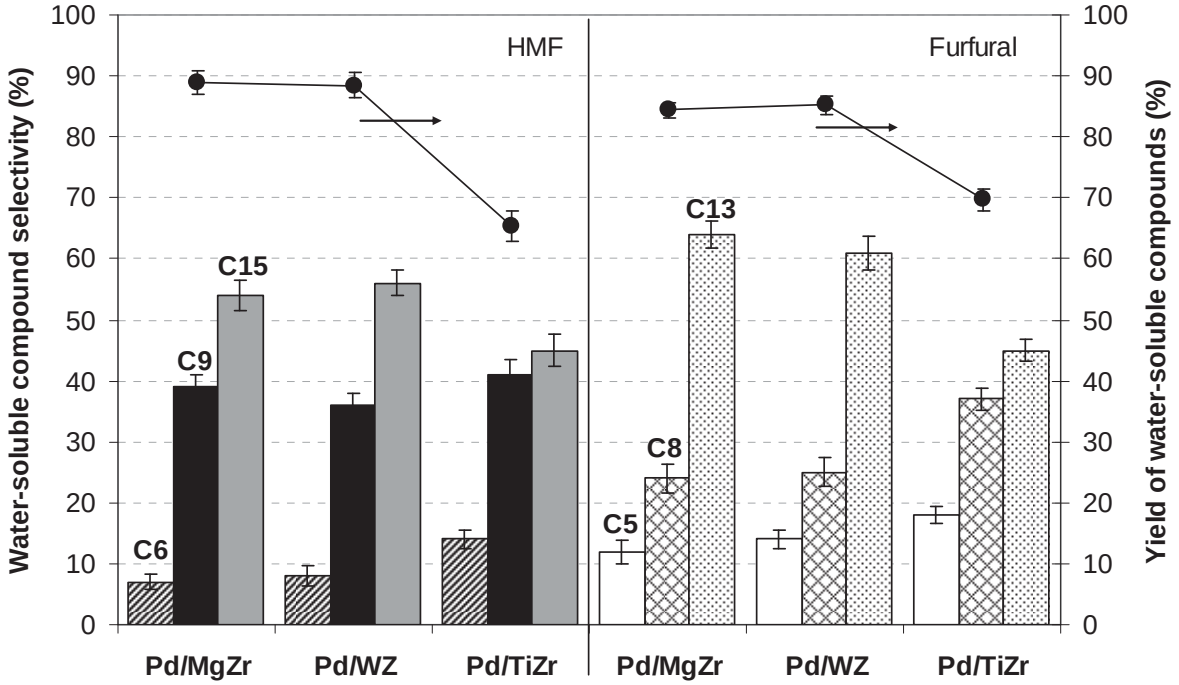

Fig. 3.12 Yields and selectivity of water-soluble C_5-C_{15} organic compounds from the sequential aldol-condensation/hydrogenation of furfural and HMF (aldol-condensation temperature of 353 K for 30 h and hydrogenation temperature of 393 K for 6 h)

It can be seen from the figure that the yield of water-soluble organic compounds from the reaction over Pd/WO_3-ZrO_2 and Pd/MgO-ZrO_2 are relatively higher than that over Pd/TiO_2-ZrO_2. From the studies, we summarized that Pd/WO_3-ZrO_2 and Pd/MgO-ZrO_2 are the good catalysts for the sequential aldol-condensation/hydrogenation reaction. Therefore, both catalysts were chosen for the further studies on the integrative hydrolysis/dehydration/aldol-condensation/hydrogenation of corncob and waste cassava to water-soluble organic compounds in the single reactor.

3.3.3 Integrative hydrolysis/dehydration/aldol-condensation/hydrogenation of biomass (lignocellulose) and biomass-derived carbohydrate

As the main purpose of this study, the integrative hydrolysis/dehydration/aldol-condensation/hydrogenation of corncob and waste cassava in the single reactor was carried out. Based on the information received from previous sections, the starting materials (i.e. corncob and waste cassava) was mixed with acetone/DMSO solution (with acetone:DMSO of 70:30) and the catalyst was added prior the pressurization and reaction. In the study, four catalyst systems (with the same total catalyst weight)

including (i) single Pd/WO_3-ZrO_2; (ii) single Pd/MgO-ZrO_2; (iii) combination of WO_3-ZrO_2 with Pd/MgO-ZrO_2; and (iv) combination of H_3PO_4 with Pd/MgO-ZrO_2 were investigated. Regarding the reaction testing conditions, the hydrolysis/dehydration was firstly carried out at 523 K and 34.5 MPa with the reaction time of 5 min. Subsequently, the reactor was cooled down and the sequential aldol-condensation/hydrogenation was continuously performed starting with the aldol-condensation step at 353 K for 30 h; following with the hydrogenation step by pressurized the reactor with hydrogen, then heated to 393 K and held for 6 h. Afterward, the reaction was stopped by quenching in the water bath and the liquid product was taken out for further analyses. Fig. 3.13 presents the yield of water-soluble organic compounds from the reactions of corncob and waste cassava (it is noted that this yield can be calculated based on Eqs. 1 and 2 but applying $moles_{corncob}$ and/or $moles_{waste\ cassava}$ instead of $moles_{HMF}$ and $moles_{furfural}$).

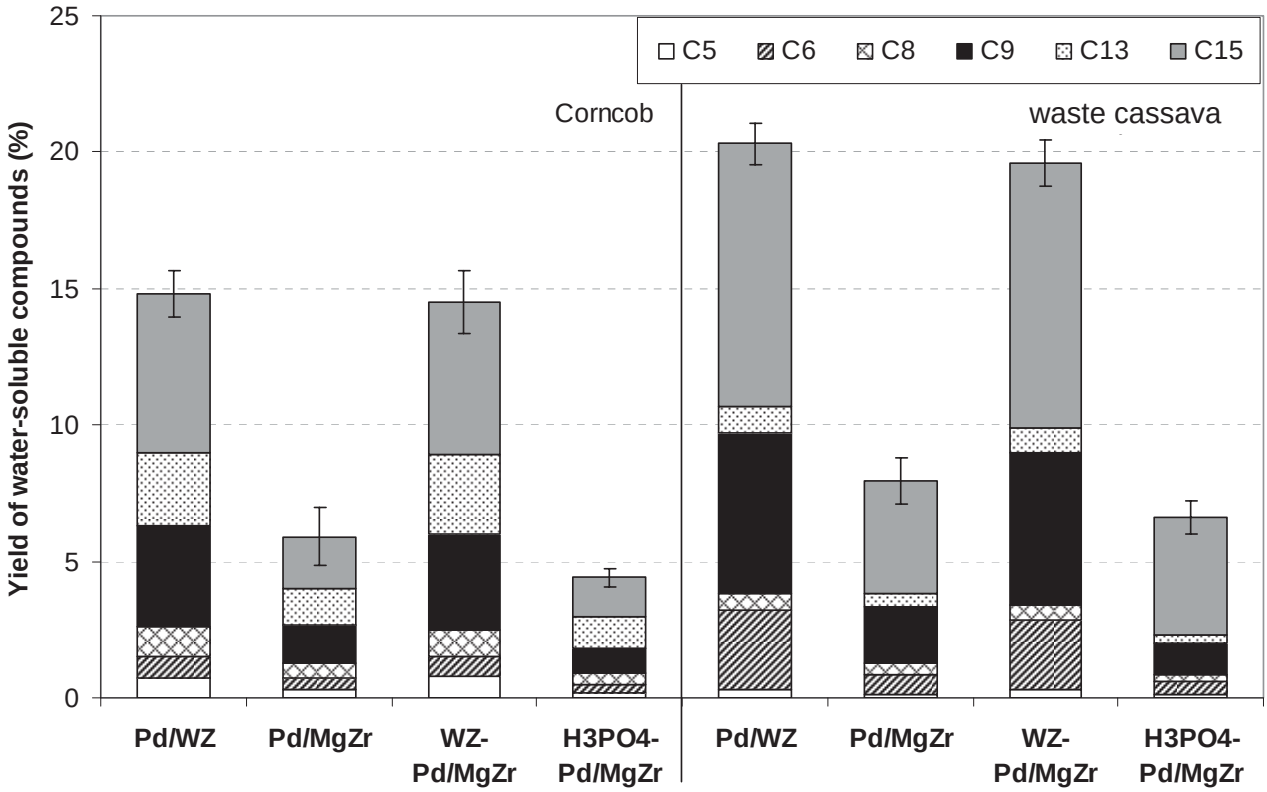

Fig. 13 Yield of water-soluble C_5-C_{15} organic compounds from the integrative hydrolysis/dehydration/aldol-condensation/hydrogenation of corncob and waste cassava in the presence of various catalyst systems (hydrolysis/dehydration temperature of 523 K for 5 min; aldol-condensation temperature of 353 K for 30 h and hydrogenation temperature of 393 K for 6 h)

It was found that the water-soluble organic compounds (with the carbon molecules of C_5, C_6, C_8, C_9, C_{13} and C_{15}) were observed with different selectivity depending on the type of feedstock; the reaction of waste cassava relatively produced higher C_6, C_9, and C_{15} selectivities, whereas the reaction of corncob generated more C_5, C_8, and C_{13} selectivities. This difference is mainly due to the containing of hemicellulose in corncob, which mainly converts to xylose and furfural via hydrolysis and dehydration

reaction, respectively. In contrast, the hydrolysis of waste cassava mostly produces glucose and fructose, which typically converts to HMF via dehydration reaction. C_5, C_8, and C_{13} compounds are the major products from the reaction of furfural, whereas C_6, C_9, and C_{15} compounds are from the reaction of HMF. It can also be seen from the figure that the yield of water-soluble organic compounds from the reaction of waste cassava is higher than that from the reaction of corncob. This is related to the containing of lignin in corncob, which is unable to hydrolyze to sugar compounds. Hence, it is clear that, compared under the same weight basis, biomass derived carbohydrate (i.e. waste cassava) would generate more alkane products than lignocellulosic biomass. Among the series of catalyst system studied, the single use of Pd/WO_3-ZrO_2 provided the highest yield of water-soluble organic compounds comparable to the combination of WO_3-ZrO_2 and Pd/MgO-$ZrO_2$for both reactions. This highlights the great benefit of Pd/WO_3-ZrO_2 as the suitable catalyst for all hydrolysis, dehydration, aldol-condensation and hydrogenation reactions. Further investigations regarding the effect of operating conditions on the yield of water-soluble organic compounds and product selectivity from the reaction of waste cassava in the presence of Pd/WO_3-ZrO_2 were then performed by varying the inlet feedstock/solvent molar ratio (from 1/1 to 1/3, 3/1, and 9/1), the hydrogenation temperature (from 393 K to 353 K, 423 K, and 453 K), and the hydrogenation time (from 6 h to 3 h, 12 h, and 18 h). As shown in Fig. 3.14, at low inlet feedstock/solvent molar ratio (i.e. 1/3), low organic compound yield was achieved due to the dilution of liquid product by excess solvent, whereas the use of too high inlet feedstock/solvent molar ratio (i.e. 9/1) also resulted in the low organic compound yield achievement due to the incomplete conversion of HMF and furfural by aldol-condensation reaction.

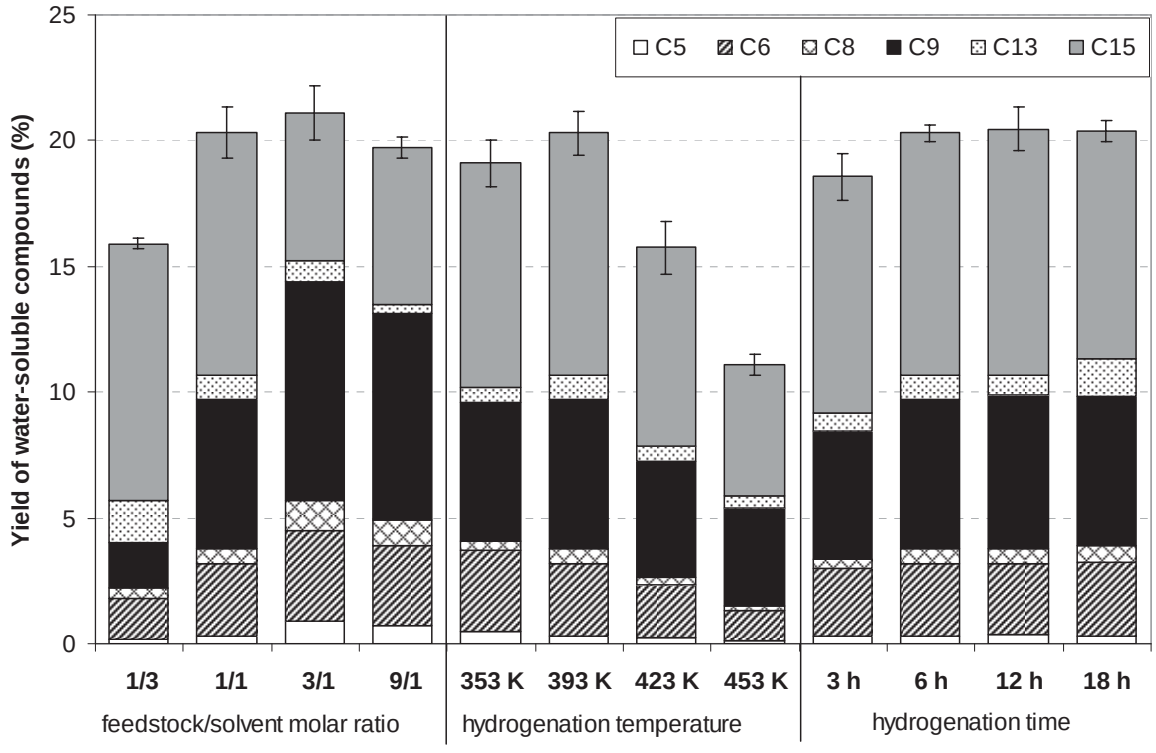

Fig. 14 Effects of feedstock/solvent molar ratio, hydrogenation temperature and hydrogenation time on the yield of water-soluble C_5-C_{15} organic compounds from the integrative hydrolysis/dehydration/aldol-condensation/hydrogenation of waste cassava in the presence of Pd/WO_3-ZrO_2 (hydrolysis/dehydration temperature of 523 K for 5 min; aldol-condensation temperature of 353 K for 30 h)

According to the effect of hydrogenation temperature, the organic compound yield increased with increasing the reaction temperature from 353 K to 393 K; nevertheless, it oppositely decreased at higher reaction temperatures (i.e. 423 K and 453 K), which could be due to the further conversion or cracking of water-soluble organic compounds at too high temperature. Lastly, regarding the effect of hydrogenation time, the organic compound yield increased with increasing the reaction time from 3 h to 6 h; afterward, the yield seems to be constant. Hence, we concluded that the optimum conditions for maximizing the yield of water-soluble organic compounds from the integrative hydrolysis/dehydration/aldol-condensation/hydrogenation of corncob and waste cassava were at feedstock/solvent molar ratio of 3/1 with the hydrogenation temperature of 393 K and hydrogenation time of 6 h.

3.4 Conclusions

The simultaneous hydrolysis/dehydration reaction of sugarcane bagasse, rice husk and corncob efficiently produced furfural and HMF at 573 K with the reaction time of 5 min. According to the studies of individual cellulose, xylan, glucose, and xylose reactions, it can be revealed that the production of HMF comes from the conversion of cellulose in biomass, while furfural is generated from the decompositions of both cellulose and hemicellulose. In the presence of TiO_2-ZrO_2 (with Ti/Zr molar ratio of 1/1), the highest furfural and HMF yields with less by-products (i.e. glucose, fructose, xylose, and AHG) formation can be achieved compared to the reaction without catalyst and/or with TiO_2 and ZrO_2 due to its strong hydrolysis, isomerization and dehydration reactivities. It was also found that the catalysts prepared by (co-) precipitation method gained higher reactivity compared to those prepared by sol-gel and physical mixing methods. Furthermore, the alcinations temperature during the catalyst preparation also made strong impact on its reactivity. According to the XRD experiment, different portion of phase formation was observed over catalysts with different alcinations temperatures (i.e. the portion of anatase/rutile for TiO_2, monoclinic/tetragonal for ZrO_2 and amorphous/crystalline for TiO_2-ZrO_2); this strongly affected the acidity-basicity and the reactivity of catalysts.

In addition to TiO_2-ZrO_2, it was also found that WO_3-ZrO_2 enables to catalyze hydrolysis/dehydration reaction and efficiently converts corncob and waste cassava to HMF and furfural. The impregnation of Pd over WO_3-ZrO_2 as Pd/WO_3-ZrO_2 was found active for sequential aldol-condensation/hydrogenation of HMF and furfural to C_5-C_{15} organic compounds. Importantly, the single use of Pd/WO_3-ZrO_2 for integrative hydrolysis/dehydration/aldol-condensation/hydrogenation of corncob and waste cassava was studied. The optimum conditions to maximize the yield of these water-soluble organic compounds were found at hydrolysis/dehydration temperature of 573 K for 5 min; aldol-condensation temperature of 353 K for 30 h; and hydrogenation temperature of 393 K for 6 h. Under these conditions, 20.4% alkane-based liquid fuel can be enhanced from waste cassava, whereas 14.6% can be enhanced from corncob. It should also be noted that the effects of pressure and catalyst amount were also tested and it was found that these parameters showed insignificant effect on the reaction yield.

3.5 References

Aida T.M., Watanabe M., Aizawa Y., Iida T., Levy C., Sue K., Inomata H., 2007. Dehydration of d-glucose in high temperature water at pressures up to 80 MPa. J. Supercritical Fluids. 40, 381-388.

Aramendía M.A., Borau V., Jiménez C., Marinas A., Marinas J.M., Ruiz J.R., Urbano F.J., 2004. Magnesium-containing mixed oxides as basic catalysts: base characterization by carbon dioxide TPD–MS and test reactions. J. Mol. Catal. A: Chem. 218, 81-90.

Asghari F.S., Yoshida H., 2006. Dehydration of fructose to 5-hydroxymethylfurfural in sub-critical water over heterogeneous zirconium phosphate catalysts. Carbohydr. Res. 341, 2379-2387.

Barrett C.J., Chheda J.N., Huber G.W., Dumesic J.A., 2006. Single-reactor process for sequential aldol-condensation and hydrogenation of biomass-derived compounds in water, Appl. Catal. B. 66, 111-118.

Bicker M., Hirth J., Vogel H., 2003. Dehydration of fructose to 5-hydroxymethylfurfural in sub- and supercritical acetone. Green Chem. 5, 280-284.

Bower S., Wickramasinghe R., Nagle N.J., Schell D.J., 2008. Modeling sucrose hydrolysis in dilute sulfuric acid solutions at pretreatment conditions for lignocellulosic biomass. Bioresource Technol. 99, 7354-7362.

Chareonlimkun A., Champreda V., Shotipruk A., Laosiripojana N., 2010. Catalytic conversion of sugarcane bagasse, rice husk and corncob in the presence of TiO_2, ZrO_2 and mixed-oxide TiO_2–ZrO_2 under hot compressed water (HCW) condition. Bioresource Technol. 101, 4179-4186.

Chareonlimkun A., Champreda V., Shotipruk A., Laosiripojana N., 2010. Reactions of C_5 and C_6-sugars, cellulose, and lignocellulose under hot compressed water (HCW) in the presence of heterogeneous acid catalysts. Fuel, In Press.

Furuta S., Matsuhashi H., Arata K., 2004. Biodiesel fuel production with solid super acid catalyst in fixed bad reactor under atmospheric pressure. Catal. Commun. 5, 721-723.

Gutsche C.D., Redmore D., Buriks R.S., Nowotny K., Grassner H., Armbruster C.W., 1967. Base-Catalyzed Triose Condensations. J. Am. Chem. Soc., 89, 1235-1245.

Huber G.W., Chheda J.N., Barrett C.J., Dumesic J.A, 2005. Production of liquid alkanes by aqueous-phase processing of biomass-derived carbohydrates. Science 308, 1446-1450.

Kabyemela B.M.., Adschiri T., Malaluan R.M., Arai K., 1999. Glucose and Fructose Decomposition in Subcritical and Supercritical Water: Detailed Reaction Pathway, Mechanisms, and Kinetics. Ind. Eng. Chem. Res. 38, 2888-2895.

Karimi K., Kheradmandinia S., Taherzadeh M.J., 2006. Conversion of rice straw to sugars by dilute-acid hydrolysis. Biomass Bioenergy. 30, 247-253.

Laopaiboon P., Thani A., Leelavatcharamas V., Laopaiboon L., 2010. Acid hydrolysis of sugarcane bagasse for lactic acid production, Bioresource Technol. 101, 1036-1043.

Lopez D.E., Goodwin Jr. J.G., Bruce D.A., Lotero E., 2005. Transesterification of triacetin with methanol on solid acid and base catalysts. Appl. Catal. A 295, 97-105.

Lourvanij K., Rorrer G.L., 1993. Reactions of aqueous glucose solutions over solid-acid Y-zeolite catalyst at 110-160C. Ind. Eng. Chem. Res. 32, 11-19.

Moreau C., Durand R., Peyron D., Duhamet J., Rivalier P., 1998. Selective preparation of furfural from xylose over microporous solid acid catalysts. Ind. Crop. Prod. 7, 95-99.

Moreau C., Durand R., Roux A., Tichit D., 2000. Isomerization of glucose into fructose in the presence of cation-exchanged zeolites and hydrotalcites. Appl. Catal. A. 193, 257-264.

Qi X., Watanabe M., Aida T.M., Richard L., Smith Jr., 2008. Selective Conversion of D-Fructose to 5-Hydroxymethylfurfural by Ion-Exchange Resin in Acetone/Dimethyl sulfoxide Solvent Mixtures. Ind. Eng. Chem. Res. 47, 9234-9239.

Qi X., Watanabe M., Aida T.M., Richard L., Smith Jr., 2009. Sulfated zirconia as a solid acid catalyst for the dehydration of fructose to 5-hydroxymethylfurfural. Catal. Comm. 10, 1771-1775.

Rao K.N., Sridhar A., Lee A.F., Tavener S.J., Young N.A., Wilson K. 2006 Zirconium phosphate supported tungsten oxide solid acid catalysts for the esterification of palmitic acid. Green Chem. 8, 790-797.

Sasaki M., Goto K., Tajima K., Adschiri T., Arai K., 2002. Rapid and selective retro-aldol condensation of glucose to glycolaldehyde in supercritical water. Green Chem. 4, 285-287.

Shigemasa Y., Yokoyama K., Sashiwa H., Saimoto H., 1994. Synthesis of threo- and erythro-3-pentulose by aldol type reaction in water. Tetrahedron Lett. 35, 1263-1266.

Watanabe M., Aizawa Y., Iida T., Aida T.M., Levy C., Sue K., Inomata H., 2005. Glucose reactions with acid and base catalysts in hot compressed water at 473 K. Carbohydr. Res. 340, 1925-1930.

Watanabe M., Aizawa Y., Iida T., Nishimura R., Inomata H., 2005. Catalytic glucose and fructose conversions with TiO_2 and ZrO_2 in water at 473 K: Relationship between reactivity and acid–base property determined by TPD measurement. Appl. Catal. A. 295, 150-156.

Yang B.Y., Montgomery R., 1996. Alkaline degradation of glucose: Effect of initial concentration of reactants. Carbohydr. Res. 280, 27-45.

Yat S.C., Berger A., Shonnard D.R., 2008. Kinetic characterization for dilute sulfuric acid hydrolysis of timber varieties and switchgrass. Bioresource Technol. 99, 3855-3863.

Chapter 4

Results and Discussion: Biodiesel production studies

4.1 Introduction and research objectives

Biodiesel is an important alternative fuel due to its environmental friendly and enable to substitute for petroleum diesel fuel. Biodiesel is created by the chemical conversion of animal fats or vegetable oils. Biodiesel production is based on tranesterification of vegetable oils and fats through the addition of methanol (or other alcohols) and catalyst, giving glycerol as a co-product. Biodiesel can be produced from a great variety of feedstocks. These feedstocks include most common vegetable oils (soybean, cottonseed, palm, peanut, rapeseed canola, sunflower, safflower, coconut, etc.) and animal fats (tallow) as well as waste oils (used frying oils, etc.). The selection of feedstock mainly depends on geography; for instance, soybean oil is the major biodiesel feedstock in the United States, rapeseed oil is the major source in Europe, and palm oil is of significance for countries with tropical climate. It may be noted that rapeseed oil as used in Europe and canola oil as used in North America are very similar regarding their fatty acid profiles. Depending on the origin and quality of the feedstock, changes to the production process may be necessary. Other sources or potential sources of biodiesel that are being investigated that include animal fats, used cooking or frying oils, greases, algae and less common vegetable oils such as jatropha, which is shown in Table 4.1.

Table 4.1 Feedstock for biodiesel production

Feedstocks	**% of free fatty acid**
Rapeseed oil	≤ 5%
Sun flower oil	≤ 5%
Soybean oil	≤ 5%
Camelina oil	≤ 5%
Choice white Grease	≤ 4%
Cooking oil	≤ 15%
Animal Fat	≤ 30%
Corn oil	≤ 15%
Jatropha oil	≤ 20%
Trap/ Brown Grease	70-95%

Focusing on the use of palm as the reactant for biodiesel production, typically, crude palm oil (CPO) contains high amount of free fatty acids (FFAs), which easily converts to soap during the transesterification reaction and consequently reduces the overall process performance (Zullaikah et al., 2005). To avoid this formation, most of FFAs in CPO must be treated or removed (as called palm fatty acid distilled or PFAD); and the treated palm oil after PFAD removal is called refined palm oil (RPO), which can be efficiently converted to biodiesel via transesterification reaction. It is noted that the conversion of PFAD to fatty acid methyl ester (FAME) via esterification reaction is a

good procedure to reduce the production cost of biodiesel and consequently to make biodiesel enable to compete economically with petroleum-based fuels.

Generally, biodiesel production starts from the natural oil feedstock (i.e. vegetable oil and animal oil) as a raw material. Importantly, the quality of biodiesel production depends mainly on the composition of reactant (in term of fatty acid content inside the raw material oil). Typically, in all crude natural oil, it contains highly content of fatty acids. In the conventional biodiesel production, the steps of biodiesel production include:

Acid Esterification

Oil feedstocks (vegetable oil or animal oil) containing more than 4% free fatty acids go through an acid esterification process to increase the yield of biodiesel. These feedstocks are filtered and preprocessed to remove water and contaminants, and then fed to the acid esterification process. The catalyst, sulfuric acid, is dissolved in methanol and then mixed with the pretreated oil. The mixture is heated and stirred, and the free fatty acids are converted to biodiesel. Once the reaction is complete, it is dewatered and then fed to the transesterification process.

Transesterification

Oil feedstocks containing less than 4% free fatty acids are filtered and preprocessed to remove water and contaminants and then fed directly to the transesterification process along with any products of the acid esterification process [http://www1.eere.energy.gov]. The catalyst, potassium hydroxide, is dissolved in methanol and then mixed with and the pretreated oil. If an acid esterification process is used, then extra base catalyst must be added to neutralize the acid added in that step. Once the reaction is complete, the major co-products, biodiesel and glycerin, are separated into two layers.

Methanol recovery

The methanol is typically removed after the biodiesel and glycerin have been separated, to prevent the reaction from reversing itself. The methanol is cleaned and recycled back to the beginning of the process.

Biodiesel refining

Once separated from the glycerin, the biodiesel goes through a clean-up or purification process to remove excess alcohol, residual catalyst and soaps. This consists of one or more washings with clean water. It is then dried and sent to storage. Sometimes the biodiesel goes through an additional distillation step to produce a colorless, odorless, zero-sulfur biodiesel.

Glycerin refining

The glycerin by-product contains unreacted catalyst and soaps that are neutralized with an acid. Water and alcohol are removed to produce 50% - 80% crude glycerin. The remaining contaminants include unreacted fats and oils. In large biodiesel plants, the glycerin can be further purified, to 99% or higher purity, for sale to the pharmaceutical and cosmetic industries [http://www1.eere.energy.gov].

Generally, the transesterification process is typical process for biodiesel production. The reaction of a triglyceride (fat/oil) with an alcohol to form esters and glycerol in the presence of the catalysts (acid or base catalyst). The feedstock for biodiesel production always come from the non-edible types of fat and oil because of the lower price. A triglyceride has a glycerine molecule as its base with three long chain fatty acids attached. The characteristics of the fat are determined by the nature of the fatty acids attached to the glycerine. The nature of the fatty acids can be affecting the characteristics of the biodiesel. The alcohol reacts with the fatty acids to form the mono-alkyl ester, or biodiesel and crude glycerol. In most production methanol or ethanol is the alcohol used (methanol produces methyl esters, ethanol produces ethyl esters).

The main drawback of the biodiesel by tranesterification is the soap formation occurred from reaction and it will decrease the yield of biodiesel. To solve this problem by using the esterification process as a pretreatment step to reduce the FFAs level and after that will follow by tranesterification process. Esterification is a chemical reaction used for making esters (biodiesel). The reaction in which a Carboxylic acid (fatty acid) reacts with an alcohol in the presence of a catalyst (homogeneous catalysts or heterogeneous catalysts) to form an ester [$CH_3COOC_2H_5$] and water as product.

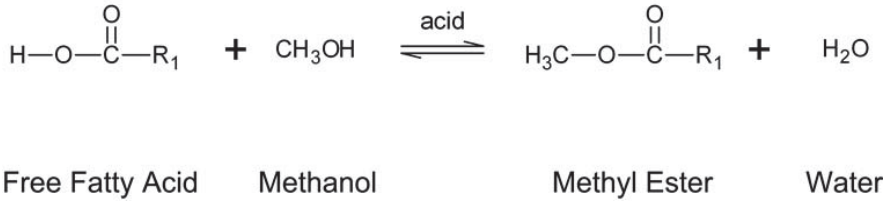

FFA can be observed in several forms i.e. lauric acid myristic acid stearic acid and linoleic acid. Normally, high content free fatty acid (FFA) feedstock has less expensive than low fatty acid feedstock because FFA is known as the major component that can interrupt the reaction of biodiesel production. Naturally, seed oil always consist of many types of fatty acid which consist of saturated and unsaturated (double bond and triple bond) as shown in Table 4.2.

Table 4.2 Fatty acid composition in difference feedstock types

Vegetable oil	Palmatic 16:0	Stearic 18:0	Palmitoleic 16:1	Oleic acid 18:1	Linoleic 18:2	Other acids
Tallow	29.0	24.5	-	44.5	-	-
Coconut oil	5.0	3.0	-	6.0	-	65.0
Olive oil	14.6	-	-	75.4	10.0	-
Cotton oil	28.6	0.9	0.1	13.0	57.2	0.2
Corn oil	6.0	2.0	-	44.0	48.0	-
Soybean oil	11.0	2.0	-	20.0	64.0	3.0
Rapeseed	3.5	0.9	0.1	54.1	22.3	9.1
Sunflower seed	6.4	2.9	0.1	17.7	72.8	0.1

Nowadays, the alternative way of processing these oil or fatty acid is to reduce fatty acid in feedstock for biodiesel production by esterification. This process has been studied by many researchers. Currently, the difference of esterification process is catalytic used that are the homogeneous catalysts and heterogeneous catalysts.

Regarding the homogeneous catalyst process, esters are produced when carboxylic acids are heated with alcohols in the presence of homogeneous acid catalyst. A great advantage with acid catalysts is that they can produce biodiesel directly from low-cost lipid feedstocks, generally associated with high FFA concentrations (low-cost feedstocks, such as used cooking oil and greases, commonly have FFAs levels > 6%). Currently, the catalysts more used in biodiesel production are the organic acids, such as the derivates of toluene sulfonic acid and, more often, mineral acids such as H_2SO_4. However, nowadays the homogeneous acid catalyst has not yielded satisfactory results. The latter process gives rise to problems linked to the corrosive action of the liquid acid catalyst and to the high quantity of by-products formed and cause of the environment impact. Another disadvantage that homogeneous acids such as sulfuric acid need long reaction times more than the alkaline catalysts becomes a serious problem [Abiney L. et al., 2008]. The use of solid acid catalysts offers an alternative and has received a lot of attention in the past years. Solid acid catalysts are not corrosive and, coated onto a support, they can be easily reused. Examples of solid acid catalysts used in esterification reactions include ion-exchange resins, zeolites and superacids like sulphated zirconia and niobium acid [Thijs A et at., 2006]. The development of alternative catalysts for the esterification of FFAs, based on the Lewis acids (Homogeneous catalysts), which operate under mild conditions of reaction and are less corrosive, rather than traditional Brønsted acids, is one of the main challenges to be overcome. Although this technology could make lower environmental impact but the production cost of biodiesel will more increase. Table 4.3 shows the performance of solid acid on esterification process [Thijs A. et al., 2006; Anton A. et al., 2007; Kyong-Hwan Chung a. et al., 2008; and Abiney L. et al., 2008].

At present, the new heterogeneous acid catalysts have been investigating to replace homogenous acid catalyst due to their easily reused after reused after regenerating and higher stability than homogenous catalyst with less harmful (Abiney L. et al., 2008). Previously, several solid catalysts have been investigated for transesterification and esterification reactions (Furuta et al., 2004; Baba et al., 2005; Lopez et al., 2005; Kiss et al., 2006; Jitputti et al., 2006). Among them, sulfated zirconia (SO_4-ZrO_2) has been known to give high activity and selectivity for transesterification and esterification of several vegetable oils and fatty acids (Lo´pez et al., 2005; Kiss et al., 2006; Jitputti et al., 2006); this catalyst can also be applied in several important industrial processes e.g. hydrocarbon isomerization and alkylation (Tanabe and Holderich, 1999). Apart from SO_4-ZrO_2, other zirconia-based catalysts e.g. TiO_2-ZrO_2 and WO_3-ZrO_2 have also been of interest to researchers for several acid- and base-catalyzed reactions. TiO_2-ZrO_2 is known to have bifunctionality for both acidity and basicity properties which benefits for acid- and base-catalyzed reactions e.g. hydrolysis and isomerization, while WO_3-ZrO_2 was also reported to active for transesterification and esterification reactions under specific conditions (Furuta et al., 2004; Lopez et al., 2005; Rao et al., 2006).

Table 4.3 Solid acid catalysts for esterification process

Catalyst	Acid : Alcohol	Amount of catalyst	Temperature (°C)	Time (min)	Conversion (%)
H-ZSM-5 (25)zeolite (c)	1L:30L Flying oil :Methanol	1 g	60	180	80
H-MOR (10)zeolite (c)	1L:30L Flying oil :Methanol	1 g	60	180	78
Amberlyst-15 (a)	1mmol:1mmol Dodecanoic acid :Hexanol	3 % wt	150	40-55	96-98
Nafion-NR50 (a)	1mmol:1mmol Dodecanoic acid :Hexanol	3 % wt	150	95-105	72-75
Nafion/silica (SAC 13) (d)	3 L : 0.9 L Sunflower oil :Methanol	1 g	60	1440	85-90
Smopex-101 (b)	0.66mol:0.66mol acetic acid : Butanol	1.85 g	75	350-400	65-68
Sulphated Zirconia(SZ) (b)	0.66mol:2mol acetic acid : Butanol	1 wt%	150	40-50	90-93
Tungsten Zirconia(WZ) (d)	3 L : 0.9 L Sunflower oil :Methanol	1 g	60	1440	20
SnCl2.2H2O (e)	1mmol:120mmol Oleic acid :Ethanol	0.4 mmol	mild	120	90-93

Source : (a)Anton A.Kiss(2005), (b)Thijs A. Peters(2005), (c)Kyong-Hwan Chung(2008),(d) J. Ni, F.C. Meunier(2007), (e) Abiney L. Cardoso(2008)

Alternative to the catalytic processes, Saka and Kusdiana (2001) proposed a method of biodiesel production via non-catalytic transesterification of vegetable oils in supercritical methanol. According to this process, the reaction takes place in a shorter time and the diffusive problem can be eliminated since the reactants form homogeneous phase in supercritical state. Furthermore, feedstock with high FFA content can be efficiently used in this process and the catalyst removal step can be eliminated. However, major disadvantages of this method are the requirement of high operating temperature, pressure and methanol to reactant ratio, which result in high energy consumption and high cost of production. In order to overcome these barriers, several approaches have been investigated i.e. the addition of appropriate solid catalyst which allows the supercritical reaction to be carried out under milder conditions (e.g. near-critical condition) (Demirbas (2007)) and the addition of co-solvent along with the feed to achieve the well-mixing phase in the reaction system (Cao et al. (2005)).

In the present work, we aimed to study the transesterification and esterification of relevant palm products i.e. CPO, RPO and PFAD under near-critical methanol in the presence of three synthesized zirconia-based catalysts i.e. SO_4-ZrO_2, TiO_2-ZrO_2 and

WO_3-ZrO_2. The effects of catalyst preparing conditions i.e. sulfate and tungsten loadings, Ti/Zr molar ratio, and calcination temperature on the catalyst performance were intensively studied; and the physical characteristics of these synthesized catalysts, i.e. acidity-basicity properties, phase formation and catalyst surface properties were analyzed in order to relate these properties with the catalytic reactivity. Then, the beneficial of these catalysts on the reaction performance in terms of reaction reactivity, reaction time, temperature and amount of alcohol requirements were investigated. In addition, the effect of co-solvent adding on reaction performance was studied by introducing three promising co-solvents (i.e. toluene, benzene and hexane) along with the reactants to the system. Lastly, since it is known that the formation of water during the esterification reaction could strongly inhibit the yield of FAME production, the effect of water removal i.e. as feedstock pre-treatment prior the reaction and during the reaction were studied by adding molecular sieve (as water sorbent) to the reactants. From all studies, the suitable catalyst, type of co-solvent, process to treat water in the system, and the optimum operating conditions for converting CPO, RPO and PFAD to biodiesel were eventually determined.

4.2 Materials and methods

4.2.1 Raw material supplies and catalyst preparations

Chemicals

CPO, RPO and PFAD samples used in this study were obtained from Pathum Vegetable Oil, Co. Ltd. (Thailand). PFAD consists of 93.2 wt% free fatty acid (FFA) (45.6% palmitic, 33.3% oleic, 7.7% linoleic, 3.8% stearic, 1.0% myristic, 0.6% tetracosenoic, 0.3% linolenic, 0.3% ecosanoic, 0.2% ecosenoic, and 0.2% palmitoleic acid) and the rest elements are triglycerides, diglycerides (DG), monoglycerides (MG) and traces of impurities, whereas CPO contains 7 wt% FFA (43.5% palmitic, 39.8% oleic, 10.2% linoleic, 4.3% stearic). Methyl ester standards (i.e. methyl palmitate, methyl stearate and methyl oleate) were obtained from Wako Chemicals, USA. Commercial grade methanol (95%) and analytical grade hexane, toluene, and benzene (99.9%) ware purchased from Fisher scientific, UK and commercial grade 3 Å molecular sieve was supplied from Fluka, Buchs, Switzerland.

Solid acid catalyst

SO_4-ZrO_2 and WO_3-ZrO_2 were prepared by incipient wetness impregnation of sulfuric acid or ammonium metatungstate over zirconium oxide (ZrO_2). Regarding the preparation of ZrO_2, a solution of zirconyl chloride ($ZrOCl_2$) precursor (0.1 M) was slowly dropped into a well-stirred precipitating solution of ammonium hydroxide (NH_4OH) at room temperature. The solution was controlled at pH of 11. The obtained precipitate was removed, and then washed with deionized water and ethanol. Then, the solid sample was dried overnight at 110°C and calcined at 500°C for 6 h. SO_4-ZrO_2 and WO_3-ZrO_2 were then prepared by immersing of synthesized ZrO_2 in 0.1 mol l^{-1} of H_2SO_4 and/or ammonium metatungstate at 70°C for 30 min, then dried overnight at 110°C and calcined at three different temperatures (500, 600 and 700°C for SO_4-ZrO_2 and 700, 800 and 900°C for WO_3-ZrO_2) for 3 h. It is noted that three different amounts of sulfuric acid

(providing sulfur contents of 0.75, 1.8 and 2.5 wt%) and ammonium metatungstate (providing tungsten weight contents of 10, 20 and 30 wt%) were applied in the present work. For TiO_2-ZrO_2, this catalyst (with Ti/Zr molar ratios of 1/3, 1/1, and 3/1) was prepared by co-precipitation method. In detail, a mixture of zirconium and titanium salt precursors (i.e. zirconyl chloride ($ZrOCl_2$) and titanium chloride ($TiCl_4$) (0.15 M)) was slowly dropped into a well-stirred precipitating solution of ammonium hydroxide (NH_4OH) (2.5 wt%) at room temperature. The solution was controlled at pH of 11. The obtained precipitate was removed, and then washed with deionized water until Cl^- was not detected by a silver nitrate ($AgNO_3$) solution. Then, the solid sample was dried overnight at 110°C and calcined at three different temperatures (i.e. 500°C, 600°C and 700°C) under continuous air flow for 6 h with a temperature ramping rate of 10°C min^{-1}.

After preparation, these synthesized catalysts were characterized by several techniques. The measurements of BET surface area, cumulative pore volume and average pore diameter were performed by N_2 physisorption technique using Micromeritics ASAP 2020 surface area and porosity analyzer. The XRD patterns of powder were performed by X-ray diffractometer, in which the crystallite size was estimated from line broadening according to the Scherrer equation. NH_3- and CO_2-TPD were used to determine the acid-base properties of catalysts. TPD experiments were carried out using a flow apparatus. The catalyst sample (0.1g) was treated at 500^oC in helium flow for 1 h and then saturated with 15% NH_3/He mixture or pure CO_2 flow after cooling to 100^oC. After purging with helium, the sample was heated to 650^oC in helium flow. The amount of acid-base sites on the catalyst surface was calculated from the desorption amount of NH_3 and CO_2, which was determined by measuring the areas of the desorption profiles obtained from the Chemisorption System analyzer.

4.2.2 Catalyst testing toward the esterification and transesterification

A batch type stainless steel reactor was applied to study the transesterification and esterification reactions in the present work. Prior to the experiment, the temperature of the heating furnace at the location of the furnace adjacent to the reactor was controlled at 200-300°C. To carry out the reaction, palm feedstock (i.e. CPO, RPO and PFAD) was mixed with methanol at a specific molar ratio of 6:1-42:1 (methanol to CPO or RPO) and 3:1-18:1 (methanol to PFAD). The solid catalyst was then added in the reactants at the concentration range of 0-1 wt %. The reactor was reached to the desired reaction temperature approximately 15 min (heating time), at which point the reaction was allowed to continue for a period of 0–15 min. The effect of co-solvent on the reaction performance was studied by adding toluene, benzene and hexane (10% v/v) along with the feed before charging the solution to the reactor. Regarding the effect of water content on the reaction performance, the experiments were carried out by (1) adding molecular sieve to dehydrate the reactant (CPO, RPO and PFAD) before filtering out from the reactant prior the reaction and (2) adding molecular sieve to dehydrate the mixture (of reactant and products) during the reaction. After the reaction, the vessel was removed from the heater and placed into a water bath to stop the reaction. The reaction products were discharged from the reactor and were centrifuged, forming three phases. The top phase was a mixture of methyl ester (biodiesel) and a small amount of un-reacted methanol which was removed by evaporation, the middle phase was glycerol and/or water, and the lower phase was solid catalyst.

FAME analysis was carried out using GC (Shimadzu 2010 model) with a flame ionization detector (FID) in which 1 ml of the sample was injected into column. The GC consists of a capillary column (DB-WAX, Carbowax 20 M, 30 m, 0.32 mm ID, 0.25 μm). The injector, detector, and column temperatures were set at 250, 260 and 200°C respectively. Pressure was 64.1 kPa and linear velocity was 25 cm s^{-1}. The carrier gas was helium and the make-up gas was nitrogen. The sample was prepared by adding 0.05 ml of FAME to 5 ml of n-hexane and methyl heptadecanoate was used as an internal standard.

4.2.3 Catalyst characterization

The solid acid catalysts were characterized by The Brunauer-Emmett-teller (BET) and Temperature-Programmed Desorption (TPD) to determine their physical properties and their acidity property.

Brunauer-Emmett-teller (BET) measurment

The specific surface area of the catalyst is characterized by Micromeritics ASAP equipment. The Micromeritics ASAP is used to characterize the active and support surfaces of catalysts, to determine the high surface areas of catalyst by using nitrogen gas adsorption. After the measurement process, data analysis, adsorption isotherm which is including surface area, pore structure and pore surface were debated.

Figure 4.1 Micromeritics ASAP

Temperature Program Decomposition (TPD)

Temperature-Programmed Desorption (TPD) is one of the most widely used and flexible techniques for characterizing the acid sites on oxide surfaces. Determining the quantity and strength of the acid sites on alumina, amorphous silica-alumina, and zeolites is crucial to understanding and predicting the performance of a catalyst. TPD experiments were carried out using a flow apparatus. The catalyst sample (0.1g) was treated at 110°C in helium flow for 1 h and then saturated with 15% NH_3/He mixture or pure CO_2 flow after cooling to 100°C. After purging with helium, the sample was heated to 140°C in helium flow. The amount of acid-base sites on the catalyst surface was calculated from

the desorption amount of NH_3. It was determined by measuring the areas of the desorption profiles obtained from the Chemisorption System analyzer.

Fatty acid methyl ester analysis

Methyl ester content in the products was measured by GC analysis according to the EN 14103 test method. At first, standard (STD) solution was prepared as 10 mg/ml of methyl heptadecanoate (C17:0) with heptane solution. The sample (250 mg) was added in the standard solution (5 ml).The mixed sample with STD solution was analyzed by GC. The methyl ester content was determined by the equation below.

$$\text{Methyl ester content } (\%) = \frac{\sum A - A_s}{A} \times \frac{C_s V_s}{m} \times 100$$

where $\sum A$ = summation of peak areas of methyl esters (C14:0–C24:1), A_s = peak area of methyl heptadecanoate (STD material), C_s = concentration of STD solution (10 mg/ml), V_s = volume of STD solution (5 ml), and m = amount of sample (250 mg).

In detail, GC is specifies for gas and liquid-phases testing. It is a physical method to separate the components and distributed between two phase. A very small amount of liquid mixing sample is injected into the instrument and is volatilized in a hot injection chamber. Then, it is swept by a stream of inert carrier gas through a heated column which contains the stationary, high-boiling liquid. As the mixture travels through this column, its components go back and forth at different rates between the gas phase and dissolution in the high-boiling liquid, and thus separate into pure components. Just before each compound exits the instrument, it passes through a detector. When the detector detects the compound, it sends an electronic message to the recorder, which responds by printing a peak on a piece of paper.

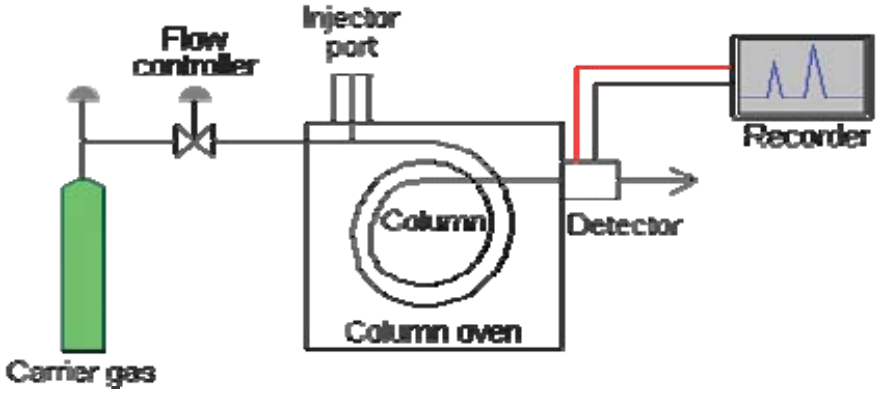

Figure 4.2 Schematic diagram of gas chromatography (GC)

The GC consists of an injection block, a column, and a detector. An inert gas flows through the system. The injection chamber is a heated cavity which serves to volatilize the compounds. The sample is injected by syringe into this chamber through a

port which is covered by a rubber septum. Once inside, the sample becomes vaporized and is carried out of the chamber and onto the column by the carrier gas. The main part of the Gas Chromatography is the detector that will give different types of selectivity. The requirement of a detector depends on the separation application that shown in Table 4.4 below.

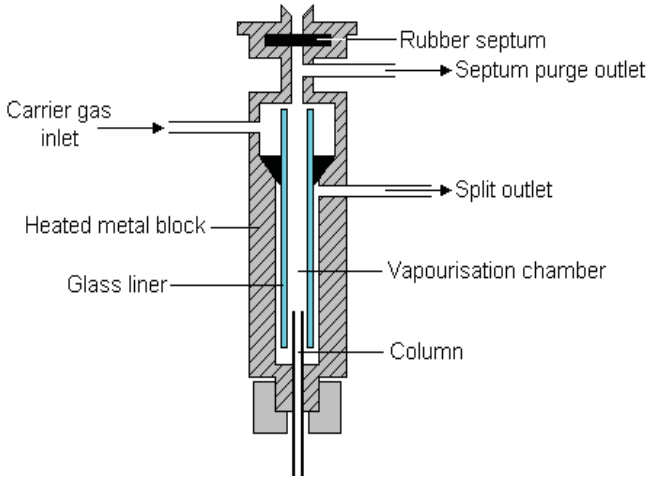

Figure 4.3 Split/splitless injection

Table 4.4 Types of detector

Detector	Selectivity
Flame ionization (FID)	Most organic compounds
Thermal conductivity (TCD)	Universal
Electron capture (ECD)	Halides, nitrates, nitriles, peroxides, anhydrides, organometallics
Nitrogen-phosphorus	Nitrogen, phosphorus
Flame photometric (FPD)	Sulphur, phosphorus, tin, boron, arsenic, germanium, selenium, chromium
Photo-ionization (PID)	Aliphatics, aromatics, ketones, esters, aldehydes, amines, heterocyclics, organosulphurs, some organometallics
Hall electrolytic conductivity	Halide, nitrogen, nitrosamine, sulphur

In this research, the Flame ionization (FID) detector is applied to analyst the organic compounds because it has high sensitivity. From the biochemical compounds have a greatest amount of carbon present than other elements and these particular compounds can be detected by Flame ionization (FID) easier than other methods because of its higher carbon concentration and its sensitivity.

4.3 Results and discussion

As described, SO_4-ZrO_2, TiO_2-ZrO_2 and WO_3-ZrO_2 catalysts were synthesized at various preparation conditions and tested for transesterification and esterification of CPO, RPO and PFAD in near-critical methanol condition. Here, the synthesized SO_4-ZrO_2, TiO_2-ZrO_2 and WO_3-ZrO_2 were denoted as SZ, TZ, and WZ. SZ catalysts prepared by loading the sulfur contents of 0.75, 1.8, and 2.5% and calcined at 500^{o}C were denoted as 0.75SZ-500, 1.8SZ-500, and 2.5SZ-500. TZ catalysts with Ti/Zr ratios of 1/3, 1/1 and 3/1 and calcined at 500^{o}C were donated as 1/3TZ-500, 1/1TZ-500 and 3/1TZ-500. Lastly, WZ catalysts prepared by loading WO_3 of 10, 20 and 30% and calcined at 800^{o}C were donated as 10WZ-800, 20WZ-800 and 30WZ-800.

4.3.1 Catalyst characterization

The specific surface area, cumulative pore volume, average pore diameter and pore size distribution of all synthesized catalysts, determined by N_2 physisorption using Micromeritics ASAP 2020 surface area and porosity analyzer, are summarized in Tables 4.1-4.3.

Table 4.1 N_2 Physisorption results of SO_4-ZrO_2 prepared from different conditions

Catalysts	BET Surface Area[a] (m^2/g)	Cumulative Pore Volume[b] (cm^3/g)	Average Pore Diameter[c] (nm)
0.75SZ-500	228	0.321	3.9
1.8SZ-500	243	0.390	3.6
2.5SZ-500	237	0.354	3.8
1.8SZ-600	179	0.314	4.0
1.8SZ-700	113	0.254	4.4

[a] Error of measurement = ±5%.
[b] BJH desorption cumulative volume of pores between 1.7 and 300 nm diameter.
[c] BJH desorption average pore diameter.

Table 4.2 N_2 Physisorption results of WO_3-ZrO_2 prepared from different conditions

Catalysts	BET Surface Areaa (m^2/g)	Cumulative Pore Volumeb (cm^3/g)	Average Pore Diameterc (nm)
20WZ-700	121	0.293	4.1
10WZ-800	91	0.157	4.0
20WZ-800	95	0.193	3.8
30WZ-800	103	0.221	3.8
20WZ-900	78	0.112	4.3

[a] Error of measurement = ±3%.
[b] BJH desorption cumulative volume of pores between 1.7 and 300 nm diameter.
[c] BJH desorption average pore diameter.

Table 4.3 N_2 Physisorption results of TiO_2-ZrO_2 prepared from different conditions

Catalysts	BET Surface Areaa (m^2/g)	Cumulative Pore Volumeb (cm^3/g)	Average Pore Diameterc (nm)
1/1TZ-500	198	0.394	2.5
3/1TZ-500	175	0.385	2.6
1/3TZ-500	189	0.392	2.5
1/1TZ-600	187	0.391	2.5
1/1TZ-700	165	0.382	2.7

[a] Error of measurement = ±6%.
[b] BJH desorption cumulative volume of pores between 1.7 and 300 nm diameter.
[c] BJH desorption average pore diameter.

It can be seen that the specific surface area of SO_4-ZrO_2 increased when the sulfur was loaded up to 1.8%, then the surface area slightly decreased when the sulfur loading content was 2.5%. The abrupt decrease in surface area with higher sulfur contents could be correlated with the alteration of crystal structure and sulfate migration into the bulk phase of the solid. It should be noted that, by loading sulfur over zirconia, the catalyst exhibited smaller crystallite sizes, which caused the increase in the cumulative pore volume, and the reduction of the average pore diameter. As for WO_3-ZrO_2, the specific surface area was also found to increase with increasing tungsten loading content, which could be due to the reducing of ZrO_2 sintering rate by WO_3 adding as reported by Iglesia et al (1993). It can also be seen from Table 4.1 that the specific surface area and cumulative pore volume of SO_4-ZrO_2 considerably decrease with increasing calcination temperature, whereas those of WO_3-ZrO_2 also decrease but with the lower rate due to the preventing of ZrO_2 sintering by WO_3 as mentioned above. For TiO_2-ZrO_2, the BET results indicated that TiO_2-ZrO_2 with Ti/Zr molar ratio of 1/1 shows the greatest specific surface area. Similar to SO_4-ZrO_2 and WO_3-ZrO_2, the specific surface area and cumulative pore volume of TiO_2-ZrO_2 linearly decreased with increasing calcination temperature, whereas the average pore diameter increased.

According to the XRD measurement, the characteristic peaks at $2\theta = 28.2^o$ and 31.5^o for (-111) and (111) reflexes were represented to the monoclinic phase in ZrO_2, while that at $2\theta = 30.2^o$ for the (111) reflex in the XRD patterns was the tetragonal phase in ZrO_2. It was found that all SO_4-ZrO_2 and WO_3-ZrO_2 catalysts contain both tetragonal and monoclinic phases with various contents depending on the preparation condition. The percents of tetragonal and monoclinic phases were calculated by a comparison of the areas for the characteristic peaks of the monoclinic phase and the tetragonal phase using means of the Gaussian areas ($h \times w$), where h and w are the height and half-height width of the corresponding XRD characteristic peak. Tables 4.4-4.5 presents the contents of both phases for these catalysts, which were calculated from the areas of corresponding XRD characteristic peaks. The results revealed that the average crystal size and the fraction of monoclinic phase for SO_4-ZrO_2 decreased when the sulfur loading content increased from 0% to 0.75% and 1.8%, then they slightly increased when the sulfur loading content was 2.5%. For WO_3-ZrO_2, the fraction of tetragonal phase increased with increasing tungsten loading; in addition, the formation of triclinic phase WO_3 was also detected at high WO_3 loadings. It can also be seen that the crystal size in monoclinic phase and the fraction of monoclinic phase for both SO_4-ZrO_2 and WO_3-ZrO_2 increased with increasing calcination temperature. For TiO_2-ZrO_2, the main phase observed from

XRD over this catalyst is $TiZrO_4$ (as amorphous phase when calcined at 500°C and turns to be crystalline at higher calcination temperature (> 500°C).

Table 4.4 SO_4-ZrO_2 characteristics obtained from XRD measurement.

Catalysts	Phase	Average Crystal Size (nm)	Crystal Size (nm)[a]		% monoclinic phase[a]
			M[b]	T[c]	
0.75SZ-500	M, T	8.1	8.3	4.2	66.3
1.8SZ-500	M,T	7.8	8.1	4.0	62.9
2.5SZ-500	M, T	7.9	8.1	3.9	63.4
1.8SZ-600	M,T	8.2	8.2	4.3	65.0
1.8SZ-700	M, T	8.7	8.5	4.7	68.7

[a] Based on XRD line broadening
[b] Monoclinic phase in ZrO_2
[c] Tetragonal phase in ZrO_2

Table 4.5 WO_3-ZrO_2 characteristics obtained from XRD measurement.

Catalysts	Phase	Average Crystal Size (nm)	Crystal Size (nm)[a]		% monoclinic phase[a]
			M[b]	T[c]	
20WZ-700	M, T	8.4	8.9	4.7	50.3
10WZ-800	M, T	9.7	9.9	5.3	53.8
20WZ-800	M, T	9.5	9.7	5.1	51.4
30WZ-800	M, T	9.4	9.6	5.1	51.2
20WZ-900	M, T	10.3	10.5	5.9	57.6

[a] Based on XRD line broadening
[b] Monoclinic phase in ZrO_2
[c] Tetragonal phase in ZrO_2

Lastly, NH_3- and CO_2-TPD techniques were used to measure the acid-base properties of the catalysts. The amounts of acid and base sites, which were calculated from the area below curves of these TPD profiles, are listed in Tables 4.6-4.8.

Table 4.6 Results from NH_3- and CO_2-TPD measurements of SO_4-ZrO_2 prepared from different conditions

Catalysts	Total Sites (μmol/g)		Density of Sites (μmol/m^2)	
	Acid Sites[a]	Base Sites[b]	Acid Sites	Base Sites
0.75SZ-500	677.2	47.9	2.97	0.21
1.8SZ-500	733.9	70.5	3.02	0.29
2.5SZ-500	734.7	78.2	3.10	0.33
1.8SZ-600	524.5	43.0	2.93	0.24
1.8SZ-700	305.1	19.2	2.70	0.17

Table 4.7 Results from NH_3- and CO_2-TPD measurements of WO_3-ZrO_2 prepared from different conditions

Catalysts	Total Sites (μmol/g)		Density of Sites (μmol/m^2)	
	Acid Sites[a]	Base Sites[b]	Acid Sites	Base Sites
20WZ-700	330.3	42.9	2.73	0.35
10WZ-800	263.1	31.8	2.89	0.34
20WZ-800	280.2	35.5	2.95	0.37
30WZ-800	286.3	37.2	2.75	0.36
20WZ-900	219.2	21.4	2.81	0.27

[a] From NH_3-TPD.
[b] From CO_2-TPD.

Table 4.8 Results from NH_3- and CO_2-TPD measurements of TiO_2-ZrO_2 prepared from different conditions

Catalysts	Total Sites (μmol/g)		Density of Sites (μmol/m^2)	
	Acid Sites[a]	Base Sites[b]	Acid Sites	Base Sites
1/1TZ-500	692	697	3.49	3.52
3/1TZ-500	594	708	3.39	4.04
1/3TZ-500	653	703	3.45	3.71
1/1TZ-600	645	712	3.45	3.81
1/1TZ-700	554	806	3.35	4.89

[a] From NH_3-TPD.
[b] From CO_2-TPD.

Along with these values, the distribution of acid and base site on the catalyst surface (namely the density of acid and base site; μmol m^{-2}) is also given in the table since this parameter is important indicator to determine the catalytic reactivity of acid and base reactions (Maniriquez et al., 2004; Tomishige et al., 2000). According to the studies over SO_4-ZrO_2, the amount and density of acid sites increased with increased percents of sulfur contents. Differently for WO_3-ZrO_2, the density of acid sites increased with increased percents of tungsten content in ZrO_2 up to 20% of tungsten content; then it decreased with more tungsten loadings (30%). Considering the base sites, the amount of base sites for both SO_4-ZrO_2 and WO_3-ZrO_2 catalysts increased proportional to the sulfur and tungsten contents in ZrO_2. By increasing the calcination temperature, the amounts of acid and base sites for both catalysts decreased. Nevertheless, it was found that the densities of acid and base sites for SO_4-ZrO_2 decreased with increasing calcination temperature (from 500^{o}C to 600 and 700 ^{o}C), whereas they increased with increasing calcination temperature from 700^{o}C to 800^{o}C for WO_3-ZrO_2 before dropped down at higher calcination temperature (900^{o}C). It can also be noticed that, at the same calcination temperature (700^{o}C), the amount and density of acid sites for WO_3-ZrO_2 are slightly higher than those of SO_4-ZrO_2. For TiO_2-ZrO_2, the catalyst with Ti/Zr molar ratio of 1/1 showed the greater amounts and densities of acid sites compared to other two ratios (3/1 and 1/3). In addition, the calcination temperature was found to affect the

acidity-basicity properties of TiO_2-ZrO_2; the amount and density of acid sites decreased with increasing calcination temperature, whereas those of base sites increased with increasing calcination temperature.

4.3.2 Catalyst reactivity toward transesterification/esterification in near-critical methanol

The catalytic reactivities toward transesterification and esterification of CPO, RPO and PFAD were firstly tested at 250°C with the reaction time of 10 min with and without the presence of three different catalysts. Figs. 4.4-4.6 show the yield of FAME production from these reactions; it can be seen that the FAME yield from the reaction of RPO is the highest, whereas that from the reaction of PFAD is relatively lower than other two feedstocks. In addition, in the presence of catalyst, the FAME yields are significantly higher than those without catalyst, particularly for WO_3-ZrO_2 and SO_4-ZrO_2 catalysts. The reusability of these solid catalysts was also carried out by washed and dried the separated catalysts from the solution before re-testing their reactivities at the same operating conditions.

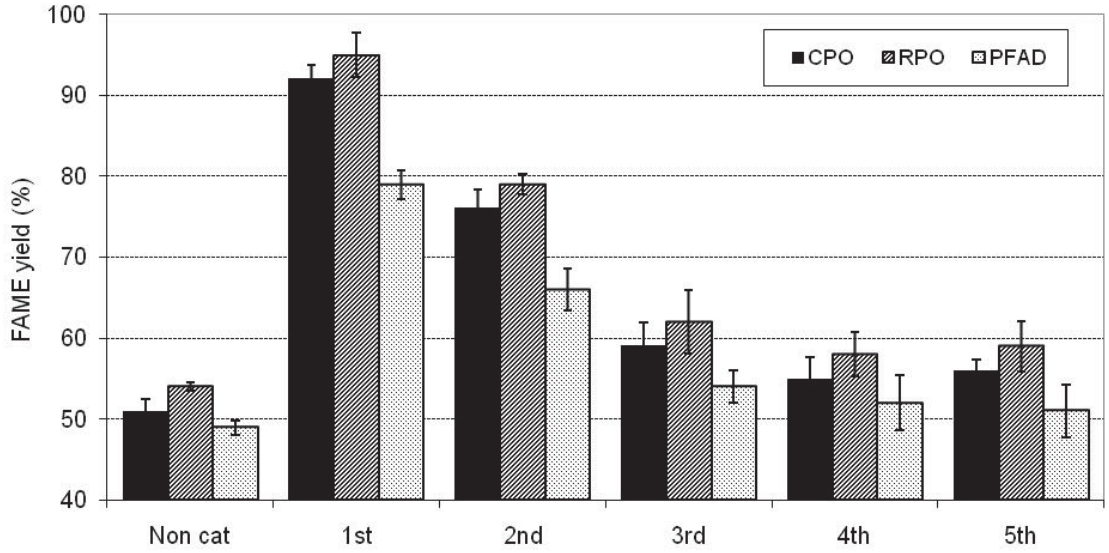

Figure 4.4 Yield of FAME production (in 5 reaction cycles) from the transesterification and esterification of CPO, RPO and PFAD with and without the presence of SO_4-ZrO_2 at 250°C with the reaction time of 10 min and methanol to feedstock molar ratios of 24:1 (for CPO and RPO) and 18:1 (for PFAD)

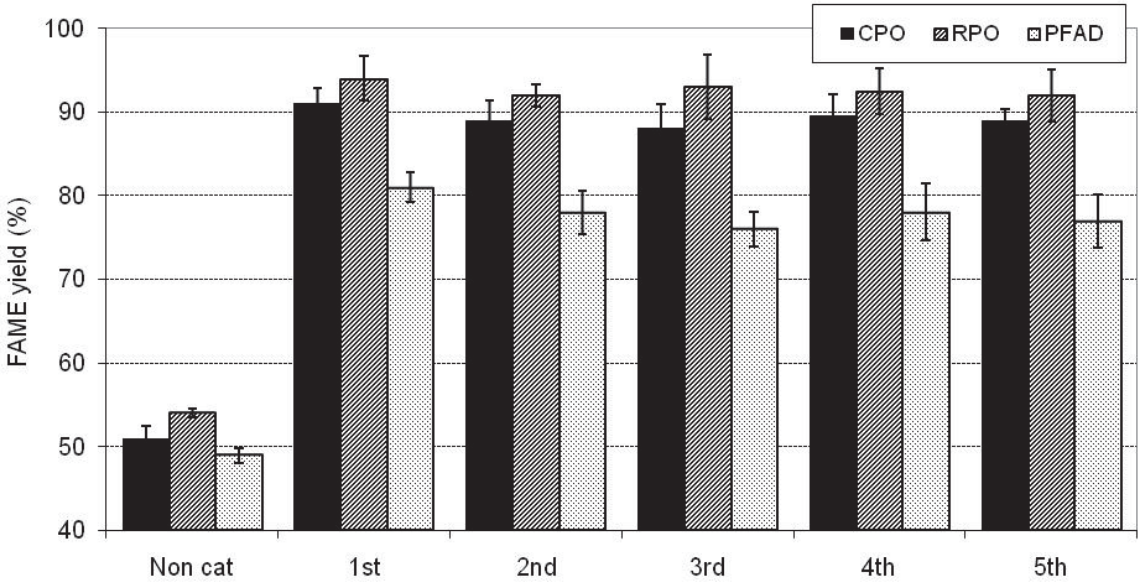

Figure 4.5 Yield of FAME production (in 5 reaction cycles) from the transesterification and esterification of CPO, RPO and PFAD with and without the presence of WO_3-ZrO_2 at 250°C with the reaction time of 10 min and methanol to feedstock molar ratios of 24:1 (for CPO and RPO) and 18:1 (for PFAD)

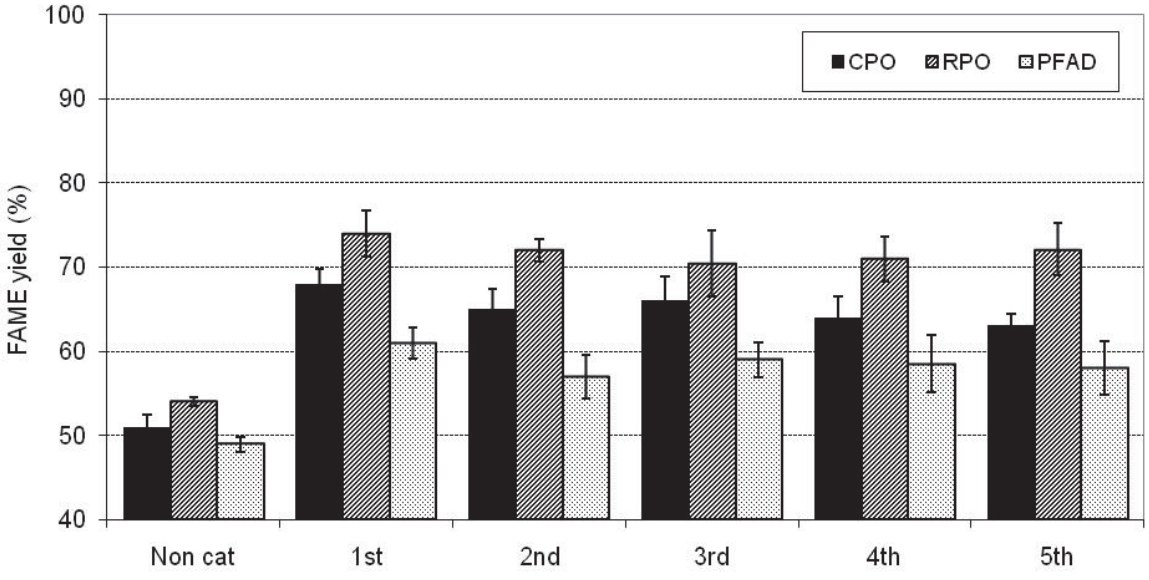

Figure 4.6 Yield of FAME production (in 5 reaction cycles) from the transesterification and esterification of CPO, RPO and PFAD with and without the presence of TiO_2-ZrO_2 at 250°C with the reaction time of 10 min and methanol to feedstock molar ratios of 24:1 (for CPO and RPO) and 18:1 (for PFAD)

As also shown in Figs. 4.4-4.6, the reactivities of spent WO_3-ZrO_2 and TiO_2-ZrO_2 are almost identical to the fresh one indicated their well-reusable; this highlights the great benefit of these modified zirconia-based catalysts. In contrast, for SO_4-ZrO_2, significant

deactivation was observed form the reused catalyst. It has widely been reported that the limitation of SO_4-ZrO_2 is the sulfur leaching from the catalyst, poisoning and pore filling during the process (Lo´pez et al., 2008; Corma, 1997; and Kiss et al., 2006). Lo´pez et al. (2008) also indicated that the high electronegative sulfate ions can be lost from the catalyst during the reaction with alcohol. In addition, the catalyst deactivation can also be due to the side blockage by adsorbed intermediates or product species that were considerably more polar than the original reagents (Lo´pez et al., 2005), and/or carbon deposition (Suwannakarn et al., 2008). Therefore, WO_3-ZrO_2 would be a good candidate for esterification of PFAD ahead of SO_4-ZrO_2 and TiO_2-ZrO_2 in terms of its high reactivity and reusability. Importantly, we found that the catalyst preparation condition (i.e. sulfate and tungsten loading contents, Ti/Zr molar ratio, and the catalyst calcination temperature) strongly affects the reaction reactivity, as shown in Figs. 4.7-4.9.

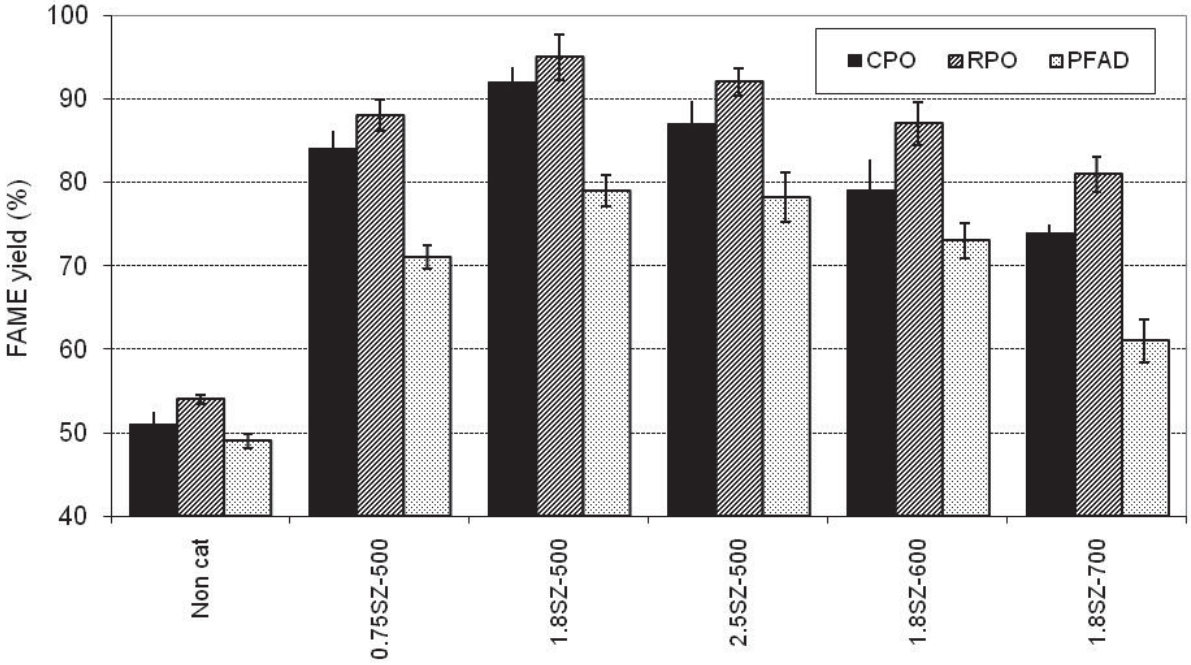

Figure 4.7 Effect of catalyst preparing condition (SO_4-ZrO_2) on the yield of FAME production from the transesterification and esterification of CPO, RPO and PFAD at 250°C with the reaction time of 10 min and methanol to feedstock molar ratios of 24:1 (for CPO and RPO) and 18:1 (for PFAD)

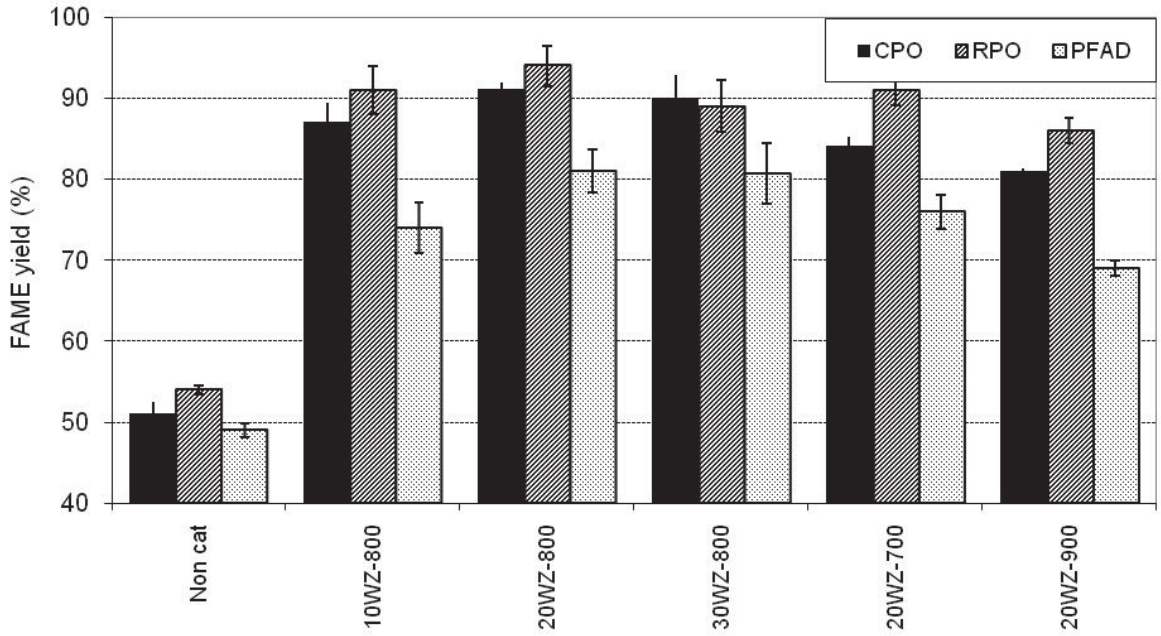

Figure 4.8 Effect of catalyst preparing condition (WO_3-ZrO_2) on the yield of FAME production from the transesterification and esterification of CPO, RPO and PFAD at 250°C with the reaction time of 10 min and methanol to feedstock molar ratios of 24:1 (for CPO and RPO) and 18:1 (for PFAD)

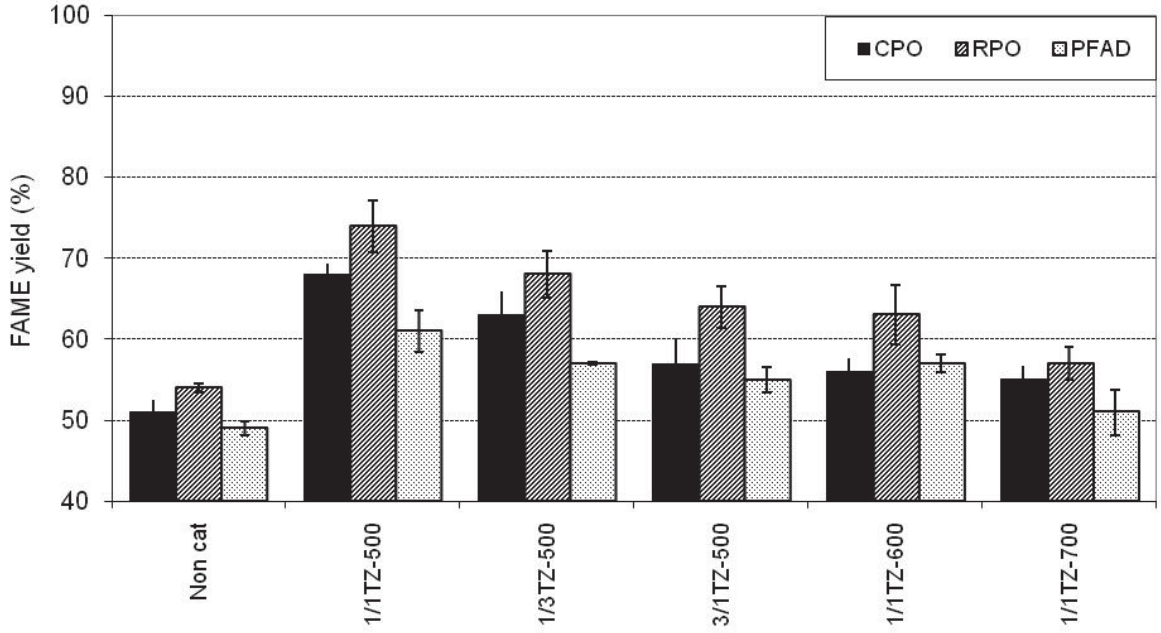

Figure 4.9 Effect of catalyst preparing condition (TiO_2-ZrO_2) on the yield of FAME production from the transesterification and esterification of CPO, RPO and PFAD at 250°C with the reaction time of 10 min and methanol to feedstock molar ratios of 24:1 (for CPO and RPO) and 18:1 (for PFAD)

Among all types of catalyst, 20WZ-800 is the most active one providing the FAME yields of 91.3, 94.1 and 81.0% from CPO, RPO and PFAD respectively. For SZ-based and TZ-based catalysts, 1.8SZ-500 and 1/1TZ-500 are the most active catalyst in their own groups. It can be seen from this figure that the loading of too high sulfur and tungsten contents (2.5SZ and 30WZ) caused a slight negative effect on the catalytic activity. The inhibitory effect for SO_4-ZrO_2 could be due to the agglomeration of the active SO_4^{2-} phase and/or the cover of basic sites by the exceeded SO_4^{2-}, which results in lower the surface areas of active components and eventually the catalytic activity as reported by Xie et al., 2007, whereas the negative effect for WO_3-ZrO_2 can be explained by the acid-base properties of catalyst, according to NH_3- and CO_2-TPD results. As seen in Tables 6-8, although the amount of acid sites for 30WZ is higher than that of 10WZ and 20WZ, the density of acid sites for 20WZ is greater than that of 10WZ and 30WZ. We therefore suggest here that the acid site density is important indicator than the amount of acid site to judge the catalyst reactivity toward our interest reactions. In the case of TiO_2-ZrO_2, the high reactivity of 1/1TZ could be due to the higher specific surface area, the amount and the density of acid sites for this catalyst compared to 1/3TZ and 3/1TZ. It is noted that although the amount and the density of acid sites for TiO_2-ZrO_2 catalysts are relatively higher than those of WO_3-ZrO_2 and SO_4-ZrO_2, the catalyst reactivities toward these reactions are obviously lower. This implies the influence of other parameters that affect the reactivity toward transesterification and esterification reactions apart from catalyst acid-base properties.

It can be seen from Figs. 4.7-4.9 that the calcination temperature showed significant impact on the catalyst reactivity. At high calcination temperature (700^{o}C), the reactivities of SO_4-ZrO_2 and TiO_2-ZrO_2 considerably decreased; this can be explained by the decreases of catalyst specific surface area and the amount of acid sites at high calcination temperature. Furthermore, it can be noticed from the XRD studies that the crystalline structure of catalysts calcined at different temperatures also closely related to the catalyst reactivity. As seen in Tables 4-5 the percentage of tetragonal phase for SO_4-ZrO_2 is in the same trend as the reaction rate; and it seems that the presence of tetragonal phase render to increase the reactivity for the interested reactions. In the case of TiO_2-ZrO_2, the best reactivity was observed from the catalyst calcined at 500^{o}C. According to the XRD studies, the phase of TiO_2-ZrO_2 turns from amorphous to crystalline phase above 500^{o}C; hence, this suggests that TiO_2-ZrO_2 with amorphous phase is more active than crystalline phase. Importantly, for WO_3-ZrO_2, it was found that the catalyst calcined at 800^{o}C achieved higher reactivity than those calcined at 700^{o}C and 900^{o}C. This result is in good agreement with Lo´pez et al. (2008) who suggested that the presence of polymeric tungsten species (at the calcination temperature of 800^{o}C) along with the tetragonal form of ZrO_2 support promote the reactivity of toward the acid- and alkali-catalyzed reactions. We summarized from our studies that the catalyst acid-base properties and the phase formation play an important role on the reactivity toward transesterification and esterification reactions under near-critical methanol condition.

4.3.3 Effect of operating conditions on the reaction reactivity

Based on the above results, 20WZ-800 was selected for further studies in order to determine the optimum operating conditions that maximize the yield of FAME production from CPO, RPO and PFAD. Firstly, the effect of reaction time on the FAME yield was determined by varying the reaction time from 0 to 90 min (using the reaction temperature of 250^{o}C and methanol to reactant molar ratios of 24:1 for CPO and RPO

and 6:1 for PFAD). As shown in Fig. 3, it was found that the FAME yield increases with increasing the reaction time until 10 min for the transesterification of CPO and RPO and around 1 min for the esterification of PFAD, providing the FAME yields of 91.3, 94.1 and 81.0% respectively. After that, the yields remained nearly constant or slightly decreased, which could be due to thermal decomposition that occurred after transesterification and esterification reached nearly reaction equilibrium (Xie et al., 2006)). Thus, we suggest here that the reactions of CPO and RPO under near-critical methanol in the presence of WO_3-ZrO_2 were completed at about 10 min, whereas that of PFAD was completed in 1 min. For comparison, the reactions without catalyst were also tested. As also shown in Figs. 4.10-4.11, the transesterification reaction requires more than 1 h to reach steady state, whereas the esterification requires 30 min. Hence, the capability to shorter the reaction time is the great benefit of adding WO_3-ZrO_2, which can reduce the energy consumption and cost of FAME production.

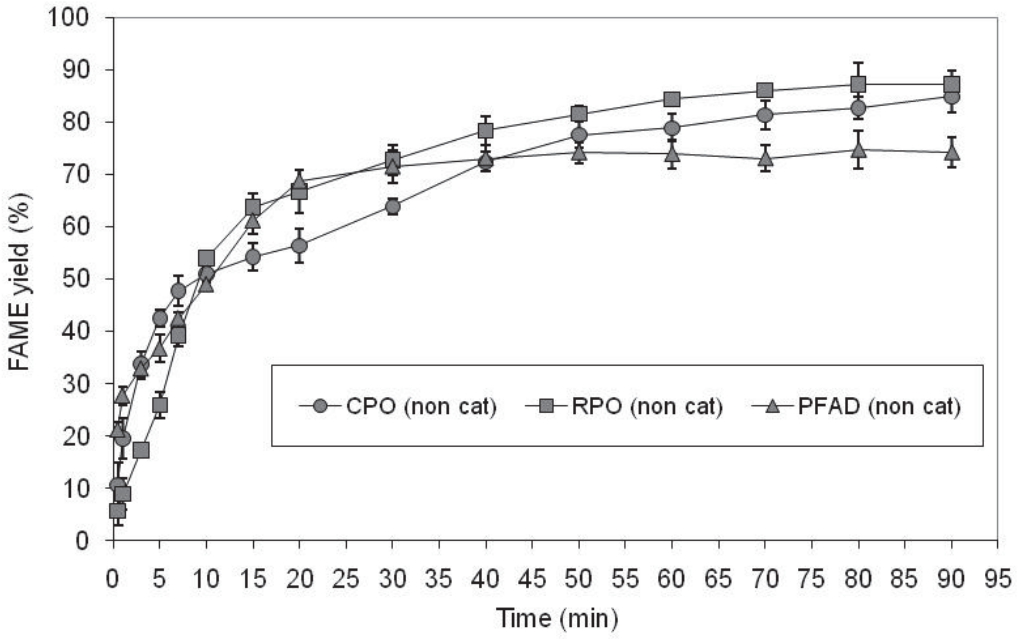

Figure 4.10 Effect of reaction time on the yield of FAME production from the transesterification and esterification of CPO, RPO and PFAD without the presence of catalyst at 250°C with the methanol to feedstock molar ratios of 24:1 (for CPO and RPO) and 18:1 (for PFAD)

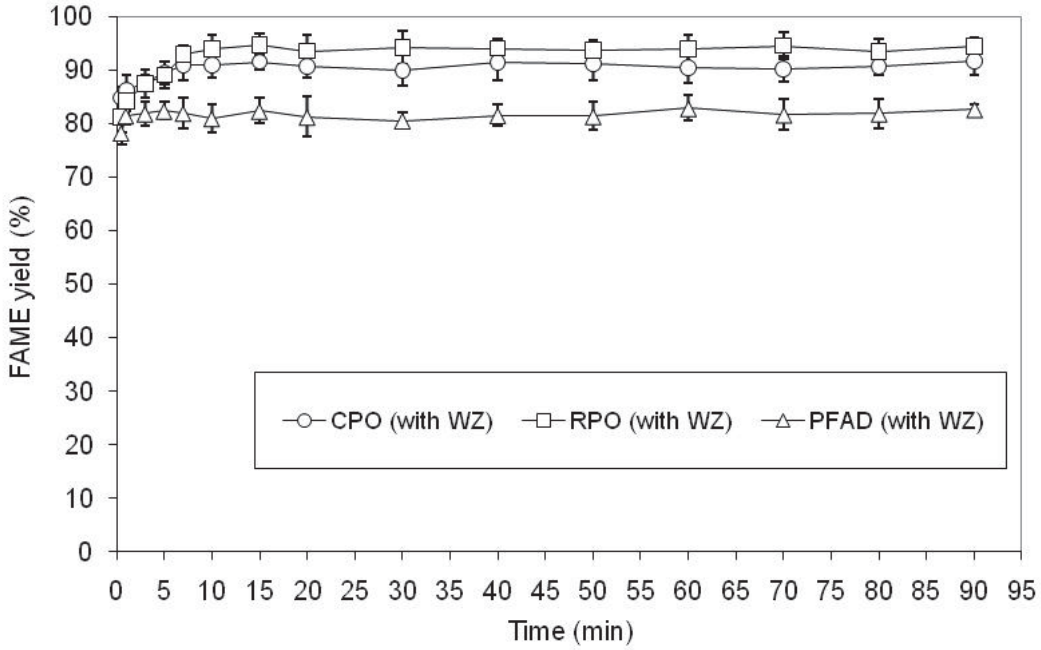

Figure 4.11 Effect of reaction time on the yield of FAME production from the transesterification and esterification of CPO, RPO and PFAD with the presence of 20WZ-800 catalyst at 250°C with the methanol to feedstock molar ratios of 24:1 (for CPO and RPO) and 18:1 (for PFAD)

Then, the effect of reaction temperature on the yield of FAME production was carried out by varying the reaction temperature from 200 to 300°C. The results in Figs. 4.12-4.13 indicate that, in the presence of WO_3-ZrO_2, the yields of FAME production increase with increasing the reaction temperature from 200-250°C for all reactions; above that temperature, the FAME yields are relatively constant. In contrast, without catalyst, the FAME yields from these reactions continue increased (from 51.2% (CPO), 54.1% (RPO), and 49.4% (PFAD) at 250°C to 81.5% (CPO), 88.6% (RPO), and 72.7% (PFAD) at 300°C). It can be seen that even at the reaction temperature as high as 300°C, the FAME yields from these reactions are relatively lower than those from the reactions in the presence of WO_3-ZrO_2 at 250°C. Thus, apart from the beneficial in term of shorter reaction time, the lower reaction temperature is another advantage of WO_3-ZrO_2 adding for these reactions.

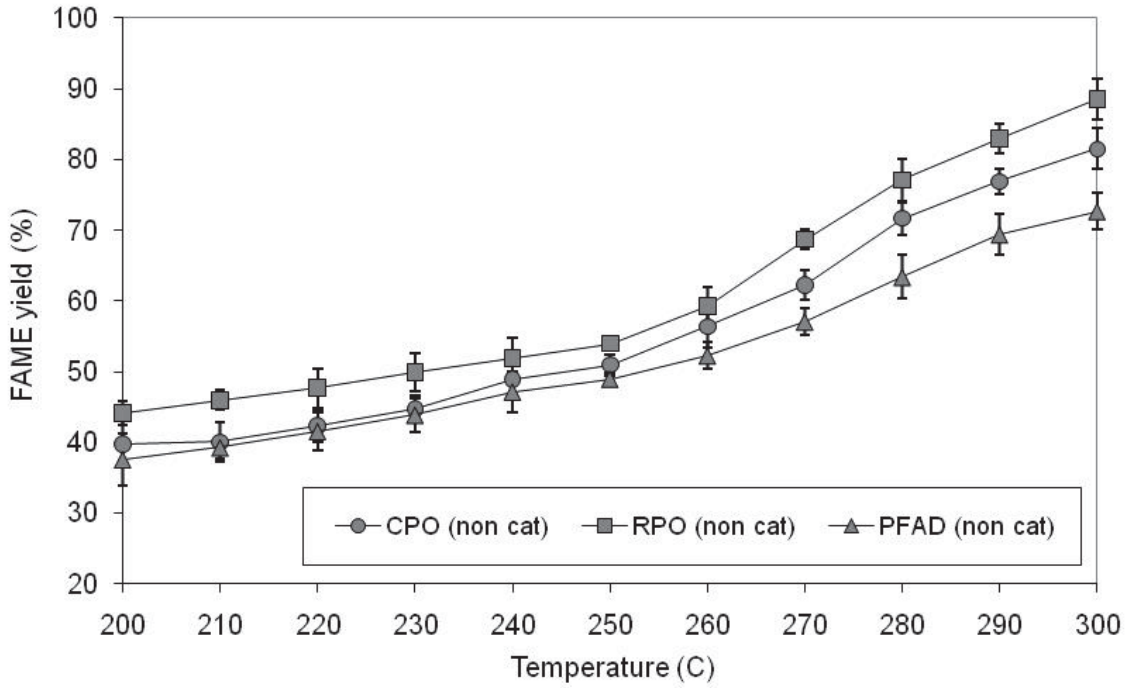

Figure 4.12 Effect of reaction temperature on the yield of FAME production from the transesterification and esterification of CPO, RPO and PFAD without the presence of catalyst at the reaction time of 10 min and methanol to feedstock molar ratios of 24:1 (for CPO and RPO) and 18:1 (for PFAD)

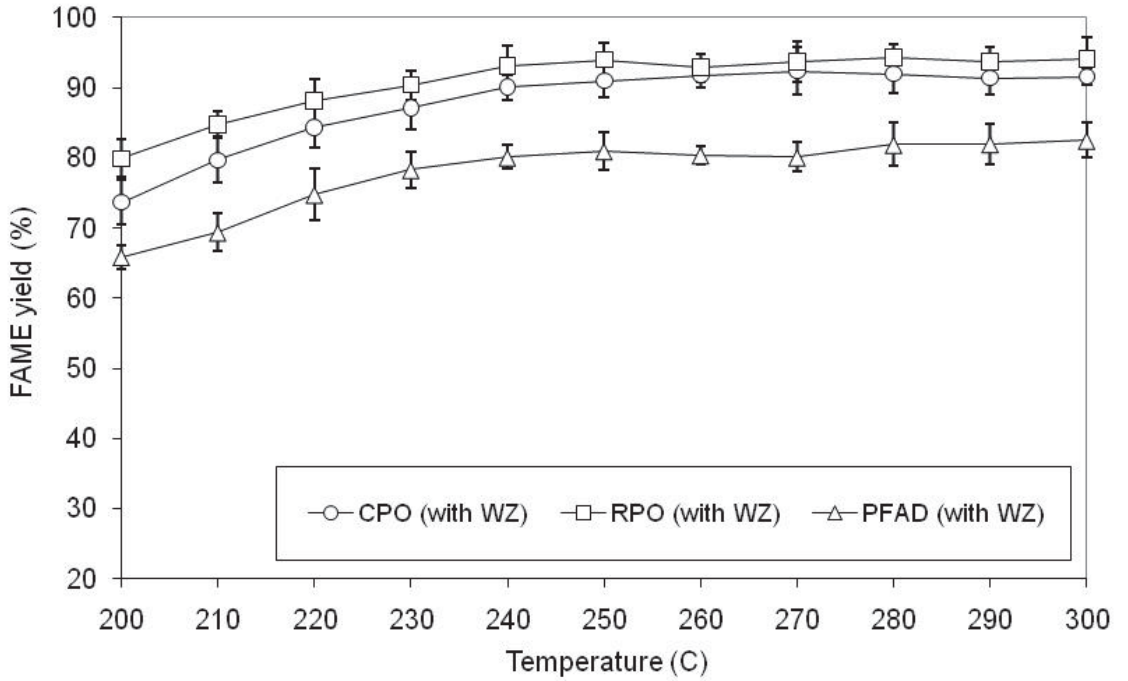

Figure 4.13 Effect of reaction temperature on the yield of FAME production from the transesterification and esterification of CPO, RPO and PFAD with the presence of 20WZ-800 catalyst at the reaction time of 10 min and methanol to feedstock molar ratios of 24:1 (for CPO and RPO) and 18:1 (for PFAD)

The effect of methanol to reactant molar ratio on the yield of FAME production was also determined. According to the typical transesterification, three moles of alcohol and one mole of triglyceride are required to produce three moles of fatty acid ester and one mole of glycerol. As for esterification, it requires one mole of alcohol and fatty acid to produce one mole of fatty acid ester and water. Practically, excess amount of alcohol is always applied in order to shift the equilibrium to the right-hand side. However, the use of too high amount of alcohol could also increase the cost of FAME and/or biodiesel production. In this study, the effect of methanol to reactant molar ratio was determined by varying the ratio between 6:1 to 42:1 for the transesterification of CPO and RPO and 3:1 to 18:1 for the esterification of PFAD. Figs. 4.14-4.15 show the effect of this molar ratio on the yield of FAME production after 10 min reaction time.

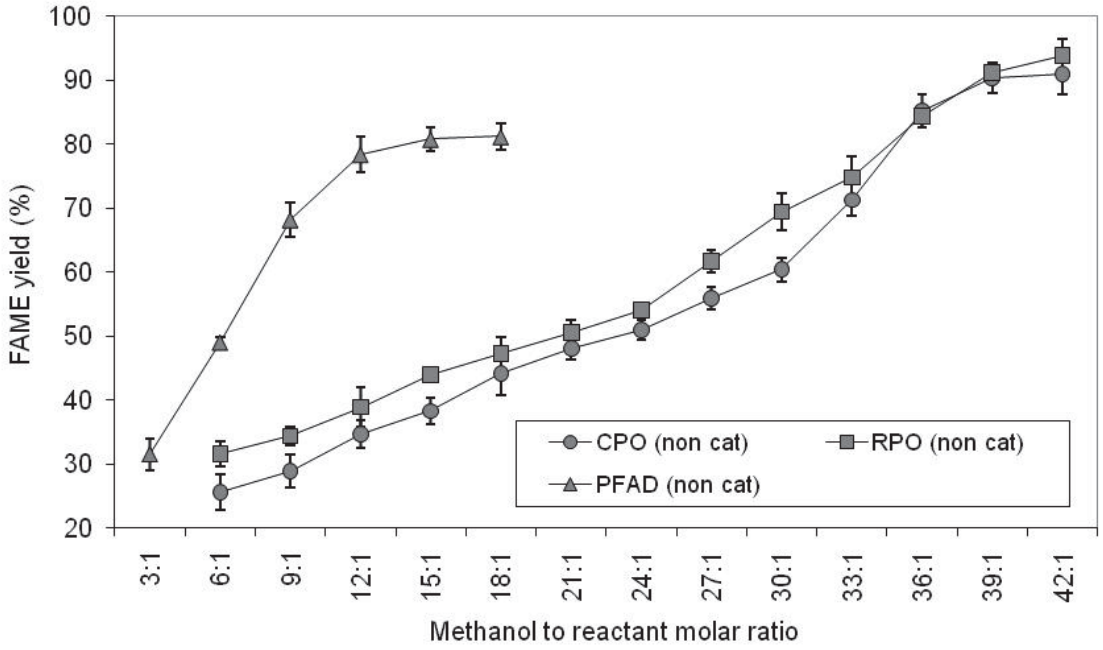

Figure 14 Effect of methanol to feedstock molar ratio on the yield of FAME production from the transesterification and esterification of CPO, RPO and PFAD without the presence of catalyst at 250°C with the reaction time of 10 min

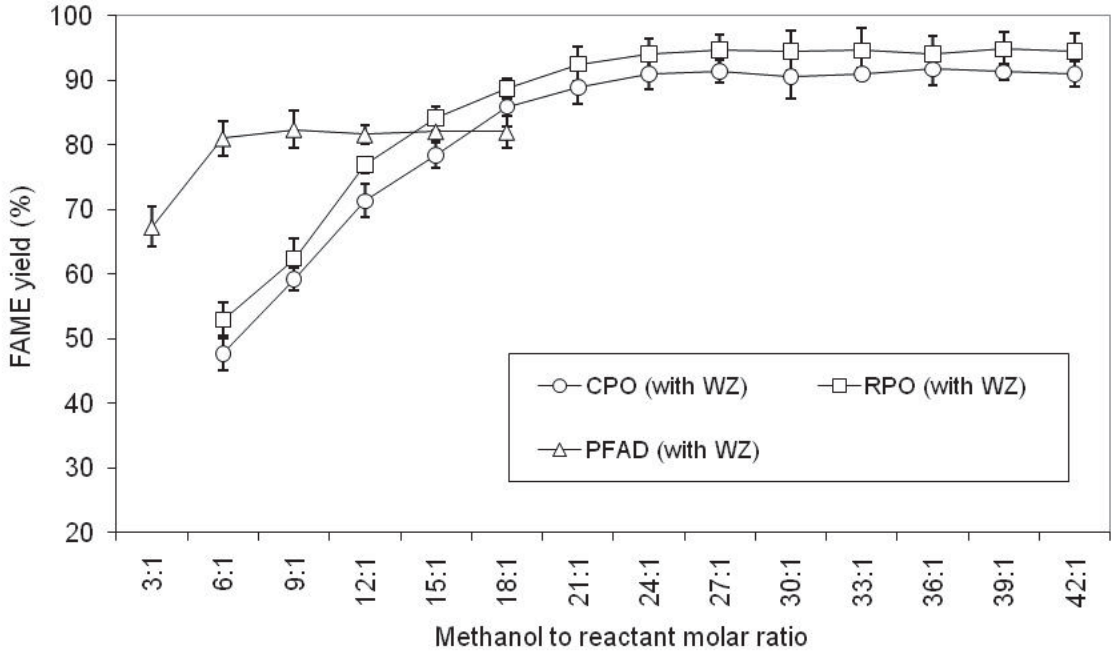

Figure 4.15 Effect of methanol to feedstock molar ratio on the yield of FAME production from the transesterification and esterification of CPO, RPO and PFAD with the presence of 20WZ-800 catalyst at 250°C with the reaction time of 10 min

Clearly, the yield increased with increasing methanol to reactant molar ratio (from 47.7% to 91.3% and 52.9% to 94.1% as the molar ratio increase from 6:1 to 24:1 for the transesterification of CPO and RPO respectively, and from 67.3% to 81.0% as the molar ratio increase from 3:1 to 6:1 for the esterification of PFAD). Upon those molar ratios, the reaction rates seem to be unaffected by the methanol content. Therefore, the optimum molar ratio of methanol to reactants for the transesterification of CPO and RPO and the esterification of PFAD in near-critical methanol were 24:1 and 6:1, respectively. For comparison, these reactions without catalyst were also carried out and it was found that the transesterification of CPO and RPO required methanol to reactant molar ratios more than 39:1, while the esterification of PFAD required the ratio of 15:1 to reach the same levels of FAME yield. Hence, another great benefit of WO_3-ZrO_2 is that it can significantly reduce the requirement of excess methanol to complete the reaction. We concluded from all experiments that the optimum conditions that maximize the yield of FAME production from the transesterification of CPO and RPO in the presence of WO_3-ZrO_2 are at 250°C with the reaction time of 10 min and methanol to reactant molar ratio of 24:1, while those for the esterification of PFAD are at 250°C with the reaction time of 1 min and methanol to PFAD molar ratio of 6:1. It is noted that the effect of catalyst to reactants mass ratio on the reaction rates was also studied and we found that the optimum mass ratio of catalyst to reactant for both transesterification and esterification under near-critical methanol was 0.5 %.

4.3.4 Reactions in the presence of co-solvents

Previously, it has been reported that the additional of suitable co-solvent could improve the performance of transesterification reaction by reducing the amount of

methanol required for the reaction; hence, the effect of co-solvent adding (i.e. hexane, benzene and toluene) was also evaluated in the present work by adding 10% v/v of these solvents in palm feedstocks. The enhancing effect of co-solvent adding in the reaction medium at different methanol to reactant molar ratios is shown in Tables 4.9-4.11.

Table 4.9 Effect of co-solvent adding on the yield of FAME production from the reaction of CPO in the presence of 20WZ-800 at various methanol to feedstock molar ratios (at 250°C with the reaction time of 10 min)

Feedstock	Methanol to feedstock ratio	FAME production yield (%)			
		No co-solvent	with hexane	with benzene	with toluene
CPO	6:1	47.7 (±2.7)	45.4 (±1.9)	49.6 (±2.5)	54.7 (±0.8)
	12:1	71.3 (±2.4)	68.3 (±2.1)	74.7 (±1.8)	78.9 (±2.3)
	18:1	85.9 (±3.1)	81.4 (±2.0)	87.2 (±2.1)	91.5 (±1.7)
	24:1	91.0 (±2.4)	88.7 (±0.4)	92.2 (±1.4)	93.9 (±2.0)

Table 4.10 Effect of co-solvent adding on the yield of FAME production from the reaction of RPO in the presence of 20WZ-800 at various methanol to feedstock molar ratios (at 250°C with the reaction time of 10 min)

Feedstock	Methanol to feedstock ratio	FAME production yield (%)			
		No co-solvent	with hexane	with benzene	with toluene
RPO	6:1	52.9 (±2.8)	49.9 (±1.3)	55.6 (±2.1)	58.8 (±3.1)
	12:1	76.9 (±1.2)	74.5 (±3.4)	79.3 (±1.9)	82.7 (±2.3)
	18:1	88.7 (±1.5)	84.7 (±2.4)	90.9 (±2.7)	94.0 (±1.4)
	24:1	94.1 (±2.5)	91.2 (±1.8)	94.7 (±0.7)	95.5 (±1.8)

Table 4.11 Effect of co-solvent adding on the yield of FAME production from the reaction of PFAD in the presence of 20WZ-800 at various methanol to feedstock molar ratios (at 250°C with the reaction time of 10 min)

Feedstock	Methanol to feedstock ratio	FAME production yield (%)			
		No co-solvent	with hexane	with benzene	with toluene
PFAD	3:1	67.3 (±3.1)	64.3 (±2.8)	71.2 (±2.2)	75.4 (±2.0)
	6:1	81.0 (±2.7)	77.9 (±2.3)	84.7 (±1.8)	87.7 (±1.9)
	9:1	82.4 (±2.9)	79.0 (±1.4)	86.1 (±2.1)	90.3 (±0.8)
	12:1	81.6 (±1.4)	80.1 (±0.8)	87.4 (±2.3)	90.2 (±1.3)

Clearly, the FAME yields increase when toluene and benzene were added particularly at low methanol to reactant molar ratio, whereas they slightly decrease when hexane was added. In the presence of toluene, more than 90% yields of FAME production can be obtained from the reactions of CPO, RPO and PFAD using methanol to reactant molar ratio of 18:1 (for CPO and RPO) and 9:1 (for PFAD), whereas these reactions without toluene adding required methanol to reactant molar ratio of 24:1 to achieve that range of FAME yields. It is noted that the reaction improvement with additions of benzene and toluene could possibly be due to the fact that benzene and toluene are good solvents for vegetable oil and both are miscible with methanol (Krisnangkura and Simamaharnnop; 1992), therefore these solvents could help the mixing of methanol with oil in reactor. The inhibitory effect of hexane could be due to the low solubility of this solvent in methanol, hence it acts as an antisolvent and reduced the biodiesel production yield.

4.3.5 Effect of water on the reaction reactivity

It is well established that the presence of water provides negative effect on the alkali- and acid-catalyzed reactions, since water interferes with the catalyst and reduces catalyst performance (Komers et al., 2001). For the alkaline-catalyzed process, the conversion was reported to reduce slightly when some water was presented in the system. As for acid-catalyzed reaction, only as little as 0.1% of water added to the reaction could lead to 6% reduction of the production yield (Canakci et al., 1999). According to the transesterification in supercritical methanol, Kusdiana and Saka (2001) demonstrated that in the presence of water up to 30% w/w triglycerides still transesterified to methyl ester efficiently with very minimal loss in conversion. For the esterification in supercritical methanol, Kusdiana and Saka (2004) reported approximately 2-5% reduction in conversion of oleic acid to methyl oleate in the presence of water (up to 30%) at 350 ºC with the oleic acid to methanol molar ratio of 1.0:42.0. In this study, the effect of water on the reaction performance were carried out by 2 methods: (1) pre-treatment of feedstock prior the reaction by adding molecular sieve to dehydrate the reactants (CPO, RPO and PFAD) before filtering out and (2) adding the molecular sieve along with reactants to the system to dehydrate the mixture of reactant and products during the reaction. As shown in Figs. 16-18, it can be seen that uses of molecular sieve by both methods shows insignificant effect on the transesterification of RPO but led to improvement in FAME yields for CPO and PFAD (particularly for PFAD at low methanol to PFAD ratios using method (2), which achieved 21.9% increasing of FAME yield).

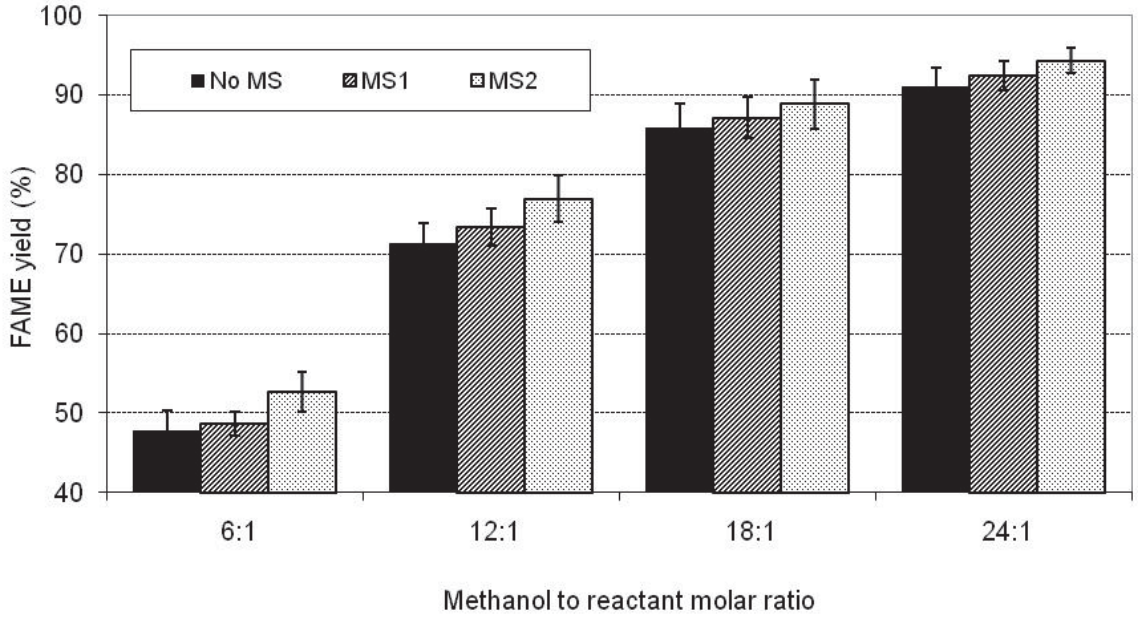

Figure 4.16 Effect of molecular sieve adding (MS1: for pre-treatment of feedstock before filtering out prior the reaction; MS2: adding along with reactants to the system) on the yield of FAME production from the transesterification and esterification of CPO at various methanol to feedstock molar ratios in the presence of 20WZ-800 (at 250°C with the reaction time of 10 min)

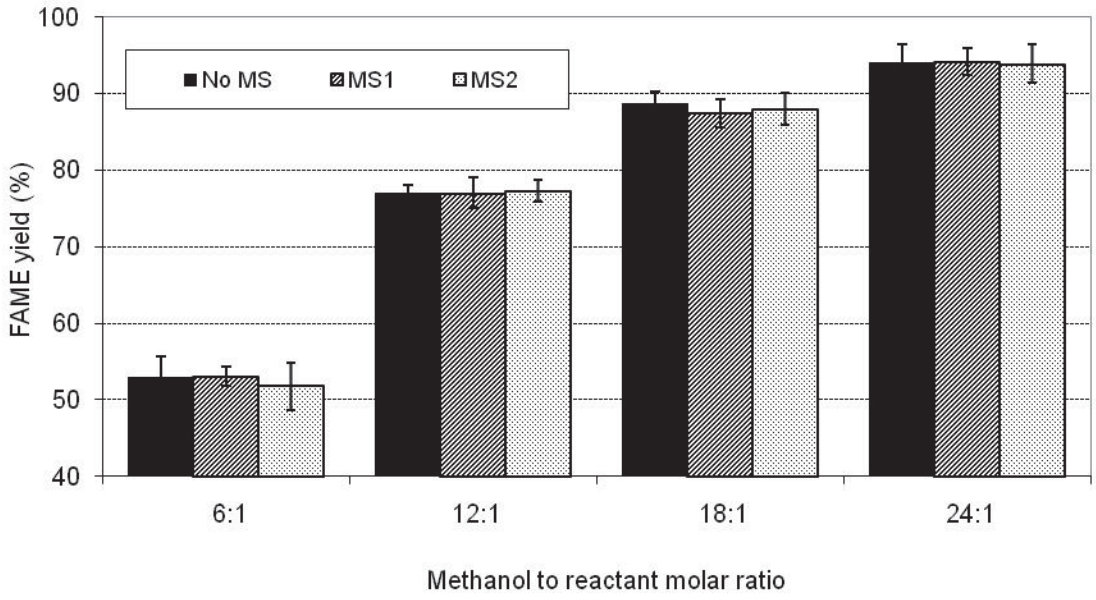

Figure 4.17 Effect of molecular sieve adding (MS1: for pre-treatment of feedstock before filtering out prior the reaction; MS2: adding along with reactants to the system) on the yield of FAME production from the transesterification of RPO at various methanol to feedstock molar ratios in the presence of 20WZ-800 (at 250°C with the reaction time of 10 min)

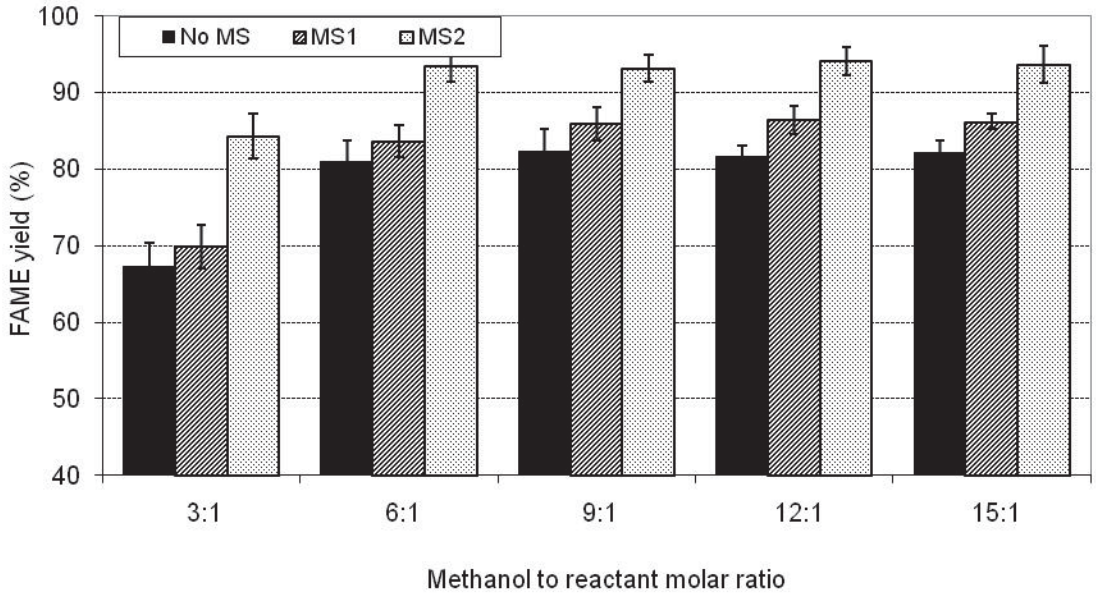

Figure 4.18 Effect of molecular sieve adding (MS1: for pre-treatment of feedstock before filtering out prior the reaction; MS2: adding along with reactants to the system) on the yield of FAME production from the esterification of PFAD at various methanol to feedstock molar ratios in the presence of 20WZ-800 (at 250°C with the reaction time of 10 min)

Water is known to affect biodiesel synthesis by favoring hydrolysis of triacylglycerol and ester products from transesterification and esterification reactions (Yamane et al., 1989; Anthonsen and Sjursens, 2000; Shah and Gupta, 2007). In this study where dried feedstocks were used (by method 1), the occurring of hydrolysis reaction is inhibited and results in the higher FAME yield achievements. The insignificant effect for the reaction of RPO could be due to its low water content after refined process and no water formation during the reaction. According to method 2, the positive effect of molecular sieve adding on the FAME yield is due to the continuous removal of water generated from the esterification of free fatty acids in PFAD and CPO (which also contains a high proportion of free fatty acids). The continuous dehydration prevents an increase of water activity in the reaction and thus results in remarked improved FAME yields from feedstocks containing high free fatty acid content. These results suggest that, in order to maximize the yield of FAME production from PFAD, care must be taken to remove water before and/or during the reaction.

4.4 Conclusions

The fatty acid methyl ester (FAME) production from the esterification reaction using palm fatty acid distilled (PFAD) as the reactant was studied under the condition of "near critical of methanol" (the temperature of 250°C with the short reaction time of 10 min) in the presence of heterogeneous catalysts. Furthermore, the transesterification and esterification of other palm products i.e. crude palm oil (CPO), and refined palm oil (RPO) were also performed for comparison. The heterogeneous catalysts selected here include the synthesized SO_4-ZrO_2, WO_3-ZrO_2 and TiO_2-ZrO_2 (with various sulfur- and tungsten-loadings, Ti/Zr ratios, and calcination temperatures). It was found that FAME production from transesterification of CPO and RPO as well as esterification of PFAD in near-critical methanol could be efficiently improved in the presences of WO_3-ZrO_2 and SO_4-ZrO_2; the reaction time, amount of methanol required and reaction temperature were reduced considerably. Although initially the reactivity of SO_4-ZrO_2 was slightly higher than WO_3-ZrO_2, SO_4-ZrO_2 showed significant deactivation after several reaction cycles due to the sulfur leaching; hence, WO_3-ZrO_2 is the better candidate for these reactions. The additional of toluene as co-solvent can reduce the requirement of methanol, while the addition of molecular sieve significantly increased FAME yield from PFAD and CPO.

4.5 References

Anthonsen T., Sjursens B.J., 2000. Importance of water activity for enzymes catalysis in non-aqueous organic systems. In: Gupta MN, editor. Methods in non-aqueous enzymology. Basel: Birkhauser Verlag. 14–35.

Canakci, M., VanGerpen, J.H., 1999. Biodiesel production via acid catalysis. Trans ASAE. 42, 1203–1210.

Cao, W., Han, H., Zhang, J., 2005. Preparation of biodiesel from soybean oil using supercritical methanol and co-solvent. Fuel 84, 347-351.

Corma, A., 1997. Solid acid catalysts. Curr. Opin. Solid State Mater. Sci. 2, 63-75.

Demirbas, A., 2007. Biodiesel from sunflower oil in supercritical methanol with calcium oxide. Energy Conver Manage 48, 937–941.

Furuta S., Matsuhashi H., Arata K., 2004. Biodiesel fuel production with solid super acid catalyst in fixed bad reactor under atmospheric pressure. Catal. Commun. 5, 721-723.

Iglesia E., Soled S.L., Kramer G.M., 1993. Isomerization of alkanes on sulfated zirconia: promotion by Pt and by adamantly hydride transfer species. J. Cat. 144, 238-253.

Jitputti J., Kitiyanan B., Rangsunvigit P., Bunyakait K., Attanatho L., Jenvanitpanjakul P., 2006. Transesterification of crude palm kernel oil and crude coconut oil by different solid catalysts. Chem. Eng. J. 116, 61-66.

Kiss A.A., Omota F., Dimian A.C., Rothenberg G., 2006. The heterogeneous advantage: biodiesel by catalytic reactive distillation. Top. Catal. 40, 141-150.

Komers J.M., Stloukal R., 2001. Biodiesel from rapeseed oil, methanol and KOH. 2. Composition of solution of KOH in methanol as reaction partner of oil. Eur. J. Lipid Sci. Tech. 103, 359–362.

Krisnangkura K., Simamaharnnop R., 1992. Continuous transmethylation of palm oil in an organic solvent. JAOCA 69, 166-169.

Kusdiana D., Saka S., 2001. Kinetics of transesterification in rapeseed oil to biodiesel fuel as treated in supercritical methanol. Fuel. 80, 693-698.

Kusdiana D., Saka S., 2004. Effects of water on biodiesel fuel production by supercritical methanol treatment. Bioresource Technol. 91, 289-295.

Lopez D.E., Goodwin Jr. J.G., Bruce D.A., Lotero E., 2005. Transesterification of triacetin with methanol on solid acid and base catalysts. Appl. Catal. A 295, 97-105.

Lopez D.E., Goodwin Jr., J.G., Bruce D.A., Furuta S., 2008. Esterification and transesterification using modified-zirconia catalysts. Appl. Catal. A 339, 76–83.

Maniriquez M.E., Lopez T., Gomez R., Navarrete J., 2004. Preparation of TiO_2-ZrO_2 mixed oxides with controlled acid–basic properties. J. Mol. Catal. A. 220, 229-237.

Rao K.N., Sridhar A., Lee A.F., Tavener S.J., Young N.A., Wilson K. 2006 Zirconium phosphate supported tungsten oxide solid acid catalysts for the esterification of palmitic acid. Green Chem. 8, 790-797.

Saka S., Kusdiana D., 2001. Biodiesel fuel from rapeseed oil as prepared in supercritical methanol. Fuel 80, 225-231.

Shah S., Gupta M.N., 2007. Lipase catalyzed preparation of biodiesel from Jatropha oil in a solvent feee system. Proc Biochem. 42, 409-414.

Suwannakarn K., Lotero E., Goodwin Jr., J.G., Lu C., 2008. Stability of sulfated zirconia and the nature of the catalytically active species in the transesterification of triglycerides. J. Catal. 255, 279-286.

Tanabe K., Holderich W.F., 1999. Industrial application of solid acid-base catalysts. Appl. Catal. 181, 399–434.

Tomishige K., Ikeda Y., Sakaihori T., Fujimoto K., 2000. Catalytic properties and structure of zirconia catalysts for direct synthesis of dimethyl carbonate from methanol and carbon dioxide. J. Catal, 192, 355-362.

Xie W., Huang X., Li H., 2007. Soybean oil methyl esters preparation using NaX zeolites loaded with KOH as a heterogeneous catalyst. Bioresource Technol. 98, 936–939.

Xie W., Peng H., Chen L., 2006. Transesterification of soybean oil catalyzed by potassium loaded on alumina as a solid-base catalyst. Appl. Catal. A 300, 67–74.

Yamane T., Kojima Y., Ichiryu T., Nagata M., Shimizu S., 1989. Intramolecular esterification by lipase powder in microaqueous benzene: effect of moisture content. Biotechnol Bioeng. 34, 838–843.

Zallaikah S., Lai C., Vali S.R., Ju Y.H., 2005. A two-step acid-catalyzed process for the production of biodiesel from rice bran oil. Bioresource Technol. 96, 1889-1896.

Chapter 5

Results and Discussion: Hydrogen production studies

5.1 Introduction

Hydrogen-rich gas is the major fuel for solid oxide fuel cell (SOFC), which can be readily produced from the reactions of several hydrocarbons i.e. methane, methanol, ethanol, liquefied petroleum gas (LPG), gasoline and other oil derivatives with oxygen-containing co-reactants i.e. O_2, H_2O, and CO_2. Partial oxidation, steam reforming and the combination of both reactions (as called autothermal reforming) have been known as feasible processes to produce hydrogen-rich fuel from several hydrocarbons[1,2]. Steam reforming is currently the most common process for producing hydrogen[1], however, it has a disadvantage of slow start-up, which makes it more suitable for a stationary system rather than for a mobile system[2]. Recently, catalytic partial oxidation[3-6] and autothermal reforming[7,8] appear to have attracted much interest. The partial oxidation consists of sub-stoichiometric oxidation of hydrocarbons, while the autothermal reforming integrates partial oxidation with steam reforming. Theoretically, both partial oxidation and autothermal reforming offer significant lower energy requirement and higher gas-space velocity than steam reforming reaction[9].

Focusing on fuel selection, due to the current oil crisis and shortage of fossil fuels, the development of H_2 production process from biomass-based feedstock attracts much attention. Among them, palm oil is one the current attractive feedstock that has widely been converted to transportation fuel (e.g. biodiesel via transesterification process). Generally, crude palm oil (CPO) always contains high amount of free fatty acid (FFA) and the presence of too high FFA could easily results in high amounts of soap produced during the transesterification reaction. To avoid this reaction, FFA must be initially removed from CPO (as called palm fatty acid distillate or PFAD). The conversion of this PFAD to valuable products e.g. hydrogen-rich gas would provide the great benefit in terms of energy and environmental aspects as well as reducing the cost of biodiesel production, enabling biodiesel to compete economically with conventional petroleum diesel fuels. Practically, PFAD consists mainly of palmitic acid ($C_{16}H_{32}O_2$; $CH_3(CH_2)_{14}COOH$), oleic acid ($C_{18}H_{34}O_2$; $CH_3(CH_2)_7CH{=}CH(CH_2)_7COOH$) and linoleic acid ($C_{18}H_{32}O_2$; $CH_3(CH_2)_4CH{=}CHCH_2CH{=}CH(CH_2)_7CO_2H$) with various ratios depending on the source of oils. These high hydrocarbon compounds should be efficiently used as the feedstock for H_2 production. Nevertheless, until now, only a few works have presented the catalytic reforming or cracking of acetic acid and/or heavy hydrocarbons to H_2[10-12]. Theoretically, the major difficulty to reform the heavy hydrocarbon compounds like PFAD is the possible degradation of catalyst due to the carbon deposition since PFAD can homogenously decompose to several gaseous hydrocarbon elements, which could further decompose to carbon species and deposit on the surface of catalyst.

In the present work, Ce-ZrO_2 was applied as oxidative catalyst since ceria-based materials were known as an alternative reforming catalyst, which can reform

hydrocarbons and oxyhydrocarbons efficiently with high resistance toward carbon formation due to their high oxygen storage capacity (OSC) and redox property [13-19]. The addition of zirconium oxide (ZrO_2) to ceria has also been known to improve the specific surface area, the OSC, redox property, thermal stability and catalytic activity of ceria[20-26]. In this study, Ce-ZrO_2 was mainly prepared by cationic surfactant-assisted method since we previously reported the achievement of nano-scale material with high surface area and good stability from this preparation technique, which is mainly due to the interaction of hydrous oxide with cationic surfactants under basic condition[27,28]. It is noted that, the performances of Ce-ZrO_2 prepared by this method in terms of partial oxidation activity, resistance toward carbon formation, and the redox properties (i.e. OSC and lattice oxygen mobility) were also compared to those of Ce-ZrO_2 synthesized by the typical co-precipitation method.

5.2 Experimental

5.2.1 Raw material

Palm fatty acid distillate (PFAD) was obtained from Chumporn Palm Oil Industry Public Company Limited., Thailand. It consists of 93 wt% free fatty acid (FFA) (mainly contains 46% palmitic acid, 34% oleic acid and 8% linoleic acid with small amount of other fatty acids i.e. stearic, myristic, tetracosenoic, linolenic, ecosanoic, ecosenoic, and palmitoleic acid). The rest elements are triglycerides, diglycerides (DG), monoglycerides (MG) and traces of impurities.

5.2.2 Catalyst preparation and characterization

Ce-ZrO_2 was chosen as an oxidative catalyst in the present work. The materials with different Ce/Zr molar ratios were prepared by co-precipitation of cerium nitrate ($Ce(NO_3)_3 \cdot H_2O$), and zirconium oxychloride ($ZrOCl_2 \cdot H_2O$) (from Aldrich) in the presence of 0.1 M cetyltrimethylammonium bromide solution (from Aldrich) as a cationic surfactant. The ratio between both solutions was altered to achieve Ce/Zr molar ratios of 1/3, 1/1 and 3/1, while the molar ratio of (([Ce]+[Zr])/ [cetyltrimethylammonium bromide] was kept constant at 0.8. The solid solution was formed by the slow mixing of this metal salt solution with 0.4 M urea. After preparation, the precipitate was filtered and washed with deionised water and ethanol to prevent an agglomeration of the particles. It was dried overnight in an oven at 383 K, and then calcined in air at 1173 K for 6 h. According to the preparation of Ce-ZrO_2 by co-precipitation method, similar procedure as described above without adding of cetyltrimethylammonium bromide solution was applied. From the preparations, high specific surface area Ce-ZrO_2 (with the specific surface area of 46.5, 47 and 49 $m^2\ g^{-1}$ for the catalysts with Ce/Zr of 3/1, 1/1 and 1/3, respectively) and average particle size of 50-80 nm (less than 100 nm; so called nano-scale Ce-ZrO_2) can be achieved from the surfactant-assisted method, whereas relatively lower specific surface area (20, 20.5 and 22 $m^2\ g^{-1}$ for the catalysts with Ce/Zr of 3/1, 1/1 and 1/3, respectively) with average particle size of 100-150 μm was obtained from the co-precipitation method. It is noted that the average catalyst particle sizes were estimated by the nanosizer and the particle size analyzer. In order to investigate the OSC and lattice oxygen mobility of synthesized catalysts, the reduction/oxidation measurement and $^{18}O/^{16}O$ isotope exchange study were applied; details of these studies are described in Section 3.1.

It is noted that, for comparison, Ni/Ce-ZrO_2 (with 5 wt% Ni) was also tested for steam reforming reaction in the present work. They were prepared by impregnating Ce-ZrO_2 with $Ni(NO_3)_2$ solution (from Aldrich). The catalysts were calcined at 1173 K and reduced under H_2 flow at 573 K for 6 h before use. After treatment, the catalysts were characterized by several physicochemical methods i.e. the weight contents of Ni were determined by X-ray fluorescence (XRF) analysis; the reducibility of catalyst was calculated from the degree of H_2 uptakes from the temperature-programmed reduction (TPR) testing; the dispersion percentage was identified from the volumetric H_2 chemisorption measurement using chemisorption analyzer; and the catalyst specific surface area was obtained from BET measurement. According to these characterizations, the catalyst consists of 5.01% Ni loading content with the reducibility and Ni dispersion of 92.6% and 8.95%, respectively. Furthermore, the specific surface area was observed to be 41.5 m^2 g^{-1}.

5.2.3 Apparatus and Procedures

An experimental system was designed and constructed as shown elsewhere[27]. The feed gases i.e. He (as carrier gas), O_2 and H_2 (used to reduce Ni/Ce-ZrO_2) were controlled by 3 mass flow controllers, whereas PFAD and water were introduced by the heated syringe pump (with the reactant feed flow rate of 2.54 cm^3 h^{-1}) and vaporized by our designed quartz vaporizer-mixer system. These gaseous feed was introduced to the 10-mm diameter quartz reactor, which was mounted vertically inside a tubular furnace. A Type-K thermocouple was placed into the annular space between the reactor and furnace. This thermocouple was mounted on the tubular reactor in close contact with the catalyst bed to minimize the temperature difference between the catalyst bed and thermocouple. Another Type-K thermocouple was inserted in the middle of quartz tube in order to re-check possible temperature gradient; this inner-system thermocouple is covered with small closed-end quartz rod to prevent the catalytic reactivity of thermocouple during reaction. The recorded values showed that maximum temperature fluctuation during the reaction was always ±1.0ºC or less from the temperature specified for the reaction. It is noted that all experiments were carried out at isothermal condition after the system temperature was raised up to its setting temperature and waited until reaching steady state.

Catalysts (50 mg) were diluted with SiC (to obtain the total weight of 500 mg) in order to avoid temperature gradients and loaded in the quartz reactor. Preliminary experiments were carried out to find suitable conditions in which internal and external mass transfer effects are not predominant. Considering the effect of external mass transfer, based on the results from our previous publications[27-28], the total flow rate was kept constant at 100 cm^3 min^{-1} under a constant residence time in all testing. The suitable average sizes of catalysts were also verified in order to confirm that the experiments were carried out without the effect of internal mass transfer limitation. After the reactions, the exit gas mixture was transferred via trace-heated lines to Porapak Q column Shimadzu 14B gas chromatograph (GC) and mass spectrometer (MS). The MS in which the sampling of exit gas was done by a quartz capillary and differential pumping was used for transient and carbon formation experiments, whereas the GC was applied in order to investigate steady state condition experiments and to recheck the results from MS. It should be noted that in the present work the reactivity was defined in terms of PFAD conversion and product distribution. PFAD conversion can be calculated based on the % difference between PFAD in the feed and in the final product. Regarding the product distribution, the gaseous products from the reaction include H_2, CO, CO_2, CH_4, C_2H_6, C_2H_4 and C_3H_6; the yield of H_2 production (Y_{H2}) was calculated by hydrogen balance

defined as molar fraction of H_2 produced to total H_2 in the products. Other by-product selectivities (i.e. S_{CO}, S_{CO2}, S_{CH4}, S_{C2H6}, S_{C2H4} and S_{C3H6}) were calculated by carbon balance, defined as ratios of each product mole to the consumed moles of hydrocarbon, accounting for stoichiometry; this information was presented in term of (relative) fraction of these by-product components, which are summed to 100%.

5.2.4 Measurement of carbon formation

In order to investigate the amount of carbon formed on catalyst surface, the oxidation reaction was carried out by introducing 10% O_2 in He (with the flow rate of 100 cm^3 min^{-1}) into the system at isothermal condition (1173 K), after being purged with He; the amount of carbon formation was determined by measuring the CO and CO_2 yields. The calibrations of CO and CO_2 productions were performed by injecting a known amount of these calibration gases from a loop, in an injection valve in the bypass line. It is noted that the spent sample was further tested with TGA-MS (PerkinElmer, USA) at the maximum temperature of 1273 K to ensure that no carbon formation remains on the surface of catalyst; and no weight loss or CO/CO_2 productions were detected from all catalysts after oxidation reaction.

5.3 Results and discussion

5.3.1 Reactivity of Ce-ZrO_2 toward partial oxidation of PFAD

The partial oxidation of PFAD over nano-scale Ce-ZrO_2 prepared by surfactant-assisted method (with Ce/Zr ratios of 1/3, 1/1, and 3/1) was firstly studied at 1123 K by feeding PFAD and O_2 with O/C molar ratio of 1.0. It can be seen in Figure 5.1a-1c that, at this condition, H_2, CO, CH_4, and CO_2 are the main products with small amount of C_2H_4, C_2H_6, and C_3H_6 generated from the reaction. Furthermore, the conversions of PFAD and O_2 are always close to 100% and small amount of water formation (less than 1%) is observed. For comparison, the homogeneous (non-catalytic) partial oxidation of PFAD was also investigated by feeding PFAD and O_2 with O/C molar ratio of 1.0 to the quartz tube filled with 500 mg of SiC at 1123 K. It was found that more than 90% of PFAD are converted; nevertheless, the main gaseous products formed are hydrocarbon compounds (i.e. CH_4, C_2H_4, C_2H_6, and C_3H_6 with the selectivities of 27.7, 23.3, 22.7, and 10.5% respectively) with slight formations of CO and CO_2 (12.8% S_{CO} and 3.0% S_{CO2}); furthermore, significant amount of carbon was also detected in the blank reactor after exposure for 6 h.

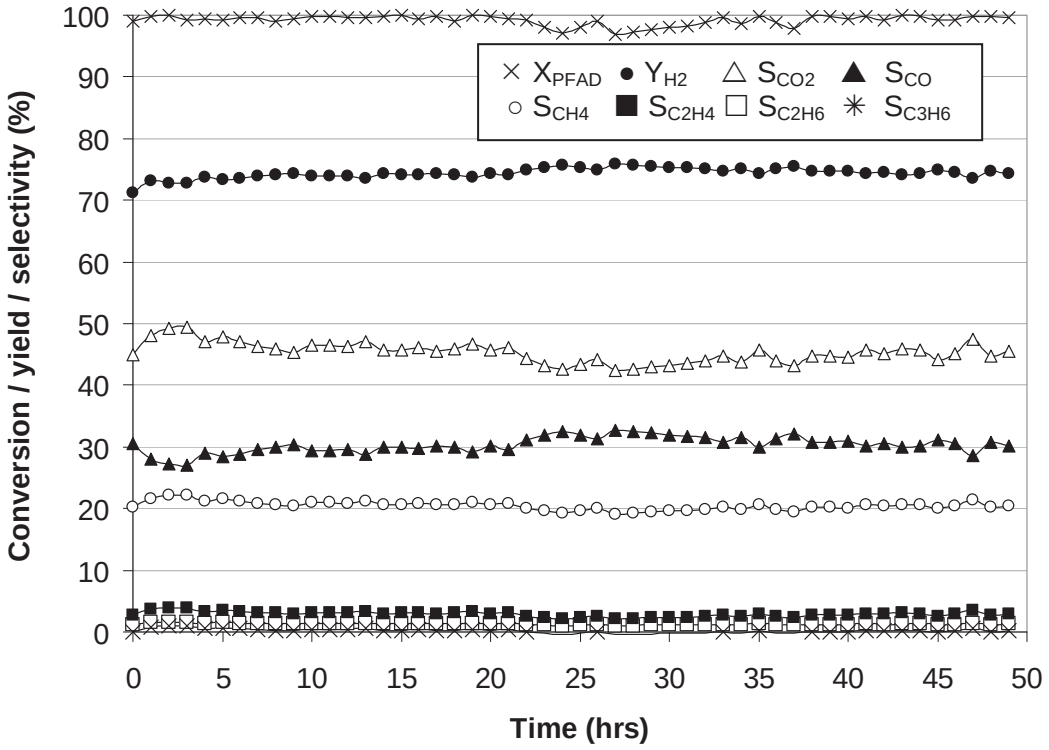

Figure 5.1a

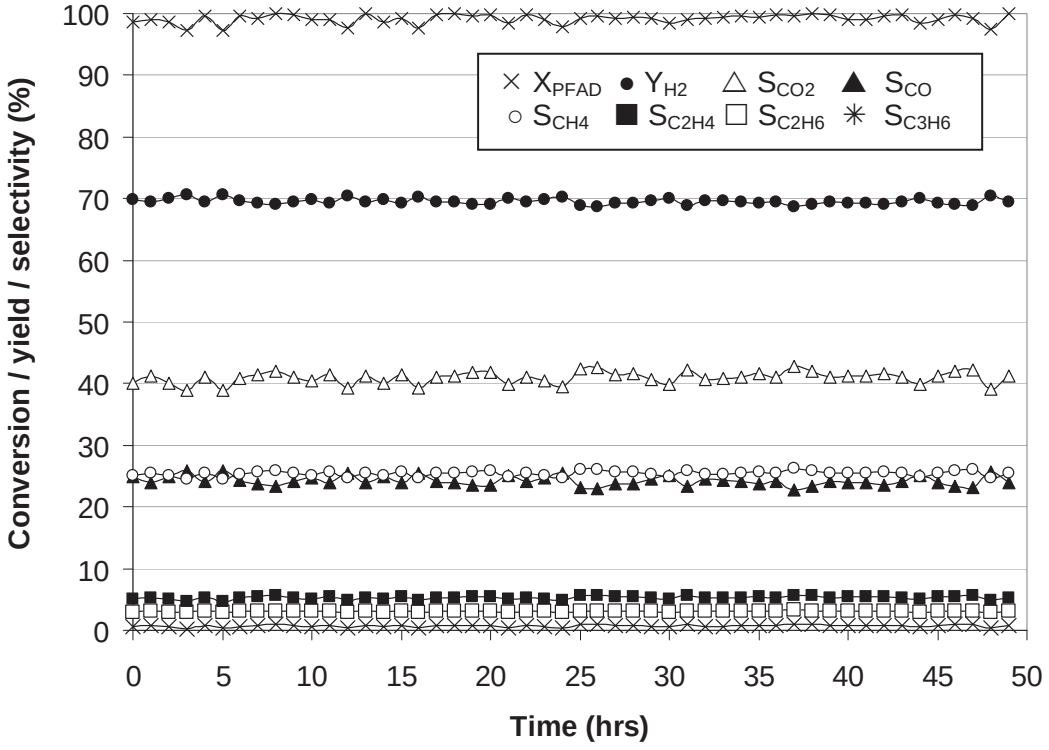

Figure 5.1b

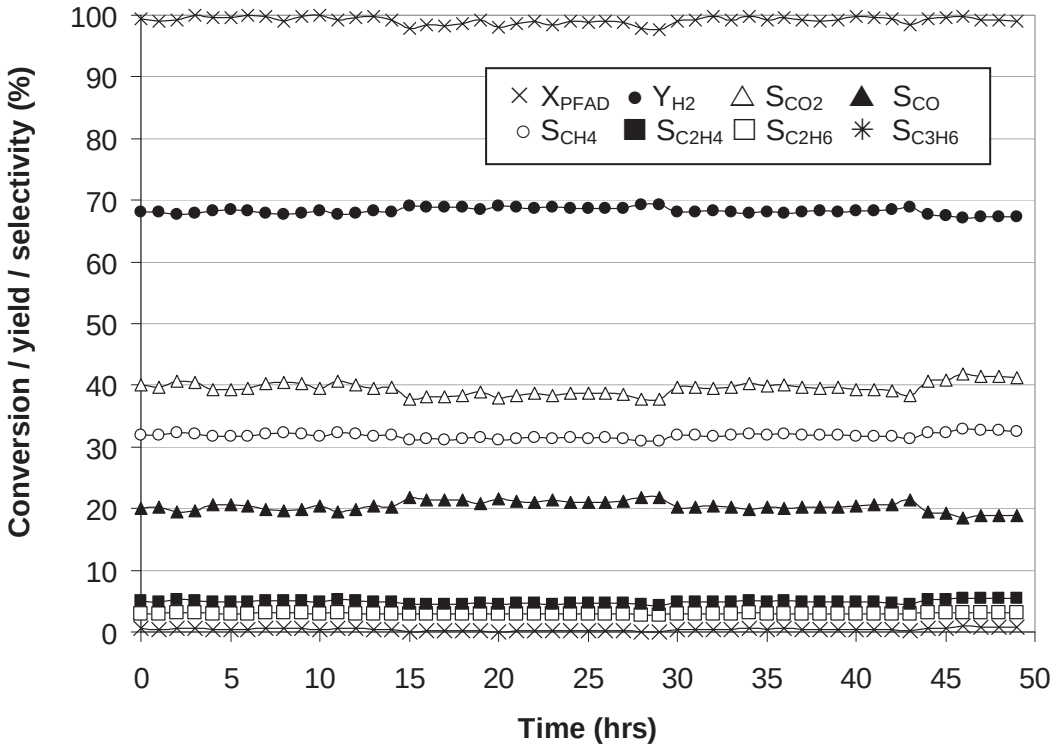

Figure 5.1c

Figure 5.1 Reactivities of nano-scale Ce-ZrO_2 with various Ce/Zr molar ratios toward the partial oxidation of PFAD (at 1123 K with O/C molar ratio of 1.0)

The variations in conversion and product distributions with time from partial oxidation of PFAD over (a) Ce-ZrO_2 (Ce/Zr molar ratio of 3/1) (b) Ce-ZrO_2 (Ce/Zr molar ratio of 1/1) and (c) Ce-ZrO_2 (Ce/Zr molar ratio of 1/3)

The results from Figure 5.1a-1c reveal that Ce-ZrO_2 with Ce/Zr ratio of 3/1 shows the best performance in term of its high H_2 production with lowest C_2H_4, C_2H_6, and C_3H_6 formations. Furthermore, according to the post-reaction oxidation experiment, the amount of carbon formation on the surface of Ce-ZrO_2 with Ce/Zr ratio of 3/1 after reaction (48 h) was relatively lower than other two ratios (3.4 mmol g_{cat}^{-1} compared to 4.3 and 4.7 mmol g_{cat}^{-1} observed over Ce-ZrO_2 with Ce/Zr ratios of 1/1 and 1/3, respectively). For comparison, the partial oxidation of PFAD over micro-scale Ce-ZrO_2 prepared by co-precipitation method (with Ce/Zr ratios of 1/3, 1/1, and 3/1) was also carried out at the same operating conditions (1123 K with O/C molar ratio of 1.0). As shown in Figure 5.2, less H_2 production with relatively higher C_2H_4, C_2H_6, and C_3H_6 formations was observed over this micro-scale Ce-ZrO_2. In addition, the post-reaction oxidation also detected significantly higher amount of carbon formation over this catalyst (4.2, 4.9 and 5.6 mmol g_{cat}^{-1} over Ce-ZrO_2 with Ce/Zr ratios of 3/1, 1/1 and 1/3). These results strongly indicate the better reaction performance for nano-scale Ce-ZrO_2 (with Ce/Zr molar ratio of 3/1); hence this catalyst was chosen for further studies and analyses.

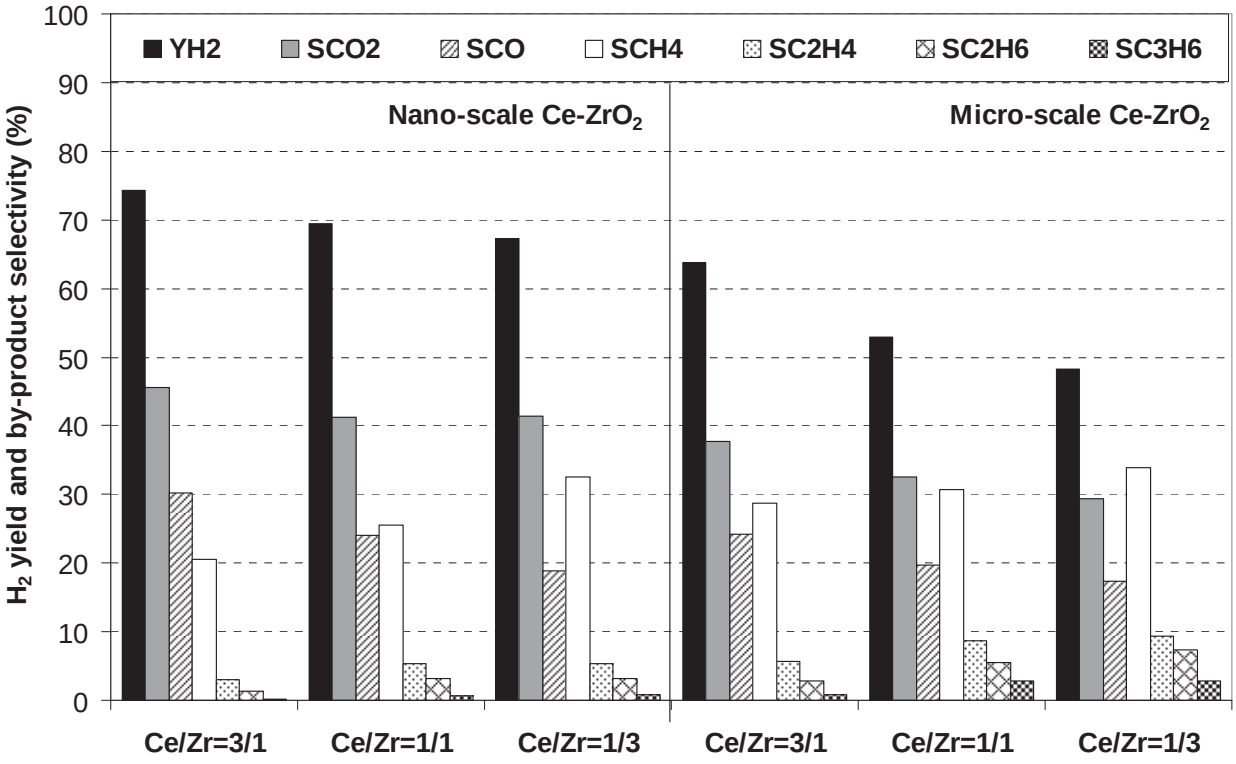

Figure 5.2 Reactivities of nano-scale and micro-scale Ce-ZrO_2 with various Ce/Zr molar ratios toward the partial oxidation of PFAD (at 1123 K with O/C molar ratio of 1.0)

The variations in product distributions from partial oxidation of PFAD at steady state (after 24 h) over nano-scale and micro-scale Ce-ZrO_2 with Ce/Zr molar ratios of 3/1, 1/1, and 1/3

The effect of inlet O_2 content on the catalytic reactivity was then studied by introducing PFAD and O_2 with O/C molar ratios of 0.5, 0.75, 1.0, 1.25 and 1.5 to the catalytic reactor. At steady state condition, H_2 production and the distribution of all gaseous by-products (i.e. hydrocarbons, CO, and CO_2) were measured as shown in Figure 5.3. It can be seen that H_2 and CO increased with increasing O_2 content until inlet O/C ratio reached 1.25. On the contrary, these products decreased when the ratio was higher, whereas the distribution of CO_2 grew up. This is mainly due to the combustion of H_2 and CO by O_2 in the feed. With increasing O_2 content, the conversions of C_2H_4, C_2H_6, and C_3H_6 increased and reached 100% at O/C molar ratio of 1.25. For CH_4 formation, it increased when inlet O/C molar ratio changed from 0.5 to 1.25 but slightly decreased at higher O_2 content. These behaviors are related to the decompositions of C_2H_4, C_2H_6, and C_3H_6 to CH_4 at low inlet O_2 concentration and the further converting of CH_4 to CO, CO_2 and H_2 at higher O_2 content. We previously reported the efficient decomposition of C_2H_6 and C_2H_4 to CH_4 in this range of temperature studied[28].

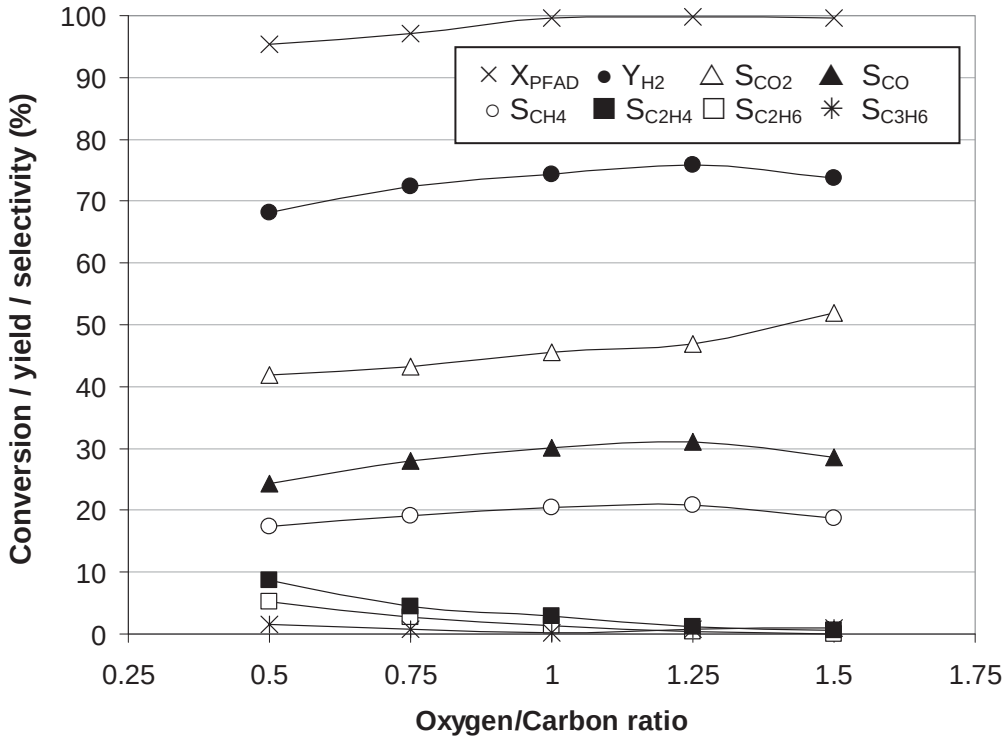

Figure 5.3 Partial oxidation of PFAD over nano-scale Ce-ZrO_2 (Ce/Zr molar ratio of 3/1) at various inlet O/C molar ratios

Effect of inlet O/C molar ratio on the product compositions from the partial oxidation of PFAD over nano-scale Ce-ZrO_2 (Ce/Zr molar ratio of 3/1)

It is noted that the effect of temperature on the conversion and product distribution was also carried out by varying the operating temperatures from 973 to 1173 K while keeping O/C molar ratio constant at 1.0. It was observed that H_2, CO and CH_4 increased with increasing temperature, whereas CO_2, C_2H_6 and C_2H_4 considerably decreased, as shown in Figure 5.4. The decrease of CO_2 is due to the influence of reverse water-gas shift reaction ($CO_2 + H_2 \rightarrow CO + H_2O$), whereas the increases of CH_4, CO and H_2 come from the decomposition and (partial) oxidation of C_2H_6 and C_2H_4 at higher temperature. Theoretically, the formations of gaseous hydrocarbon (i.e. CH_4, C_2H_4, C_2H_6, and C_3H_6) occur from the decomposition of PFAD (Eq. 1), while H_2, CO and CO_2 are generated from both thermal decomposition and partial oxidation reactions (Eqs. 2-4). It should also be noted that, apart from thermal decomposition of PFAD, CH_4 can also be generated from methanation reactions (Eqs. 5 and 6).

Thermal decomposition of fatty acids

$C_xH_yCOOH \rightarrow C_nH_mO_k$ + coke + gases (H_2, CO, CO_2, C_nH_m) (1)

Partial oxidation of gaseous hydrocarbons and possible side-reactions

$2C_nH_m + nO_2 \rightarrow n2CO + 2mH_2$ (2)

$2CO + O_2 \rightarrow 2CO_2$ (3)

$2H_2 + O_2 \rightarrow 2H_2O$ (4)

$nCO + 3nH_2 \rightarrow nCH_4 + nH_2O$ (5)

$nCO_2 + 4nH_2 \rightarrow nCH_4 + 2nH_2O$ (6)

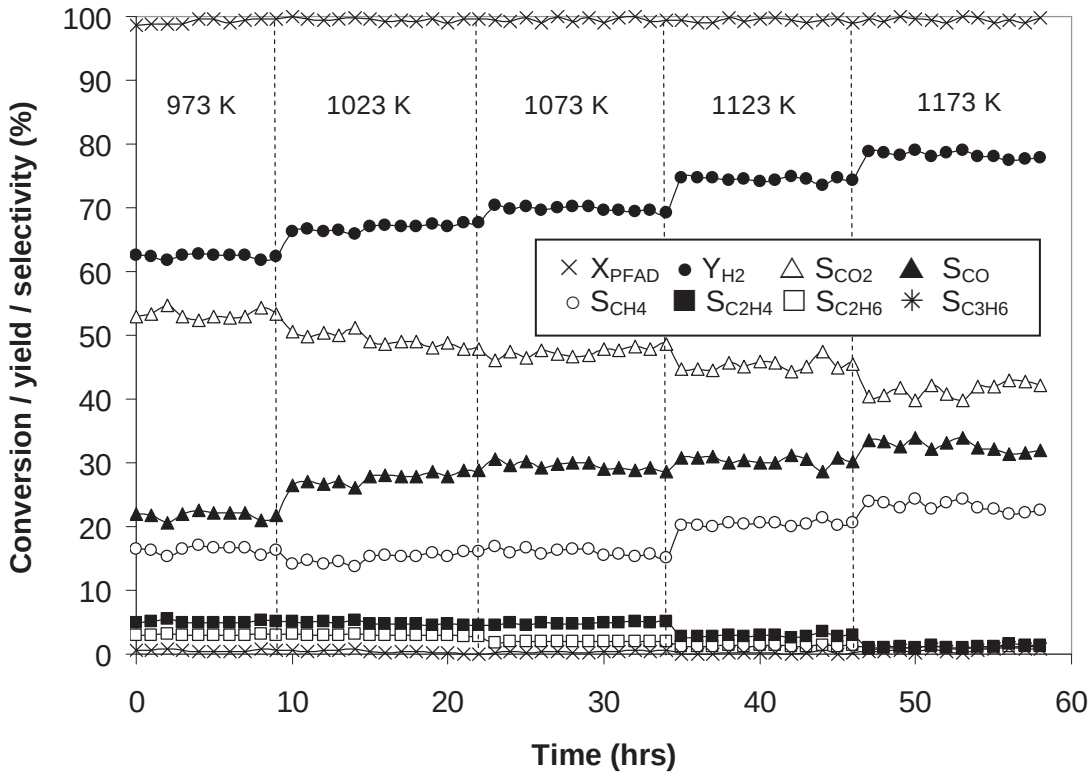

Figure 5.4 Product compositions from the partial oxidation of PFAD over nano-scale Ce-ZrO_2 (Ce/Zr molar ratio of 3/1) at various temperatures
Effect of temperature on the product compositions from the partial oxidation of PFAD over nano-scale Ce-ZrO_2 (Ce/Zr molar ratio of 3/1)

We suggested that the good partial oxidation reactivity of Ce-ZrO_2 is related to the OSC of this material since we previously reported that at moderate temperature, lattice oxygen (O_O^x) at ceria surface can oxidize gaseous hydrocarbons (e.g. CH_4) [27,28]. In addition, the doping of CeO_2 with Zr has been observed to improve OSC as well as thermal stability of the material[29-32]. These benefits were associated with enhanced reducibility of cerium (IV) in Ce-ZrO_2 due to the high O^{2-} mobility inside the fluorite lattice[26]. During partial oxidation reaction, the gas-solid reactions between hydrocarbons present in the system (i.e. CH_4, C_2H_4, C_2H_6, and C_3H_6) and O_O^x takes place forming CO and H_2 from which the formation of carbon is thermodynamically unfavorable. The possible reaction pathway for partial oxidation of PFAD over Ce-ZrO_2 is illustrated below:

C_nH_m adsorption

$$C_nH_m + (n+m)^* \rightarrow (CH_x^*) + (H^*) \rightarrow n(C^*) + m(H^*) \quad (7)$$

Co-reactant (O_2) adsorption

$$O_2 + 2^* \Leftrightarrow 2O^* \quad (8)$$

Redox reactions of lattice oxygen (O_O^x) with C and O**

$$C^* + O_O^x \rightarrow CO^* + V_O^{\bullet\bullet} + 2\,e' \quad (9)$$

$$V_O^{\bullet\bullet} + 2\,e' + O^* \Leftrightarrow O_O^x + * \quad (10)$$

Desorption of products (CO and H_2)

$$CO^* \Leftrightarrow CO + * \quad (11)$$

$$2(H^*) \Leftrightarrow H_2 + 2^* \quad (12)$$

Based on the Kroger–Vink notation, $V_O^{\bullet\bullet}$ denotes an oxygen vacancy with an effective charge 2^+, and e' is an electron which can either be more or less localized on a cerium ion or delocalized in a conduction band. * is the surface active site of ceria-based materials. During the reaction, hydrocarbons adsorbed on * forming intermediate surface hydrocarbon species (CH_x* and eventually C* and H*) (Eq. 7). This C* later reacted with lattice oxygen (O_O^x) (Eq. 9). The steady state rate is due to the continuous supply of oxygen source by inlet O_2 that reacted with the reduced-state catalyst to recover lattice oxygen (O_O^x) (Eqs. 8 and 10). It is noted that, according to our previous studies, * can be considered as unique site or same site as lattice oxygen (O_O^x)[27,28]. During the reaction, hydrocarbons adsorbed on either unique site or lattice oxygen (O_O^x) whereas O_2 reacted with the catalyst reduced site to regenerate O_O^x as well as remove the formation of carbon species on the catalyst surface. In this work, the amount of carbon formation (mmol g_{cat}^{-1}) on the surface of Ce-ZrO_2 after exposure in the partial oxidation at several inlet conditions (various O/C molar ratios and operating temperatures) was also determined, as reported in Table 5.1.

Table 5.1 Effects of temperature and oxygen/carbon molar ratio on the degrees of carbon formation over Ce-ZrO_2 after exposure in partial oxidation of PFAD

Catalyst	Temperature (K)	Oxygen/carbon Molar ratio	Carbon formation (mmol g_{cat}^{-1})
Ce-ZrO_2 (Ce/Zr=3/1)	1123	0.5	5.3 ±0.15
	1123	0.75	4.2 ±0.09
	1123	1.0	3.4 ±0.10
	1123	1.25	2.9 ±0.24
	1123	1.5	2.7 ±0.17
	973	1.0	4.3 ±0.11
	1023	1.0	3.9 ±0.02
	1073	1.0	3.6 ±0.15
	1173	1.0	3.0 ±0.19

Clearly, the carbon formation decreased with increasing temperature and oxygen content. Theoretically, the following reactions are the most probable reactions that could lead to carbon formation during the partial oxidation of PFAD:

$$2CO \Leftrightarrow CO_2 + C \quad (13)$$
$$C_nH_m \Leftrightarrow 0.5mH_2 + nC \quad (14)$$
$$CO + H_2 \Leftrightarrow H_2O + C \quad (15)$$
$$CO_2 + 2H_2 \Leftrightarrow 2H_2O + C \quad (16)$$

At low temperature, reactions (15)–(16) are favorable, while reactions (13) and (14) are thermodynamically unfavored. The Boudouard reaction (Eq. 13) and the decomposition of hydrocarbons (Eq. 14) are the major pathways for carbon formation at such a high temperature as they show the largest decreased in Gibbs energy[33,34]. Based on the range of temperature in this study, carbon formation would be formed via the decomposition of hydrocarbons and Boudouard reactions especially at low inlet O/C

molar ratio. By applying ceria-based catalysts, both reactions could be inhibited by the redox reaction between surface carbon (C) and lattice oxygen (O_O^x) (Eq. 9), while the oxygen vacancy is recovered via the reactions with supply of O_2 source (Eqs. 8 and 10).

5.3.2 Oxygen storage capacity and lattice oxygen mobility measurements

The higher reactivity with greater resistance toward carbon deposition for nano-scale Ce-ZrO_2 with Ce/Zr ratio of 3/1 compared to micro-scale Ce-ZrO_2 and Ce-ZrO_2 with Ce/Zr ratios of 1/1 and 1/3 could be due to the better redox properties (e.g. OSC) of this catalyst. In order to prove this explanation, the OSC of all Ce-ZrO_2 were determined by the isothermal reduction measurement (R-1), which was performed by purging the catalysts with 5%H_2 in He at 1173 K. The amount of H_2 uptake is correlated to the amount of O_2 stored in the catalysts. As presented in Figure 5.5 and Table 5.2, the amount of H_2 uptake over nano-scale Ce-ZrO_2 with Ce/Zr of 3/1 is significantly higher than other Ce-ZrO_2. The redox reversibilities of these catalysts were also determined by applying the oxidation measurement (Ox-1) following by second time reduction measurement (R-2) at the same conditions. The amounts of O_2 chemisorbed and H_2 uptakes (from both R-1 and R-2) are presented in Table 2. From these results, the amounts of H_2 uptake from R-2 were approximately identical to those from R-1 indicated the reversibility of OSC for these synthesized Ce-ZrO_2.

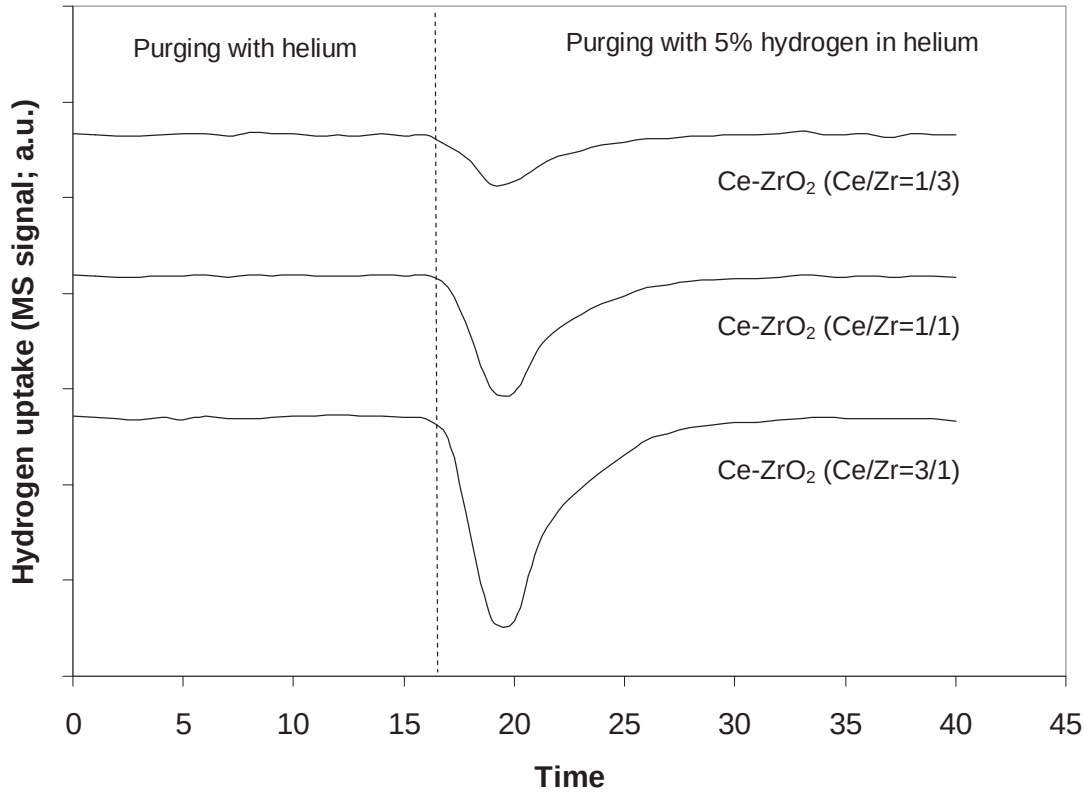

Figure 5.5 Oxygen storage capacity measurement of nano-scale Ce-ZrO_2 with various Ce/Zr molar ratios
Isothermal Reduction testing (at 1123 K) over nano-scale Ce-ZrO_2 with Ce/Zr molar ratios of 1/3, 1/1 and 3/1

Table 5.2 Results of R-1, Ox-1, and R-2 analyses of nano-scale and micro-scale Ce-ZrO_2 with different Ce/Zr ratios

Catalyst	H_2 Uptake from R-1 ($\mu mol/g_{cat}$)	O_2 Uptake from Ox-1 ($\mu mol/g_{cat}$)	H_2 Uptake from R-2 ($\mu mol/g_{cat}$)
Nano-scale Ce-ZrO_2 (Ce/Zr=1/3)	2883	1423	2879
Nano-scale Ce-ZrO_2 (Ce/Zr=1/1)	3692	1848	3687
Nano-scale Ce-ZrO_2 (Ce/Zr=3/1)	5221	2620	5213
Micro-scale Ce-ZrO_2 (Ce/Zr=1/3)	1087	551	1075
Micro-scale Ce-ZrO_2 (Ce/Zr=1/1)	1701	709	1694
Micro-scale Ce-ZrO_2 (Ce/Zr=3/1)	2625	1305	2621

In addition to the OSC, the $^{18}O/^{16}O$ isotope exchange experiment was carried out to investigate the lattice oxygen mobility of these Ce-ZrO_2. The sample (200 mg) was placed in the quartz reactor and thermally treated under the flow of high-purity helium (99.995%) at the desired temperatures for 1 h. Then, $^{18}O_2$ (in helium as carrier gas) was multiple times pulsed to the system and the outlet gases were monitored by the MS. According to our results, the productions of $^{16}O_2$ and $^{18}O^{16}O$ for nano-scale Ce-ZrO_2 with Ce/Zr of 3/1 were 18 and 14% at 600°C, whereas those for nano-scale Ce-ZrO_2 with Ce/Zr of 1/1 and Ce-ZrO_2 with Ce/Zr of 1/3 were 13 and 6% (Ce/Zr of 1/1) and 9 and 2% (Ce/Zr of 1/3) at the same temperature. Thus, the higher oxygen mobility of Ce-ZrO_2 with Ce/Zr of 3/1 can be confirmed. As for the testing over micro-scale Ce-ZrO_2, the productions of $^{16}O_2$ and $^{18}O^{16}O$ at 600°C for this Ce-ZrO_2 with Ce/Zr of 3/1, 1/1 and 1/3 were 11 and 7%, 9 and 5%, and 6 and 2%, respectively.

It can be seen that the partial oxidation reactivity, the OSC and the lattice oxygen mobility of Ce-ZrO_2 are in the same trend (nano-scale Ce-ZrO_2 < micro-scale Ce-ZrO_2; Ce-ZrO_2 with Ce/Zr of 3/1 > Ce-ZrO_2 with Ce/Zr of 1/1 > Ce-ZrO_2 with Ce/Zr of 1/3) indicated the strong impact of the catalyst specific surface area, the OSC and the lattice oxygen mobility on the catalyst reactivity.

5.3.3 The application of Ce-ZrO_2 as pre-oxidative catalyst

From Section 5.3.1, the great benefit of partial oxidation over nano-scale Ce-ZrO_2 is its high resistance toward carbon deposition; nevertheless, the remaining detectable of hydrocarbons (i.e. CH_4, C_2H_4, C_2H_6 and C_3H_6) in the product indicates the incomplete conversion of PFAD by this catalyst. Therefore, we further studied the potential for applying Ce-ZrO_2 as pre-oxidative catalyst to initial convert PFAD to light products; the product gas from this primary partial oxidation part was then mixed with steam and simultaneously fed to the secondary steam reforming over Ni/Ce-ZrO_2 to complete the hydrocarbon conversion and maximize H_2 yield. In this experiment, the initial feed was PFAD and O_2 with O/C molar ratio of 1.25. At the exit of the partial oxidation reaction, the steam was then added with H_2O/C molar ratio of 3.0. It is noted that the carbon considered for this H_2O/C ratio is based on the amount of unconverted carbon compounds (i.e. CH_4, C_2H_4, C_2H_6 and C_3H_6) from the partial oxidation part. Figure 5.6 presents the H_2 yield and other gaseous products from this coupling system at various temperatures, it can be seen that H_2 production is significantly high and the formations of hydrocarbons i.e. CH_4, C_2H_4, and C_2H_6 are closed to 0 particularly at high operating temperature.

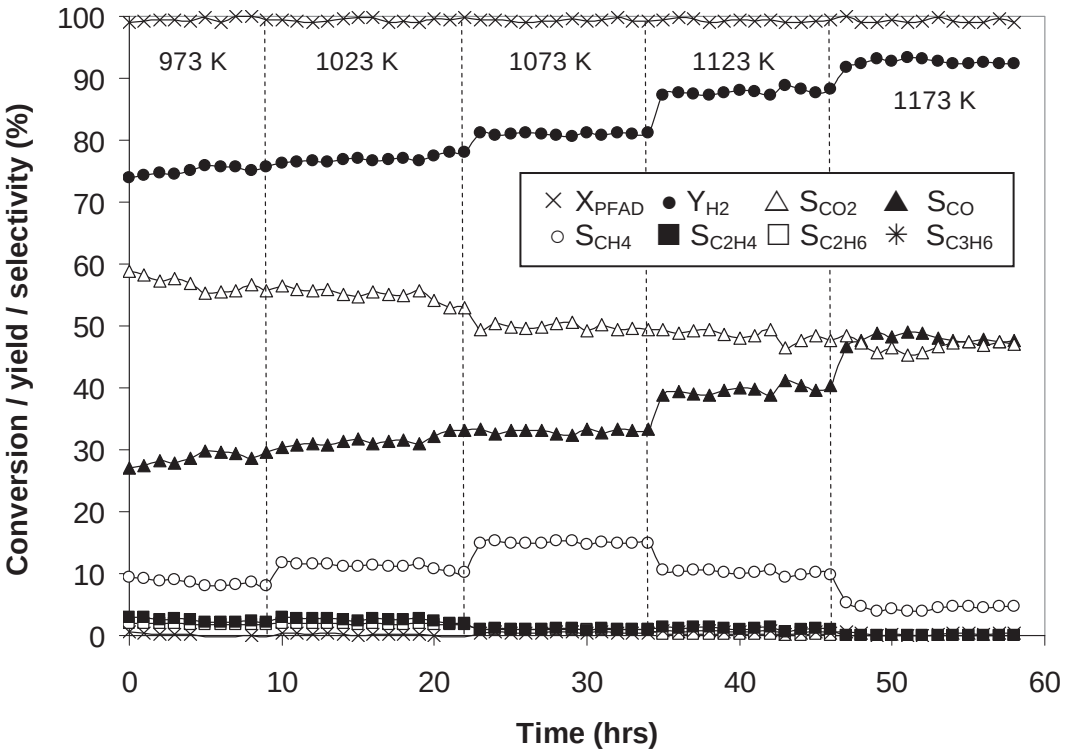

Figure 5.6 Pre-oxidation of PFAD with nano-scale Ce-ZrO_2 following by the steam reforming over Ni/Ce-ZrO_2 at various temperatures

Effect of temperature on the product compositions from the pre-oxidation of PFAD with nano-scale Ce-ZrO_2 following by the steam reforming over Ni/Ce-ZrO_2

It was also revealed that CO and H_2 increase with increasing temperature, whereas CO_2, C_2H_4, and C_2H_6 decrease. The dependence of CH_4 on the operating temperature was non-monotonic, the maximum production of CH_4 occurred at approximately 1073 K. The increase of CH_4 at low temperature comes from the decomposition of all hydrocarbons (PFAD, C_2H_4, and C_2H_6) whereas the decrease at higher temperature could be due to the further reforming to CO and H_2; the increase in H_2O conversion (from 41% at 1073 K to 45% and 48% at 1123 K and 1173 K) strongly supports this explanation. It is noted according to the post-reaction oxidation measurement that low carbon formation (in the range of 3.2-4.7 mmol g_{cat}^{-1}) was observed from the spent catalysts; moreover, the amount of carbon formation (as well as the percentage of CH_4 in the end-product) can be further minimized by increasing the inlet steam content, as presented in Table 5.3 and Figure 5.7. For comparison, the steam reforming of PFAD over Ni/Ce-ZrO_2 (without pre-oxidation with Ce-ZrO_2) was also tested. Unstable profiles of H_2 production, which related to the high formation of carbon species on the surface of catalyst, were observed. After purging in He, the post-reaction oxidation measurement detected significant amount of carbon over the catalyst (8.4 mmol g_{cat}^{-1}). This result indicates that Ni-based catalyst is inappropriate for the direct reform of PFAD and highlights the great benefit of nano-scale Ce-ZrO_2 as pre-oxidative catalyst.

Table 5.3 Effects of temperature and inlet steam/carbon molar ratio on the degrees of carbon formation after exposure in the pre-oxidation of PFAD over Ce-ZrO_2 (with O/C molar ratio of 1.25) following by the steam reforming over Ni/Ce-ZrO_2

Catalyst	Temperature (K)	Steam/carbon Molar ratio	Carbon formation (mmol g_{cat}^{-1})
Ce-ZrO_2 + Ni/Ce-ZrO_2	973	3.0	4.7 ±0.29
	1023	3.0	4.4 ±0.17
	1073	3.0	3.9 ±0.11
	1123	3.0	3.6 ±0.14
	1173	3.0	3.2 ±0.06
	1173	5.0	3.1 ±0.18
	1173	7.0	2.9 ±0.10
	1173	9.0	2.7 ±0.13
	1173	11.0	2.7 ±0.07
	1173	13.0	2.6 ±0.09

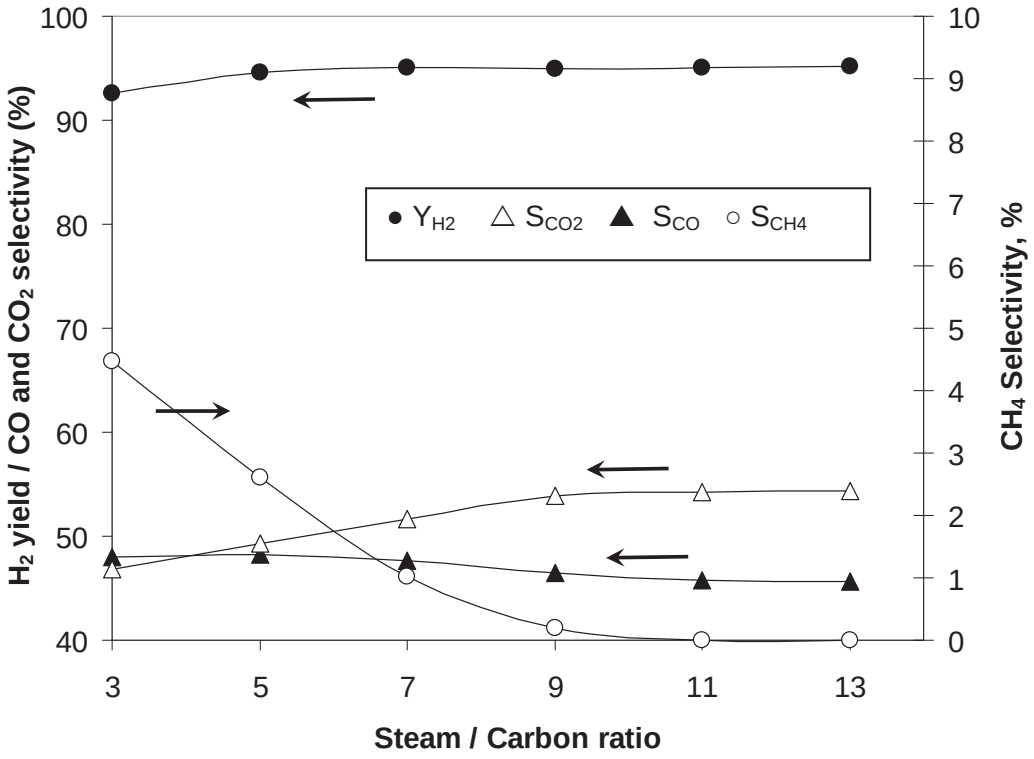

Figure 5.7 Pre-oxidation of PFAD with nano-scale Ce-ZrO_2 following by the steam reforming over Ni/Ce-ZrO_2 at various inlet steam/carbon molar ratios
Effect of inlet steam/carbon molar ratio on the product compositions from the pre-oxidation of PFAD with nano-scale Ce-ZrO_2 following by the steam reforming over Ni/Ce-ZrO_2

5.4 Conclusions

Nano-scale Ce-ZrO_2 with Ce/Zr ratio of 3/1 has useful partial oxidation activity for converting PFAD (with almost 100% conversion) to H_2, CH_4, CO, and CO_2 with slight formations of gaseous high hydrocarbon compounds i.e. C_2H_4, C_2H_6 and C_3H_6 under moderate temperature (1073-1173 K). The good reactivity was found to be closely related with the high oxygen storage capacity and lattice oxygen mobility of this synthesized catalyst, according to the reduction/oxidation measurement and $^{18}O/^{16}O$ isotope exchange study. It was also revealed that this nano-scale Ce-ZrO_2 can be efficiently used as the pre-oxidative catalyst for primary converting PFAD to light hydrocarbons, from which later reforms with steam in the presence of Ni-based catalyst to hydrogen with lower carbon formation problem.

5.5 Literature Cited

1. Ahmed S, Krumpelt M. Hydrogen from hydrocarbon fuels for fuel cells. *Int. J. Hydrogen Energy*. 2001; 26: 291-301.
2. Seo YS, Shirley A, Kolaczkowski ST. Evaluation of thermodynamically favourable operating conditions for production of hydrogen in three different reforming technologies. *J. Power Sources*. 2002; 108: 213-225.
3. Cheekatamarla PK, Finnerty CM. Synthesis gas production via catalytic partial oxidation reforming of liquid fuels. *Int. J. Hydrogen Energy*. 2008; 33: 5012-5019.
4. Wang H, Feldhoff A, Caro J, Schiestel T, Werth S. Oxygen selective ceramic hollow fiber membranes for partial oxidation of methane. *AIChE Jl.* 2009; 55: 2657-2664.
5. Tanaka H, Kaino R, Okumura K, Kizuka T, Tomishige K. Catalytic performance and characterization of Rh–CeO_2/MgO catalysts for the catalytic partial oxidation of methane at short contact time. *J. Catal.* 2009; 268: 1-8.
6. Diehl F, Barbier J, Duprez D, Guibard I, Mabilon G. Catalytic oxidation of heavy hydrocarbons over Pt/Al_2O_3. Influence of the structure of the molecule on its reactivity. *Appl. Catal. B: Environ.* 2010; 95: 217-227.
7. Alvarez-Galvan MC, Navarro RM, Rosa F, Briceño Y, Gordillo Alvarez F, Fierro JLG. Performance of La,Ce-modified alumina-supported Pt and Ni catalysts for the oxidative reforming of diesel hydrocarbons. *Int. J. Hydrogen Energy*. 2008; 33: 652-663.
8. Shi L, Bayless DJ, Prudich ME. A CFD model of autothermal reforming. *Int. J. Hydrogen Energy*. 2009; 34: 7666-7675.
9. Recupero V, Pino L, Leonardo RD, Lagana M, Maggio G. Hydrogen generator, via catalytic partial oxidation of methane for fuel cells. *J. Power Sources*. 1998; 71: 208-214.
10. Basagiannis AC, Verykios XE. Influence of the carrier on steam reforming of acetic acid over Ru-based catalysts. *Appl. Catal. B: Environ*. 2008; 82: 77-88.
11. Basagiannis AC, Verykios XE, Catalytic steam reforming of acetic acid for hydrogen production. *Int. J Hydrogen Energy*. 2007; 32: 3343-3355.
12. Davidian T, Guilhaume N, Daniel C, Mirodatos C. Continuous hydrogen production by sequential catalytic cracking of acetic acid: Part I. Investigation of reaction conditions and application to two parallel reactors operated cyclically. *Appl. Catal. A: Gen*. 2008; 335: 64-73.

13. Liu N, Yuan Z, Wang C, Wang S, Zhang C, Wang S. The role of CeO_2–ZrO_2 as support in the ZnO–$ZnCr_2O_4$ catalysts for autothermal reforming of methanol. *Fuel Process. Technol.* 2008; 89: 574-581.
14. Damyanova S, Pawelec B, Arishtirova K, Martinez Huerta MV, Fierro JLG. The effect of CeO_2 on the surface and catalytic properties of Pt/CeO_2–ZrO_2 catalysts for methane dry reforming. *Appl. Catal. B: Environ.* 2009; 89: 149-159.
15. Vagia EC, Lemonidou AA. Investigations on the properties of ceria–zirconia-supported Ni and Rh catalysts and their performance in acetic acid steam reforming. *J. Catal.* 2010; 269: 388-396.
16. Chen J, Wu Q, Zhang J, Zhang J. Effect of preparation methods on structure and performance of Ni/$Ce_{0.75}Zr_{0.25}O_2$ catalysts for CH_4–CO_2 reforming. *Fuel.* 2008; 87: 2901-2907.
17. Cao L, Pan L, Ni C, Yuan Z, Wang S. Autothermal reforming of methane over Rh/$Ce_{0.5}Zr_{0.5}O_2$ catalyst: Effects of the crystal structure of the supports. *Fuel Process. Technol.* 2010; 91: 306-312.
18. Yuan Z, Ni C, Zhang C, Gao D, Wang S, Xie Y, Okada A. Rh/MgO/$Ce_{0.5}Zr_{0.5}O_2$ supported catalyst for autothermal reforming of methane: The effects of ceria–zirconia doping. *Catal. Today.* 2009; 146: 124-131.
19. Lima SM, Cruz IO, Jacobs G, Davis BH, Mattos LV, Noronha FB. Steam reforming, partial oxidation, and oxidative steam reforming of ethanol over Pt/$CeZrO_2$ catalyst. *J. Catal.* 2008; 257: 356-368.
20. Ozawa M, Kimura M, Isogai A. The application of CeZr oxide solid solution to oxygen storage promoters in automotive catalysts. *J. Alloys Comp*. 1993; 193: 73-75.
21. Balducci G, Kaspar J, Fornasiero P, Graziani M, Islam MS. Surface and reduction energetics of the CeO_2−ZrO_2 catalysts. *J. Phys. Chem. B*. 1998; 102: 557-561.
22. Vlaic G, Fornasiero P, Geremia S, Kaspar J, Graziani M. Relationship between the zirconia-promoted reduction in the Rh-loaded $Ce_{0.5}Zr_{0.5}O_2$ mixed oxide and the Zr-O local structure. *J. Catal*. 1997; 168: 386-392.
23. Rao GR, Kaspar J, Meriani S, Dimonte R, Graziani M. NO decomposition over partially reduced metallized CeO_2-ZrO_2 solid solutions. *Catal. Lett*. 1994; 24: 107-112.
24. Fornasiero P, Dimonte R, Rao GR, Kaspar J, Meriani S, Trovarell A, Graziani M. Rh-loaded CeO_2-ZrO_2 solid-solutions as highly efficient oxygen exchangers: dependence of the reduction behavior and the oxygen storage capacity on the structural-properties. *J. Catal*. 1995; 151: 168-177.
25. Yao MH, Hoost TE, Baird RJ, Kunz FW. An XRD and TEM investigation of the structure of alumina-supported ceria-zirconia. *J. Catal*. 1997; 166: 67-74.
26. Kim D. Lattice Parameters, Ionic conductivities, and solubility limits in fluorite-structure MO_2 oxide [M = Hf^{4+}, Zr^{4+}, Ce^{4+}, Th^{4+}, U^{4+}] solid solutions. *J. Am. Ceram. Soc*. 1989; 72: 1415-1421.
27. Laosiripojana N, Assabumrungrat S. Catalytic dry reforming of methane over high surface area ceria, *Appl. Catal. B: Environ*. 2005; 60: 107-116.
28. Laosiripojana N, Assabumrungrat S. Kinetic dependencies and reaction pathways in hydrocarbon and oxyhydrocarbon conversions catalyzed by ceria-based materials, *Appl. Catal. B: Environ*. 2008; 82: 103-113.
29. Laosiripojana N, Chadwick D, Assabumrungrat S. Effect of high surface area CeO_2 and Ce-ZrO_2 supports over Ni catalyst on CH_4 reforming with H_2O in the presence of O_2, H_2, and CO_2. *Chem. Eng. J*. 2008; 138: 264-273.

30. Kruse N, Frennet A, Bastin JM (Eds.). Catalysis and automotive pollution control IV, Elsevier, Amsterdam (1998).
31. Kaspar J, Fornasiero P, Graziani M. Use of CeO_2-based oxides in the three-way catalysis. *Catal. Today*. 1999; 50: 285-298.
32. Roh HS, Potdar HS, Jun KW. Carbon dioxide reforming of methane over co-precipitated Ni-CeO_2, Ni-ZrO_2 and Ni-Ce-ZrO_2 catalysts. *Catal. Today*. 2004; 93–95: 39-44.
33. Lwin Y, Daud WRW, Mohamad AB, Yaakob Z. Hydrogen production from steam–methanol reforming: thermodynamic analysis. *Int. J. Hydrogen Energy*. 2000; 25: 47-53.
34. Amor JN. The multiple roles for catalysis in the production of H_2. *Appl. Catal. A: Gen*. 1999; 176: 159-176.

ผลงานที่ได้ตีพิมพ์ลงวารสารวิชาการระดับนานาชาติจากโครงการนี้

1. Laosiripojana N, Charojrochkul S, Lohsoontorn P, Assabumrungrat S, *Role and advantages of H_2S on the catalytic steam reforming over nano-scale CeO_2-based catalysts*. Journal of Catalysis **2010**; 276: 6-15.
2. Laosiripojana N, Kiatkittipong W, Assabumrungrat S. *Effects of support and co-fed elements on steam reforming of palm fatty acid distillate (PFAD) over Rh-based catalysts*. Applied Catalysis A: General **2010**; 383: 50-57.
3. Chettapongsaphan C, Charojrochkul S, Assabumrungrat S, Laosiripojana N. *Synthesis and testing of highly active $La_{0.8}Sr_{0.2}Cr_{0.9}Ni_{0.1}O_3$ toward H_2O and CO_2 reforming of CH_4: Effect of co-reactant/CH_4 on its reforming characteristic*. Applied Catalysis A: General **2010**; 386: 194-200.
4. Chareonlimkun A, Champreda V, Shotipruk A, Laosiripojana N. *Catalytic conversion of sugarcane bagasse, rice husk and corncob in the presence of TiO_2, ZrO_2 and mixed-oxide TiO_2-ZrO_2 under hot compressed water (HCW) condition*. Bioresource Technology **2010**; 101: 4179-4186.
5. Laosiripojana N, Kiatkittipong W, Assabumrungrat S. *Synthesis of methyl esters from relevant palm products in near-critical methanol with modified-zirconia catalysts: Effects of catalyst, co-solvent and water formation*. Bioresource Technology **2010**; 101: 8416-8423.
6. Laosiripojana N, Sutthisripok W, Lohsoontorn P, Assabumrungrat S. *Hydrogen production from partial oxidation of liquefied petroleum gas over Ce-ZrO_2 doped with La-, Gd-, Nb-, and Sm-: The application as primary oxidative catalyst*. International Journal of Hydrogen Energy **2010**; 35: 6747-6756.
7. Raita M, Champreda V, Laosiripojana N. *Biocatalytic ethanolysis of palm oil for biodiesel production using microcrystalline lipase*. Process Biochemistry **2010**; 45: 829-834.
8. Chareonlimkun A, Champreda V, Shotipruk A, Laosiripojana N. *Reactions of C_5 and C_6-sugars, cellulose, and lignocellulose under hot compressed water in the presence of heterogeneous acid catalysts*. Fuel **2010**; 2873-2880.
9. Mongkolbovornkij P, Champreda V, Shotipruk A, Laosiripojana N. *Reactivity of modified ZrO_2 with WO_3-, SO_4- and TiO_2- toward esterification of palm fatty acid distillate: Effects of catalyst preparation, co-solvent adding and water formation*. Fuel Processing Technology **2010**; 91: 1510-1516.
10. Sansernnivet M, Laosiripojana N, Assabumrungrat S, Charojrochkul S. *Fabrication of $La_{0.8}Sr_{0.2}CrO_3$ Film via Flame Assisted Vapour Deposition Technique*. Chemical Vapor Deposition **2010**; 16: 311-321.
11. Wetwatana U, Lohsoontorn P, Assabumrungrat S, Laosiripojana N. *Catalytic steam and autothermal reforming of use lubricating oil over Rh- and Ni-based catalysts*. Industrial & Engineering Chemistry Research. **2010**; 49: 10981-10985.
12. Sinsereekul N, Wangkam T, Thamchaipenet A, Srikhirin T, Eurwilaichitr L, Champreda V. *Recombinant expression of BTA hydrolase in Streptomyces rimosus*. Applied Microbiology and Biotechnology **2010**; 86: 1775-1784.
13. Laobuthee A, Veranitisagul C, Koonsaeng N, Bhavakul V, Laosiripojana N, *Catalytic activity of ultrafine $Ce_xGd_ySm_zO_2$ synthesized by metal organic complex method toward steam reforming of methane*. Catalysis Communications **2010**; 12: 25-29
14. Dedsuksophon W, Faungnawakij K, Champreda V, Laosiripojana N, *Hydrolysis/ dehydration/aldol-condensation/hydrogenation of lignocellulosic biomass and*

biomass-derived carbohydrates in the presence of Pd/WO_3-ZrO_2 in a single reactor. Bioresource Technology **2011**; 102: 2040-2046.
15. Laosiripojana N, Sutthisripok W, Charojrochkul S, Assabumrungrat S. *Steam reforming of LPG over Ni and Rh supported on Gd-CeO_2 and Al_2O_3: Effect of support and feed composition*. Fuel **2011**; 90: 136-141.
16. *of palm oil fatty acids for biodiesel production using cross-linked protein coated microcrystalline lipase*. Journal of Molecular Catalysis B: Enzymatic **2011**; 73: 74-79.
17. Laosiripojana N, Kiatkittipong W, Assabumrungrat S. *Partial oxidation of palm fatty acids over Ce-ZrO_2: Roles of catalyst surface area, lattice oxygen, mobility*, AIChE Journal. **2011**; 57: 2861-2869.
18. Laosiripojana N, Assabumrungrat S. *Conversion of poisonous methanethiol to hydrogen-rich gas by chemisorption/reforming over nano-scale CeO_2: The use of CeO_2 as catalyst coating material*, Applied Catalysis B: Environmental. **2011**; 102: 267-275.

(รายละเอียด Reprint ดังแสดงในหน้าถัดไป)

Journal of Catalysis 276 (2010) 6–15

Contents lists available at ScienceDirect

Journal of Catalysis

journal homepage: www.elsevier.com/locate/jcat

Role and advantages of H_2S in catalytic steam reforming over nanoscale CeO_2-based catalysts

N. Laosiripojana [a,*], S. Charojrochkul [b], P. Kim-Lohsoontorn [c], S. Assabumrungrat [d]

[a] The Joint Graduate School of Energy and Environment, CHE Center for Energy Technology and Environment, King Mongkut's University of Technology Thonburi, Thailand
[b] National Metal and Materials Technology Center (MTEC), Pathumthani, Thailand
[c] Department of Chemical Engineering, Faculty of Engineering, Mahidol University, Thailand
[d] Department of Chemical Engineering, Faculty of Engineering, Chulalongkorn University, Thailand

ARTICLE INFO

Article history:
Received 4 June 2010
Revised 8 August 2010
Accepted 14 August 2010
Available online 29 September 2010

Keywords:
CeO_2
Steam reforming
H_2S
Hydrogen

ABSTRACT

The activity of nanoscale CeO_2 and doped CeO_2 (with Gd, Y, Nb, La, and Sm) toward the steam reforming of CH_4 in the presence of H_2S was investigated for later application as an in-stack reforming catalyst in a solid oxide fuel cell. Although H_2S is commonly known as a poisonous gas for metallic-based catalysts, it was found that the presence of appropriate H_2S content increases the reforming activity of these CeO_2-based catalysts. According to postreaction catalyst characterizations by X-ray diffraction, X-ray photoelectron spectroscopy, temperature-programmed reduction, temperature-programmed desorption, $H_2/H_2O + H_2S$ titration, and $^{18}O/^{16}O$ isotope exchange, it was revealed that this behavior is related to the formation of various Ce–O–S phases ($Ce(SO_4)_2$, $Ce_2(SO_4)_3$, and Ce_2O_2S) during the reaction. Our studies indicated that the formation of $Ce(SO_4)_2$ promotes the oxygen storage capacity, the lattice oxygen mobility, and eventually the reforming activity, whereas the formation of Ce_2O_2S oppositely reduces both properties and lowers the reforming rate.

1. Introduction

Hydrogen is widely regarded as a promising energy carrier for fuel cells to generate energy with great improvements in air quality, human health, and climate [1]. It can be produced readily from the reforming of hydrocarbons with oxygen-containing co-reactants [2–5]. Metallic catalysts such as Ni, Rh, and Pd are known to be active for these reactions, but catalyst deactivation due to carbon formation and sulfur poisoning is a major concern when heavy hydrocarbons and/or sulfur-containing feeds such as natural gas, biogas, and liquefied petroleum gas are used [6,7]. Typically, prereforming and/or desulfurization units are needed to reform these feedstocks; however, both installations reduce the flexibility and the potential for applying hydrogen/fuel cell technologies. Research on developing catalysts with high resistance to carbon formation and sulfur interaction is therefore continuing.

Cerium oxide (CeO_2) is extensively used as a catalyst and support for a variety of reactions involving oxidation of hydrocarbons [4,8,9]. This material contains a high concentration of highly mobile oxygen vacancies, which act as local sources or sinks for oxygen involved in reactions taking place on its surface; this behavior renders CeO_2-based materials of interest for a wide range of catalytic applications [10–13]. One of the great potential applications of CeO_2-based material is in solid oxide fuel cells (SOFC) as cell materials and in-stack reforming catalysts (IIR-SOFC) [14–19]. Furthermore, doping CeO_2 with Gd, Nb, La, and Sm has also been reported to improve the redox properties of CeO_2, and these doped forms are now widely used as catalysts in a wide variety of reactions involving oxidation or partial oxidation of hydrocarbons (e.g., automotive catalysis). Previously, we successfully synthesized nano-scale CeO_2 with high specific surface area and thermal stability by a cationic surfactant-assisted method [20]. We then studied H_2O and CO_2 reforming of CH_4, C_2H_4, C_2H_6, C_3H_8, C_4H_{10}, CH_3OH, and C_2H_5OH over this ultrafine CeO_2 and found that this material efficiently converts these hydrocarbons to H_2-rich gas with high resistance toward carbon formation under given conditions [20,21]. We proposed that the turnover rates are strongly influenced by the amount of lattice oxygen (O_O^x) in CeO_2, whereas the kinetic dependencies of hydrocarbon conversions and the activation energies were unaffected by the material's specific surface area, the doping element, the degree of oxygen storage capacity (OSC), and the reactions (i.e., H_2O reforming and CO_2 reforming). Furthermore, identical turnover rates for H_2O and CO_2 reforming (at similar C_nH_m partial pressure) with linear dependence on C_nH_m partial pressure and independence of CO_2 and H_2O partial pressures were observed. These results provide strong evidence that the sole kinetically relevant elementary step is the reaction of intermediate surface hydrocarbon species with O_O^x

* Corresponding author. Fax: +66 662 872 6736.
E-mail address: navadol_l@jgsee.kmutt.ac.th (N. Laosiripojana).

0021-9517/$ - see front matter © 2010 Elsevier Inc. All rights reserved.
doi:10.1016/j.jcat.2010.08.015

and that oxygen is replenished by a rapid surface reaction of reduced-state CeO_2 with oxygen sources (i.e., CO_2 or H_2O) in the system [21].

Recently, the regenerative H_2S adsorption capability of CeO_2 at high temperature was reported [22]. In the present work, the activity of CeO_2 and doped CeO_2 (with several rare earths, Gd, Y, Nb, La, and Sm), synthesized by a cationic surfactant-assisted method, toward the steam reforming of CH_4 in the presence of H_2S was investigated under several operating conditions (i.e., various inlet H_2S contents, inlet steam/carbon (S/C) molar ratios, and operating temperatures). Several characterizations, including X-ray diffraction (XRD), X-ray photoelectron spectroscopy (XPS), temperature-programmed reduction (TPR), temperature-programmed desorption (TPD) under reducing conditions, $H_2/H_2O + H_2S$ titration, and $^{18}O/^{16}O$ isotope exchange methods were also performed over the fresh and spent catalysts from the reactions in order to observe the changes in catalyst phase formation and the redox properties associated with the OSC and the mobility of lattice oxygen. Based on the experimental results and the above analyses, the mechanism of methane steam reforming in the presence of H_2S over nano-scale CeO_2-based catalysts was established. In addition, a practical application with respect to the study using this ultrafine CeO_2 as a primary reforming catalyst to reform natural gas, biogas, and liquefied petroleum gas (LPG) without prior desulfurization was proposed.

2. Experimental

2.1. Catalyst preparations

Nano-scale CeO_2-based materials were synthesized by a cationic surfactant-assisted method. We previously reported that the preparation of ceria-based materials by this method can provide materials with ultrafine particle size, high surface area, and good stability after thermal treatment [20,21]. The achievement of high-surface-area material with good thermal stability by this preparation technique is related to the interaction of hydrous oxide with cationic surfactants under basic conditions and the incorporation of surfactants during preparation, which reduces the interfacial energy and eventually decreases the surface tension of water contained in the pores. It has been reported that this incorporation reduces the shrinkage and collapse of the catalyst during heating, which consequently helps the catalyst maintain high surface area after calcination [23]. In the present work, the undoped CeO_2 was prepared by mixing 0.1 M of cerium nitrate ($Ce(NO_3)_3{\cdot}H_2O$ from Aldrich) solution with 0.1 M of cetyltrimethylammonium bromide (from Aldrich) and keeping the [Ce]/[cetyltrimethylammonium bromide] molar ratio constant at 0.8. This solution was stirred by magnetic stirring (100 rpm) for 3 h and then aqueous ammonia was slowly added until the pH was 11.5. The mixture was continually stirred, sealed, and placed in a thermostatic bath maintained at 263 K. The precipitate was then filtered and washed with deionized water and acetone to remove the free surfactant. It was dried overnight in ambient air at 110 °C and then calcined in flowing dry air by increasing the temperature to 900 °C at a rate of 0.167 °C s^{-1} and holding at 900 °C for 6 h. After calcination, fluorite-structured CeO_2 with good homogeneity was obtained. According to the SEM image (Fig. 1), ultrafine particles of CeO_2 can be achieved from this method (compared to the microscale CeO_2 obtained from the conventional precipitation method). Doped CeO_2 with Gd, Y, Nb, La, and Sm was prepared by mixing $Ce(NO_3)_3$ with $RE(NO_3)_x$ (Re = Gd, Nb, La, Y, and Sm) to achieve a RE ratio in the material of 0.1; $RE_{0.1}$–CeO_2 (in the presence of 0.1 M cetyltrimethylammonium bromide solution). After treatments, the specific surface areas of all doped and undoped CeO_2 were determined by BET measurement (Table 1), and as expected, the surface area for all ceria decreased at high calcination temperatures.

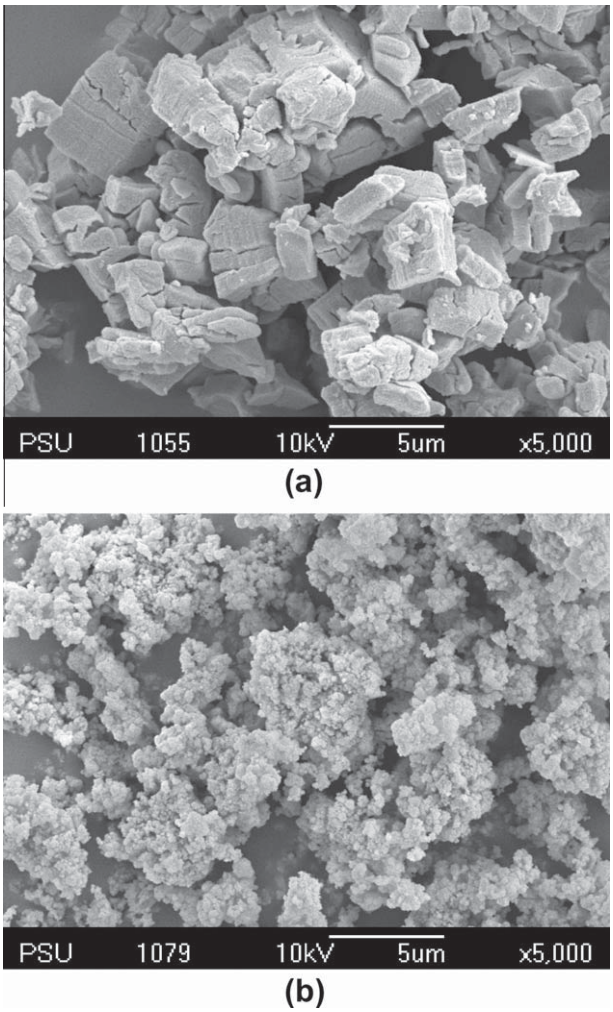

Fig. 1. SEM micrograph of (a) CeO_2 prepared by precipitation method and (b) CeO_2 prepared by cationic surfactant-assisted method (after calcination at 900 °C).

Table 1
Specific surface area of ceria-based materials at several calcination temperatures.

Catalysts	Surface area ($m^2\ g^{-1}$) after calcination at		
	700 °C	800 °C	900 °C
CeO_2	52	35	18
La-doped CeO_2	68	51	26
Gd-doped CeO_2	61	47	23
Sm-doped CeO_2	62	45	23
Nb-doped CeO_2	40	23	11
Y-doped CeO_2	59	41	20

It is noted that, for comparison, Ni/Al_2O_3 and Rh/Al_2O_3 (5 wt.% Ni and Rh) were also prepared and tested toward the steam reforming reaction. In detail, these catalysts were prepared by the wet impregnation of α-Al_2O_3 with aqueous solutions of $Ni(NO_3)_2$ and $Rh(NO_3)_2$ (from Aldrich). According to the fresh catalyst (after reduction) characterizations by X-ray fluorescence (XRF) analysis, temperature-programmed reduction (TPR) with 5% H_2 in helium, and temperature-programmed desorption (TPD) studies, the Ni and Rh weight content was 4.9% and 5.1%, the metal reducibility was 92.1% and 94.8%, and the metal reducibility percentage was 4.87% and 5.04%, respectively.

2.2. Catalytic steam reforming and relevant reactions

To undertake the reaction testing, an experimental reactor system was constructed. The feed gases, including the components of interest, i.e. CH_4, natural gas, biogas, LPG, and H_2S, were controlled and introduced to the system by the mass flow controllers, while deionized H_2O was fed by a syringe pump passing through an evaporator. For methane steam reforming testing, the inlet concentration of CH_4 was 20%, whereas the steam concentration was varied to achieve H_2O/CH_4 ratios between 0.5 and 3.0 and the inlet H_2S concentration was between 10 and 1000 ppm to capture a range of H_2S content in various fuels. As for the steam reforming of sulfur-containing fuels (i.e., natural gas, biogas, LPG) testing, the inlet concentration of total hydrocarbons in these fuels was kept constant at 20%, whereas various steam concentrations were added to achieve S/C ratios between 0.5 and 3.0. It is noted that the reforming tests with and without predesulfurization of these hydrocarbons were compared. Regarding the desulfurization unit, ZnO was applied to adsorb H_2S from the feed (the outlet gases were rechecked by gas chromatography with a flame photometric detector (FPD) to ensure that all H_2S were removed before purging to the reforming testing unit).

The inlet gas mixtures were introduced to the reaction section, in which a 10-mm-diameter quartz reactor was mounted vertically inside a tubular furnace. The catalysts (500 mg) were diluted with SiC (to obtain a total weight of 3.0 g) in order to avoid temperature gradients and loaded into the quartz reactor, which was packed with quartz wool to prevent the catalyst from moving. In the system, a type-K thermocouple was placed in the annular space between the reactor and furnace. This thermocouple was mounted in close contact with the catalyst bed to minimize the temperature difference. It is noted that another type-K thermocouple, covered by a closed-end quartz tube, was inserted into the middle of the quartz reactor in order to recheck the possible temperature deviation due to the heat transfer limitation. The record showed that the maximum temperature fluctuation during the reaction was always ±0.75 °C or less from the temperature specified for the reaction. After the reactions, the exit gas mixture was transferred via trace-heated lines (100 °C) to the analysis section, which consisted of a Porapak Q column Shimadzu 14B gas chromatograph (GC) and a quadrupole mass spectrometer (MS). The GC was applied in the steady state studies, whereas the MS was used for the transient experiments. In the present work, the outlet of the GC column was directly connected to a thermal conductivity detector (TCD), frame ionization detector, and FPD. In order to satisfactorily separate all elements, the temperature setting inside the GC column was programmed to vary with time. In the first 3 min, the column temperature was constant at 60 °C; it was then increased steadily at a rate of 15 °C min^{-1} to 120 °C and last decreased to 60 °C.

In this study, the catalyst activity was identified in terms of the turnover frequencies, H_2 yields, and other outlet gas selectivities. The turnover frequencies can be calculated from the equation [18]

$$\text{turnover frequencies} = \frac{rN_A A_{N_2}}{m_c S} \tag{1}$$

where r is the moles of CH_4 (or hydrocarbons) changing per unit time (mol_{CH_4} min^{-1}), N_A is Avogadro's number, A_{N_2} is the area occupied by an adsorbed nitrogen molecule (16.2×10^{-20} m^2); it is assumed that all surface sites accessible by nitrogen adsorption. m_c is the weight of catalyst used, and S is the specific surface area of the catalyst (m^2 g^{-1}). The yield of H_2 production (Y_{H_2}) was defined as the molar fraction of H_2 produced out of the total hydrogen-based compounds in the products. Other by-product selectivities (i.e., S_{CO}, S_{CO_2}, S_{CH_4}, $S_{C_2H_6}$, and $S_{C_2H_4}$) were defined as the mole ratios of the specified component in the outlet gas to the total carbon-based compounds in the product, accounting for stoichiometry. The following equations present the calculations of these selectivities:

$$S_{CO} = 100 \times \left(\frac{(\%CO)}{(\%CO) + (\%CO_2) + (\%CH_4) + 2(\%C_2H_6) + 2(\%C_2H_4)} \right) \tag{2}$$

$$S_{CO_2} = 100 \times \left(\frac{(\%CO_2)}{(\%CO) + (\%CO_2) + (\%CH_4) + 2(\%C_2H_6) + 2(\%C_2H_4)} \right) \tag{3}$$

$$S_{CH_4} = 100 \times \left(\frac{(\%CH_4)}{(\%CO) + (\%CO_2) + (\%CH_4) + 2(\%C_2H_6) + 2(\%C_2H_4)} \right) \tag{4}$$

$$S_{C_2H_4} = 100 \times \left(\frac{2(\%C_2H_4)}{(\%CO) + (\%CO_2) + (\%CH_4) + 2(\%C_2H_6) + 2(\%C_2H_4)} \right) \tag{5}$$

$$S_{C_2H_6} = 100 \times \left(\frac{2(\%C_2H_6)}{(\%CO) + (\%CO_2) + (\%CH_4) + 2(\%C_2H_6) + 2(\%C_2H_4)} \right) \tag{6}$$

It is noted that, for the studies on methane and biogas steam reforming, the terms for C_2H_6 and C_2H_4 are eliminated.

2.3. Measurement of carbon formation

After reaction, temperature-programmed oxidation (TPO) was used to investigate the amount of carbon formed on the spent catalyst surface by introducing 10% O_2 in helium, after the system was purged with helium. The operating temperature increased from room temperature to 1000 °C at a rate of 10 °C min^{-1}. The amount of carbon formation on the surface of catalysts was determined by measuring the CO and CO_2 yields from the TPO results (using Microcal Origin Software). The calibrations of CO and CO_2 were performed by injecting a known amount of these calibration gases from the sampling loop. In addition to the TPO method, the amount of carbon deposition was confirmed by the carbon balance calculation, in which the amount of carbon deposition theoretically equals the difference between the inlet hydrocarbon fuel and the outlet carbon components (e.g., CO, CO_2, CH_4, and C_{2+}).

2.4. The study of CeO_2 as prereforming catalyst

In the present work, a practical application using CeO_2 as a primary reforming catalyst to reform natural gas, biogas, and LPG (without prior desulfurization) was investigated. In detail, CeO_2 was applied to adsorb H_2S from the feed and primarily reform heavy hydrocarbons (C_{2+}) to light hydrocarbon (i.e., CH_4). The product from this section was continuously passed though a secondary reforming bed, where Ni/Al_2O_3 was packed, to complete the conversion and maximize H_2 yield. The design of this system consists of two tubular-containing CeO_2 columns and one Ni/Al_2O_3 column (with diameters of 25 mm and lengths of 50 cm). In each column, 25 g of either CeO_2 or Ni/Al_2O_3 (mixed with SiC) was packed, and these three columns were placed in the same burner, in which the temperature was controlled isothermally at SOFC temperature (900 °C) for later application as IIR-SOFC. Details of system operation are presented in Section 3.5.

3. Results and discussion

3.1. Preliminary experiments

Preliminary experiments were carried out to find a suitable condition under which internal and external mass transfer effects are

not predominant. Considering the effect of external mass transfer, the total gas flow rate was varied between 10 and 200 $cm^3\ min^{-1}$ for a constant residence time of $5 \times 10^{-4}\ g_{cat}\ min\ cm^{-3}$. It was found that the turnover frequencies are independent of the gas velocity when the gas flow rate is higher than 60 $cm^3\ min^{-1}$, indicating the absence of external mass transfer effects at this high velocity (Fig. 2). Furthermore, the reaction on different average sizes of catalyst was studied in order to ensure that the experiments were carried out within the region of intrinsic kinetics. It was observed that the catalysts with particle size less than 200 μm showed no intraparticle diffusion limitation under the range of conditions studied. Therefore, in the following studies, the total flow rate was kept constant at 100 $cm^3\ min^{-1}$, whereas the catalyst diameters were kept within the above-mentioned range in all experiments.

3.2. Activity of CeO_2 toward steam reforming of CH_4 in the presence of H_2S

First, the steam reforming of CH_4 over nano-scale CeO_2 in the presence of various H_2S contents was investigated. In our studies, H_2S contents of 10, 100, 500, and 1000 ppm (capturing a range of H_2S content in various fuels) were added during the reaction at 900 °C with an H_2O/CH_4 ratio of 3.0. As shown in Fig. 3, we found that the presence of H_2S under appropriate conditions increases the steam reforming rate. Without H_2S, the steady state turnover frequencies were 0.054 s^{-1}. When 10 ppm H_2S was added, the turnover frequencies increased steadily with time and reached a higher steady state value at 0.074 s^{-1}. When more H_2S was added in the feed (100 and 500 ppm), the turnover frequencies increased more rapidly to 0.098 and 0.095 s^{-1}. Nevertheless, when as much as 1000 ppm H_2S was introduced, although the turnover frequencies initially increased to 0.115 s^{-1}, they later gradually dropped to 0.071 s^{-1}. After exposure to H_2S for 3 h, the experiment was continued by removing H_2S from the feed. As also seen in this figure, the turnover frequencies (after 10 ppm H_2S was removed) remain constant, whereas after the experiments with 100 and 500 ppm H_2S the turnover frequencies were slightly reduced to 0.085 and 0.086 s^{-1}, respectively. After 1000 ppm H_2S was removed, the turnover frequencies increased considerably before decreasing to 0.088 s^{-1}. It is noted according to the error analysis that the

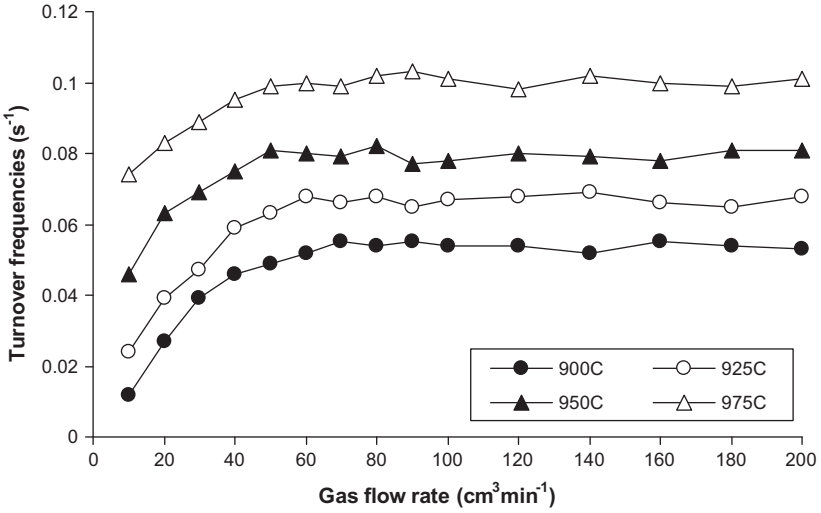

Fig. 2. Effect of the total gas flow rate on the turnover frequencies from the steam reforming at 900–975 °C with constant residence time 5×10^{-4} g min cm^{-3}.

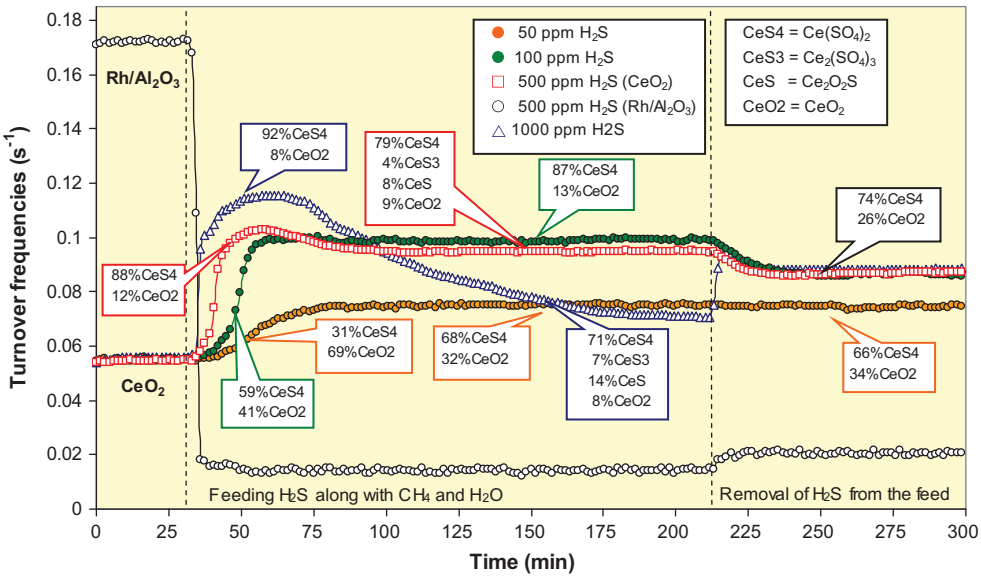

Fig. 3. Effect of H_2S on the turnover frequencies from methane steam reforming and Ce–O–S phase compositions at various H_2S concentrations.

deviations of these turnover frequencies are in the range of ±4.5%. Furthermore, the turnover frequencies observed in the present work are in good agreement with the values previously reported in the literature [18,20].

For comparison, the effect of H_2S on the steam reforming activity of highly active Rh/Al_2O_3 was also studied by adding 500 ppm H_2S along with CH_4 and H_2O. It was found that, in the presence of H_2S, the turnover frequencies from the steam reforming over Rh/Al_2O_3 dramatically dropped from 0.172 to 0.013 s^{-1} in a short time and could not be recovered even when H_2S was removed from the system (Fig. 3). It is noted that the XRD study on the spent Rh/Al_2O_3 catalyst indicated the formation of rhodium sulfide, which is rarely regenerated.

3.3. Effects of temperature and inlet H_2O/CH_4 ratio

As the next step, the effects of operating temperature and inlet H_2O/CH_4 molar ratio on the steam reforming of CH_4 over CeO_2 in the presence of H_2S were determined by varying the temperature (from 900 °C to 925, 950, and 975 °C) and inlet H_2O/CH_4 molar ratio (from 3.0 to 2.0, 1.5, and 1.0). It was found that the influence of H_2S on the turnover frequencies over CeO_2 strongly depends on the operating temperature and inlet H_2O/CH_4 ratio (Fig. 4). When 100 ppm H_2S was added at 900 °C, the turnover frequencies increased by 81% (from 0.054 to 0.098 s^{-1}); this difference increased to 83% (from 0.063 to 0.117 s^{-1}), 86% (from 0.075 to 0.139 s^{-1}), and 88% (from 0.089 to 0.168 s^{-1}) when the temperature increased to 925, 950, and 975 °C, respectively. In contrast, at 900 °C, when the inlet H_2O/CH_4 ratio was reduced to 2.0, 1.5, and 1.0, the positive deviation of the turnover frequencies with H_2S was reduced to +53%, +25%, and +7.9%; and when an H_2O/CH_4 ratio below 1.0 was applied, H_2S then reduced the turnover frequencies (from 0.054 s^{-1} to 0.041, 0.038, and 0.033 s^{-1} at inlet H_2O/CH_4 ratios of 0.75, 0.5, and 0.25). It is suggested from the XRD studies on spent CeO_2 after several reaction periods and conditions that this contradictory effect of H_2S is related to the formation of various Ce–O–S phases: $Ce(SO_4)_2$, $Ce_2(SO_4)_3$, and Ce_2O_2S, during the reaction (as illustrated in Fig. 5). The relevant reactions between CeO_2 and H_2S, which result in these phases, may be.

$$2CeO_2 + 8H_2O + 3H_2S \leftrightarrow Ce_2(SO_4)_3 + 11H_2 \quad (7)$$

$$Ce_2(SO_4)_3 + 4H_2O + H_2S \leftrightarrow 2Ce(SO_4)_2 + 5H_2 \quad (8)$$

$$2CeO_2 + H_2 + H_2S \leftrightarrow Ce_2O_2S + 2H_2O \quad (9)$$

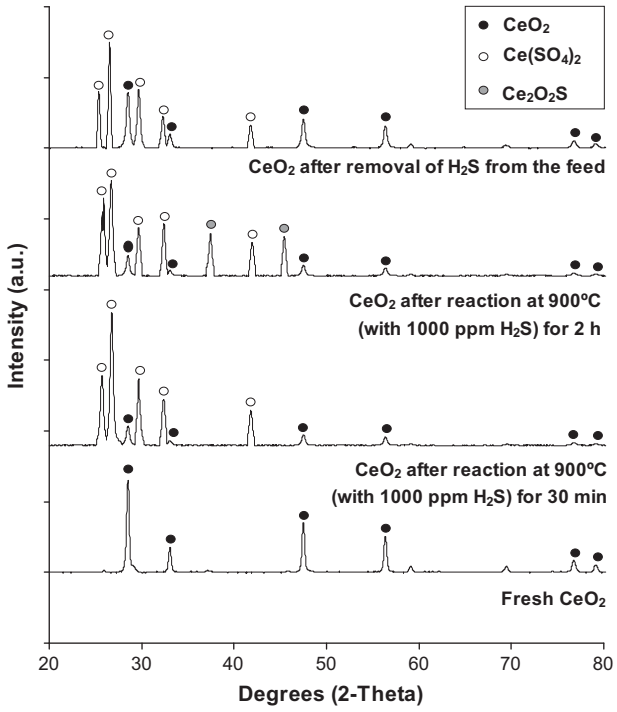

Fig. 5. XRD patterns of CeO_2 at various reaction times.

When 10 and 100 ppm H_2S was introduced during the reaction (with an H_2O/CH_4 ratio of 3.0 at 900 °C), $Ce(SO_4)_2$ was formed (via Eqs. (7) and (8)) and its proportion increased with increasing operating time (from 31% after 20 min to 68% after 2 h for 10 ppm H_2S; and from 59% after 20 min to 87% after 2 h for 100 ppm H_2S). In the experiments with 500 and 1000 ppm H_2S, as well as $Ce(SO_4)_2$ formation (79% and 71% for 500 and 1000 ppm H_2S), $Ce_2(SO_4)_3$ (4% and 7% for 500 and 1000 ppm H_2S) and Ce_2O_2S (8% and 14% for 500 and 1000 ppm H_2S) were also observed. At higher operating temperatures, the portion of $Ce(SO_4)_2$ phase increased considerably. On the other hand, when inlet H_2O/CH_4 ratios less than 1.0 were applied, Ce_2O_2S (occurs via Eq. (9)) became the dominant Ce–O–S phase. It has been suggested that with decreasing oxygen fugacity, the sulfate form of ceria decomposes to CeO_2 and then to

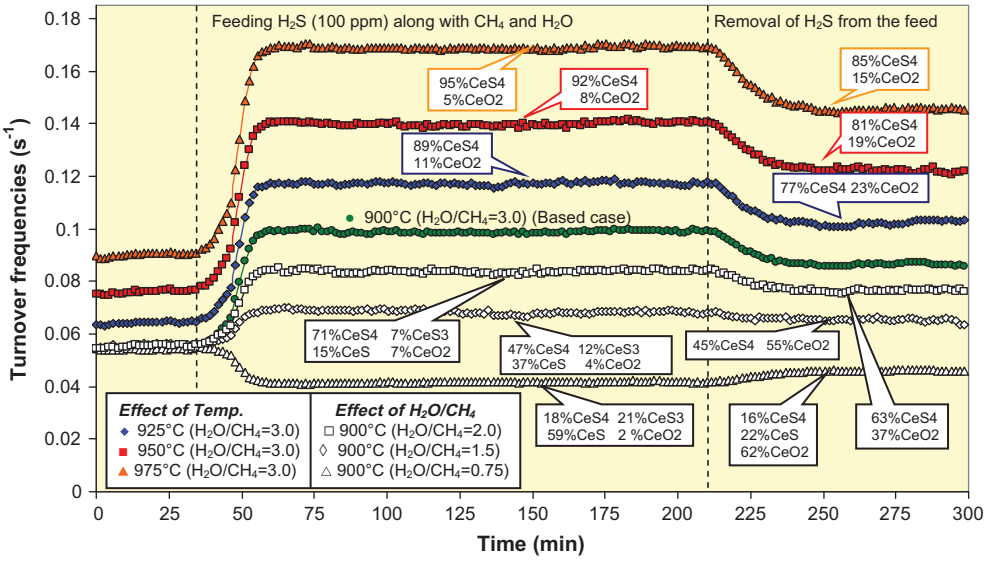

Fig. 4. Effect of H_2S on the turnover frequencies from methane steam reforming and Ce–O–S phase compositions at various temperatures and H_2O/CH_4 ratios.

Ce_2O_2S [24]. After H_2S removal, XRD patterns revealed that the Ce_2O_2S phase disappeared (due to the reversal of Eq. (9)), while the portion of $Ce(SO_4)_2$ phase slightly decreased but that of the CeO_2 phase increased.

3.4. Determination of the OSC and lattice oxygen mobility

Based on the results from Sections 3.1 and 3.2, we suggest that the formation of $Ce(SO_4)_2$ during the reaction leads to a high reforming activity, whereas the presence of Ce_2O_2S reduces the activity. To test this idea, the redox properties associated with the OSC and the mobility of lattice oxygen for $Ce(SO_4)_2$ were examined and compared to those for CeO_2 by applying TPR, TPD under reducing condition, $H_2/H_2O + H_2S$ titration, and $^{18}O/^{16}O$ isotope exchange methods. Furthermore, the ratio of Ce^{3+}/Ce^{4+} under reducing and oxidizing conditions was characterized by XPS. In detail, the TPR experiment was carried out in a 10-mm-diameter quartz reactor, which was mounted vertically inside tubular furnace. A type-K thermocouple was placed into the annular space between the reactor and furnace, while another thermocouple, covering by a closed-end quartz tube, was inserted into the middle of the quartz reactor in order to recheck the possible temperature gradient. The sample (100 mg) was heated from 25 to 1000 °C under 5% H_2 in nitrogen with a flow rate of 50 cm^3 min^{-1}, and the amount of H_2 consumed during the TPR process at different temperatures was monitored online by the TCD and quantified by calibrating the peak areas against the TPR of a known amount of CuO. The TPD over $Ce(SO_4)_2$ under the reducing-condition experiment was performed in the same scale of reactor with the same weight of sample as the TPR study (under 5%H_2 in nitrogen), but the effluent gases from the TPD experiment were monitored by the MS. It is noted that the MS signals were calibrated with a known amount of outlet gases (e.g., H_2S) to determine the absolute coverages corresponding to these TPD signals. As for $H_2/H_2O + H_2S$ titration, this experiment was conducted over $Ce(SO_4)_2$ to confirm the consecutive cycles of $Ce(SO_4)_2 \leftrightarrow CeO_2 \leftrightarrow Ce_2O_2S$. Similarly to the TPR and TPD experiments, the sample (100 mg of $Ce(SO_4)_2$) was placed in the middle of a quartz reactor packed with two layers of quartz wool to prevent the sample from moving. After the system was purged with helium for 1 h, known amounts of H_2 and $H_2O + H_2S$ were sequentially pulsed to the reactor for five consecutive cycles and the effluent gases were monitored with the MS. Last, an $^{18}O/^{16}O$ isotope exchange experiment was carried out to investigate the lattice oxygen mobility of the samples (CeO_2 and $Ce(SO_4)_2$). The sample (200 mg) was placed in the quartz reactor and thermally treated under a flow of high-purity helium (99.995%) at the desired temperatures for 1 h. Then $^{18}O_2$ (in helium) was multiply pulsed into the system and the outlet gases were monitored by the MS.

We found in the studies that the TPR of $Ce(SO_4)_2$ indicated a sharp reduction band at 470 °C and a broader band at 810 °C, whereas for CeO_2 smaller peaks were detected at slightly higher temperatures (600 and 850 °C). The TPD under reducing conditions showed an amount of H_2S desorption approximately corresponding to half of the initial coverage of sulfate relevant to the formation of Ce_2O_2S. After TPD, all sulfates were reduced to Ce_2O_2S. The $H_2/H_2O + H_2S$ titration was conducted to ensure that Ce_2O_2S can be reoxidized to sulfate forms. In five consecutive cycles, the amounts of H_2 uptake were nearly identical (Fig. 6), suggesting that the redox behavior of $Ce(SO_4)_2$ and CeO_2 is reversible. The amounts of H_2 uptake and H_2S produced were applied to indicate the amount and percentage of reducible oxygen in the catalysts. From the calculation, the amount of reducible oxygen for $Ce(SO_4)_2$ was estimated to be 1.27 mmol g^{-1} (17.3% of total oxygen in catalyst) compared to 0.71 mmol g^{-1} (10.1% of total oxygen in catalyst) for CeO_2; this clearly indicates the higher OSC of $Ce(SO_4)_2$. Furthermore, regarding the $^{18}O/^{16}O$ isotope exchange study, it is known that the exchange of $^{18}O/^{16}O$ isotopes over CeO_2 surface theoretically consists of (i) homoexchange in the gas phase ($^{18}O_2$ (g) + $^{16}O_2$ (g) → $^{18}O^{16}O$ (g)) and (ii) heteroexchange with the participation of oxygen atoms from CeO_2 ($^{18}O_2$ (g) + $^{16}O_2$ (S) → $^{18}O^{16}O$ (g) + ^{18}O (S) and $^{18}O^{16}O$ (g) + $^{16}O_2$ (S) → $^{16}O_2$ (g) + ^{18}O (S)). According to our results at 600 °C, the production of $^{16}O_2$ and $^{18}O^{16}O$ for $Ce(SO_4)_2$ is 24 and 17%, whereas the production of $^{16}O_2$ and $^{18}O^{16}O$ for CeO_2 is 12 and 2%. Therefore, the homoexchange in the gas phase is negligible under these operating conditions, since $^{18}O^{16}O$ concentration from both materials should be identical if the exchange in the gas phase is dominant for the overall reaction [25]. Fig. 7 shows the Arrhenius plots from $^{18}O/^{16}O$ isotope exchange studies over $Ce(SO_4)_2$ compared to CeO_2. It was found that the conversion of $^{18}O_2$ increases with increasing temperature to form $^{16}O_2$ and $^{18}O^{16}O$ for both materials and the production of $^{16}O_2$ and $^{18}O^{16}O$ from $Ce(SO_4)_2$ is greater than that from CeO_2, indicating its higher oxygen mobility. Furthermore, the observed activation energy from $^{18}O/^{16}O$ isotope exchange over $Ce(SO_4)_2$ is 85 kJ mol^{-1}, whereas that over CeO_2 was 110 kJ mol^{-1}.

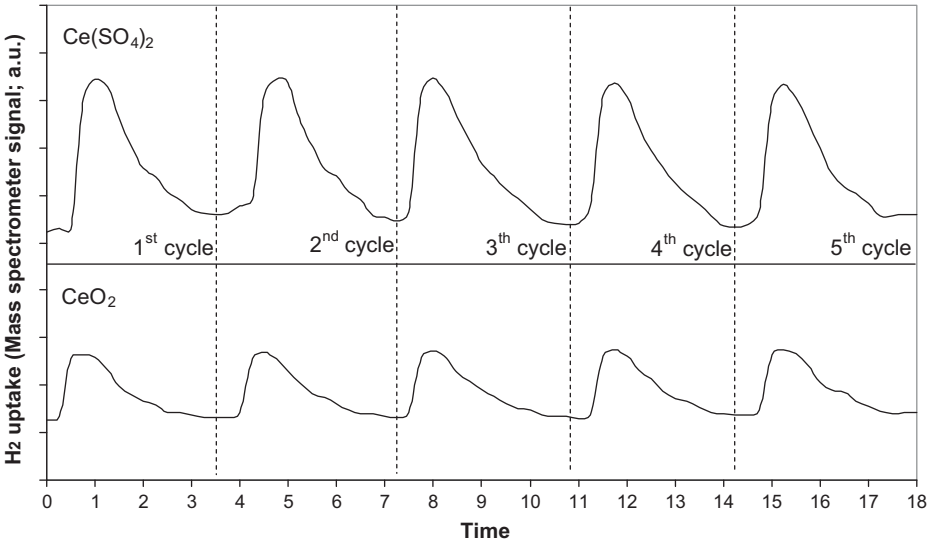

Fig. 6. H_2 uptake from $H_2/H_2O + H_2S$ titration over $Ce(SO_4)_2$ and CeO_2 for five cycles.

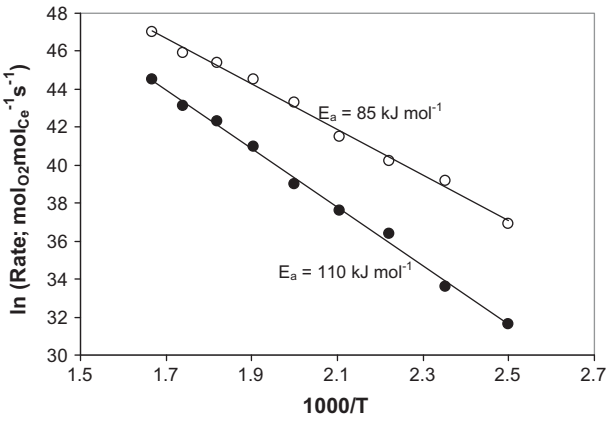

Fig. 7. Arrhenius plots from $^{18}O/^{16}O$ isotope exchange studies over (○) $Ce(SO_4)_2$ and (●) CeO_2.

Last, the XPS studies were also carried out to quantify the Ce^{4+} and Ce^{3+} levels of reduced and oxidized states of sulfate-form samples (Ce_2O_2S and $Ce(SO_4)_2$) compared to reduced and oxidized states of CeO_2. The XPS spectra implied that, under reducing conditions, the contents of Ce^{3+} for the sulfate-form sample and CeO_2 were 34.6% and 24.9%, respectively, while under oxidizing conditions, the contents of Ce^{3+} for the sulfate-form sample and CeO_2 were 17.3% and 19.8%, respectively. These results suggest that CeO_2 in sulfate form promotes the reduction of Ce^{4+} to Ce^{3+} under reducing conditions and the oxidation of Ce^{3+} to Ce^{4+} under oxidizing conditions. It is noted that these results should be further confirmed by an *in situ* XPS study, which can determine the Ce^{4+}/Ce^{3+} values during the reaction. Nevertheless, based on all characterization results, the greater redox properties of $Ce(SO_4)_2$ compared to CeO_2, which lead to the higher reforming activity, can be confirmed.

3.5. Long-term stability testing, effect of doped CeO_2 (with Gd, Y, Nb, La, and Sm), and activity toward the steam reforming of several hydrocarbons

Long-term stability testing with consecutive cycles at various scenarios (i.e., $CH_4 + H_2O/CH_4 + H_2O + H_2S/CH_4 + H_2O$ and $CH_4 + H_2O/CH_4 + H_2O + H_2S/O_2$ with different inlet H_2S concentrations) was carried out (Fig. 8). Over 50 h with 10 cycles, good stability and reversibility were observed for all conditions. Furthermore, the effect of doping CeO_2 with Gd, Y, Nb, La, and Sm on the contradictory behavior of H_2S was also studied, since doping with these rare earths is known to affect the OSC of CeO_2 [26,27]. It was first observed that doping with La, Sm, Gd, and Y increased the turnover frequencies of CeO_2 (which relates to their OSC improvement), whereas doping with Nb shows an inhibitory effect due to the strong segregation of Nb from the CeO_2 surface. It was then found that the effect of H_2S on doped and undoped CeO_2 followed the same trend but with different magnitude depending on the OSC of materials. Based on TPR and H_2–O_2 titration testing, the amounts of reducible oxygen over doped CeO_2 with Gd, Y, Nb, La, and Sm were 0.93, 0.82, 0.45, 1.09, and 0.95 mmol g^{-1} compared to 0.71 mmol g^{-1} for undoped CeO_2. These values are closely related to the turnover frequencies of the materials, in that the order of turnover frequencies without and with 100 ppm H_2S is La–CeO_2 (0.083 s^{-1}/0.121 s^{-1}) > Sm–CeO_2 (0.071 s^{-1}/0.113 s^{-1}) > Gd–CeO_2 (0.069 s^{-1}/0.109 s^{-1}) > Y–CeO_2 (0.061 s^{-1}/0.104 s^{-1}) > undoped CeO_2 (0.054 s^{-1}/0.098 s^{-1}) > Nb–CeO_2 (0.041 s^{-1}/0.066 s^{-1}).

With regard to more practical applications, the steam reforming of sulfur-containing hydrocarbons, i.e., natural gas (67%CH_4, 8.6%C_2H_6, 4.5%C_3H_8, 2.5%C_4H_{10}, and 14.5%CO_2 with 50 ppm H_2S sup-

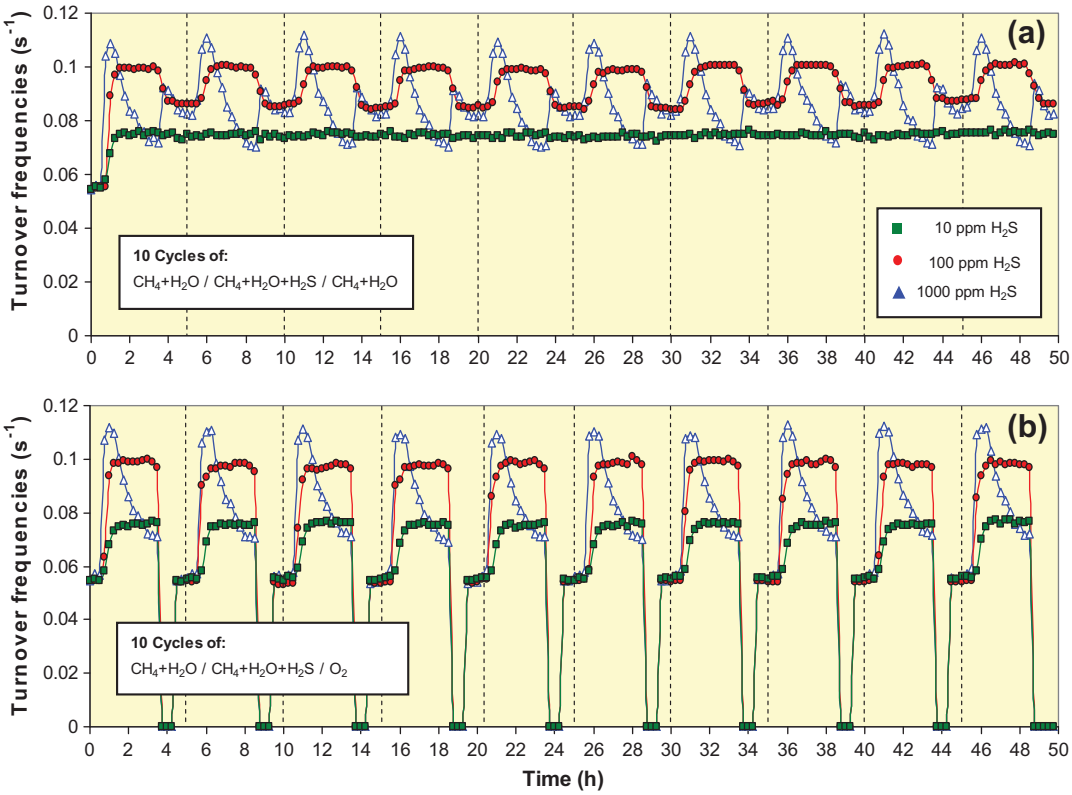

Fig. 8. Prolonged testing with 10 consecutive cycles of $CH_4 + H_2O/CH_4 + H_2O + H_2S/CH_4 + H_2O$ (a) and $CH_4 + H_2O/CH_4 + H_2O + H_2S/O_2$ (b) at three different H_2S concentrations.

Table 2
Turnover frequencies, H_2 yield, and other outlet gas selectivities from the steam reforming of natural gas, LPG, and biogas over CeO_2 at several temperatures and S/C molar ratios (with and without prior desulfurization).

Fuel	Temp. (°C)	S/C ratio	Turnover frequencies (s^{-1})				H_2 yield (%)	By-product selectivity (%)			
			CH_4	C_2H_6	C_3H_8	C_4H_{10}		CO	CO_2	CH_4	C_{2+}
Natural gas	900	3.0	0.070 (0.043)[a]	0.018 (0.017)	0.010 (0.010)	0.006 (0.006)	49 (32)	37 (20)	25 (18)	38 (59)	0 (3)
	925	3.0	0.085 (0.052)	0.019 (0.017)	0.010 (0.010)	0.006 (0.006)	57 (37)	48 (26)	23 (16)	29 (58)	0 (0)
	950	3.0	0.105 (0.059)	0.021 (0.018)	0.010 (0.010)	0.006 (0.006)	69 (41)	57 (32)	21 (15)	22 (53)	0 (0)
	1000	3.0	0.138 (0.078)	100 (0.019)	0.010 (0.010)	0.006 (0.006)	81 (50)	65 (40)	19 (11)	16 (49)	0 (0)
	900	2.0	0.070 (0.043)	0.018 (0.017)	0.010 (0.010)	0.006 (0.006)	48 (30)	39 (23)	23 (15)	38 (59)	0 (3)
	900	1.5	0.056 (0.043)	0.018 (0.017)	0.010 (0.010)	0.006 (0.006)	43 (28)	33 (25)	20 (12)	47 (60)	0 (3)
	900	1.0	0.049 (0.043)	0.017 (0.017)	0.010 (0.010)	0.006 (0.006)	37 (26)	31 (26)	12 (10)	55 (60)	2 (4)
	900	0.5	0.043 (0.038)	0.017 (77)	0.010 (0.010)	0.006 (0.006)	28 (24)	29 (28)	9 (3)	59 (63)	3 (6)
			C_3H_8	C_4H_{10}				CO	CO_2	CH_4	C_{2+}
LPG	900	3.0	0.108 (0.108)	0.108 (0.108)			69 (61)	58 (50)	27 (21)	13 (21)	2 (8)
	925	3.0	0.108 (0.108)	0.108 (0.108)			76 (65)	65 (57)	24 (19)	10 (19)	0.2 (5)
	950	3.0	0.108 (0.108)	0.108 (0.108)			83 (68)	72 (64)	20 (17)	8 (18)	0 (1.4)
	1000	3.0	0.108 (0.108)	0.108 (0.108)			89 (71)	78 (71)	17 (14)	5 (15)	0 (0)
	900	2.0	0.108 (0.108)	0.108 (0.108)			65 (58)	57 (52)	21 (18)	17 (22)	5 (8)
	900	1.5	0.108 (0.108)	0.108 (0.108)			59 (55)	55 (54)	18 (15)	20 (22)	7 (9)
	900	1.0	0.108 (0.108)	0.108 (0.108)			54 (52)	53 (55)	13 (10)	24 (25)	10 (10)
	900	0.5	0.108 (0.108)	0.108 (0.108)			45 (49)	51 (56)	6 (7)	30 (26)	13 (11)
								CO	CO_2	CH_4	
Biogas	900	3.0	0.071 (0.054)				43 (33)	27 (24)	33 (31)	40 (45)	
	925	3.0	0.088 (0.067)				50 (38)	34 (30)	31 (29)	35 (41)	
	950	3.0	0.108 (0.078)				58 (40)	42 (37)	29 (26)	29 (37)	
	1000	3.0	0.147 (0.101)				75 (51)	54 (45)	26 (24)	20 (31)	
	900	2.0	0.062 (0.054)				37 (31)	26 (27)	32 (28)	42 (45)	
	900	1.5	0.056 (0.054)				31 (29)	25 (30)	31 (25)	44 (45)	
	900	1.0	0.047 (0.052)				24 (28)	23 (33)	30 (21)	47 (46)	
	900	0.5	0.041 (0.049)				21 (25)	21 (35)	30 (18)	49 (47)	

[a] Values in blanket are those observed from the steam reforming of feedstocks with prior desulfurization.

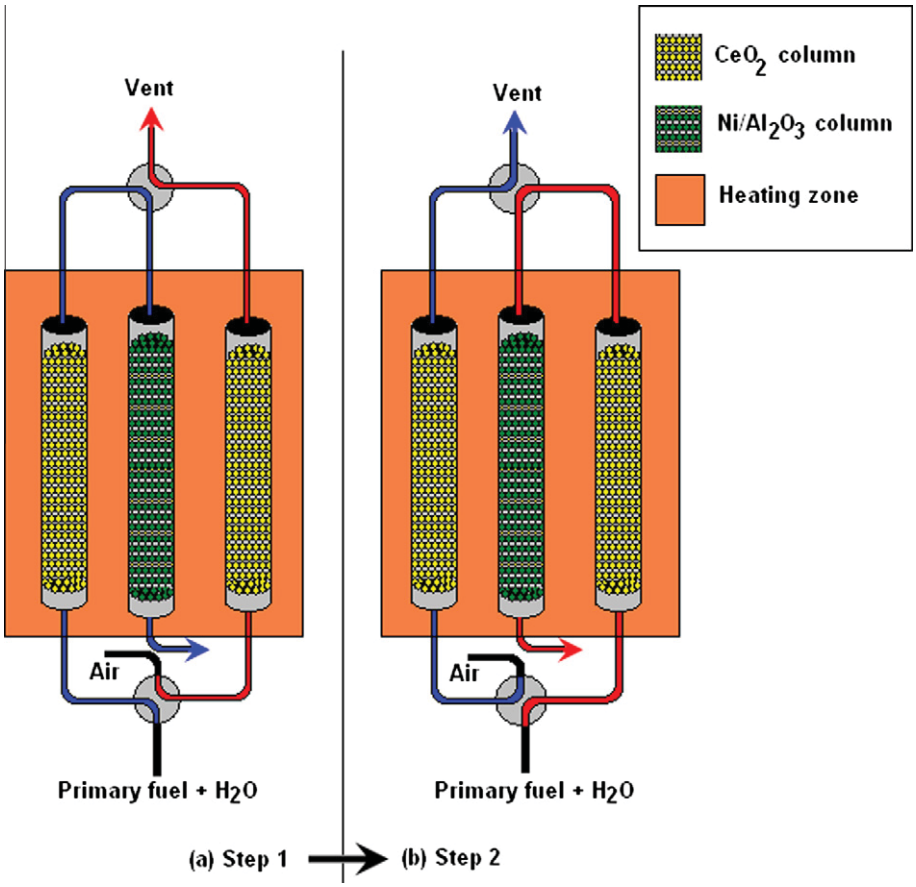

Fig. 9. Design and operation of CeO_2 as prereforming catalyst in the present work.

plied by PPT Plc., Thailand), LPG (60%C_3H_8, 40%C_4H_{10} with 100 ppm H_2S), and biogas (60%CH_4, 40%CO_2 with 1000 ppm H_2S) with and without desulfurization over CeO_2 was examined. Table 2 presents the catalytic activity in terms of turnover frequencies, H_2 yield, and by-product selectivities for various operating conditions. At suitable conditions, i.e., inlet S/C ratio 3.0, higher turnover frequencies could be achieved from the steam reforming of these feedstocks without desulfurization. Furthermore, after reaction for 18 h, the amounts of carbon deposition under each condition were analyzed by TPO and carbon balance calculation. It was found that, with an inlet S/C molar ratio of 3.0, the observed carbon deposition from the steam reforming of natural gas, LPG, and biogas (at 900 °C) was in the range of 0.22–0.26, 0.62–0.65, and 0.04–0.07 mmol g_{cat}^{-1}, respectively. These low amounts of carbon deposition indicate the excellent resistance toward carbon deposition of CeO_2.

Nevertheless, as seen from this table, CeO_2 alone as a reforming catalyst gives relatively low reforming activity and some hydrocarbons (mainly CH_4) were detected in the product, indicating incomplete conversion. Thus, we proposed the pairing of CeO_2 with a suitable metallic catalyst to achieve the benefits of self-desulfurization, improved resistance to carbon deposition, and higher reforming activity. For the approach in the present work, CeO_2 was applied as a prereforming catalyst in order to adsorb H_2S from the feed and primarily reform heavy hydrocarbons (C_{2+}) in the feed to CH_4. The product from this section was continuously passed though a secondary reforming bed, where Ni/Al_2O_3 was packed, to complete the conversion and to maximize H_2 yield. Design and operation of this prototype system are shown in Fig. 9. As for the operation, the primary fuels (i.e., natural gas, LPG, and biogas) were mixed with steam and flowed past a switching valve through the first CeO_2 column to remove all H_2S and partially reform all heavy hydrocarbons to CH_4. At the end of this tube, the gas mixture flowed backward past another switching valve to the Ni/Al_2O_3 column to complete the reforming reaction. At proper

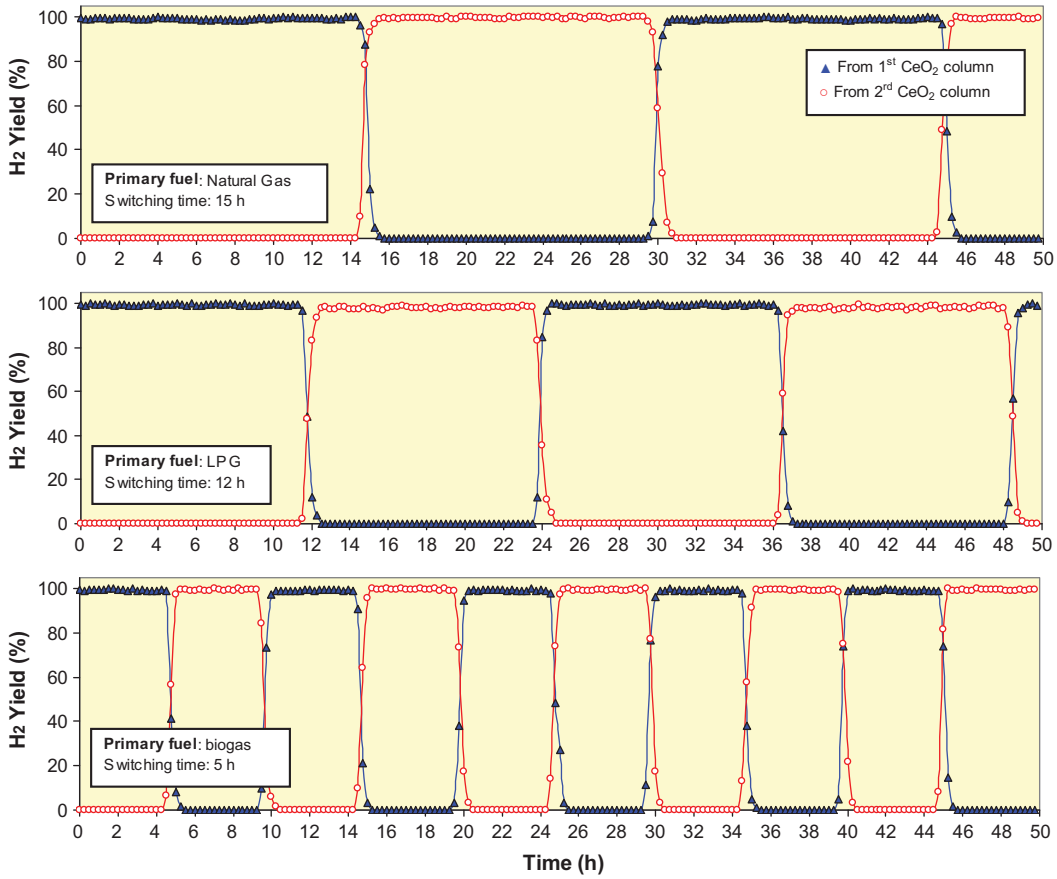

Fig. 10. H_2 yield produced from the use of CeO_2 as prereforming catalyst fed by different primary fuels at 900 °C with appropriate switching times (from first CeO_2 column to second CeO_2 column).

Table 3
Activity in terms of turnover frequencies, H_2 yield, other outlet gas selectivities, and the amount of carbon formation from the steam reforming of natural gas, LPG, and biogas (using CeO_2 as primary reforming catalyst and Ni/Al_2O_3 as secondary reforming catalyst) at 900 °C with S/C molar ratio 3/1.

Fuel	Regeneration time (h)	Turnover frequencies (s^{-1})				H_2 yield (%)	By-product selectivity (%)				Carbon formation (mmol g_{cat}^{-1})
		CH_4	C_2H_6	C_3H_8	C_4H_{10}		CO	CO_2	CH_4	C_2H_4	
Natural gas	15	0.173	0.022	0.011	0.006	99.7	66.3	33.5	0.2	0	0.36[a] (0.33)[b]
LPG	12	–	–	0.108	0.108	99.0	74.6	25.0	0.4	0	0.91 (0.95)
Biogas	5	0.214	–	–	–	99.7	61.3	38.5	0.2	–	0.09 (0.12)

[a] Calculated using CO and CO_2 yields from the TPO study.
[b] Calculated from the balance of carbon-based compounds in the system.

exposure times (5 h for biogas, 12 h for LPG, and 15 h for natural gas, where H_2S start came out in the outlet gas), two switching valves as mentioned above automatically switched the port direction and the primary fuels were flowed through the second CeO_2 column instead. Simultaneously, the air was purged through the first CeO_2 column to remove all sulfur elements in the column and vent out from the system. In our study, the switching process was repeated five times or for 50 h without detection of any activity deactivation, as shown in Fig. 10. The results in Table 3 also indicate that almost 100% H_2 yield could be achieved from all feedstocks; furthermore, low amounts of carbon deposition (less than 1.0 mmol g_{cat}^{-1}) were detected from all reactions after the prolonged testing. We concluded that the novelties of this reforming unit are the flexibility of inlet fuels and the nonrequirements for a desulfurization unit, a separate prereforming unit, and/or the use of expensive noble metal catalysts to reform sulfur-containing heavy hydrocarbon feedstocks. Importantly, this reforming unit would promote the practical application of IIR-SOFC, particularly with the use of a sulfur-tolerant SOFC anode, by eliminating the requirements for costly desulfurization units.

4. Conclusions

The presence of appropriate H_2S content makes it possible to promote the steam reforming rate of nano-scale CeO_2 and doped CeO_2 (with Gd, Y, Nb, La, and Sm). This contradictory effect was related to the formation of various Ce–O–S phases (i.e., $Ce(SO_4)_2$, $Ce_2(SO_4)_3$, and Ce_2O_2S) during the reaction. It was revealed that the formation of $Ce(SO_4)_2$ promotes the OSC, the lattice oxygen mobility, and eventually the reforming activity, whereas the formation of Ce_2O_2S reduces the OSC, the lattice oxygen mobility, and the reforming rate. The capability of these CeO_2 catalysts to adsorb and use poisoning H_2S gas to enhance its catalytic activity offers great benefits in terms of energy and environmental management, and importantly, this behavior would help to promote the hydrogen/fuel cell economy by eliminating the requirements for costly desulfurization units.

Acknowledgments

Financial support from the Thailand Research Fund (TRF) throughout this project is gratefully acknowledged. The authors acknowledge Dr. John T.H. Pearce for the English correction of this manuscript.

References

[1] M.Z. Jacobson, W.G. Colella, D.M. Golden, Science 308 (2005) 901.
[2] J.R. Rostrup-Nielsen, J. Sehested, J.K. Nørskov, Adv. Catal. 47 (2002) 65.
[3] J.R. Rostrup-Nielsen, T.S. Christensen, I. Dybkjaer, Stud. Surf. Sci. Catal. 113 (1998) 81.
[4] G.A. Deluga, J.R. Salge, L.D. Schmidt, X.E. Verykios, Science 303 (2004) 993.
[5] G.W. Huber, J.W. Shabaker, J.A. Dumesic, Science 300 (2003) 2075.
[6] J.R. Rostrup-Nielsen, Stud. Surf. Sci. Catal. 147 (2004) 121.
[7] G. Jones, J.G. Jakobsen, S.S. Shim, J. Kleis, M.P. Andersson, J. Rossmeisl, F. Abild-Pedersen, T. Bligaard, S. Helveg, B. Hinnemann, J.R. Rostrup-Nielsen, I. Chorkendorff, J. Sehested, J.K. Nørskov, J. Catal. 259 (2008) 147.
[8] A. Grirrane, A. Corma, H. García, Science 322 (2008) 1661.
[9] J.A. Rodriguez, S. Ma, P. Liu, J. Hrbek, J. Evans, M. Pérez, Science 318 (2007) 1757.
[10] A. Trovarelli, Catal. Rev. Sci. Eng. 38 (1996) 439.
[11] P. Fornasiero, G. Balducci, R.D. Monte, J. Kaspar, V. Sergo, G. Gubitosa, A. Ferrero, M. Graziani, J. Catal. 164 (1996) 173.
[12] T. Miki, T. Ogawa, M. Haneda, N. Kakuta, A. Ueno, S. Tateishi, S. Matsuura, M. Sato, J. Phys. Chem. 94 (1990) 339.
[13] C.T. Campbell, C.H.F. Peden, Science 309 (2005) 713.
[14] T. Hibino, A. Hashimoto, T. Inoue, J. Tokuno, S. Yoshida, M. Sano, Science 288 (2000) 2031.
[15] Z. Zhan, S.A. Barnett, Science 308 (2005) 844.
[16] R.J. Gorte, J.M. Vohs, S. McIntosh, Solid State Ion. 175 (2004) 1.
[17] O. Costa-Nunes, R.J. Gorte, J.M. Vohs, J. Power Sources 141 (2005) 241.
[18] E. Ramírez-Cabrera, A. Atkinson, D. Chadwick, Appl. Catal. B 47 (2004) 127.
[19] D.J.L. Brett, A. Atkinson, D. Cumming, E. Ramírez-Cabrera, R. Rudkin, N.P. Brandon, Chem. Eng. Sci. 60 (2005) 5649.
[20] N. Laosiripojana, S. Assabumrungrat, Appl. Catal. B 60 (2005) 107.
[21] N. Laosiripojana, S. Assabumrungrat, Appl. Catal. B 82 (2008) 103.
[22] M. Flytzani-Stephanopoulos, M. Sakbodin, Z. Wang, Science 312 (2006) 1508.
[23] D. Terribile, A. Trovarelli, J. Llorca, C. Leitenburg, G. Dolcetti, J. Catal. 178 (1998) 299.
[24] D.A.R. Kay, W.G. Wilson, V. Jalan, J. Alloys Compd. 192 (1993) 11.
[25] Y. Zeng, S. Kaytakoglu, D.P. Harrison, Chem. Eng. Sci. 55 (2000) 4893.
[26] H. He, H.X. Dai, K.W. Wong, C.T. Au, Appl. Catal. A 251 (2003) 61.
[27] L. Cao, C. Ni, Z. Yuan, S. Wang, Catal. Commun. 10 (2009) 1192.

Applied Catalysis A: General 383 (2010) 50–57

Contents lists available at ScienceDirect

Applied Catalysis A: General

journal homepage: www.elsevier.com/locate/apcata

Effects of support and co-fed elements on steam reforming of palm fatty acid distillate (PFAD) over Rh-based catalysts

N. Laosiripojana[a,*], W. Kiatkittipong[b], S. Charojrochkul[c], S. Assabumrungrat[d]

[a] The Joint Graduate School of Energy and Environment, King Mongkut's University of Technology Thonburi, Bangkok, 10140, Thailand
[b] Department of Chemical Engineering, Faculty of Engineering and Industrial Technology, Silpakorn University, Nakhon Pathom 73000, Thailand
[c] National Metal and Materials Technology Center (MTEC), Pathumthani, Thailand
[d] Department of Chemical Engineering, Faculty of Engineering, Chulalongkorn University, Bangkok, Thailand

ARTICLE INFO

Article history:
Received 22 October 2009
Received in revised form 29 April 2010
Accepted 17 May 2010
Available online 25 May 2010

Keywords:
Hydrogen
Palm fatty acid distillate
Reforming
Rhodium

ABSTRACT

The steam reformings of palm fatty acid distillate (PFAD) over Rh on $MgO–Al_2O_3$, Al_2O_3, and $Ce–ZrO_2$ (with Ce/Zr ratios of 3/1, 1/1, and 1/3) supports were studied. At 1023 K, the conversions of PFAD are almost 100%, while H_2, CO, CO_2, and CH_4 are the major products from the reaction with some amount of high hydrocarbon compounds i.e. C_2H_4, C_2H_6, and C_3H_6 also detectable. Among all catalysts, the highest H_2 yield with the greatest resistance toward carbon deposition and lowest formation of hydrocarbons in the product was achieved from $Rh/MgO–Al_2O_3$.

The activities of all catalysts increased with increasing temperature; interestingly at temperatures above 1173 K, H_2 yields from the steam reforming over $Rh/Ce–ZrO_2$ (with Ce/Zr ratio of 3/1) become greater than those observed over Rh/Al_2O_3 and $Rh/MgO–Al_2O_3$. This great improvement is due to gas–solid reactions between hydrocarbons present in the system with lattice oxygen (O_O^x) at $Ce–ZrO_2$ surfaces simultaneously with the reaction taking place on the active sites of Rh. $Rh/Ce–ZrO_2$ with Ce/Zr ratios of 3/1 was then selected for further study by adding O_2 and H_2 along with PFAD and steam at the feed. An addition of both components significantly reduced the degree of carbon deposition and promoted the conversion of hydrocarbons to CO and H_2. Nevertheless, the presence of too much O_2 could oxidize Rh particles and combust H_2 to H_2O, which results in low reforming reactivity. Addition of too much H_2 also reduced the catalyst activity due to the active site competition with Rh particles and the inhibition of gas–solid redox reactions between the gaseous hydrocarbon components with lattice oxygen (O_O^x) on the surface of $Ce–ZrO_2$ support.

1. Introduction

The solid oxide fuel cell (SOFC) has attracted considerable interest as it generates electricity with a wide range of applications, flexibility in the choice of fuel, and high system efficiency with low emission [1]. Hydrogen is the major fuel for SOFC; it can be produced efficiently from catalytic steam reforming of several conventional hydrocarbon fuels such as methane, natural gas, liquefied petroleum gas (LPG), gasoline and other oil derivatives. Nevertheless, due to the current oil crisis and the shortage of fossil fuels, the development of H_2 production process from biomass-based fuels attracts much attention. Among biomass-based fuels, palm oil is one of the current attractive resources and has been widely applied for alternative transportation fuel (i.e. biodiesel) production. Importantly, palm oil always contains high amounts of free fatty acid (FFA) and the presence of too much FFA could easily result in high amounts of soap produced simultaneously with transesterification reactions. To avoid this reaction, one must first process most of FFA or remove it from the oil (as in the form of palm fatty acid distillate (PFAD)). The conversion of this separate PFAD to valuable products, e.g. alternative clean fuels, is a method to reduce the cost for biodiesel production and to allow biodiesel enables to compete economically with conventional petroleum diesel fuels. Therefore, as a major aim of this research, PFAD is applied as feedstock to produce hydrogen-rich gas for later utilization in SOFCs. On this basis, it will provide great benefits in terms of energy, environmental, and economical aspects.

Focusing on the catalytic reforming process for H_2 production, many researchers have investigated reforming of several oxygenated hydrocarbons, e.g. methanol, acetic acid, ethanol, acetone, phenol or cresol [2–10]. Nevertheless, until now, no publication has reported the conversion of fatty acids or PFAD to H_2; only a few works have previously reported the catalytic reforming or cracking of acetic acid to H_2 [11–13]. PFAD mainly consists of palmitic acid ($C_{16}H_{32}O_2$; $CH_3(CH_2)_{14}COOH$), oleic acid ($C_{18}H_{34}O_2$; $CH_3(CH_2)_7CH{=}CH(CH_2)_7COOH$) and linoleic acid

* Corresponding author. Tel.: +66 2 872 9014; fax: +66 2 872 6736.
E-mail address: navadol_l@jgsee.kmutt.ac.th (N. Laosiripojana).

0926-860X/$ – see front matter © 2010 Elsevier B.V. All rights reserved.
doi:10.1016/j.apcata.2010.05.022

Table 1
Physicochemical properties of the catalysts before and after exposure in the steam reforming at 1023 K for 48 h.

Catalyst	C formation (mmol g_{cat}^{-1})	BET surface ($m^2\ g^{-1}$)	Metal-load[a] (wt.%)	Metal-red.[b] (Rh%)	Metal-disp.[c] (Rh%)
Rh/Ce–ZrO_2 (Ce/Zr = 3/1)	10.0	40.2 (40.9)[d]	5.05 (5.05)	92.0(92.1)	4.52(4.61)
Rh/Ce–ZrO_2 (Ce/Zr = 1/1)	10.2	40.8(41.3)	5.26 (5.28)	93.2 (93.9)	4.73 (4.86)
Rh/Ce–ZrO_2 (Ce/Zr = 1/3)	9.5	43.1 (43.7)	5.16(5.16)	92.9(93.1)	5.01(5.12)
Rh/Al_2O_3	10.4	41.5(42.1)	5.11(5.13)	94.4 (94.8)	4.97 (5.04)
Rh/MgO–Al_2O_3	6.1	45.0 (45.3)	5.00 (5.04)	95.1 (95.3)	7.35 (7.41)

[a] Measured from X-ray fluorescence analysis.
[b] Rhodium reducibility (Measured from temperature-programmed reduction (TPR) with 5%hydrogen).
[c] Rhodium dispersion (Measured from the volumetric H_2 chemisorption measurement using chemisorption analyzer).
[d] Values in the blanket are those observed before the reaction.

($C_{18}H_{32}O_2$; $CH_3(CH_2)_4CH{=}CHCH_2CH{=}CH(CH_2)_7CO_2H$) with various ratios depending on the source of spent oils. The major difficulty in converting these acid compounds is the possible deactivation of catalyst due to carbon deposition, as these heavy compounds can easily decompose homogenously to several gaseous high hydrocarbon elements, which act as very strong promoters for carbon formation.

Currently, the commercial reforming catalysts are metallic-based materials (e.g. Ni or Rh) on several oxide supports (e.g. Al_2O_3, MgO, and MgO–Al_2O_3). It has been evident that the selection of support material is an important issue as metal catalysts are not very active for the steam reforming when supported on inert oxides [14]. Recently, one promising catalyst for the reforming reactions appears to be a metal on ceria–zirconia (Ce–ZrO_2) support, where the metal can be Ni, Rh, Pt or Pd [15–22]. Ce–ZrO_2 is well established to be useful in a wide variety of applications involving oxidation or partial oxidation of hydrocarbons (e.g. automotive catalysis) and as components of anodes for SOFCs. This material has high oxygen storage capacity, which is beneficial in oxidation processes and carbon combustion. The excellent resistance toward carbon formation from methane reforming reactions over Ni supported by Ce–ZrO_2 compared to commercial Ni on Al_2O_3 support was recently reported [23]. Furthermore, previously we reported the achievement of high reforming reactivity by applying high surface area (HSA) ceria-based supports compared to the conventional low surface area ones, due to the improvement in metal dispersion and high redox properties of HSA ceria-based supports [23]. The cationic surfactant-assisted approach was employed to prepare HSA ceria-based materials in our works; by this preparation procedure, materials with good homogeneity and stability especially after thermal treatments were achieved [23,24].

In the present work, Rh was selected as a metal catalyst as it has been widely reported to present high reforming activity with great resistance toward carbon formation. Recently, several researchers have studied the steam reforming, autothermal reforming and partial oxidation of several hydrocarbon feedstocks, e.g. methane, ethanol, light and heavy hydrocarbons, over Rh-based catalysts; they all reported the excellent performance of this catalyst toward these reactions [25–31]. Here, Rh was impregnated on high surface area (HSA) Ce–ZrO_2 synthesized by the cationic surfactant-assisted approach. The stability, activity and product distribution of this Rh/Ce–ZrO_2 toward the steam reforming of PFAD were studied and compared to these of Rh/MgO–Al_2O_3 and Rh/Al_2O_3. Furthermore, the resistance toward carbon formation and the influences of temperature and possible inlet co-reactant, i.e. O_2 (as autothermal reforming) and H_2, on the reforming performance were also determined and discussed.

2. Experimental

2.1. Raw material

In the present work, palm fatty acid distillate (PFAD) was obtained from Chumporn Palm Oil Industry Public Company Limited, Thailand. It consists of 93 wt% free fatty acid (FFA) (that mainly contains 46% palmitic acid, 34% oleic acid and 8% linoleic acid with small amount of other fatty acids i.e. stearic, myristic, tetracosenoic, linolenic, ecosanoic, ecosenoic, and palmitoleic acid). The remaining components are triglycerides, diglycerides (DG), monoglycerides (MG) and traces of impurities.

2.2. Catalyst preparations and characterizations

$Ce_{1-x}Zr_xO_2$ (or Ce–ZrO_2) with different Ce/Zr molar ratios were prepared by the cationic surfactant-assisted method of cerium nitrate ($Ce(NO_3)_3{\cdot}H_2O$), and zirconium oxychloride ($ZrOCl_2{\cdot}H_2O$) (from Aldrich). In the preparation, an aqueous solution of an appropriate cationic surfactant, 0.1 M cetyltrimethylammonium bromide solution (from Aldrich), was added to the mixture of cerium nitrate and zirconium oxychloride. The ratio between each metal salts was altered to achieve nominal Ce/Zr molar ratios: $Ce_{1-x}Zr_xO_2$, where x = 0.25, 0.50, and 0.75, respectively, whereas the molar ratio of ([Ce] + [Zr])/[cetyltrimethylammonium bromide] was kept constant at 0.8. The mixture was stirred and then aqueous ammonia was slowly added with vigorous stirring until the pH was 11.5. The mixture was continually stirred for 3 h, then sealed and placed in a thermostatic bath maintained at 263 K for 3 days. Next, the mixture was cooled and the resulting precipitate was filtered and washed repeatedly with water and ethanol to prevent agglomeration of the particles. It was dried overnight in an oven at 383 K, and then calcined at 1173 K for 6 h.

Rh/Ce–ZrO_2 (5 wt% Rh) was then prepared by impregnating Ce–ZrO_2 with the solution of $Rh(NO_3)_3$ (from Aldrich). The catalyst was reduced with 10%H_2 at 773 K for 6 h before use. For comparison, Rh/Al_2O_3 and Rh/MgO–Al_2O_3 (5 wt% Rh) were prepared by impregnating γ-Al_2O_3 (from Aldrich) and MgO–Al_2O_3 with $Rh(NO_3)_3$. MgO–Al_2O_3 was prepared by impregnating γ-Al_2O_3 with $Mg(NO_3)_2$ (the MgO content was 15% by mass). All catalysts were reduced under H_2 flow at 573 K for 6 h before use. After treatment, the catalysts were characterized by several physicochemical methods. The weight content of Rh was determined by X-ray fluorescence (XRF) analysis. The reducibility percentage of rhodium was measured and calculated from the degree of H_2 uptakes from the temperature-programmed reduction (TPR) test using 5% H_2 with the total flow rate of 100 $cm^3\ min^{-1}$ and temperature from room temperature to 773 K, while the dispersion percentage of rhodium was identified from the volumetric H_2 chemisorption measurement using a chemisorption analyzer. Lastly, the catalyst specific surface areas were obtained from BET measurements. All physicochemical properties of the synthesized catalysts are presented in Table 1.

2.3. Apparatus and procedures

For the catalytic testing, an experimental reactor system was constructed as shown elsewhere [24]. The feed gases i.e. He (as carrier gas), O_2 and H_2 were controlled by 3 mass flow controllers, whereas PFAD and H_2O were introduced by the heated syringe pump (with the reactant feed flow rate of 2.54 $cm^3\ h^{-1}$) and vapor-

ized by our designed quartz vaporizer-mixer system. All feeds were introduced to a 10-mm diameter quartz reactor, which is mounted vertically inside the tubular furnace. The catalyst (100 mg) was loaded in the quartz reactor, which was packed with a small amount of quartz wool to prevent the catalyst from moving. Preliminary experiments were carried out to find suitable conditions in which internal and external mass transfer effects are not predominant. Considering the effect of external mass transfer, we kept the total flow rate constant at 100 $cm^3\ min^{-1}$ under a constant residence time in all testing. The suitable average sizes of catalysts were also verified in order to confirm that the experiments were carried out within the region of isothermal kinetics. Based on the verification, the catalyst particle size diameter was between 100 and 200 μm in all experiments.

In our system, a Type-K thermocouple was placed into the annular space between the reactor and the furnace. This thermocouple was mounted on the tubular reactor in close contact with the catalyst bed to minimize the temperature difference between the catalyst bed and the thermocouple. Another Type-K thermocouple, which is covered with small closed-end quartz rod to prevent any catalytic reactivity of the thermocouple during the reaction, was inserted in the middle of the quartz tube in order to re-check the possible temperature gradient. The recorded values showed that the maximum temperature fluctuation during the reaction was always ±1.0 °C or less from the temperature specified for the reaction.

After the reactions, the exit gas mixture was transferred via trace-heated lines to the analysis section, which consists of a Porapak Q column Shimadzu 14B gas chromatograph (GC) and a mass spectrometer (MS). The mass spectrometer in which the sampling of the exit gas was done by a quartz capillary and differential pumping was used for the transient and carbon formation experiments, whereas the gas chromatography was applied in order to investigate the steady state condition experiments and to re-check the results from the mass spectrometer. In the present work, the reactivity was defined in terms of conversion and product distribution. The yield of H_2 production was calculated by hydrogen balance, defined as molar fraction of H_2 produced to total H_2 in the products. Distributions of other by-product selectivities (e.g. CO, CO_2, CH_4, C_2H_6, and C_2H_4) were calculated by carbon balance, defined as ratios of each mole of product to the moles of hydrocarbons in the product gas, accounting for stoichiometry; this information was presented in term of (relative) fractions of these by-product components, which are summed to 100%. Eqs. (1)–(8) present the calculations of PFAD conversion, H_2 yield and by-product selectivities.

$$X_{PFAD} = 100 \times \left(\frac{(\%PFAD_{in} - \%PFAD_{out})}{\%PFAD_{in}} \right) \quad (1)$$

$$Y_{H_2} = 100 \times \left(\frac{(\%H_2)}{2(\%CH_4) + 3(\%C_2H_6) + 2(\%C_2H_4)} \right) \quad (2)$$

$$S_{CO} = 100 \times \left(\frac{(\%CO)}{(\%CO) + (\%CO_2) + (\%CH_4) + 2(\%C_2H_6) + 2(\%C_2H_4) + 3(\%C_3H_6)} \right) \quad (3)$$

$$S_{CO_2} = 100 \times \left(\frac{(\%CO_2)}{(\%CO) + (\%CO_2) + (\%CH_4) + 2(\%C_2H_6) + 2(\%C_2H_4) + 3(\%C_3H_6)} \right) \quad (4)$$

$$S_{CH_4} = 100 \times \left(\frac{(\%CH_4)}{(\%CO) + (\%CO_2) + (\%CH_4) + 2(\%C_2H_6) + 2(\%C_2H_4) + 3(\%C_3H_6)} \right) \quad (5)$$

$$S_{C_2H_4} = 100 \times \left(\frac{2(\%C_2H_4)}{(\%CO) + (\%CO_2) + (\%CH_4) + 2(\%C_2H_6) + 2(\%C_2H_4) + 3(\%C_3H_6)} \right) \quad (6)$$

$$S_{C_2H_6} = 100 \times \left(\frac{2(\%C_2H_6)}{(\%CO) + (\%CO_2) + (\%CH_4) + 2(\%C_2H_6) + 2(\%C_2H_4) + 3(\%C_3H_6)} \right) \quad (7)$$

$$S_{C_3H_6} = 100 \times \left(\frac{3(\%C_3H_6)}{(\%CO) + (\%CO_2) + (\%CH_4) + 2(\%C_2H_6) + 2(\%C_2H_4) + 3(\%C_3H_6)} \right) \quad (8)$$

2.4. Measurement of carbon formation

The oxidation reaction was applied to investigate the amount of carbon formed on the catalyst surface by introducing 10% O_2 in He into the system at 1173 K, after purging with helium. The amount of carbon formation on the surface of catalysts was determined by measuring the CO and CO_2 yields from the test. The calibrations of CO and CO_2 productions were performed by injecting a known amount of these calibration gases from a loop, in an injection valve in the bypass line. The response factors were obtained by dividing the number of moles for each component over the respective areas under the peaks. It is noted that the spent sample was further tested with TGA–MS (PerkinElmer, USA) at the maximum temperature of 1273 K to ensure that no carbon formation remains on the surface of the catalyst; and no weight loss or CO/CO_2 productions were detected from all catalysts after the oxidation reaction.

3. Results and discussion

3.1. Reactivity toward steam reforming of PFAD

Rh over three different supports (Al_2O_3, $MgO–Al_2O_3$, $Ce–ZrO_2$) were firstly studied in the steam reforming of PFAD at 1023 K. The feed was PFAD/H_2O in He with the H_2O/carbon molar ratio of 3.0. The variations in PFAD conversion and product distribution with time at 1023 K over different catalysts are shown in Fig. 1a–c. It can be seen that the conversion of PFAD was always 100% for all catalysts. Regarding the product composition, apart from the productions of H_2, CO, and CO_2, significant amounts of CH_4 and C_2H_4 with small amounts of other high hydrocarbon compounds i.e. C_2H_6, and C_3H_6 were also detected from the reaction. If one compares among three catalysts, considerable higher H_2 yields were detected for $Rh/MgO–Al_2O_3$, whereas lower H_2 yields with significant formations of CH_4, C_2H_4, C_2H_6, and C_3H_6 were observed from the steam reforming of PFAD over Rh/Al_2O_3 and $Rh/Ce–ZrO_2$ catalysts (with all Ce/Zr ratios). At steady state, H_2 yield from the steam reforming of PFAD over $Rh/MgO–Al_2O_3$, Rh/Al_2O_3 and $Rh/Ce–ZrO_2$ (with Ce/Zr ratio of 1/3) were 72.6, 60.8 and 63.4%, respectively. It is noted that, among $Rh/Ce–ZrO_2$ (with various Ce/Zr ratios), $Rh/Ce–ZrO_2$ with Ce/Zr ratio of 1/3 gave the highest H_2 yield with the lowest amount of carbon formation (H_2 yield from the steam reforming of PFAD over $Rh/Ce–ZrO_2$ with Ce/Zr ratios of 1/1 and 3/1 were 60.1 and 58.4%, respectively; the difference in reactivity could be due to the high dispersion percentage of $Rh/Ce–ZrO_2$ with Ce/Zr ratio of 1/3 compared to $Rh/Ce–ZrO_2$ with Ce/Zr ratios of 3/1 and 1/1, according to the pre- and post-reaction H_2 chemisorption analysis (Table 1).

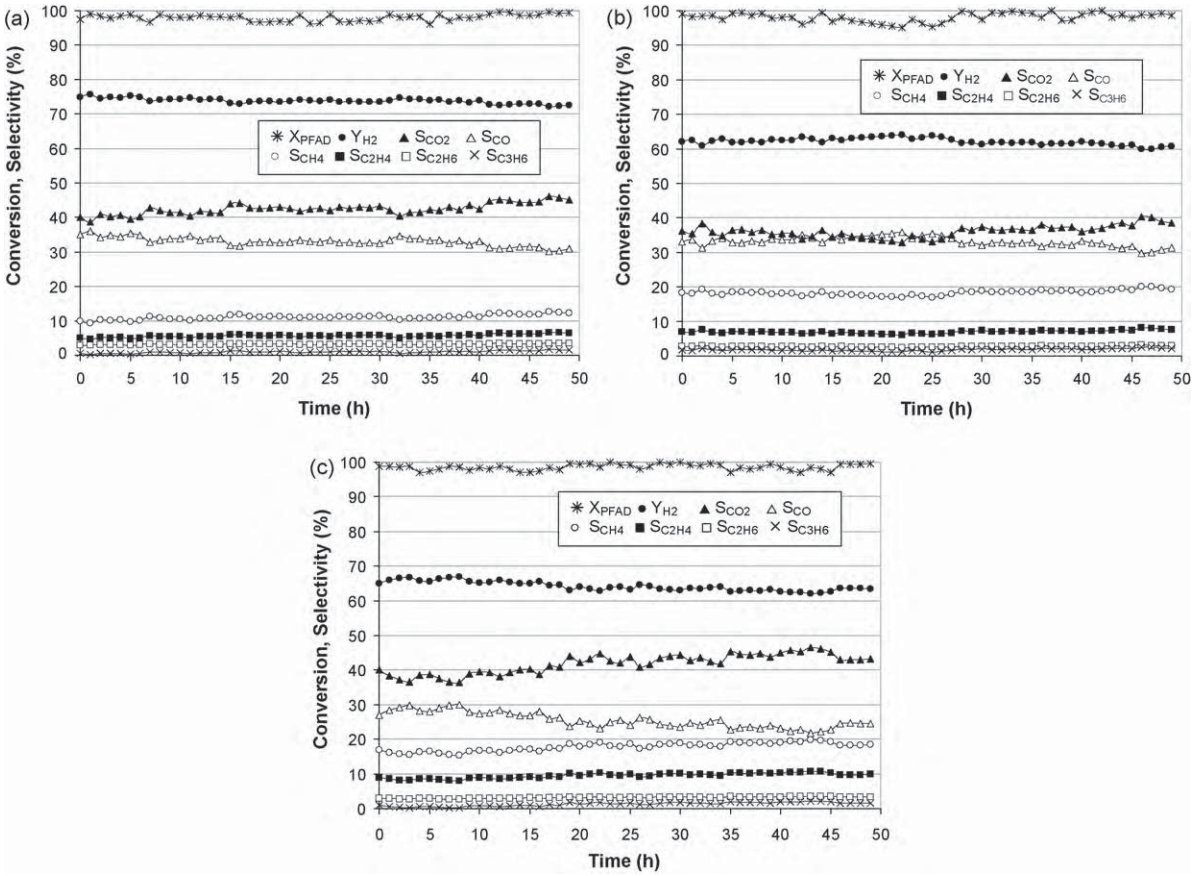

Fig. 1. (a) Variations in conversion and product distributions with time from the steam reforming of PFAD at 1023 K over (a) $Rh/MgO–Al_2O_3$, (b) Rh/Al_2O_3 and (c) $Rh/Ce–ZrO_2$ (Ce/Zr = 1/3).

According to the mechanistic viewpoint, the overall reactions involved in the steam reforming of PFAD are very complex. At such a high operating temperature in the present work, the thermal decomposition of PFAD takes place producing several gaseous products as well as coke from the following reaction:

$$C_xH_yCOOH \rightarrow C_nH_mO_k + \text{coke} + \text{gases}(H_2, CO, CO_2, C_nH_m) \quad (9)$$

when steam is introduced, the catalytic steam reforming of hydrocarbons (C_nH_m) occurs along with some side-reactions (e.g. water gas shift reaction and methanation).

$$C_nH_m + nH_2O \rightarrow nCO + (n + 0.5m)H_2 \quad (10)$$

$$nCO + nH_2O \rightarrow nCO_2 + nH_2 \quad (11)$$

$$nCO + 3nH_2 \rightarrow nCH_4 + nH_2O \quad (12)$$

$$nCO_2 + 4nH_2 \rightarrow nCH_4 + 2nH_2O \quad (13)$$

The generations of saturated and unsaturated C_{2+} hydrocarbons (e.g. ethylene and ethane) are the major difficulties for the catalytic steam reforming, as these components act as very strong promoters for carbon formation. Theoretically, Eqs. (14)–(17) below are the most probable reactions that could lead to carbon deposition during the reforming processes:

$$C_nH_m \Leftrightarrow 0.5mH_2 + nC \quad (14)$$

$$2CO \Leftrightarrow CO_2 + C \quad (15)$$

$$CO + H_2 \Leftrightarrow H_2O + C \quad (16)$$

$$CO_2 + 2H_2 \Leftrightarrow 2H_2O + C \quad (17)$$

C means the carbonaceous deposits. According to the range of temperature in this study, carbon formation would be formed via the decomposition of hydrocarbons and Boudouard reactions [32,33]. In order to determine the amount of carbon formation occurred in the system, the post-reaction oxidation experiments were carried out after a helium purge by introducing of 10% O_2 in He. The amounts of carbon formations on the surface of these catalysts were determined by measuring CO_2 yield (using Microcal Origin Software). The results clearly indicated the strong resistance toward carbon formation at this operating condition for $Rh/MgO–Al_2O_3$ as compared to Rh/Al_2O_3 and $Rh/Ce–ZrO_2$ (Table 1).

The good reforming reactivity with high resistance toward carbon deposition of $Rh/MgO–Al_2O_3$ is related to the formation of magnesium aluminate spinel, which offers enhanced O and –OH anion spillover from the support surface onto the metallic particles, according to the report from Basagiannis and Verykios [11]. They studied the steam reforming of acetic acid over Ru-based catalysts and indicated that, based on the mechanistic viewpoint, the ability of the catalyst to keep the metal surface clean through O and –OH spillover process is an important step toward catalytic activity. In addition, they also suggested that the high resistance toward carbon deposition of $Rh/MgO–Al_2O_3$ is also due to the reduction of total surface acidity by addition of MgO to Al_2O_3, which is widely known to reduce the rate of carbon deposition.

3.2. Effects of inlet steam/carbon ratio and temperature

As the next step, the inlet H_2O/carbon ratio was varied from 3 to 5, 7, 9, and 11, and the operating temperature was increased from 1023 to 1223 K. Table 2 presents the effect of inlet H_2O/carbon ratio

Table 2
Effect of inlet steam/carbon molar ratio on the product distributions and degree of carbon formation after exposure in steam reforming of PFAD at 1023 K for 48 h.

Catalyst	H_2O/carbon molar ratio	Product distribution (%)							Carbon formation (mmol g_{cat}^{-1})
		YH_2	SCO_2	SCO	SCH_4	SC_2H_4	SC_2H_6	SC_3H_6	
Rh/Ce–ZrO_2 (Ce/Zr = 3/1)	3.0	56.7	40.8	19.6	26.3	8.9	2.4	2.0	10.0
	5.0	58.4	43.6	17.9	28.4	7.3	1.6	1.2	9.4
	7.0	60.3	45.9	16.9	29.9	5.4	1.2	0.7	9.1
	9.0	61.2	46.9	15.9	30.9	5.1	0.9	0.3	8.6
	11.0	63.4	47.5	15.3	32.1	4.2	0.8	0.1	8.2
Rh/Ce–ZrO_2 (Ce/Zr = 1/1)	3.0	60.1	40.0	21.5	24.9	9.0	4.1	0.5	10.2
	5.0	61.2	41.7	19.7	27.3	8.1	2.8	0.4	10.1
	7.0	64.5	45.5	16.5	28.2	7.5	2.1	0.2	9.7
	9.0	66.7	48.5	14.2	30.1	5.6	1.5	0.1	9.3
	11.0	68.7	50.2	13.1	31.5	4.2	1.0	0	9.0
Rh/Ce–ZrO_2 (Ce/Zr = 1/3)	3.0	63.5	43.2	23.8	18.4	9.9	3.3	1.5	9.5
	5.0	65.7	45.3	22.9	19.4	8.4	3.1	0.9	9.1
	7.0	66.9	48.9	18.9	22.4	6.3	2.9	0.6	8.4
	9.0	68.4	51.2	16.1	23.6	6.1	2.5	0.5	8.0
	11.0	69.2	53.4	15.5	24.7	5.2	1.1	0.1	8.0
Rh/Al_2O_3	3.0	60.7	38.5	30.1	18.8	7.6	2.9	2.2	10.4
	5.0	63.4	40.5	29.4	20.4	5.3	2.4	2.0	9.8
	7.0	65.8	42.3	26.1	23.9	4.1	2.1	1.5	9.8
	9.0	67.2	46.5	22.2	24.9	3.2	1.9	1.3	9.6
	11.0	69.9	47.8	20.1	27.2	2.6	1.3	1.0	8.6
Rh/MgO–Al_2O_3	3.0	72.6	45.1	31.4	12.2	6.4	3.4	1.5	7.1
	5.0	74.9	47.8	29.3	13.9	5.4	2.5	1.1	6.8
	7.0	75.4	52.3	26.8	14.8	3.2	2.0	0.9	6.4
	9.0	75.9	57.9	21.9	15.7	2.2	1.8	0.5	6.3
	11.0	76.3	60.4	20.3	15.9	2.1	1.0	0.3	6.1

on H_2 yield and other product distributions from the steam reforming of PFAD at 1023 K. The degree of carbon deposition observed from the post-reaction oxidation measurements over spent catalysts from various conditions are also given in that table. It can be seen that H_2 and CO_2 increase with increasing H_2O content, whereas CO decreases; this could be mainly due to the contribution of the water gas shift reaction. In addition, the increase of CH_4 and decreases of C_2H_4, C_2H_6, and C_3H_6 with increasing inlet H_2O content could be due to the decomposition of high hydrocarbons to CH_4. As shown in Table 2, although the amount of carbon deposition was found to decrease with increasing H_2O content, significant amounts of carbon deposition remain observed.

Figs. 2–4 illustrate the influence of temperature on the steam reforming of PFAD over Rh/Al_2O_3, Rh/Ce–ZrO_2 and Rh/MgO–Al_2O_3. It can be seen that the activities of the catalyst significantly increased with increasing temperature, particularly for Rh/Ce–ZrO_2. Interestingly, at temperatures above 1173 K, the H_2 yield from the steam reforming over Rh/Ce–ZrO_2 with Ce/Zr ratio of 3/1 (Fig. 4(c)) becomes higher than those observed over Rh/Ce–ZrO_2 with Ce/Zr ratios of 1/1 and 1/3 (Fig. 4(a) and (b)). In addition, its reactivity is also greater than those observed from Rh/MgO–Al_2O_3 and Rh/Al_2O_3. At 1223 K, the main products from the steam reforming over Rh/Ce–ZrO_2 with Ce/Zr ratio of 3/1 were H_2, CO, CO_2, and CH_4, with insignificant amounts of C_2H_4. The absolute amounts of H_2 generated from Rh/MgO–Al_2O_3, Rh/Al_2O_3, Rh/Ce–ZrO_2 (Ce/Zr of 1/3), Rh/Ce–ZrO_2 (Ce/Zr of 1/1) and Rh/Ce–ZrO_2 (Ce/Zr of 3/1) were 6.32, 5.63, 6.09, 6.01, and 6.79 mmol/Rh, respectively. It is noted from our experiments that some deviations on H_2 yield and product selectivities with time were observed at the low operating temperature range. According to the post-reaction oxidation measurements (as presented in Table 3), this is due to the formation of carbon species on the surface of catalysts. The post-reaction oxidation experiments also indicated the greater resistance toward carbon deposition for Rh/Ce–ZrO_2 compare to the other two catalysts at high temperature.

The greater reforming reactivity with improvement in resistance toward carbon deposition for Rh/Ce–ZrO_2 at high temperature could be due to the gas–solid reactions between the

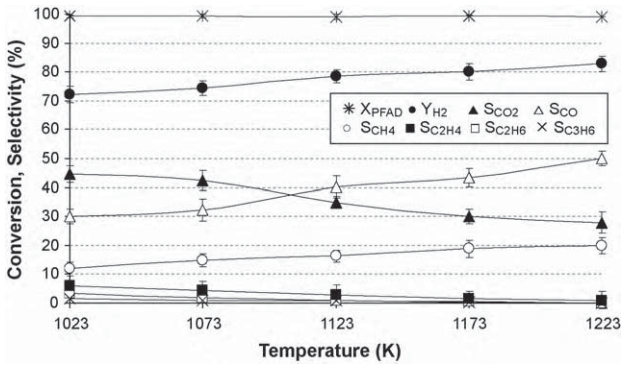

Fig. 2. Effect of temperature on product distributions from the steam reforming of PFAD over Rh/MgO–Al_2O_3 (with inlet steam/carbon molar ratio of 3.0).

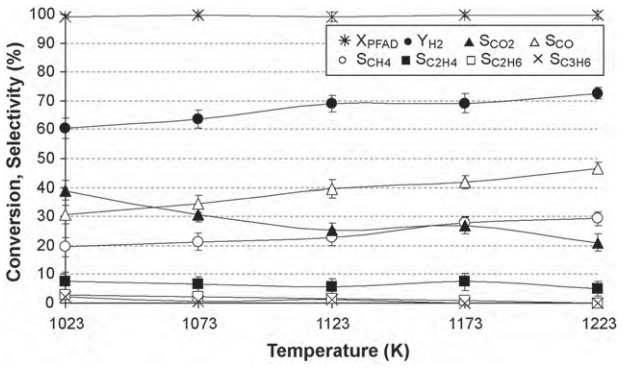

Fig. 3. Effect of temperature on product distributions from the steam reforming of PFAD over Rh/Al_2O_3 (with inlet steam/carbon molar ratio of 3.0).

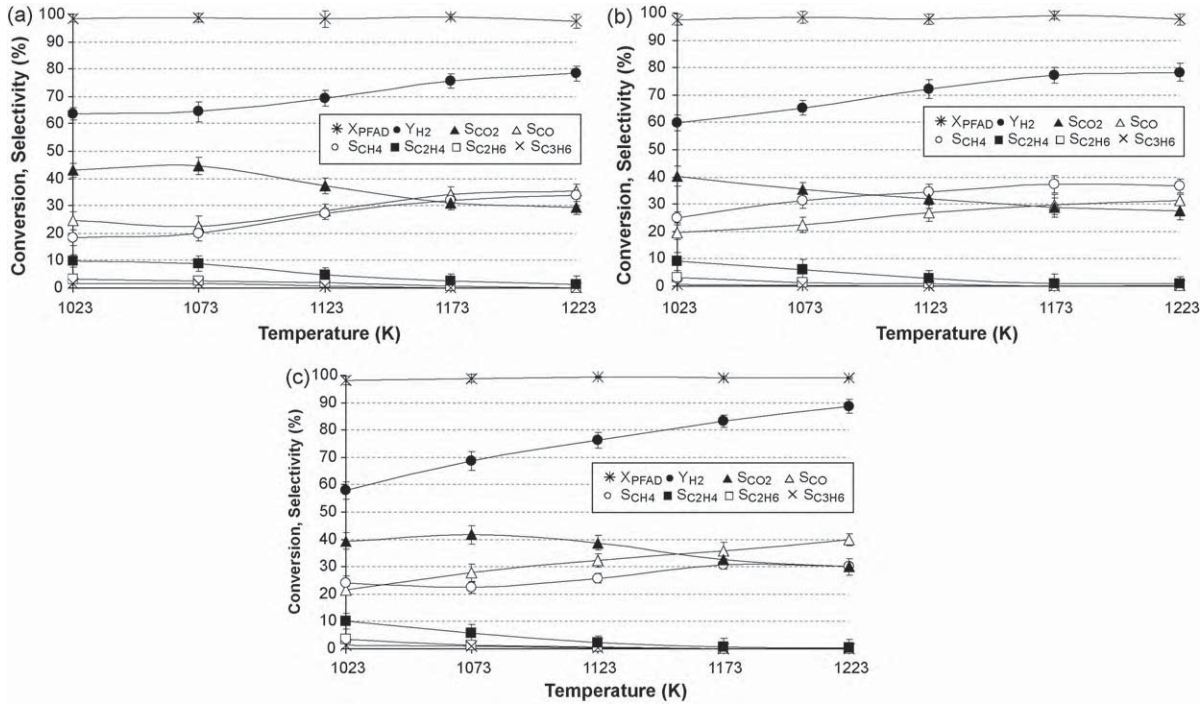

Fig. 4. Effect of temperature on product distributions from the steam reforming of PFAD with inlet steam/carbon molar ratio of 3.0 over (a) Rh/Ce–ZrO_2 (Ce/Zr = 1/3), (b) Rh/Ce–ZrO_2 (Ce/Zr = 1/1) and (c) Rh/Ce–ZrO_2 (Ce/Zr = 3/1).

hydrocarbons present in the system with the lattice oxygen (O_O^x) at Ce–ZrO_2 surface, since we previously reported the redox reactivity of CeO_2 and Ce–ZrO_2 toward steam reforming of PFAD at this range of temperature [34]. Apart from the reactions taking place on the active sites of Rh, the redox reactions between gaseous hydrocarbons (e.g. CH_4, C_2H_4, C_2H_6, and C_3H_6) with the lattice oxygen (O_O^x) can occur as illustrated below:

C_nH_m adsorption

$$C_nH_m + (n+m)* \rightarrow (CH_x*) + (H*) \rightarrow n(C*) + m(H*) \quad (18)$$

Co-reactant (H_2O) adsorption

$$H_2O + 2* \Leftrightarrow OH* + H* \quad (19)$$

$$OH* + * \Leftrightarrow H* + O* \quad (20)$$

Redox reactions of lattice oxygen (O_O^x) with C and O**

$$C* + O_O{}^x \rightarrow CO* + V_o{}^{\bullet\bullet} + 2e' \quad (21)$$

$$V_o{}^{\bullet\bullet} + 2e' + O* \Leftrightarrow O_O{}^x + * \quad (22)$$

Desorption of products (CO and H_2)

$$CO* \Leftrightarrow CO + * \quad (23)$$

$$2(H*) \Leftrightarrow H_2 + 2* \quad (24)$$

In the Kroger–Vink notation, $V_o^{\bullet\bullet}$ means an oxygen vacancy with an effective charge 2^+, and e′ is an electron which can either be more or less localized on a cerium ion or delocalized in a conduction band. * is a surface active site of ceria-based materials. During the reactions, gaseous hydrocarbons (C_nH_m) adsorbed on * forming intermediate surface hydrocarbon species (CH_x*) and later reacted with the lattice oxygen (O_O^x) (Eq. (21)). The steady state reforming rate is due to the continuous supply of the oxygen source by H_2O (Eqs. (19) and (20)) that reacted with the reduced-state catalyst to recover O_O^x (Eq. (22)); this fast step maintains O_O^x essentially unreduced by adsorbed intermediate surface hydrocarbons. It should be noted that the measured value of the oxygen diffusion coefficient for ceria is high and the reaction rate is controlled by a surface reaction, not by diffusion of oxygen from the bulk of the solid particles to ceria surfaces [35].

When Rh/Ce–ZrO_2 was used as a catalyst, in addition to the reactions on Rh surface, C_2H_4, C_2H_6, and C_3H_6 formations and

Table 3
Effect of temperature on the degree of carbon formation after exposure in steam reforming of PFAD for 48 h.

Catalyst	Temperature (K)	Carbon formation (mmol g_{cat}^{-1})
Rh/Ce–ZrO_2 (Ce/Zr = 3/1)	1023	10.0
	1073	8.2
	1123	7.5
	1173	5.4
	1223	4.8
Rh/Ce–ZrO_2 (Ce/Zr = 1/1)	1023	10.2
	1073	8.5
	1123	7.6
	1173	6.5
	1223	5.2
Rh/Ce–ZrO_2 (Ce/Zr = 1/3)	1023	9.5
	1073	8.1
	1123	7.3
	1173	6.9
	1223	6.4
Rh/Al_2O_3	1023	10.4
	1073	9.5
	1123	8.6
	1173	7.8
	1223	7.1
Rh/MgO–Al_2O_3	1023	7.1
	1073	6.7
	1123	6.0
	1173	5.3
	1223	5.1

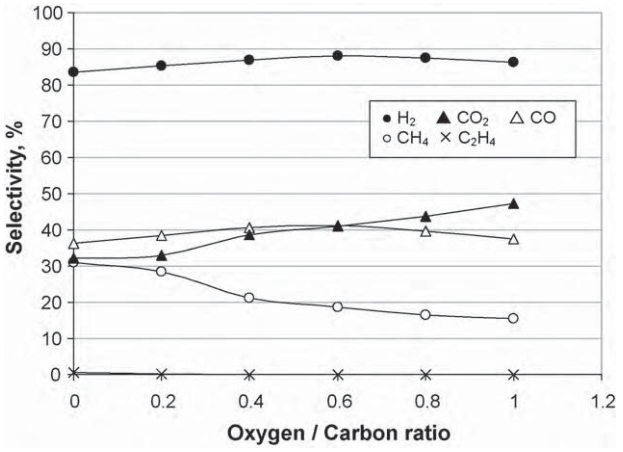

Fig. 5. Effect of inlet O_2/carbon molar ratio on product distributions from the steam reforming of PFAD at 1173 K over Rh/Ce–ZrO_2 (Ce/Zr = 3/1).

the possible carbon depositions from these hydrocarbons could be inhibited by the gas–solid reactions between these hydrocarbons and O_O^x at Ce–ZrO_2 surface forming H_2 and CO_2, which are thermodynamically unfavored to form carbon species. O_O^x can then be regenerated by reaction with oxygen containing compounds (H_2O) present in the system. The higher reactivity and greater resistance toward carbon deposition for Rh/Ce–ZrO_2 with Ce/Zr ratio of 3/1 compared to Rh/Ce–ZrO_2 with other Ce/Zr ratios could be due to the higher oxygen storage capacity (OSC) of Ce/ZrO_2 with Ce/Zr of 3/1 compared to 1/1 and 1/3. This explanation was proven by the testing of OSC over Rh/Ce–ZrO_2. After treatment, the degree of OSC for Rh/Ce–ZrO_2 with different Ce/Zr ratios were determined by the temperature-programmed reduction (TPR), which was performed by heating the catalysts up to 1273 K in 5%H_2 in He. The amount of H_2 uptake is correlated to the amount of oxygen stored in the catalysts. It was observed that the amount of H_2 uptake over Rh/Ce–ZrO_2 with Ce/Zr of 3/1 is significantly higher than that observed over Rh/Ce–ZrO_2 with Ce/Zr ratios of 1/1 and 1/3 (5065 μmol g_{cat}^{-1} compared to 3482 and 2543 μmol g_{cat}^{-1}, respectively); this indicated the highest OSC for this catalyst.

3.3. Reactivity toward reforming of PFAD with co-fed oxygen

Rh/Ce–ZrO_2 with Ce/Zr ratios of 3/1 was selected for further studies by adding O_2 together with PFAD and H_2O as an autothermal reforming operation. The inlet H_2O/carbon molar ratio was kept constant at 3, while the inlet O_2/carbon molar ratios were varied from 0.2, 0.4, 0.6, 0.8, to 1.0. The effect of O_2 concentration on the product composition at 1173 K is shown in Fig. 5. It can be seen that the main products are similar to these of the steam reforming (e.g., H_2, CO, CO_2, and CH_4); nevertheless, at suitable O_2/carbon molar ratios, higher H_2, CO, and CO_2 were observed from the autothermal reforming, whereas less CH_4, C_2H_6, C_2H_4, and C_3H_6 were found compared to the steam reforming at the same operating conditions. Importantly, the dependences of O_2 on H_2 yield are non-monotonic. H_2 increased with increasing O_2/carbon molar ratio until the ratio reached 0.6; then, oxygen presented a negative effect on H_2 production at higher inlet O_2/carbon molar ratio values. The post-reaction oxidation measurements were then carried out to determine the degree of carbon formation on catalyst surfaces. The TPO results in Table 4 show that significantly lower qualities of carbon deposited were observed at high O_2/carbon molar ratios.

By addition of O_2 along with PFAD and H_2O, the partial oxidation of fatty acids takes place and fatty acids are converted to CH_4 and CO. Thus, the rate of fatty acid decomposition reduces and less C_2H_6, C_2H_4, and C_3H_6 are generated, which consequently results

Table 4
Effect of inlet oxygen/carbon molar ratio on the degrees of carbon formation and metal reducibility after exposure in steam reforming of PFAD at 1173 K for 48 h.

Catalyst	Oxygen/carbon molar ratio	Carbon formation (mmol g_{cat}^{-1})	Metal reducibility (%)
Rh/Ce–ZrO_2 (Ce/Zr = 3/1)	0.0	5.4	92.0
	0.2	5.1	91.7
	0.4	4.7	91.8
	0.6	4.1	91.4
	0.8	3.6	90.1
	1.0	3.5	89.7

in the lower degree of carbon deposition on the surface of catalyst. In addition, O_2 also prevents the formation of carbon species via the hydrocarbon depositions by oxidizing these hydrocarbons to gaseous elements that are unfavored to form carbon species. In addition, for the catalyst over ceria-based supports, the presence of oxygen also helps steam to regenerate the lattice oxygen (O_O^x) on Ce–ZrO_2 surface ($0.5O_2 + V_O^{\bullet\bullet} + 2\ e' \rightarrow O_O^x$), which eventually help promoting the reforming reactivity of Ce–ZrO_2. Nevertheless, regarding the temperature-programmed reduction (TPR) experiments over the spent catalysts after exposure in autothermal reforming condition, the addition of too much O_2 (higher than 0.8) results in the oxidation of Rh to RhO as shown in the last column of Table 4, which could consequently reduce the catalyst reactivity for the long term operating. In addition, the decrease of H_2 yield at inlet O_2/carbon molar ratio above 0.6 could also be due to the combustion of H_2 with excess O_2 to form H_2O. Therefore, the inlet O_2/carbon molar ratio of 0.6 is the optimum ratio, it provides the highest resistance toward carbon deposition and is able to operate without the possible oxidation of Rh.

3.4. Reactivity toward reforming of PFAD with co-fed hydrogen

As another alternative procedure, H_2 was added as co-feeding along with PFAD and H_2O at the feed. The inlet H_2O/carbon molar ratio was kept constant at 3.0, while the inlet H_2/carbon molar ratios were varied from 0.5 to 5.0. Since H_2 was also added at the feed, the effect of this component on the catalyst performance was investigated in term of other product distributions (CO, CO_2, CH_4 and C_2H_4). Fig. 6 presents the product composition from the steam reforming of PFAD in the presence of various H_2 partial pressures over Rh/Ce–ZrO_2 at 1173 K. The productions of CH_4 and C_2H_4 clearly decrease with increasing H_2 content, which relates to the increase

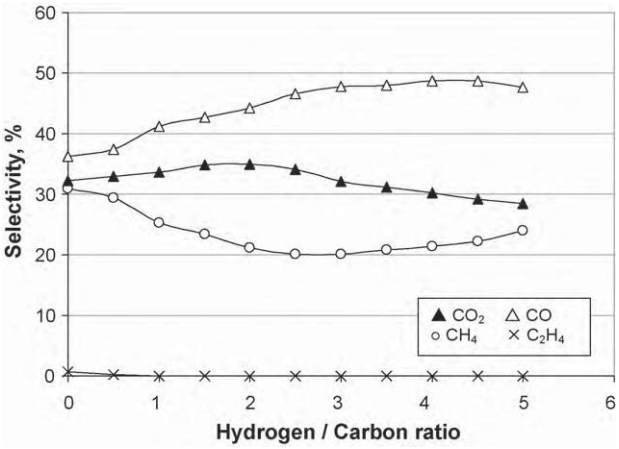

Fig. 6. Effect of inlet H_2/carbon molar ratio on CO, CO_2, CH_4, and C_2H_4 distributions from steam reforming of PFAD at 1173 K over Rh/Ce–ZrO_2 (Ce/Zr = 3/1).

in conversion of these hydrocarbons by addition of H_2. At higher H_2 content, the effect of this component becomes less pronounced and at inlet H_2/carbon ratio higher than 3.0, the presence of CH_4 slightly grows. The positive effect of H_2 on hydrocarbon conversions could be due to the reduction of oxidized state on the surface active site of Rh (*) by H_2 ($H_2 + O{-}^* \Leftrightarrow H_2O + {}^*$), whereas the increase in CH_4 at high H_2 appearance could be related to the promotion of methanation, reverse water–gas shift reactions and reverse methane steam reforming [36,37]. Furthermore, the occupying of H_2 atoms on some active sites of rhodium particles ($H_2 + 2^* \Leftrightarrow 2H{-}^*$) could also lead to the decrease in CH_4 conversion due to the catalyst active site competition, as explained by Xu and Froment [36,37]. It should be noted, in addition, that for the catalyst supported by Ce–ZrO_2 the increase in CH_4 production at high H_2 partial pressure could also be due to the reduction of O_O^x by H_2 (Eqs. (25) and (26)), which consequently inhibits the reaction of O_O^x with surface hydrocarbon species (Eq. (13)).

$$H_2 + 2* \Leftrightarrow H* + H* \quad (25)$$

$$H* + {O_O}^x \Leftrightarrow OH* + {V_o}^{\bullet\bullet} + 2e' \quad (26)$$

The post-reaction TPO were also carried out to determine the degree of carbon formation. In the presence of H_2, lower amounts of carbon deposited were observed on the surfaces of catalyst (decreased from 5.4 to 4.3 mmol g_{cat}^{-1} in the presence of 5 kPa H_2), which could possibly be due to the hydrogenation reactions.

4. Conclusion

The steam reformings of palm fatty acid distillate (PFAD) over Rh on MgO–Al_2O_3, Al_2O_3, and Ce–ZrO_2 (with Ce/Zr ratios of 3/1, 1/1, and 1/3) supports were studied. At 1023 K, the steam reforming of PFAD over Rh/MgO–Al_2O_3 showed good reforming performance in terms of H_2 yield and the resistance toward carbon deposition. Nevertheless, at temperatures above 1173 K, the steam reforming performance over Rh/Ce–ZrO_2 with Ce/Zr ratio of 3/1 becomes greater due to the gas–solid reactions between hydrocarbons present in the system with lattice oxygen (O_O^x) at Ce–ZrO_2 surface simultaneously with the reactions taking place on the active sites of Rh. The additions of O_2 and H_2 significantly reduced the degree of carbon deposition from the steam reforming of PFAD over Rh/Ce–ZrO_2. The presence of both reactants also promoted the conversion of hydrocarbons to CO and H_2. Nevertheless, the major consideration is the suitable co-fed reactant/PFAD ratio since the presence of too high O_2 or H_2 concentration could result in a lower reforming reactivity. From our work, the optimum O_2/carbon and H_2/carbon ratios are 0.6 and 3.0, respectively.

Acknowledgements

The financial support from The Thailand Research Fund (TRF) and National Metal and Materials Technology Center (MTEC) throughout this project is gratefully acknowledged.

References

[1] R. George, Fuel Cell Handbook, sixth edition, EG&G Technical Services, Inc., Science Applications International Corp., Under Contract No. DE-AM-26-99FT40575, U.S. Dept. of Energy, Office of Fossil Energy, National Energy Technology Laboratory, Morgantown, W. Virginia, 2002.
[2] A.C. Basagiannis, X.E. Verykios, Appl. Catal. A: Gen. 308 (2006) 182–193.
[3] J.R. Galdámez, L. García, R. Bilbao, Energy Fuels 19 (2005) 1133–1142.
[4] S. Czernik, R.J. French, K.A. Magrini-Bair, E. Chornet, Energy Fuels 18 (2004) 1738–1743.
[5] D. Wang, S. Czernik, D. Montané, M. Mann, E. Chornet, Ind. Eng. Chem. Res. 36 (1997) 1507–1518.
[6] D. Wang, D. Montané, E. Chornet, Appl. A: Gen. 143 (1996) 245–270.
[7] K. Polychronopoulou, C.N. Costa, A.M. Efstathiou, Appl. Catal. A: Gen. 272 (2004) 37–52.
[8] K. Takanabe, K. Aika, K. Seshan, L. Lefferts, J. Catal. 227 (2004) 101–108.
[9] A.N. Fatsikostas, D.I. Kondarides, X.E. Verykios, Catal. Today 75 (2002) 145–155.
[10] D.K. Liguras, D.I. Kondarides, X.E. Verykios, Appl. Catal. B: Environ. 43 (2003) 345–354.
[11] A.C. Basagiannis, X.E. Verykios, Appl. Catal. B: Environ. 82 (2008) 77–88.
[12] A.C. Basagiannis, X.E. Verykios, Int. J. Hydrogen Energy 32 (2007) 3343–3355.
[13] T. Davidian, N. Guilhaume, C. Daniel, C. Mirodatos, Appl. Catal. A: Gen. 335 (2008) 64–73.
[14] X. Wang, R.J. Gorte, Appl. Catal. A: Gen. 224 (2002) 209–218.
[15] M. Mamak, N. Coombs, G. Ozin, Adv. Mater. 12 (2000) 198–202.
[16] M. Mamak, N. Coombs, G. Ozin, J. Am. Chem. Soc. 122 (2000) 8932–8939.
[17] M. Mamak, N. Coombs, G.A. Ozin, Chem. Mater. 13 (2001) 3564–3570.
[18] P. Bera, S. Mitra, S. Sampath, M.S. Hegde, Chem. Commun. (2001) 927–928.
[19] A. Martinez-Arias, J.M. Coronado, R. Cataluna, J.C. Conesa, J.C. Soria, J. Phys. Chem. B 102 (1998) 4357–4365.
[20] D. Skarmoutsos, F. Tietz, P. Nikolopoulos, Fuel Cells 1 (2001) 243–248.
[21] T. Takeguchi, S.N. Furukawa, M. Inoue, J. Catal. 202 (2001) 14–24.
[22] J. Sfeir, P.A. Philippe, P. Moseki, N. Xanthopoulos, R. Vasquez, J.M. Hans, V.H. Jan, K.R. Thampi, J. Catal. 202 (2001) 229–244.
[23] N. Laosiripojana, S. Assabumrungrat, Appl. Catal. A: Gen. 290 (2005) 200–211.
[24] N. Laosiripojana, S. Assabumrungrat, Appl. Catal. B: Environ. 60 (2005) 107–116.
[25] S. Naito, H. Tanaka, S. Kado, T. Miyao, S. Naito, K. Okumura, K. Kunimori, K. Tomishige, J. Catal. 259 (2008) 138–146.
[26] T. Miyazawa, T. Kimura, J. Nishikawa, K. Kunimori, K. Tomishige, Sci. Tech. Adv. Mater. 6 (2005) 604–614.
[27] B. Li, K. Maruyama, M. Nurunnabi, K. Kunimori, K. Tomishige, Appl. Catal. A: Gen. 275 (2004) 157–172.
[28] A. Bitsch-Larsen, R. Horn, L.D. Schmidt, Appl. Catal. A: Gen. 348 (2008) 165–172.
[29] R. Horn, K.A. Williams, N.J. Degenstein, L.D. Schmidt, J. Catal. 242 (2006) 92–102.
[30] B.J. Dreyer, I.C. Lee, J.J. Krummenacher, L.D. Schmidt, Appl. Catal. A: Gen. 307 (2006) 184–194.
[31] J.R. Salge, G.A. Deluga, L.D. Schmidt, J. Catal. 235 (2005) 69–78.
[32] Y. Lwin, W.R.W. Daud, A.B. Mohamad, Z. Yaakob, Int. J. Hydrogen Energy 25 (1) (2000) 47–53.
[33] J.N. Amor, Appl. Catal. A: Gen. 176 (1999) 159–176.
[34] A. Shotipruk, S. Assabumrungrat, P. Pavasant, N. Laosiripojana, Chem. Eng. Sci. 64 (2009) 459–466.
[35] B.C.H. Steele, J.M. Floyd, Proc. Br. Ceram. Soc. 19 (1971) 55–76.
[36] J. Xu, G.F. Froment, AIChE 35 (1989) 88–96.
[37] J. Xu, G.F. Froment, AIChE 35 (1989) 97–103.

Applied Catalysis A: General 386 (2010) 194–200

Contents lists available at ScienceDirect

Applied Catalysis A: General

journal homepage: www.elsevier.com/locate/apcata

Catalytic H_2O and CO_2 reforming of CH_4 over perovskite-based $La_{0.8}Sr_{0.2}Cr_{0.9}Ni_{0.1}O_3$: Effects of pre-treatment and co-reactant/CH_4 on its reforming characteristics

C. Chettapongsaphan [a,b], S. Charojrochkul [b], S. Assabumrungrat [c], N. Laosiripojana [a,*]

[a] The Joint Graduate School of Energy and Environment, CHE Center for Energy Technology and Environment, King Mongkut's University of Technology, Thonburi, Thailand
[b] National Metal and Materials Technology Center (MTEC), Pathumthani, Thailand
[c] Department of Chemical Engineering, Faculty of Engineering, Chulalongkorn University, Thailand

ARTICLE INFO

Article history:
Received 4 March 2010
Received in revised form 24 July 2010
Accepted 29 July 2010
Available online 6 August 2010

Keywords:
Perovskite
Reforming
Hydrogen
SOFC

ABSTRACT

The H_2O and CO_2 reformings of CH_4 over perovskite-based $La_{0.8}Sr_{0.2}Cr_{0.9}Ni_{0.1}O_3$ prepared by precipitation, sol–gel and surfactant-assisted methods (calcined with air, nitrogen and hydrogen) were studied under solid oxide fuel cell (SOFC) conditions. It was found that the catalyst prepared by the surfactant-assisted method and calcined with hydrogen provided the highest specific surface area and reforming reactivity. Under typical conditions (H_2O/CH_4 and CO_2/CH_4 of 1.0), the reforming reactivity of $La_{0.8}Sr_{0.2}Cr_{0.9}Ni_{0.1}O_3$ was comparable to that of Ni/Al_2O_3 but relatively less than that of precious-metal Rh/Al_2O_3. Nevertheless, at specific condition (H_2O/CH_4 and CO_2/CH_4 of 0.5–0.7), its activity dramatically increased to the same level as that of Rh/Al_2O_3.

According to the study on the kinetic dependencies of $La_{0.8}Sr_{0.2}Cr_{0.9}Ni_{0.1}O_3$, the reforming rate was proportional to CH_4 partial pressure with the reaction order increased from 0.50 (at co-reactant/CH_4 ratio of 1.0–3.0) to 0.95 (at co-reactant/CH_4 ratio of 0.5). In addition, the rate was inhibited by H_2 addition at high inlet co-reactant/CH_4 ratio; however the inhibitory effect becomes less pronounced at an inlet co-reactant/CH_4 ratio less than 0.7. It is suggested that one of two reforming mechanisms occurred depending on the operating conditions applied. $La_{0.8}Sr_{0.2}Cr_{0.9}Ni_{0.1}O_3$ behaves like an oxide-based catalyst at high co-reactant/CH_4 ratio, whereas it tends to behave more like a metallic-based catalyst at low co-reactant/CH_4 ratios resulting in the high reforming reactivity. The study has shown that high surface area perovskite-based $La_{0.8}Sr_{0.2}Cr_{0.9}Ni_{0.1}O_3$ catalyst has great potential to be applied as a steam reforming catalyst since it requires low inlet steam content, which provides significant benefits in terms of minimizing the water management in reformer and SOFC systems.

1. Introduction

Hydrogen is widely regarded as a promising energy carrier for fuel cells to generate energy with significant improvements in air quality, human health, and climate [1]. It can be readily produced from the reforming of hydrocarbons with oxygen-containing co-reactants [2,3]. Metallic catalysts, e.g. Ni, Rh, and Pd are known to be active for these reactions, but catalyst deactivation due to carbon formation is a major concern; research is therefore continuing to develop catalysts with high resistance toward carbon formation. Recently, there has been an interest in the use of perovskite-based material with the general formula of ABO_3 as an alternative reforming catalyst for hydrogen production and fuel cell technologies [4–8].

Perovskite materials with La at the A-site and a first-row transition metal at the B-site, i.e. Cr, Ti, Fe, or Co promise good reforming reaction in terms of their high resistance toward carbon formation [9,10]. Among them, $LaCrO_3$-based perovskite material has been widely investigated for solid oxide fuel cell (SOFC) applications, i.e. as an anode component and as an internal reforming catalyst (IR-SOFC). Nevertheless, it is well known that pure lanthanum chromite shows a decrease in mechanical strength under reducing conditions as well as phase segregation in the microstructure due to the evaporation of gaseous CrO_3 from $LaCrO_3$ particles at high temperature [9]; the partial substitution of Cr on the B-site by Ni (Cr/Ni of 0.9/0.1) has been reported to improve the structural stability without a significant decrease in its catalytic reactivity [11]. Furthermore, the partial substitution of the A-site cation with alkaline earths (i.e. Sr and Ca) has been found to increase the catalytic reactivity of $LaCrO_3$-based perovskite material due to the stabilizing of the B-site cation as well as the introducing of structural defects, e.g. oxygen vacancies [11]. Focusing on the reaction

* Corresponding author. Tel.: +66 2 872 9014; fax: +66 2 872 6736.
E-mail address: navadol_l@jgsee.kmutt.ac.th (N. Laosiripojana).

0926-860X/$ – see front matter © 2010 Elsevier B.V. All rights reserved.
doi:10.1016/j.apcata.2010.07.053

pathway of methane steam reforming and cracking over $LaCrO_3$-based perovskite materials, the reaction with dry methane over $La_{0.8}Ca_{0.2}CrO_3$ was reported to have two pathways depending on the operating temperature [12]. At intermediate temperatures, the complete oxidation reaction occurred, as the lattice oxygen was unlikely to be mobile over this temperature range; hence, methane reacted with surface oxygen and produced CO_2 and H_2O as the main products with only small amounts of H_2 and CO. At high temperature, methane dissociation occurred, as the lattice oxygen was likely to be mobile over this temperature range; therefore, methane adsorbed on to the oxide surface and formed unsaturated carbon and monatomic hydrogen. Some carbon then oxidized to produce CO, while monatomic hydrogen combined rapidly to form H_2. The main products in this temperature range were then CO, and H_2. Importantly, the addition of steam along with methane as methane steam reforming can give good recovery of the oxide surface of $LaCrO_3$-based perovskite material. It has also been reported that carbon is mainly deposited on the catalyst surface due to methane dissociation. Baker and Metcalfe [13] investigated the carbon formation rate of $La_{0.8}Ca_{0.2}CrO_3$ compared to a Ni-YSZ cermet. They reported that the carbon formation rate over Ni-YSZ cermet was much higher than that over $La_{0.8}Ca_{0.2}CrO_3$ at the same operating conditions; furthermore, by adding steam at the feed, no carbon formation was detected on $La_{0.8}Ca_{0.2}CrO_3$, when 3% water was added together with 5% methane feed [13]. The methane steam reforming activities of $La_{0.8}Sr_{0.2}Cr_{0.97}V_{0.03}O_3$, $La_{0.8}Sr_{0.2}Cr_{0.8}Mn_{0.2}O_3$, and $La_{0.8}Sr_{0.2}Cr_{0.8}Fe_{0.2}O_3$ were investigated with respect to potential SOFC application [14]. It was reported that $La_{0.8}Sr_{0.2}Cr_{0.8}Fe_{0.2}O_3$ cannot be used as the anode material in SOFC due to its high methane cracking activity. $La_{0.8}Sr_{0.2}Cr_{0.97}V_{0.03}O_3$ exhibited effective electrochemical oxidation of hydrogen at this temperature, while $La_{0.8}Sr_{0.2}Cr_{0.8}Mn_{0.2}O_3$ gave similar electrochemical behavior to nickel without any carbon formation at 800 °C.

The present work focuses on the synthesis and testing of $La_{0.8}Sr_{0.2}Cr_{0.9}Ni_{0.1}O_3$ with respect to the steam and dry (CO_2) reforming of methane at various operating conditions for possible application in IR-SOFC. Although $LaCrO_3$-based perovskite materials have great potential to be used as the reforming catalyst for IR-SOFC, the main weaknesses of this material are its low specific surface area and high thermal sintering when operated under SOFC stack conditions. This work proposes that the use of a high surface area material would be an effective alternative method to minimize the sintering impact and consequently improve the stability and reactivity toward the reforming reaction. Several preparation procedures (i.e. precipitation, sol–gel and surfactant-assisted methods) were applied under various pre-treatment techniques (i.e. calcined under air, nitrogen and hydrogen). The activity toward the steam and dry reforming of methane over these synthesized materials were studied at various methane/oxidant molar ratios and operating temperature in order to determine the suitable operating conditions; furthermore, the resistance toward carbon formation of these materials was also studied. The reforming reactivities of these perovskite-based catalysts were compared to those of the metallic-based Ni/Al_2O_3 and precious-metal-based Rh/Al_2O_3 catalysts.

2. Experimental

2.1. Catalyst preparation and characterization

$La_{0.8}Sr_{0.2}Cr_{0.9}Ni_{0.1}O_3$ was prepared by three different techniques: i.e. precipitation method, sol–gel method and surfactant-assisted method. For the precipitation method, the starting solution was prepared by mixing 0.1 M of all nitrate precursors (La, Sr, Cr and Ni; from Aldrich) with 0.4 M of ammonium hydroxide at a 2:1 volumetric ratio. This solution was stirred by using a magnetic stirrer (100 rpm) for 3 h, then sealed and placed in a thermostatic bath maintained at 90 °C for 3 days. The resultant precipitate was filtered and washed with deionized water and acetone to remove the free surfactant. It was dried overnight in an oven at 110 °C, and then calcined at 900 °C for 6 h. Three different atmospheres were used during calcination, i.e. under airflow, nitrogen flow and hydrogen (10% balance in helium) flow.

For the surfactant-assisted method, according to work by Terribile et al. [15], $La_{0.8}Sr_{0.2}Cr_{0.9}Ni_{0.1}O_3$ was prepared by adding an aqueous solution of the appropriate cationic surfactant, 0.1 M cetyltrimethylammonium bromide ($C_{17}H_{42}BrN$) solution from Aldrich, to a 0.1 M cerium chloride. The molar ratio of [La + Sr + Cr + Ni]/[cetyltrimethylammonium bromide] was kept constant at 0.8. The mixture was stirred and then ammonium hydroxide was slowly added with vigorous stirring until the pH was 11.5 [15]. The mixture was continually stirred for 3 h, then sealed and placed in a thermostatic bath maintained at 90 °C for 3 days. After that, the mixture was cooled and the resulting precipitate was filtered and washed repeatedly with water and acetone. The filtered powder was then treated under the same procedures as those used in the precipitation method. Lastly, for the sol–gel method, the procedure of Bilger et al. [16] was followed, in which all nitrate precursors were mixed with excess methanol (corresponding to CH_3OH/(La + Sr + Cr + Ni) ratio of 150). After complete dissolution, the mixture was refluxed for 30 min at the boiling point of the solvent (65 °C) to give a dark green alcoholic solution. The exothermic precipitation of solid methoxide occurred by adding ammonium hydroxide to pH ≥11. Then the precipitate was washed to remove NO_3-free by methanol. The blue-gray methoxide residue was hydrolyzed in deionized water and peptized by adding nitric acid to stabilize the sol. Then it was dried and calcined at the same conditions as those for the precipitation method. $LaCrO_3$ with non-partial substitution was also prepared by the surfactant-assisted method for comparison. After preparation, measurements of BET surface area, cumulative pore volume and average pore diameter for all calcined powders were performed by the N_2 physisorption technique using Micromeritics ASAP 2020 surface area and porosity analyzer, while the XRD patterns of these powders were determined by an X-ray diffractometer.

For comparison, Ni/Al_2O_3 and Rh/Al_2O_3 (5 wt% Ni and Rh) were also prepared by wet impregnation of α-Al_2O_3 with $NiCl_3$ and $RhCl_3$ (from Aldrich). Both catalysts were ultimately treated and evacuated in H_2 at 700 °C before characterization and subsequent reaction. In this work, the weight contents of Ni and Rh loadings were confirmed by X-ray fluorescence (XRF) analysis, while the dispersion percentages were measured by the volumetric H_2 chemisorption measurement after reduction and evacuation. According to these measurements, the % Ni and Rh loadings were approximately 5.0 (±0.2) and the % metal dispersion for Ni/Al_2O_3 was 28.5% whereas that for Rh/Al_2O_3 was 31.8%.

2.2. Testing of catalytic steam and dry reforming of methane

To perform catalytic testing, we constructed an experimental reactor system as shown elsewhere [17]. The feed gases including the components of interest, i.e. CH_4, deionized H_2O (injected via a syringe pump), CO_2, and H_2 were introduced to the reaction section, in which a 10-mm diameter quartz reactor was mounted vertically inside a tubular furnace. The catalysts (50 mg) were diluted with SiC (to obtain the total weight of 500 mg) in order to avoid temperature gradients and then loaded in the quartz reactor, which was packed with quartz wool to prevent the catalyst moving. In the system, a type-K thermocouple was placed into the annular space between the reactor and the furnace. This thermocouple was mounted in close contact with the catalyst bed to give a measurement of tem-

perature as accurate as possible. Another type-K thermocouple, covering by a closed-end quartz tube, was inserted in the middle of the quartz reactor in order to re-check the possible temperature gradient. The record showed that the maximum temperature fluctuation during the reaction was always ±0.75 K or less from the temperature specified for the reaction.

The steam and dry reforming of methane were studied over wide ranges of temperature (850–1000 °C) and reactant partial pressures (H_2O/CH_4 and CO_2/CH_4 of 0.3–3.0; with inlet CH_4 partial pressure between 0.01 and 0.04 atm). After the reactions, the exit gas mixture was transferred via trace-heated lines (100 °C) to the analysis section, which consists of a Porapak Q column Shimadzu 14B gas chromatograph (GC) and a mass spectrometer (MS). The GC was applied for the steady state studies, whereas the MS, in which the sampling of the exit gas was done by a quartz capillary and differential pumping was used for the transient experiments. In the present work, the outlet of the GC column was directly connected to a thermal conductivity detector (TCD) and a frame ionization detector (FID). In order to satisfactorily separate all elements, the temperature setting inside the GC column was programmed to vary with time. In the first 3 min, the column temperature was constant at 60 °C; it was then increased steadily by the rate of 15 °C min^{-1} until 120 °C and finally decreased to 60 °C.

2.3. Measurement of carbon formation

After reaction, the temperature programmed technique (TP) was applied to study the resistance toward carbon formation. The temperature programmed oxidation (TPO) was carried out by introducing 10% oxygen in helium with a total flow rate of 100 cm^3 min^{-1} into the system, after purging with helium for 1 h. The temperature was increased from room temperature to 900 °C at the rate of 10 °C min^{-1}. The amounts of carbon formation on the surface of catalysts were determined by measuring the CO and CO_2 yields from the TPO results. In addition, the amount of carbon deposition was confirmed by calculating the carbon balance of the system. The amount of carbon deposited on the surface of catalyst would theoretically be equal to the difference between the inlet carbon containing components (CH_4, and CO_2) and the outlet carbon containing components (CO, CH_4, and CO_2).

3. Results and discussion

The steam and dry reforming of methane in the presence of several catalysts were studied under various operating conditions. In the present work, the synthesized $La_{0.8}Sr_{0.2}Cr_{0.9}Ni_{0.1}O_3$ and $LaCrO_3$ were denoted as LSCN and LC. The catalysts (e.g. LSCN) synthesized by precipitation, sol–gel and surfactant-assisted methods were represented as LSCN-PP, LSCN-SG, and LSCN-SF. Lastly, the catalysts (e.g. LSCN-SF) calcined under air, nitrogen and hydrogen atmospheres were symbolized as LCSN-SF-A, LCSN-SF-N and LCSN-SF-H, respectively.

3.1. Preliminary testing

Prior to the experimental studies, same preliminary tests were carried out to determine the suitable conditions in which internal and external mass transfer effects are not predominant. Considering the effect of external mass transfer, we varied the total gas flow rate under a constant residence time of 5×10^{-4} g min cm^{-3}. The CH_4 reaction rate was independent of the gas velocity when the gas flow rate was higher than 60 cm^3 min^{-1}, indicating the absence of external mass transfer effects at this high velocity. The reactions on different average sizes of catalysts were also carried out to confirm that the experiments were carried out within the region of intrinsic kinetics. It was observed that the catalysts with a particle size less than 200 μm showed no intraparticle diffusion limitation in the range of conditions studied. Hence, in all studies, the total flow rate was kept constant at 100 cm^3 min^{-1}, whereas the catalyst diameters were kept below 200 μm.

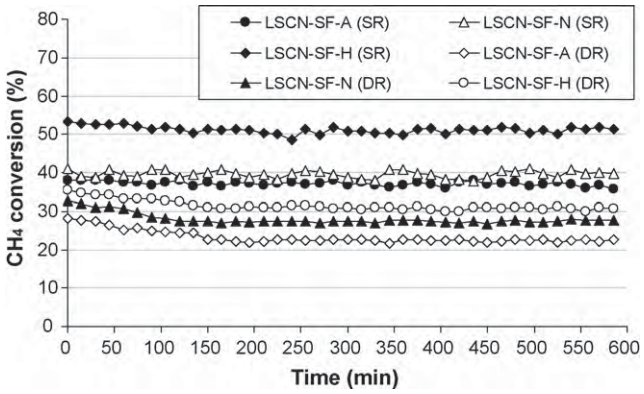

Fig. 1. Variation of CH_4 conversion with time (for 10 h) from the steam reforming (SR) and dry reforming (DR) of CH_4 over $La_{0.8}Sr_{0.2}Cr_{0.9}Ni_{0.1}O_3$ (prepared by the surfactant-assisted method and calcined in air, nitrogen or hydrogen) at 900 °C with H_2O/CH_4 and CO_2/CH_4 molar ratio of 1.0/1.0.

3.2. Reactivity toward steam and dry reforming of methane

All synthesized materials were studied in the steam and dry reforming of methane at 900 °C with H_2O/CH_4 and CO_2/CH_4 molar ratio of 1.0/1.0 as the base condition. It was found that the main products from both reactions were H_2 and CO with some CO_2 formation for steam reforming and some H_2O formation for dry reforming, indicating the influences of water-gas shift and reverse water-gas shift reactions, respectively. Based on the measured concentrations of reactants and products during the reforming, the approach to water-gas shift equilibrium condition (η_{WGS}) in the range of temperature studied (850–1000 °C) is always close to 1.0 in all types of catalysts; this indicated that the water-gas shift (WGS) reaction is at equilibrium.

Within 10 h of operation, all materials exhibited high stability with slight deactivation in methane conversion (the deactivations from the steam reforming testing are in the range of 3.2–6.7%, whereas those from the dry reforming testing are in between 13.1% and 19.2%). Fig. 1 shows the example for the variation of CH_4 conversion with time from the steam and dry reforming of CH_4 over $La_{0.8}Sr_{0.2}Cr_{0.9}Ni_{0.1}O_3$ prepared by the surfactant-assisted method and calcined in air, nitrogen and hydrogen; high stabilities toward the reactions are clearly observed. After exposure in the reaction for 10 h, Fig. 2 presents the methane conversion from the steam and dry reforming of methane over all synthesized catalysts. Among all catalysts, $La_{0.8}Sr_{0.2}Cr_{0.9}Ni_{0.1}O_3$ prepared by surfactant-assisted method and calcined under hydrogen flow (LSCN-SF-H) gave the highest methane conversion for both reactions; furthermore, it can be seen that the methane conversions from the steam reforming reaction are relatively higher than those from the dry reforming reaction for all catalysts. In this study, the H_2/CO production ratios from methane steam reforming were in the ranges of 3.8–4.7 (4.2–4.7 for the perovskite catalysts and 3.8–4.0 for the Rh- and Ni-based catalysts), whereas those from the dry reforming were in the ranges of 0.77–0.92 (0.77–0.83 for the perovskite catalysts and 0.89–0.92 for the Rh- and Ni-based catalysts). According to the BET measurement, also shown in Fig. 2, it can be seen that the perovskite catalysts calcined under hydrogen flow present significantly higher specific surface areas than those calcined under nitrogen and air flows. Insignificant changes in BET surface area were observed from all perovskite catalysts after exposure in the reforming condition

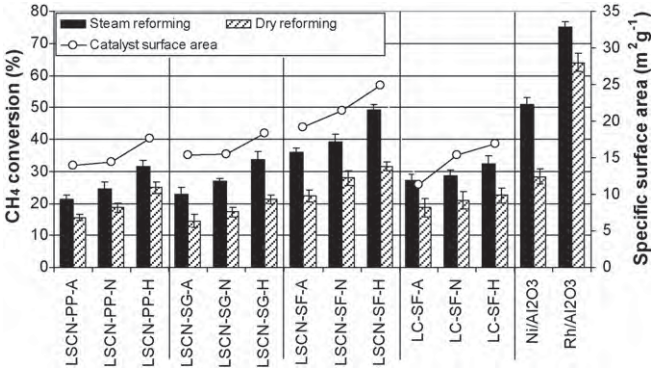

Fig. 2. Relation between specific surface area of synthesized catalysts and their reactivities toward H_2O and CO_2 reforming of CH_4 (at 900 °C with H_2O/CH_4 and CO_2/CH_4 molar ratio of 1.0/1.0).

for 10 h (the surface area reducing percentages are in the range of 3.6–4.3%); this indicates the high resistance toward the thermal sintering of these synthesized materials. Importantly, it can be noticed from Fig. 2 that the reforming reactivities of these perovskite catalysts are linearly related to their specific surface area; this highlights the importance of the catalyst calcination condition on its catalytic reactivity. When compared to the reactivity toward steam and dry reforming of methane over metallic-based Ni/Al_2O_3 and Rh/Al_2O_3 catalysts, the reactivity of LSCN-SF-H is comparable to that of Ni/Al_2O_3 (51.2% methane conversion) but still relatively less than that of Rh/Al_2O_3 (75.7% methane conversion).

After being purged with helium, the post-reaction TPO experiments were carried out over all spent catalysts. As presented in Table 1, the experiment always detected higher amounts of carbon deposition on the surface of catalysts from the dry reforming compared to the steam reforming; this is the reason for the relatively low methane conversion values observed from the dry reforming testing compared to the steam reforming testing with the same catalysts (as shown in Fig. 2). Furthermore, between perovskite and metallic catalysts, less carbon was found on the surface of perovskite materials (between 0.22 and 0.31 mmol g_{cat}^{-1} for the steam reforming and between 0.38 and 0.51 mmol g_{cat}^{-1} for the dry reforming) compared to the values on Ni/Al_2O_3 (0.83 mmol g_{cat}^{-1} for the steam reforming and 2.17 mmol g_{cat}^{-1} for the dry reforming); these results are in good agreement with other work which also indicated the better resistance of perovskite materials toward carbon formation compared to conventional metallic-based catalysts [9,10]. The amounts of carbon deposited were confirmed by the calculations of carbon balance. Regarding the calculation, the moles of carbon remaining in the system (as also given in Table 1) are in good agreement with the values observed from the TPO studies.

3.3. Effect of inlet H_2O and CO_2 contents

The steam and dry reforming at various inlet H_2O/CH_4 and CO_2/CH_4 ratios (from 0.3 to 0.5, 0.7, 1.0, 2.0, and 3.0) were then studied for all perovskite materials at the operating temperatures of 850–950 °C. It can be seen from Fig. 3(a) and (b) that the methane conversion is strongly affected by the concentration of co-reactants (i.e. H_2O and CO_2). At inlet H_2O/CH_4 and CO_2/CH_4 ratios of 0.3, the conversions were relatively low for both reactions. Nevertheless, when the inlet H_2O/CH_4 and CO_2/CH_4 ratios were raised to 0.3–0.5, methane conversions dramatically increased, particularly for the steam reforming. The maximum methane conversion of 77.3% was obtained from the steam reforming over LSCN-SF-H; this

Table 1
CH_4 conversion, H_2/CO production ratio and amount of carbon formation from H_2O and CO_2 reforming of CH_4 over synthesized catalysts (after exposure for 10 h).

Catalyst	Reaction	CH_4 conversion (%)	H_2/CO ratio	Carbon formation (mmol g^{-1})
LSCN-PP-A	SR	21.2 ± 1.4	4.2	0.24[a] (0.25)[b]
	DR	15.6 ± 0.9	0.83	0.40 (0.38)
LSCN-PP-N	SR	24.5 ± 2.3	4.4	0.25 (0.25)
	DR	18.7 ± 1.5	0.81	0.41 (0.43)
LSCN-PP-H	SR	31.6 ± 1.9	4.5	0.23 (0.22)
	DR	24.9 ± 1.9	0.79	0.39 (0.37)
LSCN-SG-A	SR	22.9 ± 2.1	4.3	0.24 (0.24)
	DR	14.5 ± 2.2	0.82	0.43 (0.44)
LSCN-SG-N	SR	26.9 ± 0.9	4.5	0.24 (0.27)
	DR	17.3 ± 1.6	0.82	0.41 (0.38)
LSCN-SG-H	SR	33.7 ± 2.5	4.5	0.22 (0.24)
	DR	21.2 ± 1.3	0.78	0.40 (0.41)
LSCN-SF-A	SR	35.8 ± 1.4	4.4	0.25 (0.22)
	DR	22.4 ± 1.9	0.79	0.39 (0.40)
LSCN-SF-N	SR	39.2 ± 2.3	4.6	0.22 (0.21)
	DR	27.9 ± 2.4	0.77	0.41 (0.41)
LSCN-SF-H	SR	49.3 ± 1.5	4.7	0.22 (0.23)
	DR	31.5 ± 1.3	0.77	0.38 (0.35)
LC-SF-A	SR	27.3 ± 1.8	4.2	0.31 (0.29)
	DR	18.7 ± 2.9	0.81	0.51 (0.51)
LC-SF-N	SR	28.7 ± 1.9	4.2	0.29 (0.27)
	DR	21.0 ± 2.7	0.81	0.49 (0.52)
LC-SF-H	SR	32.4 ± 2.3	4.3	0.28 (0.31)
	DR	22.5 ± 2.4	0.78	0.48 (0.47)
Ni/Al_2O_3	SR	51.1 ± 2.1	3.8	0.83 (0.82)
	DR	28.4 ± 2.4	0.92	2.17 (2.11)
Rh/Al_2O_3	SR	75.7 ± 1.6	4.0	0.29 (0.33)
	DR	64.0 ± 2.9	0.89	0.58 (0.62)

[a] Calculated form the TPO measurement.
[b] Calculated from the carbon balance.

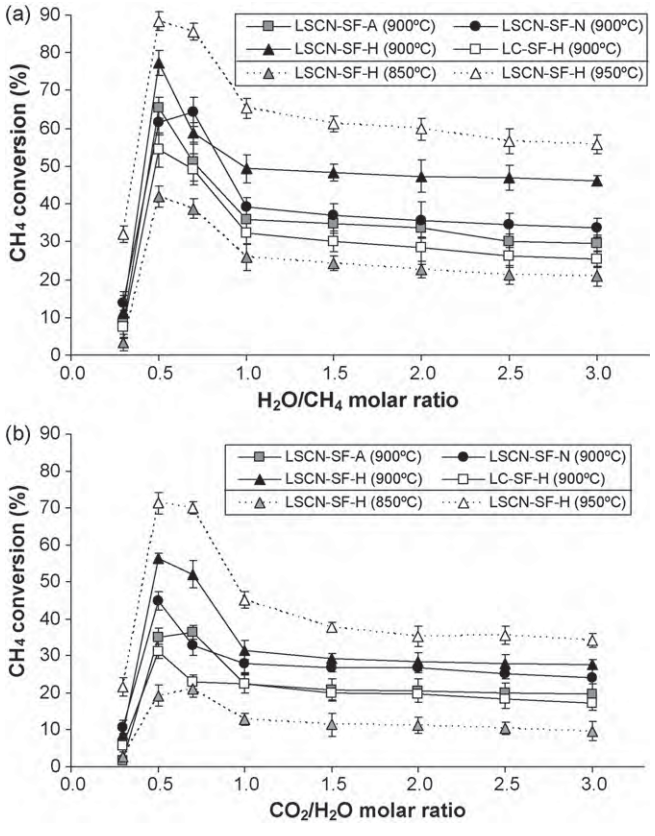

Fig. 3. Effect of inlet H_2O/CH_4 ratios (a) and CO_2/CH_4 ratios (b) on the CH_4 conversion from H_2O and CO_2 reforming over perovskite-based catalysts.

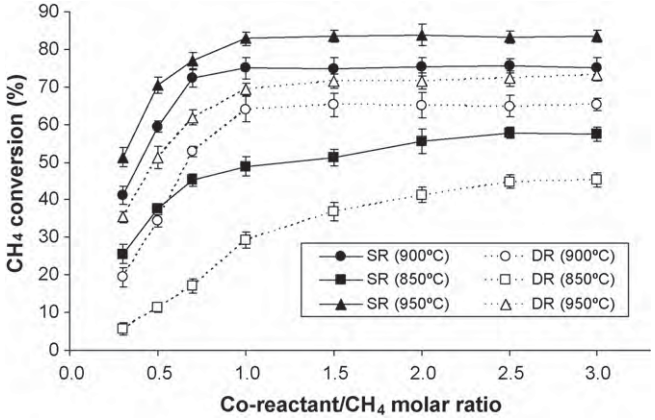

Fig. 4. Effect of inlet H_2O/CH_4 and CO_2/CH_4 ratios on the CH_4 conversion from H_2O and CO_2 reforming over Rh/Al_2O_3.

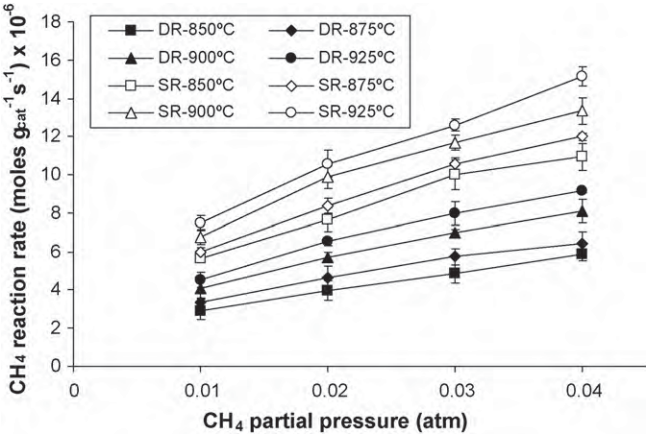

Fig. 5. Effect of CH_4 partial pressure on the reforming rate of LSCN-SF-H at 850–925 °C (with inlet H_2O/CH_4 and CO_2/CH_4 ratios constant at 1.0).

value is in the same range as that obtained from the steam reforming over precious-metal Rh/Al_2O_3 catalyst. At higher H_2O/CH_4 and CO_2/CH_4 ratios (from 0.5 to 1.0), the methane conversion considerably decreased; but beyond these ratios (from 2.0 to 3.0), the inlet H_2O and CO_2 contents showed insignificant effects on the methane conversion. The amounts of carbon formation from the reactions at various H_2O/CH_4 and CO_2/CH_4 ratios were also tested by TPO experiments. A noticeable amount of carbon was detected from the reactions at H_2O/CH_4 and CO_2/CH_4 ratios of 0.3 (0.72–0.76 and 1.32–1.44 mmol g^{-1}, respectively); this could be due to the occurrence of methane decomposition reaction, which leads to the loss of lattice oxygen from the surface of perovskite materials without the proper replacement via external oxygen-containing sources (i.e. H_2O and CO_2). Nevertheless, the amount of carbon formation could be rapidly reduced when only small contents of H_2O or CO_2 were added (0.27–0.31 and 0.41–0.49 mmol g^{-1} under the inlet H_2O/CH_4 and CO_2/CH_4 ratios of 0.5).

For comparison, the effects of H_2O and CO_2 contents on the reforming reactivity of Rh/Al_2O_3 were also carried out by varying H_2O/CH_4 and CO_2/CH_4 ratios from 0.3 to 3.0 (under the operating temperatures of 850–950 °C). As shown in Fig. 4, it was found that the methane conversions were considerably lower at H_2O/CH_4 and CO_2/CH_4 ratios less than 1.0 due to the carbon formation by the decomposition of methane. Nevertheless, at H_2O/CH_4 and CO_2/CH_4 ratios above 1.0, the methane conversions were relatively constant; this result is in good agreement with the work of Wei and Iglesia [18], who studied the kinetics of CH_4 reforming over Rh-based catalysts and also reported the independence of co-reactant (i.e. H_2O and CO_2) concentrations on the reforming rate. The different behavior between perovskite catalysts and metallic catalysts strongly indicates the difference in their reforming mechanisms. Therefore, the kinetic dependencies of selected perovskite material (LSCN-SF-H) were further studied and compared to those of Rh/Al_2O_3 in order to explain the reforming mechanism of perovskite-based $LaCrO_3$ material.

3.4. Kinetic dependencies of methane reforming over $La_{0.8}Sr_{0.2}Cr_{0.9}Ni_{0.1}O_3$

The kinetic dependencies of CH_4 reforming rates on the partial pressures of CH_4 were determined in the temperature range of 850–925 °C. All experiments were carried out under the operating conditions where the carbon formation is assumed negligible (by controlling H_2O/CH_4 and CO_2/CH_4 inlet ratios above 0.3) according to the results from Section 3.3. Fig. 5 shows the effect of CH_4 partial pressure on the reforming rate of LSCN-SF-H at several reaction temperatures (by keeping the inlet H_2O/CH_4 and CO_2/CH_4 ratios constant at 1.0). The reforming rate expressed in the figures is obtained from the relation between the measured net reaction rate (r_m; $mol_{CH4}\, g_{cat}^{-1}\, s^{-1}$) and the approach to equilibrium condition (η) using the following equation [18]:

$$r_t = r_m(1-\eta)^{-1} \quad (1)$$

where η is either the approach to equilibrium for steam reforming (η_s) or the approach to equilibrium for dry reforming (η_d). These parameters are determined from the following equations:

$$\eta_s = \frac{[P_{CO}][P_{H_2}]^3}{[P_{CH_4}][P_{H_2O}]}\frac{1}{K_s} \quad (2)$$

$$\eta_d = \frac{[P_{CO}]^2[P_{H_2}]^2}{[P_{CH_4}][P_{CO_2}]}\frac{1}{K_d} \quad (3)$$

where P_i is partial pressure of component i (atm); K_s and K_d are the equilibrium constants for H_2O and CO_2 reforming of CH_4 at a given temperature. It should be noted that, in the present work, the values of η were always kept below 0.2 in all experiments. It can be seen that the rate increased linearly with increasing CH_4 partial pressures and operating temperature for both reactions. The reaction order in CH_4 was determined by plotting $\ln(r_t)$ versus $\ln(P_{CH_4})$ (the effects of product concentrations are taken into account via the term equilibrium condition (η)). From the calculation, the values were positive fraction approximately 0.49 (±0.04) for both reactions, and seemed to be essentially independent of the operating temperature in the range of conditions studied.

As the next step, the reaction order in CH_4 at different inlet H_2O/CH_4 and CO_2/CH_4 ratios (0.5, 0.7, 2.0 and 3.0) was determined. It was found (as shown in Fig. 6) that the reaction order in CH_4 is 0.50 at co-reactant/CH_4 ratio of 1.0–3.0; nevertheless, it steadily increased with decreasing H_2O/CH_4 and CO_2/CH_4 ratios and was close to 0.98 (±0.02) at the H_2O/CH_4 and CO_2/CH_4 ratios of 0.5. For comparison, the same set of experiments was carried out over Rh/Al_2O_3. It was found that the turnover rate increased linearly with increasing CH_4 partial pressures and operating temperature for both reactions. In addition, the first-reaction order in CH_4, independent of the operating temperature and H_2O/CH_4 and CO_2/CH_4 ratios, was always observed (Fig. 7). This observation is in agreement with the literature [19–21], which generally reported the first-reaction order in CH_4 from the methane reforming over metallic-based catalysts and indicated that the sole kinetically relevant elementary step for the reaction is the adsorption of methane on catalyst active site.

For clearer understanding, the effects of H_2 addition on the steam and dry reforming over $La_{0.8}Sr_{0.2}Cr_{0.9}Ni_{0.1}O_3$ were also

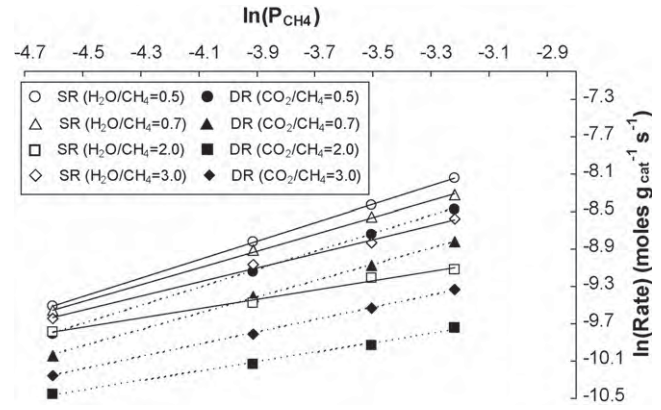

Fig. 6. Relation between ln(rate) and ln(P_{CH_4}) from H_2O and CO_2 reforming of CH_4 over LSCN-SF-H (at various inlet H_2O/CH_4 and CO_2/CH_4 ratios (0.5, 0.7, 2.0 and 3.0)).

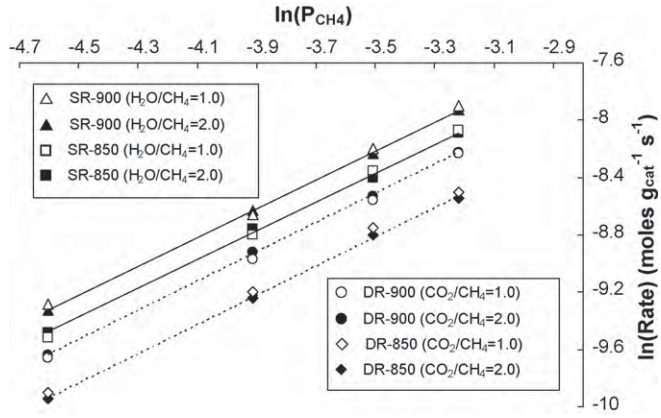

Fig. 7. Relation between ln(rate) and ln(P_{CH_4}) from H_2O and CO_2 reforming of CH_4 over Rh/Al_2O_3 (at various temperatures and inlet H_2O/CH_4 and CO_2/CH_4 ratios).

investigated (at several inlet H_2O/CH_4 and CO_2/CH_4 ratios). The results in Fig. 8 suggest that, at high inlet H_2O/CH_4 and CO_2/CH_4 ratios, the rate is significantly inhibited by H_2 addition. Nevertheless, at lower inlet H_2O/CH_4 and CO_2/CH_4 ratios, this inhibitory effect becomes less pronounced (the reaction order in H_2 changed from −0.35 (±0.04) to −0.05 (±0.01)) when the inlet H_2O/CH_4 and CO_2/CH_4 ratios decreased from 1.0 to 0.5. It is noted that the effect of H_2 addition was also performed over Rh/Al_2O_3 for comparison. By adding H_2 at the feed, it was found that the rates were not affected

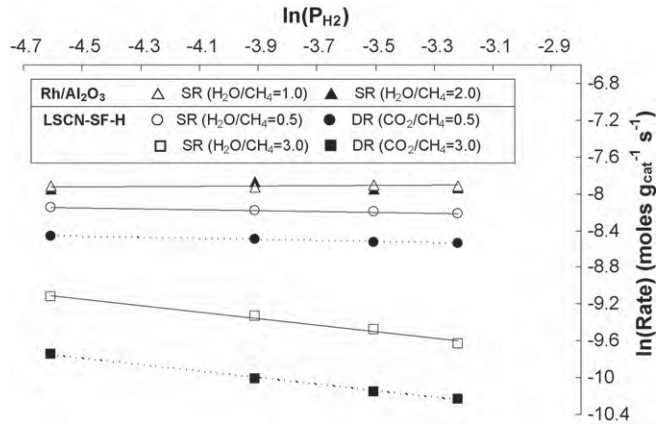

Fig. 8. Effect of H_2 adding on the reforming rate (in terms of ln(rate)) from H_2O and CO_2 reforming of CH_4 over LSCN-SF-H and Rh/Al_2O_3 (at various inlet H_2O/CH_4 and CO_2/CH_4 ratios).

by this component (Fig. 8); thus, the reaction order in H_2 was zero; this result is also in good agreement with the work by Wei and Iglesia [18], who reported the independence of H_2 addition on the reforming rate over Rh-based catalysts.

According to these observations, we suggested that there are two possible reforming mechanisms in the methane reforming over perovskite-based catalyst depending on the applied operating conditions. At the operating condition with high H_2O/CH_4 and CO_2/CH_4 ratios, the oxygen nonstoichiometry value (δ) of $La_{0.8}Sr_{0.2}Cr_{0.9}Ni_{0.1}O_{3-\delta}$ is theoretically close to 0 and the material behaves like oxide-based catalysts (e.g. ceria-based catalysts). We previously proposed the redox mechanism to explain the steam and dry reforming behaviors of ceria-based catalysts [17,22]. Our studies provided the evidence that the sole kinetically relevant elementary step is the reaction of intermediate surface hydrocarbon species with the lattice oxygen on the surface of catalyst; in addition, that oxygen is replenished by oxygen supply from either CO_2 or H_2O [17,22]. Furthermore, the negative effect of H_2 could be due to reactions between the adsorbed hydrogen (H^*) and the lattice oxygen, which consequently results in the inhibition of CH_4 conversion. On the other hand, at the operating condition with low H_2O/CH_4 and CO_2/CH_4 ratios, the δ value of $La_{0.8}Sr_{0.2}Cr_{0.9}Ni_{0.1}O_{3-\delta}$ increases and the material behaves more like the partly reduced metal-oxide catalysts; its high reforming reactivity comparable to the metallic-based Rh/Al_2O_3 under this reaction regime with the reaction order in CH_4 close to 1.0 and reaction order in H_2 close to 0.0 providing the practical evidence for this claim.

In summary, the present work suggests that high surface area perovskite-based $La_{0.8}Sr_{0.2}Cr_{0.9}Ni_{0.1}O_3$ catalyst (prepared by surfactant-assisted method and calcined under hydrogen flow) has good potential to be applied for steam and dry reforming reactions. Under specific operating conditions (low inlet H_2O/CH_4 and CO_2/CH_4 ratios), its catalytic reactivity is comparable to those of metallic-based catalysts but with greater resistance toward carbon formation. It is noted that the requirement of lower inlet steam content compared to metallic-based catalyst is a major benefit of this catalyst since concerns over water management in the system (e.g. reformer and fuel cell system) are minimal.

4. Conclusions

$La_{0.8}Sr_{0.2}Cr_{0.9}Ni_{0.1}O_3$ prepared by surfactant-assisted method and calcined with hydrogen was found to have high methane reforming reactivity with high resistance toward carbon formation. At low inlet H_2O/CH_4 and CO_2/CH_4 ratios, its reforming reactivity was as high as that of precious-metal Rh/Al_2O_3. According to the study on the kinetic dependencies of $La_{0.8}Sr_{0.2}Cr_{0.9}Ni_{0.1}O_3$, it is suggested that there are two possible reforming mechanisms depending on the applied operating conditions. At high co-reactant/CH_4 ratio, $La_{0.8}Sr_{0.2}Cr_{0.9}Ni_{0.1}O_3$ behaves like oxide-based catalysts providing relatively low reforming reactivity with positive fraction value of reaction order in CH_4 and negative value of reaction order in H_2. However, at low co-reactant/CH_4 ratio, it behaves more like metallic-based catalysts resulting in high reforming reactivity with almost first-reaction order in CH_4 and zero-reaction order in H_2.

Acknowledgements

The financial support from the Thailand Research Fund (TRF) and National Metal and Materials Technology Center (MTEC) throughout this project is gratefully acknowledged. The authors would like to acknowledge Dr. John T.H. Pearce for the English correction of this manuscript.

References

[1] M.Z. Jacobson, W.G. Colella, D.M. Golden, Science 308 (2005) 1901–1905.
[2] J.R. Rostrup-Nielsen, J. Sehested, J.K. Nørskov, Adv. Catal. 47 (2002) 65–139.
[3] J.R. Rostrup-Nielsen, T.S. Christensen, I. Dybkjaer, Stud. Surf. Sci. Catal. 113 (1998) 81–95.
[4] J. Sfeir, P.A. Buffat, P. Möckli, N. Xanthopoulos, R. Vasquez, H.J. Mathieu, J.V. Herle, K.R. Thampi, J. Catal. 202 (2001) 229–244.
[5] A.L. Sauvet, J.T.S. Irvine, Solid State Ionics 167 (2004) 1–8.
[6] J. Rynkowski, P. Samulkiewicz, A.K. Ladavos, P.J. Pomonis, Appl. Catal. A: Gen. 263 (2004) 1–9.
[7] M.R. Goldwasser, M.E. Rivas, M.L. Lugo, E. Pietri, J. Pérez-Zurita, M.L. Cubeiro, A. Griboval-Constant, G. Leclercq, Catal. Today 107/108 (2005) 106–113.
[8] G. Valderrama, M.R. Goldwasser, C.U. de Navarro, J.M. Tatibouët, J. Barrault, C. Batiot-Dupeyrat, F. Martínez, Catal. Today 107/108 (2005) 785–971.
[9] G. Pudmich, B.A. Boukamp, M. Gonzalez-Cuenca, W. Jungen, W. Zipprich, F. Tietz, Solid State Ionics 135 (2000) 433–438.
[10] J.R. Rostrup-Nielsen, J. Sehested, J.K. Nørskov, Adv. Catal. 47 (2002) 65–138.
[11] J.R. Mawdsley, T.R. Krause, Appl. Catal. A: Gen. 334 (2008) 311–320.
[12] R.T. Baker, I.S. Metcalfe, P.H. Middleton, B.C.H. Steele, Solid State Ionics 72 (1994) 328–333.
[13] R.T. Baker, I.S. Metcalfe, Appl. Catal. A: Gen. 126 (1995) 297–317.
[14] P. Vernoux, J. Guindet, E. Gehain, in: P. Stevens (Ed.), Proceedings of the Third European Solid Oxide Fuel Cell Forum, Nantes, France, 1998, p. 237.
[15] D. Terribile, A. Trovarelli, J. Llorca, C. Leitenburg, G. Dolcetti, Catal. Today 43 (1998) 79–88.
[16] S. Bilger, G. Blaß, R. Förthmann, J. Eur. Ceram. Soc. 17 (1997) 1027–1031.
[17] N. Laosiripojana, S. Assabumrungrat, Appl. Catal. B: Environ. 60 (2005) 107–116.
[18] J. Wei, E. Iglesia, J. Catal. 225 (2004) 116–127.
[19] A.L. Dicks, K.D. Pointon, A. Siddle, J. Power Sources 86 (2000) 523–530.
[20] J. Xu, G.F. Froment, AIChE J. 35 (1989) 88–96.
[21] S.S.E.H. Elnashaie, A.M. Adris, A.S. Al-Ubaid, M.A. Soliman, Chem. Eng. Sci. 45 (1990) 491–501.
[22] N. Laosiripojana, S. Assabumrungrat, Appl. Catal. B: Environ. 82 (2008) 103–113.

Bioresource Technology 101 (2010) 4179–4186

Contents lists available at ScienceDirect

Bioresource Technology

journal homepage: www.elsevier.com/locate/biortech

Catalytic conversion of sugarcane bagasse, rice husk and corncob in the presence of TiO_2, ZrO_2 and mixed-oxide TiO_2–ZrO_2 under hot compressed water (HCW) condition

A. Chareonlimkun [a], V. Champreda [b], A. Shotipruk [c], N. Laosiripojana [a,*]

[a] The Joint Graduate School of Energy and Environment, King Mongkut's University of Technology Thonburi, Thailand
[b] National Center for Genetic Engineering and Biotechnology (BIOTEC), Pathumthani, Thailand
[c] Department of Chemical Engineering, Faculty of Engineering, Chulalongkorn University, Thailand

ARTICLE INFO

Article history:
Received 23 October 2009
Received in revised form 5 January 2010
Accepted 10 January 2010

Keywords:
Lignocellulosic biomass
Furfural
TiO_2–ZrO_2
Hot compressed water

ABSTRACT

The simultaneous hydrolysis/dehydration reaction of sugarcane bagasse, rice husk and corncob was studied under hot compressed water in the presence of TiO_2, ZrO_2 and TiO_2–ZrO_2 at 473–673 K. Among them, the reaction of corncob at 573 K in the presence of TiO_2–ZrO_2 produced the highest furfural and 5-hydroxymethylfurfural (HMF) yields (10.3% and 8.6%) with less by-products (i.e. glucose, fructose, xylose, and 1,6-anhydroglucose) selectivities. It was found that the catalyst preparation procedure and calcination temperature strongly affected its reactivity. Catalysts prepared by (co-) precipitation method gained higher reactivity than those prepared by sol–gel and physical mixing methods. The suitable calcination temperature for TiO_2 and ZrO_2 was at 773 K, whereas that for TiO_2–ZrO_2 was at 873 K; the XRD patterns revealed that different portions of phase formation were observed over catalysts with different calcination temperature. The portion of these phase formations affected the acidity–basicity of catalyst and thus the catalyst reactivity.

1. Introduction

Currently, fuel shortage is one of the global concern due to the continue rising of world energy demand, particularly in the industry and transportation sections, while the energy sources have been depleting. Therefore, research on the development of alternative fuels to replace conventional fuels is being interested. Lignocellulosic biomass (e.g. rice husk, rice straw, corncob, coconut shell, palm shell, cassava pulp and sugarcane bagasse) has been considering a potent alternative energy resource in the near future, particularly for agricultural countries. With advances in chemical engineering and biotechnologies, several processes have been established to convert these feedstocks to energy. Among them, the conversion of biomass to alkane-based liquid fuel (as called biomass-to-liquid or BTL) is one of the promising technologies to replace the conventional oil in transportation section. Currently, the typical process for BTL production is the gasification following by Fischer–Tropsch process. Nevertheless, this technology is feasible economically only for large scale application and the cost of synthesized alkane-based liquid fuel form this technology remains relatively high.

Recently, Huber et al. (2005) reported a novel low cost process to convert sugar-based compounds to C_7–C_{15} alkane-based fuel by acid-catalyzed dehydration, followed by aldol condensation and hydrogenation over solid base catalysts. The important primary step in their process is the conversion of sugar-based compounds to furfural and 5-hydroxymethylfurfural (HMF) via dehydration reaction; in which these intermediates are later converted to alkane-based fuel via aldol condensation and hydrogenation reactions in the presences of acetone and hydrogen. It is well known that furfural and HMF are valuable and promising compounds for several chemical and petrochemical processes. Apart from the use as intermediate in the above process, these compounds have also been widely utilized as chemical intermediate and solvent (due to its solubility in ethanol, ether and water) and as sustainable substitutes for petroleum-based building blocks used in production of fine chemicals and plastics (Weil et al., 2002). Hence, the production of HMF and furfural (particularly from renewable sources) is currently of great interest for research and application. Previously, there are several research and development on the production of these compounds from sugar- or carbohydrate-based feedstocks via acid hydrolysis (Laopaiboon et al., 2010; Yat et al., 2008; Karimi et al., 2006; Bower et al., 2008) and hot compressed water (HCW), subcritical water and supercritical water technologies (Watanabe et al., 2005a,b; Asghari and Yoshida, 2006; Bicker

* Corresponding author. Tel.: +66 2 872 9014; fax: +66 2 872 6736.
E-mail address: navadol_l@jgsee.kmutt.ac.th (N. Laosiripojana).

0960-8524/$ - see front matter © 2010 Elsevier Ltd. All rights reserved.
doi:10.1016/j.biortech.2010.01.037

et al., 2003; Aida et al., 2007; Yang and Montgomery, 1996; Kabyemela et al., 1997; Moreau et al., 2000; Sasaki et al., 2002). Watanabe et al. (2005a) studied the hydrolysis of glucose in HCW in the presence of H_2SO_4 and NaOH solutions as catalysts; they reported the beneficial of these homogeneous catalysts on glucose reactions that the acid-catalysts i.e. H_2SO_4 promoted the formation of HMF via dehydration reaction while base catalyst i.e. NaOH endorsed the isomerization of glucose to fructose. Asghari and Yoshida (2006) studied acid-catalyzed production of HMF from D-fructose in subcritical water condition; they found that, in the presence of H_3PO_4, the excellent HMF production yield can be achieved. Although it is clear that the additional of homogeneous acid-catalysts e.g. H_2SO_4 and H_3PO_4 can promote the dehydration reaction, the typical limitation for homogeneous catalyzed reactions is the difficulty for catalyst recovery and treatment, which causes large amount of wastewater and increase the overall cost of the process. As an alternative procedure, heterogeneous catalyst has widely been reported to overcome these problems due to its easily separate and recover from the process. Recently, a few literatures have proposed the use of heterogeneous acid-based catalysts for dehydration reaction e.g. Watanabe et al. (2005b) studied dehydration of glucose in the presence of solid TiO_2 and ZrO_2 and indicated that ZrO_2 catalyzed the isomerization reaction, whereas anatase TiO_2 promoted both dehydration and isomerization reactions. They also proposed that catalytic activity of each reaction strongly depends on the acidity and basicity of catalysts.

Considering lignocellulosic biomass, the typical biomass composes mainly of cellulose, hemicellulose, and lignin with various ratios depended on the source of biomass; the first two compositions (i.e. cellulose and hemicellulose) can be converted to sugar- and furan-based compounds by hydrolysis reaction under various conditions (Karimi et al., 2006; Sasaki et al., 2008; Ando et al., 2004; Minowa and Inoue, 1999; Cheng et al., 2008; Sun and Cheng, 2002; Thomsen et al., 2008; Zhang and Zhao, 2010; Vázquez et al., 2007). In detail, Karimi et al. (2006) studied the hydrolysis of rice straw to sugars in the presence of H_2SO_4, whereas Sasaki et al. (2008) investigated the cellulose hydrolysis in subcritical and supercritical water at 563–673 K and 25 MPa. In addition, Ando et al. (2004) studied decomposition behavior of several biomasses in HCW conditions and found that hemicelluloses started to decompose at the temperature above 453 K, while cellulose decomposed above 503 K; they also reported that most lignin could be extracted by HCW at low temperature and flowed out with the decomposed products of hemicellulose. Furthermore, (Minowa and Inoue, 1999) studied the cellulose decomposition under HCW condition in the presence of alkali and nickel catalysts; and revealed that alkali inhibits the char formation, while nickel catalyzes the steam reforming and methanation reactions of aqueous intermediate products.

In the present work, we aimed at the coupling of hydrolysis and dehydration reactions to produce HMF and furfural from three promising lignocellulosic biomasses (i.e. sugarcane bagasse, rice husk and corncob) in a single unit for later utilization as intermediate compounds for alkane-based fuel production. The HCW operation in the presence of several heterogeneous catalysts i.e. TiO_2, ZrO_2 and mixed-oxide TiO_2–ZrO_2 (with three different Ti/Zr ratios i.e. 3/1, 1/1, and 1/3 and three different calcination temperatures i.e. 773, 873 and 973 K) was applied. The impact of these catalysts on the hydrolysis and dehydration of selected biomasses were compared at various operating conditions to determine the suitable catalyst system for enhancing maximum yield of HMF and furfural productions. It is noted that the effect of catalyst preparation methods i.e. sol–gel, (co-) precipitation and physical mixing (for TiO_2–ZrO_2) on the catalytic reactivity was also studied since several reports indicated the significant impact of catalyst preparation method on its catalytic reactivity. Lastly the physical characteristics of these synthesized catalysts, i.e. acidity–basicity properties, phase formation and catalyst surface properties were also carried out in order to relate these properties with the preparation method and catalytic performance.

2. Methods

2.1. Material

Sugarcane bagasse, rice husk and corncob were used as the samples of lignocellulosic biomasses in the present work. The percentages of cellulose, hemicellulose, and lignin for these samples are 0.44:0.29:0.20, 0.28:0.28:0.24, and 0.50:0.31:0.15. Before undergoes the reaction testing, these feedstocks were ground with a ball-milling to become fine particle with the average particle size of 75 μm. It should be noted that the reactions of sugar (i.e. glucose and xylose), cellulose, and xylan (representative for hemicellulose) were also carried out. These materials were supplied from Aldrich and Ajax Finechem.

2.2. Catalyst preparation and characterization

In the present work, zirconia (ZrO_2) and titania (TiO_2) were synthesized by precipitation and sol–gel methods. For the precipitation method, a solution of either zirconium or titanium salt precursors (i.e. zirconyl chloride ($ZrOCl_2$) and titanium chloride ($TiCl_4$) (0.15 M)) was slowly dropped into a well-stirred precipitating solution of ammonium hydroxide (NH_4OH) (2.5 wt.%) at room temperature. The solution was controlled at pH of 11. The obtained precipitate was removed, and then washed with deionized water until Cl^- was not detected by a silver nitrate ($AgNO_3$) solution. Then, the solid sample was dried overnight at 383 K and calcined at various temperatures (i.e. 773, 873 and 973 K) under continuous air flow for 6 h with a temperature ramping rate of 10 K min^{-1}. For sol–gel method, titanium-tetra-isopropoxide (TTIP) and zirconium (IV) isopropoxide isopropanol (supplied from Aldrich) were applied as the starting precursors. They were dissolved in 2-propanol with the molecular ratio of 1:40 and stirred for 15 min. The reaction was then maintained at pH 2 for 30 min by adding HNO_3. After that, the solution was kept at ambient temperature until become gel then it was dried at 373 K for 12 h and calcined at 773, 873 and 973 K for 6 h.

As for TiO_2–ZrO_2, this catalyst (with Ti/Zr molar ratios of 1/3, 1/1, and 3/1) was prepared by co-precipitation (using $ZrOCl_2$ and $TiCl_4$ as salt precursors), sol–gel (using titanium-tetra-isopropoxide and zirconium (IV) isopropoxide isopropanol as precursors), and physical mixing of TiO_2 and ZrO_2 (obtained from precipitation method). After similar treatment to ZrO_2 and TiO_2, several characterizations i.e. BET, XRD and TPD were performed over all synthesized catalysts. BET measurements was carried out by N_2 physisorption technique using Micromeritics ASAP 2020 surface area and porosity analyzer to determine the specific surface area, cumulative pore volume and average pore diameter of material. The X-ray diffraction (XRD) patterns of powder were analyzed by X-ray diffractometer, in which the crystallite size was estimated from line broadening according to the Scherrer equation. Temperature-programmed desorption techniques with ammonia and carbon dioxide (NH_3- and CO_2-TPD) were applied to determine the acid–base properties of catalysts. In detail, TPD experiments were carried out using a flow apparatus; the catalyst sample (0.1 g) was treated at 773 K in helium for 1 h and then saturated with 15% NH_3/He mixture or pure CO_2 flow after cooling to 373 K. After purging with helium, the sample was heated to 923 K under helium and the amount of acid–base sites on the catalyst surface

was calculated from the desorption amount of NH_3 and CO_2, which was determined by measuring the areas of the desorption profiles obtained from the Chemisorption System analyzer.

2.3. Reaction testing

In the present work, the reaction was carried out in a 0.5 in. diameter stainless steel reactor placing vertically inside tubular furnace. Nitrogen was used to purge and increase the pressure of the reactor. For the base condition, 0.1 g of sample was mixed with 1 cm^3 of water (with and without the presence of 0.1 g catalyst) and N_2 was loaded to raise the reactor pressure up before placing the reactor in the furnace. In our system, a Type-K thermocouple was placed into the annular space between the reactor and furnace with close contact to the catalyst bed to minimize the temperature difference between the furnace temperature and reaction temperature). The reaction temperature was varied from 473 to 523, 573, 623, and 673 K, while the pressure inside the reactor, measured by a pressure transducer (Kyowa, PGM-500 KD) connected to the reactor, was kept constant at 34.5 MPa in all experiments. Under these operating conditions, water was in the state of liquid phase. After the reaction time was reached, the reactor was quenched in a water bath to stop the reaction.

2.4. Product analysis

The quantification and identification of gaseous products were conducted by Gas Chromatography (Shimadzu GC-14B with Porapak Q column) connected with a thermal conductivity detector (TCD) and a frame ionization detector (FID). In order to satisfactorily separate all elements, the temperature setting inside the GC column was programmed varying with time. In the first 3 min, the column temperature was constant at 333 K, it was then increased steadily by the rate of 15 K min^{-1} until 393 K and lastly decreased to 333 K. The quantification and identification of liquid products were conducted by High Performance Liquid Chromatography (Summit, Dionex Co., Germany) in which consist of a Dionex PDA-100 photodiode array detector, a Dionex P680 pump system, a Dionex STH585 column oven and a Dionex ASI-100 automated sample injector equipped with a Shodex RSpak KC-811 (8.0 mmID $*$ 300 mm) column. The injection volume was 20 μl and the concentrations of HMF and furfural were analyzed based on UV absorbance at 280 nm by comparing to the corresponding standard curves. It is noted that H_3PO_4 was used as the eluent with the flow rate of 0.4 cm^3 min^{-1}.

It is noted that, according to the measurement of total carbon amount in the water solution after reaction, the TOC (total organic carbon) values for all experiments were always higher than 90% indicated that the quantity of gaseous products from the reactions were considerably less than that of liquid products. Hence, we here reported the results and discussion only for the liquid products from the reactions. In this study, we focus on the hydrolysis and dehydration reactions with the possible side reaction of isomerization; therefore, the possible product species i.e. glucose, fructose, xylose, furfural, HMF and 1,6-anhydroglucose (AHG) were quantified. The yield of each product was calculated by the carbon balance, defined as the ratios of the amount of carbon atom in the specified product to the amount of carbon atom in the loaded feedstock.

3. Results and discussion

The reactions of sugarcane bagasse, cellulose, hemicellulose, C_5 and C_6-based sugars in the presence of various catalysts i.e. TiO_2, ZrO_2 and TiO_2–ZrO_2 prepared by various methods and treated under different conditions were studied. The synthesized TiO_2, ZrO_2 and TiO_2–ZrO_2 by (co-) precipitation, sol–gel, and physical mixing were denoted as Ti–P, Ti–S, Zr–P, Zr–S, TiZr–P, TiZr–S and TiZr–M. The catalysts calcined at different temperatures (i.e. 773, 873 and 973 K) were denoted as Ti–P-773, Ti–P-873 and Ti–P-973 (which means TiO_2 prepared by precipitation method and calcined at 773, 873 and 973 K, respectively).

3.1. Lignocellulosic biomass reactions under HCW condition

As the base condition, the reaction of sugarcane bagasse was firstly studied under HCW condition with and without adding of solid catalysts. It was found that the main products from the reaction were glucose, fructose, xylose, furfural, HMF and AHG indicated the occurring of hydrolysis, isomerization and dehydration reactions. The yields of these liquid products from the reaction at various conditions are shown in Fig. 1. It can be seen that, at 523 K with the reaction time of 5 min, the presence of catalyst makes significant impact on the yield and selectivity of products; furthermore, the preparation procedure and calcination temperature also affect the catalyst performance. For TiO_2 and ZrO_2, the precipitation method with low calcination temperature (773 K) provide higher yield of total liquid products than the catalysts prepared by sol–gel method with high calcination temperature (873 and 973 K), whereas for TiO_2–ZrO_2 the highest total product yield was observed from the catalyst prepared by co-precipitation method with the calcination temperature of 873 K.

Clearly, among all catalysts, TiO_2–ZrO_2 was the most active one in terms of total product yields and HMF–furfural selectivities. It can also be seen that the reaction in the presence of ZrO_2 provided the greatest amount of fructose in the product indicated the promotion of isomerization reaction by this catalyst as previously reported by Watanabe et al. (2005a,b), whereas the presence of TiO_2 and TiO_2–ZrO_2 obviously inhibited the yield of AHG. The high HMF and furfural productions with low AHG and fructose formations observed over TiO_2 and TiO_2–ZrO_2 could be due to the strong isomerization of glucose to fructose following with the rapid dehydration of fructose to HMF by these catalysts. To prove this clarification, the experiments with various reaction times (1, 2, 3, 4 and 5 min) were carried out. It was found that initially within the first 1–2 min, high amount of fructose was observed; but it decreased with increasing reaction time, whereas the yield of HMF increased rapidly with increasing reaction time before reaching steady state value at 5 min.

It is noted that the reactivities of TiO_2–ZrO_2 with Ti/Zr molar ratios of 3/1 and 1/3 was also determined. Among them, TiO_2–ZrO_2 with Ti/Zr molar ratio of 1/1 provides the highest HMF and furfural productions (with the total yield of 16.4% compared to 12.8% and 8.8% observed from TiO_2–ZrO_2 with Ti/Zr molar ratios of 3/1 and 1/3, respectively). The effect of reaction temperature was then studied by varying the temperature from 473 to 673 K as shown in Fig. 2; the highest yield of liquid products can be achieved at the reaction temperature of 523 K for all catalysts. For comparison, the reactions of rice husk and corncob were then studied at selected conditions (523 K in the presence of TiO_2–ZrO_2 with Ti/Zr molar ratio of 1/1 and calcined at 873 K). The yields of liquid products from these three different lignocellulosic biomasses are presented in Fig. 3. Among them, the reaction of corncob provided the highest furfural and HMF productions, whereas those produced from the reaction of rice husk were the lowest. These results are closely related to the amounts of cellulose and hemicellulose in each feedstock since the portions of cellulose and hemicellulose in corncob are significantly higher than those in sugarcane bagasse and rice huck. For the clearer understanding of hydrolysis/dehydration reactions over lignocellulosic biomass, more studies on (1) the hydrolysis/dehydration reactions of individual cellulose

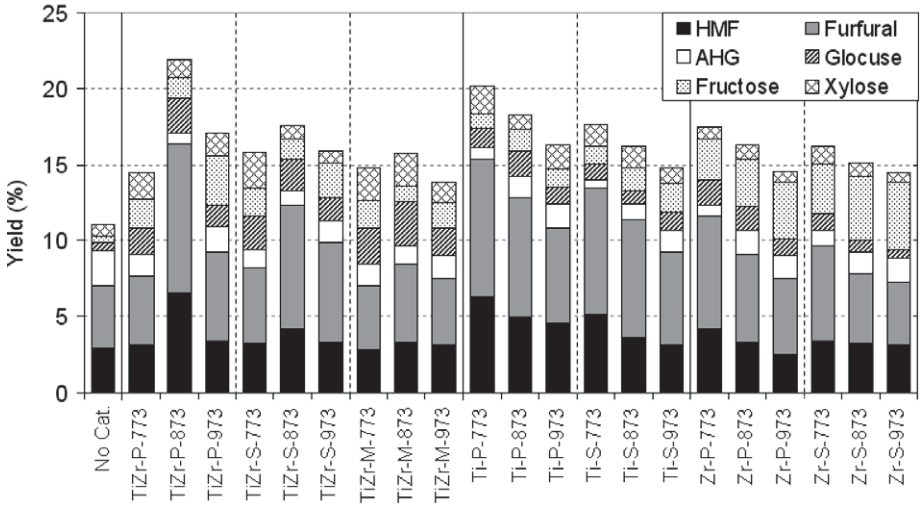

Fig. 1. Yield of liquid products from the reaction of sugarcane bagasse at 523 K and 5 min in the presence of several catalysts (prepared by various methods and treated under different conditions).

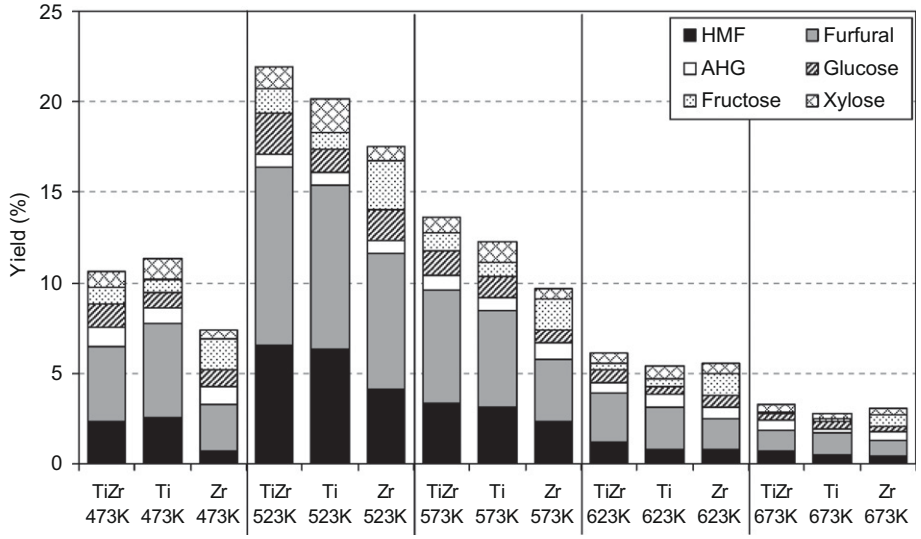

Fig. 2. Effect of reaction temperature (473–673 K) on the yield of liquid products from the reaction of sugarcane bagasse in the presence of various catalysts.

and hemicellulose and (2) the dehydration reaction of C_6-sugar (i.e. glucose) and C_5-sugar (i.e. xylose) were also carried out as presented in Section 3.2, while the role of each catalyst on the reactions is determined by catalyst characterizations and discussed in Section 3.3. It is noted that the reusability of catalysts was also tested. After separated from water solution, the catalysts were washed and dried before re-testing the reaction at the same operating conditions. It was found that the total product yields from the spent catalysts were in the range of ±4% compared to the fresh one, which indicated the well-reusable of these catalysts. Fig. 4 shows the reusability testing of TiZr–P-883 toward the reaction of corncob at 523 K; it can be seen that HMF and furfural yields were in the range of 7.3–8.5% and 9.6–11.3%, respectively, while the total yields were between 24.3% and 25.7% within five reaction cycles. This highlights the great benefit of heterogeneous oxide-based catalyst compared to the typical homogeneous catalysts (e.g. H_2SO_4).

3.2. Cellulose, hemicellulose and C_5, C_6-based sugar reactions under HCW condition

To understand the hydrolysis and dehydration of lignocellulosic biomass, the reactions of cellulose, xylan, glucose, and xylose (as intermediate compounds) were also carried out over various catalysts at 553 K. Fig. 5 shows the conversion and product yield from the reaction over cellulose and xylan, respectively. Clearly, the main product from the conversion of cellulose is HMF with some amounts of glucose, fructose, furfural and AHG also observed in the liquid product. In contrast, the main product from the conversion of xylan is only furfural with small amount of xylose detected in the product. Among all catalysts, the most active one is TiO_2–ZrO_2, which is in good agreement with the results in Section 3.1. Hence, it can be concluded that HMF production from the reaction of lignocellulosic biomass comes from the conversion of cellulose, while furfural is generated from the decompositions of both cellulose and hemicellulose.

Theoretically, it is known that the main product from the hydrolysis of cellulose is glucose; the presence of fructose comes from the isomerization of glucose, while HMF and furfural are produced from the further dehydration of glucose and fructose. In addition, AHG is another by-product from the dehydration of glucose. As for the hydrolysis of xylan, xylose is the only product from the reaction, which is further converted to furfural via dehydration reaction. These clarifications were proven by the studies of glucose and xylose reactions, Fig. 6. According to both figures, it can be

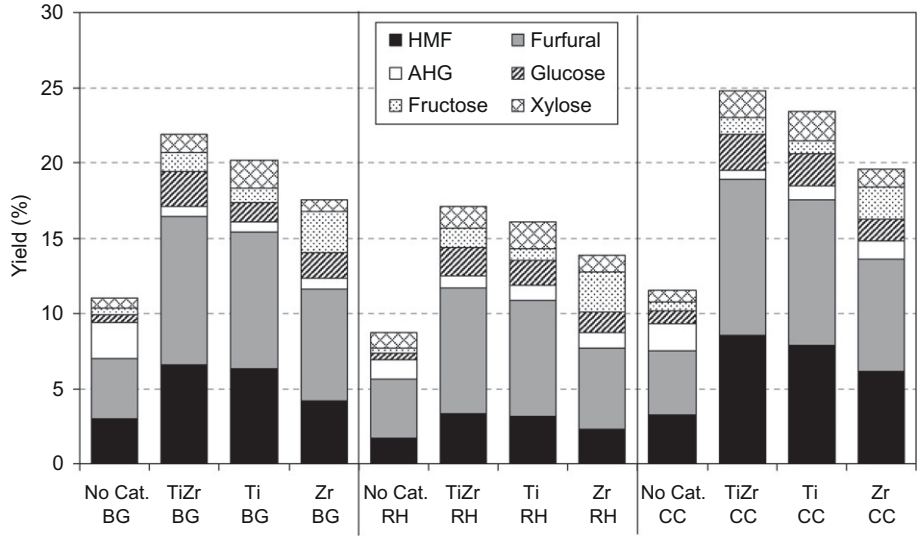

Fig. 3. Yield of liquid products from the reaction of sugarcane bagasse (BG), rice husk (RH) and corncob (CC) (at 523 K and 5 min with and without the presence of catalysts).

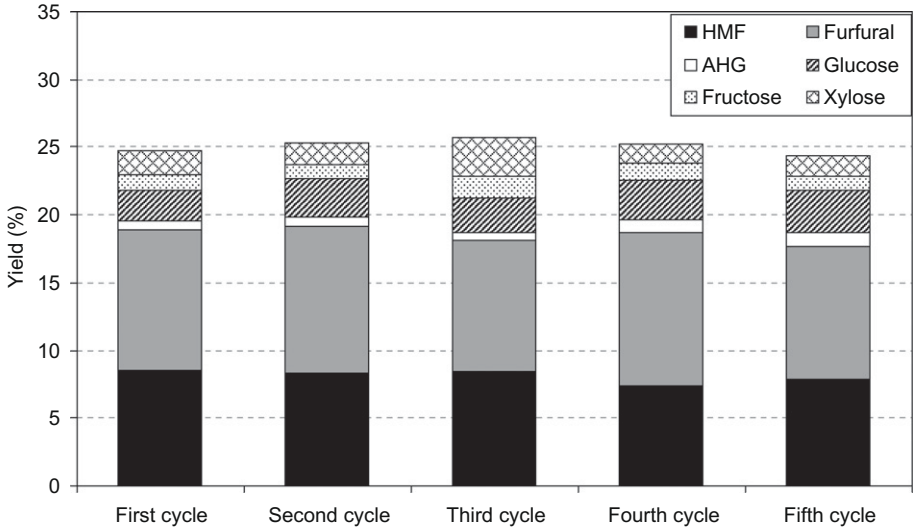

Fig. 4. Reusability testing of TiZr–P-883 toward the reaction of corncob at 523 K.

seen that all results are in good agreement with the above explanation; the products from the dehydration of glucose are HMF, furfural, fructose, and AHG, whereas that from the dehydration of xylose is only furfural.

3.3. Catalyst characterizations

To understand the role of each catalyst (prepared by different methods and conditions) on the interested reactions, the physical characteristics of all synthesized catalysts i.e. surface properties, phase formation, and acidity–basicity properties were determined by BET, XRD and NH_3- and CO_2-TPD measurements; the results of these characterizations are summarized in Tables 1 and 2. As seen in Table 1, the BET results indicated that among all catalyst TiO_2–ZrO_2 (with Ti/Zr molar ratio of 1/1) shows the greatest specific surface area. It can also be seen that the calcination temperature, preparation procedure and Ti/Zr molar ratio (for TiO_2–ZrO_2) significantly affect the specific surface area, cumulative pore volume and average pore diameter of all synthesized catalysts. The specific surface area and cumulative pore volume linearly decreased with increasing calcination temperature, whereas the average pore diameter dramatically increased. Furthermore, among all preparation procedures, (co-) precipitation method can synthesize material with highest specific surface area. According to the XRD measurements, the main phase observed for TiO_2–ZrO_2 is $TiZrO_4$. It is noted that TiO_2–ZrO_2 is in amorphous phase when calcined at 773 K, but the phase turns to be crystalline at higher calcinations temperature (>873 K). As for TiO_2, the anatase crystalline phase was mainly found when calcined at 773 K; however, with increasing the calcinations temperature (973 K), rutile phase was also detected along with anatase crystalline phase. Lastly, the XRD pattern of ZrO_2 indicated the containing of both tetragonal and monoclinic phases with various contents depending on the calcinations temperature; we found that the crystal size in monoclinic phase and the fraction of monoclinic phase increased considerably with increasing calcinations temperature, whereas tetragonal phase decreased.

NH_3- and CO_2-TPD techniques were used to measure the acid–base properties of the catalysts; the amounts of acid and base sites, which were calculated from the area below curves of these TPD